THE UNIVERSITY OF ASTON IN BIRMINGHAM

RECRYSTALLISATION IN TWO-PHASE ALUMINIUM ALLOYS

A thesis submitted in part fulfilment
for the degree of Doctor of Philosophy

by

Firyal A.R.H.Al-Khayat

July 1984

The University of Aston in Birmingham

Recrystallisation in Two-Phase Aluminium Alloys

Firyal A.R.H.Al-Khayat

Ph.D. Thesis 1984

SUMMARY

Recrystallisation behaviour in Al-Mg-Si and Al-Zn-Mg alloys has been studied after rolling reduction from 70% to 90%. A variety of microscopical and analytical techniques has been used in order to examine the as-deformed, partially and fully-annealed microstructures. Optical metallography, X-ray diffraction, scanning electron microscopy in the back-scattered mode, transmission electron microscopy , and conventional scanning electron microscopy have been used. Studies were made on foils prepared from longitudinal sections of the rolled and partially annealed specimens. Recrystallisation is considered to start with preferential nucleation in high deformation regions (i.e. near to the particles and within the shear bands), and the growth of new grains into a deformed matrix. In order to understand the recrystallisation in two-phase alloys and in materials which exhibit shear bands during deformation and their effect on rolling and annealing textures, a number of experiments involving cold rolling and annealing were made on single crystals with various orientations, and polycrystalline materials of Al-Mg-Si and Al-Zn-Mg, and finally in a pure aluminium single crystal.

The orientations of significant regions in the deformation zones around second phase particles, the crystallites within the shear bands and the orientation of newly recrystallised grains in partially annealed specimens were determined by selected area diffraction patterns (SADP) and electron channelling patterns (ECP). In all cases micro-beam diffraction was used to produce Kikuchi patterns for accurate measurement of orientation. The textures were examined using conventional pole figures for as-rolled and as fully recrystallised material.

The presence of coarse, non-deformable particles prior to rolling increased the random annealing texture. In the case of Al-Zn-Mg, where shear bands were present, these were found to act as nucleation sites and produce a wide spread of orientation, but their relation with the final annealing texture is not clear.

Keywords: Recrystallisation Al-alloys;
second phase particles;
shear bands.

CONTENTS

LIST OF TABLES

LIST OF FIGURES

INTRODUCTION

The recrystallisation textures of aluminium and its alloys are of great importance as they strongly influence the mechanical properties. Material properties of importance to formability are strength, ductility and plastic anisotropy, which are in turn related to other factors such as grain size, solute content and distribution, and texture. The microstructural features of interest are produced through solidification, deformation and annealing, and are controlled by the whole process which is the main object of this present work. Recrystallisation of cold worked materials containing second phase particles in F.C.C. metals has been studied by optical, electron microscopy and x-ray diffraction including texture studies. The recrystallisation is normally accelerated when the particles are large. Most of the work has been on second phase materials and in particular on Al-Mg-Si alloys. In this alloy the formation of recrystallisation nuclei and their growth were studied. Preliminary experimental work is concerned to produce coarse and non-deformable particles prior to rolling. Polished surfaces of deformed specimens between 10 to 90% reduction in thickness were studied by optical and scanning electron microscopy. Two theories have been proposed to explain the recrystallisation texture in F.C.C. metals, and the generally accepted theory is based on oriented nucleation[23].

The work presented in Chapter Two of this thesis reviews

the relevant literature. The experimental work presented in Chapter Three of the thesis described two programmes of work. First, to consider the mechanisms of recrystallisation in two phase alloys with large particles. Second, the development and effect of shear bands in the recrystallisation of Al-Zn-Mg alloys. A wide range of techniques has been used in the present work to study the deformation structure, and partially and fully annealed microstructures in two aluminium alloys.

CHAPTER TWO

LITERATURE REVIEW

2.1 Precipitation Sequences in Aluminium Alloy

2.1.1 A Generalised Example of Precipitation From Solid Solution

The initial stage in the precipitation sequence from solid solution is the formation of solute atom aggregates which constitute stable regions having a chemical composition different from the parent solid solution. Within these regions the atoms are situated at the average lattice points of the solid solution. It is possible to develop these regions during ageing or during the quench after solution treatment. Also the aggregates may have associated with them a larger or smaller number of vacant lattice sites than will be found in an equal volume of matrix. As precipitation continues the aggregates grow, and may undergo internal ordering, such that a precipitate having a crystal structure quite different from that of the matrix, can be produced.

Their size, shape, nature (i.e. whether they are hard or soft) and the nature of the interface between the precipitate and its matrix are extremely important. It is important to know whether glide dislocations moving in the matrix can pass through the precipitate, i.e. whether the glide dislocations in the matrix and precipitate have

similar Burgers Vectors or not.

The shape of the precipitate is greatly influenced by the nature of the interface which exists between the precipitate and the matrix. This interface may fall into one of three categories. Firstly one can have a "fully coherent" interface, when the atoms constituting the interface between the particle and matrix have an atomic arrangement which is common to both crystal structures. In general the separation of the atoms in a coherent interface is not quite the same in both matrix and precipitate, so that only when the interface is small in area can it be fully coherent since any misfit must be accommodated by elastic strain, as indicated in Figure (1a). The magnitude of the "coherent strain" will depend upon the relative atomic diameter of the atoms concerned. The second type of interface which results when the interfacial area becomes larger may be defined as one in which the strain energy is reduced by the introduction of structural dislocations lying in the interface[1,2]. This interface is generally termed "quasi coherent" or "semi coherent" and is illustrated by Figure (1b). For this type, the dislocation density per unit area of interface is small. This means that the interface may appear to be fully coherent between these dislocations[3].

The third type of interface is termed "non coherent" interface, in which there is no special relationship between the two crystals and may be regarded as a situation in which individual dislocations have become so closely

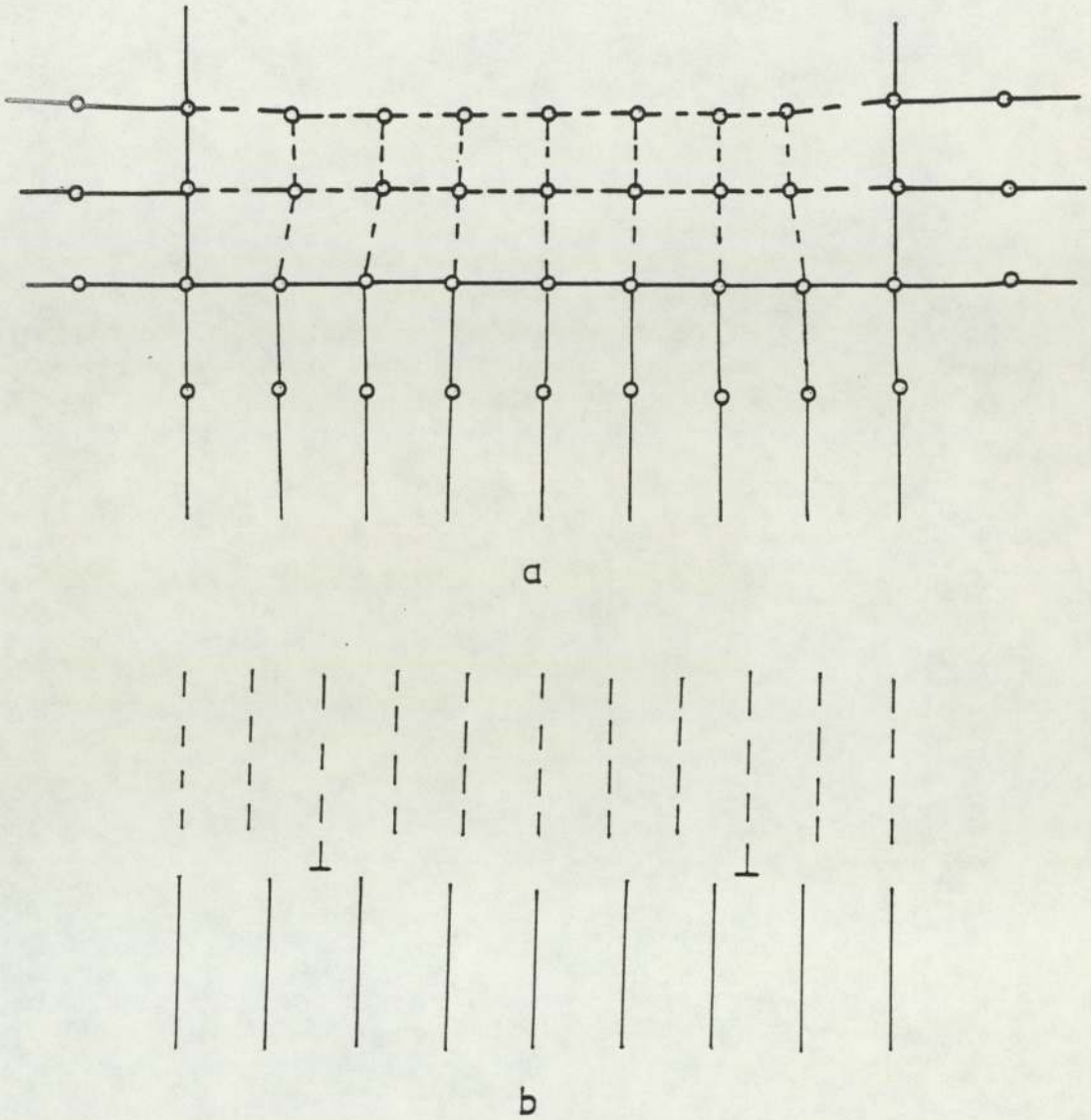

Figure (1) a - Diagram of a coherent interface between two crystals of slightly different atomic spacing.

b - A quasi-coherent interface between two crystals: both lattices have their natural lattice parameter and dislocations lie in the interface.

Ref.(3)

spaced that their individuality is lost and they can no longer be recognised as separate defects. One may now define a completely "coherent precipitate" as one in which all the interfaces with the matrix are coherent and the Bravais lattice in two crystal structures are identical. Since the Bravais lattice in the matrix and precipitate are the same, it is geometrically possible for a dislocation in the matrix to pass through a coherent precipitation as the Burgers Vector of a dislocation in the matrix will differ little, if at all, from that in the precipitate. A partially coherent precipitate is one in which at least one interface is coherent. This type of precipitate may have an orientation relationship with the matrix, although the observation of an orientation relationship does not necessarily imply any coherency. For example, the θ precipitate in aluminium-copper, if produced by ageing, possesses an orientation relationship with the matrix, but is not coherent[4]. A non-coherent precipitate is one in which none of the interfaces with the matrix are coherent. The alloy decomposes during or immediately after quenching, and the solute atoms segregate to form small clusters. These clusters grow until they give rise to the x-ray diffraction effects typical of G.P.Zones. Where there is no size difference between solute and solvent, the shape of the zones is spherical. However where a size difference does exist the zones and probably the first clusters are asymmetrical and may take the form of rods or plates. There is no effective nucleation barrier to the formation of these segregates so the process takes place entirely by competitive growth, the rate of growth being

determined by the vacancy flux. The process controlling diffusion may be the absorption of vacancies from zones[5].

2.1.2 Coherent Nucleation

Since the precipitation occurs by a process of diffusion which is essentially a simple interchange of atoms on a fixed array of sites, the first segregates of solute atoms formed must be completely coherent with the matrix. The energy of coherent or quasi-coherent interfaces is less than that for the incoherent type, and a considerable reduction in the free energy of formation of nucleus results if the embryos are bounded by coherent interfaces Figure (1b). Nabarro[6,7] showed that if the precipitate remains completely coherent with the matrix, the strain energy of the particle increases as the size of the precipitate increases. If a sphere of unstrained radius $(1+\delta)r_o$ is inserted into a hole of radius r_o in the matrix, the total elastic strain energy of a sphere of volume $V = \frac{4}{3}\pi r_o^3$ and bulk modulus K, in a matrix having a rigidity modulus G is given by:-

$$6\,G\,V\,\delta^2 / 1 + \frac{4G}{3K}$$

where δ - is misfit parameter

The energy thus increases as the volume of the precipitate particle increases. Eventually a size is reached, when it is energetically more favourable to form dislocations in the interfaces than to increase the lattice strain, and

a quasi-coherent interface will form, Figure (1b). Nabarro also showed that the energy can only be reduced, due to anisotropy of the elastic constants, by a change in the shape of the precipitate.

The small decrease in energy which can be obtained by altering the precipitate shape in an elastically anisotropic material may influence the initial shape of the precipitate which is still coherent, a plate-like precipitate is likely to have the lowest strain energy. Many precipitates in F.C.C. metals precipitate as plates on the {100} planes of the matrix due to the anisotropy of elastic modulus of the matrix[6]. Young's modulus for all F.C.C. metals has a minimum along the <100> direction[8]. The maximum strain therefore lies along the direction of minimum elastic modulus, thus minimising the strain energy. However, in the case of aluminium the anisotropy is very small. The shape of a coherent nucleus is governed by the relative values of the elastic constants, the magnitude of mismatch and the anisotropy of surface energy. If the atomic mismatch for a solute is small, so that a highly strained precipitate or zone is not formed, the particle shape will be dictated by the criterion of minimum surface area to volume ratio. Spheres are generally formed when the atomic misfit is 3%, and discs when the misfit is 5%.

2.2 Precipitation of a Second Phase

Several aluminium alloys can be hardened by the precipitation of second phase in the solid solution. The main

requirement is, basically, for a high solid solubility at elevated temperature decreasing to a low level at room temperature, or above, and therefore enabling the formation of a super saturated solid solution. This feature is found in a dilute Al-Mg-Si alloy. Once a supersaturated solid solution has been formed, it is necessary to precipitate the solute at room temperature or at moderately elevated temperatures. The changes occurring during this process account for age hardening, and the considerable amount of work published on the subject has been reviewed by Mondolfo[9] and Kelly et al[3].

2.2.1 Aluminium-Magnesium-Silicon

This is a pseudo-binary system since the compound Mg_2Si (β) is extremely stable. The probable sequence of precipitation[10] is Needle-shaped zones along <100> $\longrightarrow$ Needle-shaped zones with internal order $\longrightarrow \beta' \longrightarrow \beta(Mg_2Si)$.

Thomas[11] has carried out an extensive study of Al-1%Mg-0.6%Si alloy using the transmission electron microscope and deduced the following sequence of precipitates:

$$\text{Needle} \longrightarrow \text{rods} \longrightarrow \text{plates}\,(Mg_2Si)$$

Rods are an intermediate form of the equilibrium plates of Mg_2Si. He has found needle-shaped zones in alloy aged at temperatures $\leqslant 204^{\circ}C$ which are ~ 60 Å diameter, 200-100 Å long and the density of precipitation is $\sim 3 \times 10^{15}\ cm^{-3}$. The needles lie along the <100> matrix direction. After

further ageing the diffraction pattern shows an F.C.C. superlattice structure which may correspond to the phase and the precipitates grow to form rods ~ 100 Å diameter and ~ 1 μm long. The orientation relationship is:-

$$(100)_{\beta'} \,//\, (100)_{Al} \qquad \text{and}$$

$$[011]_{\beta'} \,//\, [100]_{Al}$$

The structure of β' is determined by Jacobs[12] to be Hexagonal with lattice spacing a=0.705 nm, and c=0.405 nm. It was also concluded that the structure of the β''-needles probably was nearly the same[12]. The difference between β'' and β' is then essentially a question of size.

Another well-known structural element is the plate shaped equilibrium Mg_2Si β-phase, which has a F.C.C. structure with lattice parameter a=0.639 nm[12] and the orientation relationship is invariably reported to be:-

$$(001)_{\beta} \,//\, (001)_{matrix} \qquad \text{and}$$

$$\langle 110 \rangle_{\beta} \,//\, \langle 100 \rangle_{matrix}$$

2.3 Rolling Textures of F.C.C. Metals

A random polycrystalline aggregate will develop preferred orientations or textures, upon sufficient plastic deformation. The nature of the deformation texture depends essentially upon the crystal structure of the metal and its flow characteristics. The resulting texture may be

affected to some extent by many other factors, such as the initial texture, the chemical composition, the previous thermal or mechanical treatment, the temperature, rate or physical constraints during deformation, etc. Many theories have been proposed to date to explain the formation of textures in polycrystalline aggregates. However, the complexity of the deformation process of the individual grains in a polycrystal, particularly at large strains, and the usual complexity of the polycrystalline texture itself impose great difficulty in the derivation of a theory on rigorous grounds. As a first step towards the understanding of the texture formation in polycrystals, much effort has been made in the study of texture developments in single crystals.

2.3.1 Rolling Textures of F.C.C. Single Crystals

Texture studies on single crystals have been conducted most extensively with the F.C.C. metals copper and aluminium. On the other hand, much less work has been done on single crystals of silver of F.C.C. alloys, such as brass. Most of the data available in the literature relates to single crystals of copper, aluminium, silver, brass and other copper-base alloys. Barrett et al[13]. Liu et al[14] and Hibbard et al[15] have studied the orientational changes in copper single crystal on rolling. They found that single crystals of copper in (110)[$\bar{1}$12] orientation do not undergo detectable rotation,even after very large reductions in thickness (>95%) reduction the texture remained remarkably sharp with a maximum orientation

spread of only ± 5 to 10 degrees from the initial orientation of the crystal. Thus (110)[$\bar{1}$12] seems to be quite a stable orientation in cold rolled copper crystals. High stability of the initial orientation after deformation was also noted in crystal having an orientation near the stable (110)[$\bar{1}$12] end orientation - such as (110)[$\bar{1}$15][13]. Moreover, the small orientation spread noted in the deformation texture of single crystals of these orientations indicated that the trend of lattice rotation was toward the (110)[$\bar{1}$12] end rotation. For (110)[001] single crystals[13] of copper the trend of the orientational changes upon rolling was also found to be toward the stable end orientation (110)[$\bar{1}$12]. Hu et al[16] compared the textures developed in (110)[1$\bar{1}$2] crystals of high-purity copper and Cu-4%Al alloy after rolling unidirectionally at room temperature to 95% reduction in thickness. There is no essential change in orientation observed in both crystals. The texture of higher purity copper crystal is remarkably sharp, whereas Cu-4% Al crystal showed a considerably larger orientation spread. The maximum intensity for the Cu-4% Al crystal was substantially lower than that observed in the pure copper crystal (Figures 2 & 3). After 99% reduction, while the texture of the copper crystal retained a high degree of sharpness, than that of the Cu-4% Al crystal already assumed a double (110)[1$\bar{1}$2] orientation which closely resembles the polycrystalline texture of brass.

Single crystals of high-purity aluminium (>99.99% pure) having the (110)[1$\bar{1}$2] orientation after being rolled to

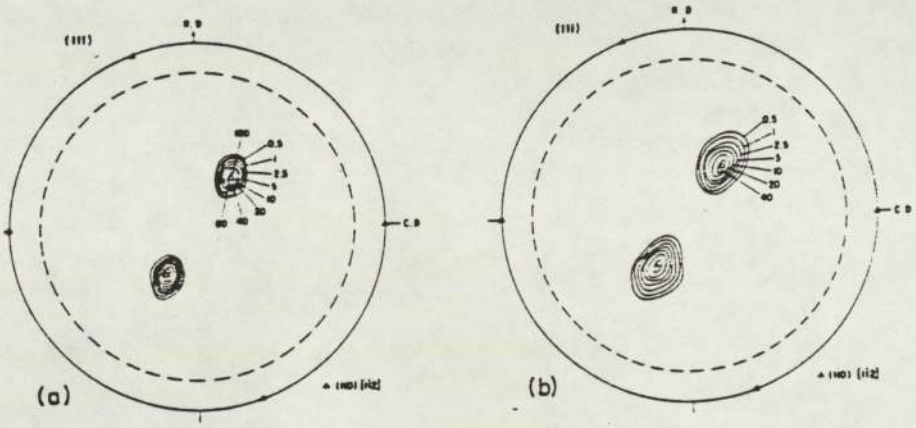

Figure (2)

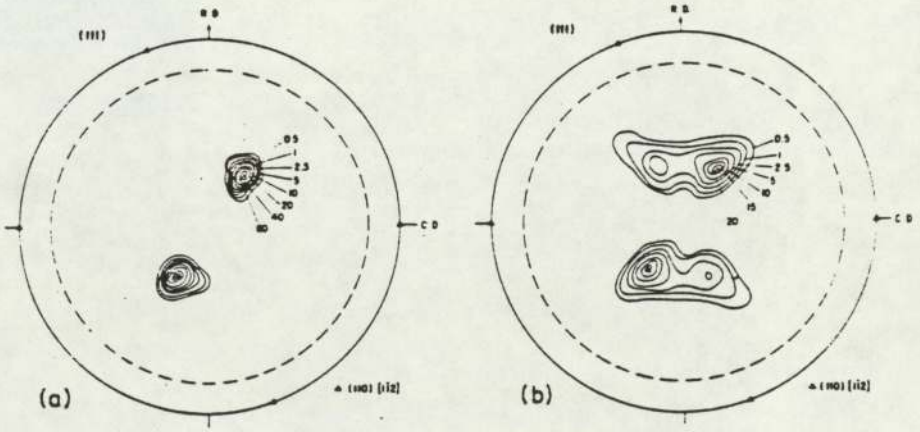

Figure (3)

Figure (2) - Texture of the (110)[1$\bar{1}$2] crystal rolled 95% at 25°C
a) High purity copper, b) Cu-4% Al

Figure (3) - Texture of the (110)[1$\bar{1}$2] crystal rolled 99% at 25°C
a) High purity copper, b) Cu-4% Al

Ref.(16)

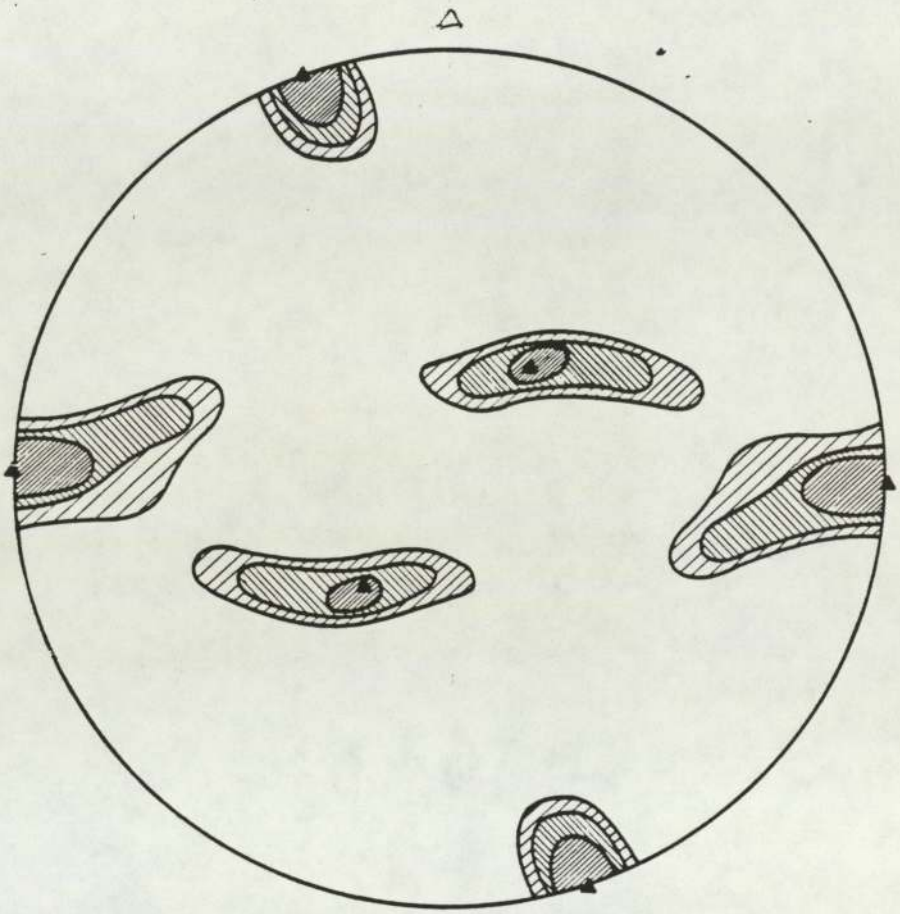

Figure (4) - (111) pole figure of an aluminium single crystal cold rolled 99.6% reduction in thickness from the (110)[$1\bar{1}2$] orientation. ▲ represents (111) poles of (110)[$1\bar{1}2$] orientation.

Ref.(19)

80% reduction did not show much change in orientation in the as-deformed texture[17,18]. From their work on pure aluminium single crystals Liu et al[19] concluded that considerable orientation spread takes place after the crystals are rolled to 99.6% reduction in thickness, Figure (4). They, however, attribute this to the initial orientation of the crystal, which deviates from (110)[1$\bar{1}$2] by 3°. Dillamore et al[20], on the other hand, consider this result as an indication of the instability of the (110)[1$\bar{1}$2] orientation in aluminium crystals in contrast with single crystals of copper,and suggested that this is due to cross-slip being easier in aluminium than in copper. Hu et al[21] have observed that for a (110)[1$\bar{1}$2] crystal of zone-refined aluminium (>99.9999% pure) rolled at -78°C to 80% reduction in thickness, the deformation texture was also a remarkably sharp (110)[1$\bar{1}$2]. Possibly, the lower temperature is sufficient to reduce the incidence of cross-slip or alternatively, at very heavy reductions, surface effects may predominate. The rolling texture of a (110)[1$\bar{1}$2] brass crystal has never been seriously investigated.

The rolling texture of (110)[$\bar{1}$10] single crystals of aluminium, copper and Cu-0.05% P were examined by Verbraak[22]. After being rolled to 99% the principal orientations of the rolling textures in each of these crystals were found to be essentially the same. As shown in Figure (5) the main components of the rolling texture in all three cases were a pair of complementary {112}⟨111⟩

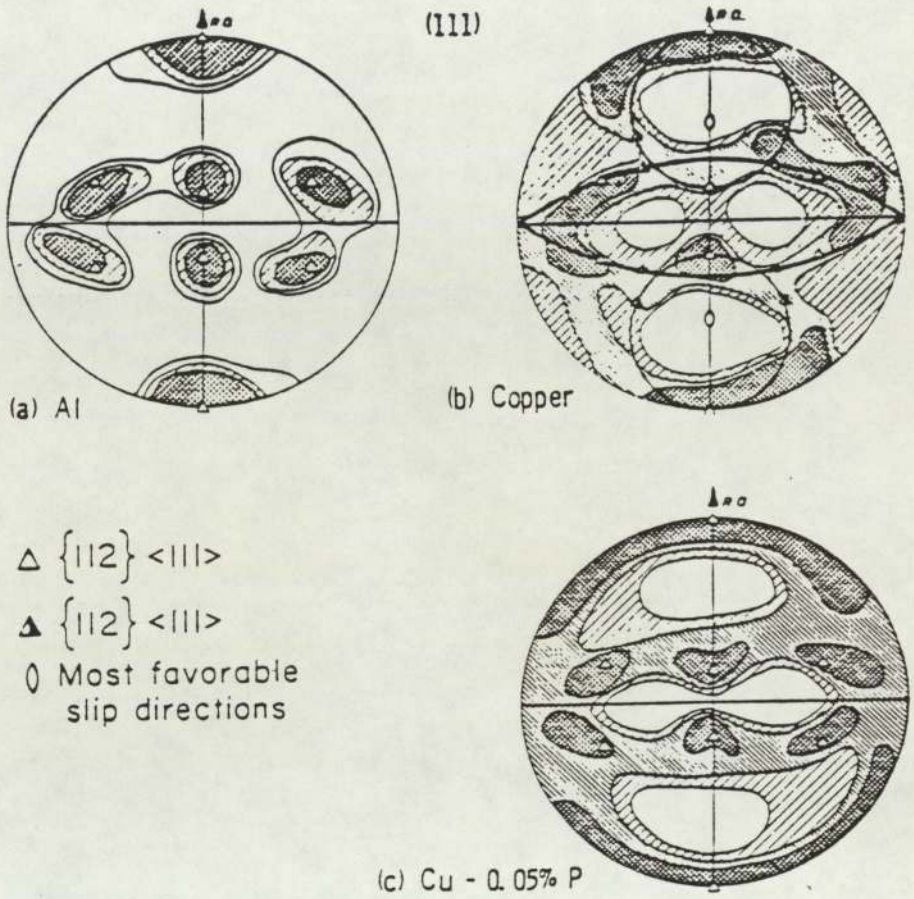

Figure (5) - Texture of the $(\bar{1}10)[110]$ crystal of
a) Al, Δ {112}<111>,
b) Cu, Δ {112}<111>, Δ {112}<111> components rotated 90° around the most favourable slip directions, and
c) Cu-0.05% P, Δ {112}<111>. All crystals rolled 99%

Ref.(22)

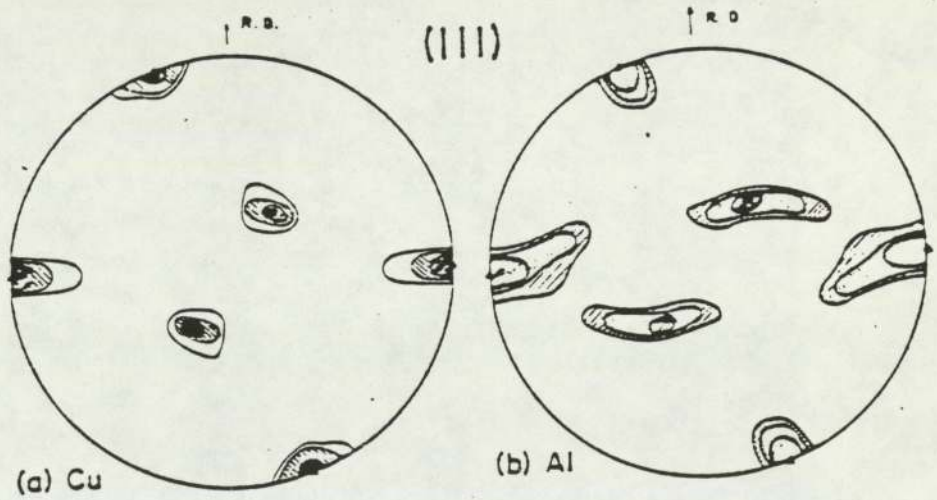

Figure (6) - Texture of the $(110)[1\bar{1}2]$ crystal of
a) Copper and
b) Aluminium rolled 99.5%

Ref.(14,19)

orientations - the range of orientation spread differing considerably amongst the three. The Cu-0.05% P crystal had the most extensive orientation spread whereas the aluminium crystal had the least orientation spread with copper lying in between these two extremes. Verbraak described the orientation spread in the copper single crystal approximately as a rotation around the most favourable slip direction, [110] after the (112)[111] - type orientation was developed. Based on these results of Verbraak and those of Liu et al[14,19], Figure (6) the textural behaviour of aluminium and copper is apparently not identical. The results of texture studies made on copper single crystals of (112)[$\bar{1}$10] [13,22] and (113)[$\bar{1}$10][13] orientations after rolling were largely similar to those having (110)[$\bar{1}$10] initial orientation. The rolling texture of (001)[110] oriented single crystals of copper was found to consist of a (110)[001] component in addition to the two complementary (112)[111] orientations[22]. These texture components are related to the initial orientation of the crystal by rotations around the [$\bar{1}$10] axis in the transverse direction. Burgers et al[23] have obtained similar results for an aluminium single crystal rolled in the (001)[110] orientation.

The rolling texture of (001)[100] crystals of copper[13,22] corresponded almost to the polycrystalline texture of copper with a strong component of the cube-orientation. The development of the rolling texture in a (350)[001] oriented single crystal of 70/30 brass was examined at

various stages of rolling by Brick[24]. The change in orientation during rolling was found to be from (350)[001] to (110)[$\bar{1}$17] after 85% reduction, then a pair of complementary (110)[113] orientations after 99% reduction. Thus it was clearly indicated that rotation toward the (110)[112] end orientation occurred during rolling.

The results obtained by Barrett et al[13] and Verbraak[22] on (112)[111] copper crystals are in good agreement in that they develop the complementary (112)[11$\bar{1}$] orientation after being rolled to 90 and 99% reduction. Hibbard et al[15] did not observe the complementary orientation in their crystal rolled 95%. Hu et al[16] have reported a comparative study of texture development on rolling in (112)[11$\bar{1}$] oriented crystals of high-purity copper and Cu-4% Al alloy. They observed a marked difference in the rolling textures of the pure metal and its alloy even at low deformation level 50% reduction. While the copper crystal was found to retain its initial orientation and showed a very sharp texture, the Cu-4% Al crystal developed a large orientation spread and a strong component of (552)[$\bar{1}\bar{1}$5] orientation which is a twin orientation of the (112)[11$\bar{1}$]. After further reduction up to 95%, a minor component of the (552)[$\bar{1}\bar{1}$5] twin orientation was developed in the copper crystal, whereas the texture of the Cu-4% Al crystal showed further changes from both the matrix and the twin orientations to the (111)[11$\bar{2}$] and (110)[001] orientations respectively.

The behaviour of rolled silver crystals in the (112)[11$\bar{1}$] orientation was found to be quite different from that of copper crystals of the same orientation rolled at room temperature. Verbraak[22] measured the peak intensities of three different reflections, from planes parallel to the rolling plane, of a silver crystal with the (112)[11$\bar{1}$] orientation at various reductions. From his results he suggested that during deformation the crystal rotated around the cross-rolling direction from the initial (112) position in the rolling plane through the (111), and finally to the (110) position with increasing reduction. In order to explain the observed difference in the rolling textures of copper and silver single crystals of the same orientation, namely, (112)[11$\bar{1}$]. Verbraak postulated that in a (112)[11$\bar{1}$] copper crystal, slip is possible on cube planes, that is, the (001)[110] slip is operative; but in silver only the (111)[$\bar{1}$01] and (111)[0$\bar{1}$1] slip systems are operative, hence the crystal rotates in one direction only.

Hu et al[16] pointed out that Verbraak's interpretation was not consistent with the results that they obtained for the Cu-4% Al crystal, since the (110)[001] orientation in the Cu-4% Al crystal was derived from the twin orientation rather than from the matrix orientation by a large angle rotation. They suggested that their results were in good agreement with the observation of Ahlborn et al[25] on a (112)[11$\bar{1}$] silver crystal. Their results indicate that the (112)[11$\bar{1}$] silver crystal, after 30% reduction, developed a new component of the (552)[$\bar{1}\bar{1}$5] orientation in the

texture and that upon further deformation this component rotated into (110)[001].

Single crystals of a few special initial orientations of copper and aluminium were also studied by various workers to determine their textural behaviour. These include the (123)[$\bar{4}\bar{1}$2] oriented crystals of copper[15] and aluminium[26] and the (3$\bar{5}$8)[$\bar{5}$23] oriented crystal copper[15]. It has been found that all these orientations were essentially retained with a reasonable scatter up to high rolling reduction.

2.3.2 Rolling Textures in Polycrystalline F.C.C. Metals and Alloys

In general two types of rolling textures are normally recognised in F.C.C. metals and alloys. Quantitative pole figure measurements were made by Beck et al[27,28] on copper, aluminium and α-brass after 96% cold reduction. They found that the rolling textures of copper and aluminium were similar and at the same time different from the texture of α-brass, Figure (7). The α-brass texture could be adequately characterised by the ideal orientation (110)[112] plus a minor (110)[001] component. The copper and aluminium textures could not, however, be so readily described and the texture shown in Figure (7 a) for copper has been called an irrational texture. Hu et al[28] using quantitative pole figures, suggested an "ideal orientation" of approximately (123)[$\bar{4}\bar{1}$2] to designate the type of textures encountered in copper and aluminium. To account

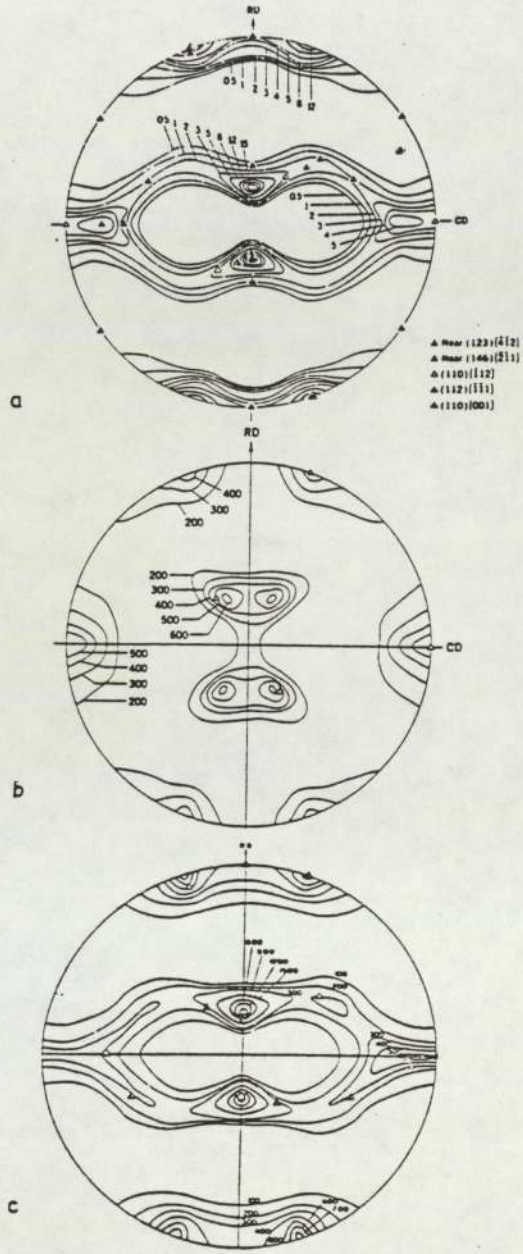

(7,12,22)[84$\bar{5}$]

Near (123)[1$\bar{2}$1]

(110)[$\bar{1}$12]

(112)[11$\bar{1}$]

Figure (7) (111) pole figures of

a) copper

b) 70/30 brass

c) aluminium after 95% cold reduction

Ref.(28)

for the maxima on the pole figures, a second ideal orientation of near (146)[21$\bar{1}$] was also used to describe the texture of copper. Results from a number of quantitative texture studies[29-31] indicate that the textures of most F.C.C. metals except silver are of the copper type, whereas those of silver and most F.C.C. alloys are of the brass type. The principal texture of most F.C.C. metals and alloys can be described by the (135)[121] orientation. This actually represents the central regions spread between the orientation (110)[112] and (112)[111]. In recent years the development of orientation distribution function (ODF) using computer analysis of the pole figure[32] has allowed an unambiguous description of the rather complex texture found in cold rolled pure F.C.C. metals. The texture does in fact consist of a range of orientations or a continuous tube of orientation from near{112}<111> through {123}<412> to {110}<112>.

Due to the Kallend et al[23] experimental results on the development of brass texture using the three-dimensional orientation distribution function (ODF) used to explain the transition texture in F.C.C. materials. Their results show that the initial development of texture in cold rolled copper and α-brass is the same, but that at a reduction of above 40%, a transition occurred in the α-brass texture. The texture of the material, which consisted of a continuous tube of orientations between {110}<112> through an orientation between {111}<112> and {552}<115>. Similar results were found by Wakefield et al[34]

using the (ODF) in copper-6.4 Wt% Al.

In Cu-30% Zn annealing textur developed the normal alloy type recrystallisation textur in both conditions, Figure (8 a,b). This texture consists of a complex tube of orientations running betwe {368}<423> and {203}<312> through orientation as {225}< >, {326}<835>, and {214}<523>.

n attempt to
rials from a
It has been
on similar
the "pure metal"
ersa, can occur
treatment

Please note that Ref.(35) is deleted.

rass texture
or decreasing

the deformation temperature (i.e. decreasing the effect of SFE). The effect of solutes on the development of rolling textures of a number of F.C.C. metals has been investigated by many workers. Smallman[29] showed that the texture transition from copper to α-brass type was caused by the addition of elements like aluminium, zinc and germanium. In the case of copper-aluminium alloys Wakefield et al[34] found that the complete texture transition was obtained after adding 6.4%Wt Al to copper. Similar observations for copper texture transition have been reported by [30,31,36,37] by adding aluminium, zinc,

using the (ODF) in copper-6.4 Wt% Al.

In Cu-30% Zn annealing texture developed the normal alloy type recrystallisation texture in both conditions, Figure (8 a,b). This texture consists of a complex tube of orientations running between {368}<423> and {203}<312> through orientation as {225}<734>, {326}<835>, and {214}<523>.

Various theories have been put forward in an attempt to predict the rolling textures in F.C.C. materials from a knowledge of their deformation mechanisms. It has been established that all F.C.C. materials slip on similar slip takes place. Texture transitions from the "pure metal" type to the "alloy type" texture and vice versa, can occur by the alterations of material variables or treatment variables, or both.

Transition from the copper texture to the brass texture can be obtained by increasing alloy content or decreasing the deformation temperature (i.e. decreasing the effect of SFE). The effect of solutes on the development of rolling textures of a number of F.C.C. metals has been investigated by many workers. Smallman[29] showed that the texture transition from copper to α-brass type was caused by the addition of elements like aluminium, zinc and germanium. In the case of copper-aluminium alloys Wakefield et al[34] found that the complete texture transition was obtained after adding 6.4%Wt Al to copper. Similar observations for copper texture transition have been reported by [30,31,36,37] by adding aluminium, zinc,

germanium, tin, phosphorus, arsenic and antimony to copper. In general, for a given solute, a minimum amount is required to initiate the transition and the degree of transition increases with increasing solute concentration.

Transition of texture in F.C.C. metals and alloys can also be effected by changing the deformation temperature. In cold rolling copper the ordinary copper-type obtained near room temperature changes gradually to the brass-type when rolling temperatures are reduced through the range -80 to -200°C[38]. A detailed study of the texture transition in relation to the deformation mechanisms involved has been studied by Hutchinson et al[39], they showed "alloy" texture component {110}<112> was due to normal octahedral slip (Group A) and texture transition to the pure-metal texture due to:

i) Non-crystallographic shear:- New type of shear were becomes active after rolling about 50% reduction[40].

ii) Slip on cube planes:- "Alloy" texture was generated by normal octahedral {111}<110> slip, while "pure metal" texture due to normal slip with additional slip on {001} planes (cubic slip), proposed by Haessner[41], which was proposed previously by Richards et al[42] during their study of the structural and textural changes during rolling 99.99% pure aluminium. They concluded that the early stage of rolling occurs by normal slip {111}<110>, which produce alloy-type texture {110}<112> components, whereas in the later stage of rolling a second shear were operates. After (>50%) reduction by rolling the {100}<110>

slip is operated which leads to the "pure metal" type texture {112}<111>, which is a typical texture of F.C.C. metals.

iii) Cross-slip:- Dillamore et al[43] and Smallman et al[44] both proposed that the present difference between the "pure metal" and "alloy" texture, and the transition from one to another is due to the difference in the cross-slip behaviour of glide dislocation. They claimed that cross-slip was responsible for "pure metal" texture to generate. Dillamore et al[43] suggest that all f.c.c. metals during deformation first develop "alloy" texture {110}<113> by normal slip, similar to that proposed by Richards[40], and later it will be transformed by cross-slip to metal-type texture. This is due to cross-slip in high SFE metals occurring more easily than in low SFE metals where the deformation occurs by normal slip and the final texture will remain as {110}<112> or "alloy" texture. Whereas in high SFE cross slip occurs easily and therefore develops "pure-metal" texture.

iv) Dislocation interaction:- A theory for f.c.c texture based on dislocation interaction was proposed by Liu[45]. During deformation and on the basis of the dislocation interaction the selectivity of active slip systems gives a minimum energy during deformation. He showed that in low SFE metals the ideal orientation was $(110)[\bar{1}12]$ plus orientation spread in plane normal (110). While in high SFE metals the ideal orientation was to be close to $(358)[52\bar{3}]$.

"Pure metal" texture generated by normal octahedral slip (group B) and transition to "alloy" texture caused by:

i) Latent hardening (over shooting):- This theory was proposed by Bishop[46] and Calnan[47] and was based on the idea that over shooting due to the unequal hardening of primary and latent slip systems had an effect on texture formations.

ii) Twinning:- Wasserman[48] has proposed that if the deformation mode such as twinning is present in addition to the normal slip the pure metal texture {112}<111> can be transformed to {552}<115> and further slip, the twinned material is then rotated to {110}<001>.

iii) Slip by partials:- This is proposed by Hu et al[ ] in order to explain the rolling texture of Cerium metal with very low SFE.

In recent techniques of analyses, using the orientation distribution function, results of texture development were obtained, and on the basis of these results it is accepted that the group (B) hypothesis is nearer to the experimental results. Recent orientation distribution function (ODF) analysis gives more detail of orientation and identifies the small texture component present which is not identified in the pole figure used in cold rolled copper and brass by Lücke et al[49]. In a more detailed study they confirm the mechanisms proposed by Hutchinson et al[39].

2.4 Recrystallisation Textures of Rolled F.C.C. Metals and Alloys

2.4.1 Recrystallisation Textures of Rolled F.C.C. Single Crystals

Most of the work in this field has been confined to copper and aluminium single crystals of various orientations. Liu et al[14,19] rolled copper and aluminium single crystals in the (110)[$\bar{1}$12] orientation. This orientation is stable in copper up to 99.5% reduction but shows some spread in aluminium[19]. With the copper after annealing, the recrystallisation components were related to the deformation orientation by 30° rotations clock-wise and anti-clock-wise about common <111> poles. They observed that for annealing temperatures of 400°C and below, all four <111> poles of the deformed crystal occurred as rotation axes, whereas above 400°C only three could be found. With the aluminium crystals, which showed much greater spread, the relationship was not as simple. Liu et al[19] report that for annealing temperatures between 400 and 600°C the relationship is described by 40° unidirectional rotation about three of the four octahedral poles and 30° unidirectional rotation about three <110> poles. On annealing at 650°C, only three of these components were present, two of which were found to bear the <110> rotation relationships. Beck et al[18,50] have studied the annealing textures of some aluminium single crystals which were rolled 80% and whose surface was abraded before annealing to induce random nucleation.

For both the (110)[1$\bar{1}$2] orientation and the (123)[41$\bar{2}$] orientation, and regardless of whether there was iron and silicon in solution or not, the relationship between deformation and recrystallisation orientation was described by a rotation of 40^{o} around common <111> poles. Lücke et al[51-53] found that in a single crystal of aluminium prestrained by 20-30%, in which recrystallisation was started at one end by clipping off the end with shears and immersing this end in a salt bath, random nucleation occurred, but grains bearing <111> rotation relationships with the matrix eventually filled the cross-section of the wire. Graham et al[54,55] on the other hand, detected no clear orientation relationship. Green et al[56] have shown that differences in the processing conditions used by the two groups account for the conflicting results. Graham et al used aluminium with a high iron and silicon content, which was retained in solution after their treatment, while Liebmann et al used an aluminium with a lower iron and silicon content, which was precipitated.

The results thus suggested that, in the absence of solution effects, the relationship between the deformed matrix and recrystallised grain is one of rotation about a <111> pole. Some controversy has surrounded the reasons for this relationship. Youshida et al[53] and Beck et al[18,50] claim random nucleation followed by growth selection, but Barrett et al[57] showed that in the work of Youshidá random nucleation was not proved and Haessner et al[58-60] found in experiments of a similar nature to those of Liebmann et al, that there was a strong component

of oriented nucleation of grains with a 28° or 40° rotation relationship about a particular <111> pole. This was imposed on a random spread of nuclei. In Haessner's work 99.99% pure aluminium was used and solution effects were, to a large extent, absent. Czjzek et al[59] studied the growth anisotropy of sheet single crystals of aluminium and concluded that this was determined more by the deformed structure than by the orientation relationship.

Liu[61] rolled a single crystal of copper in the $(3\bar{5}8)[\bar{5}23]$ orientation by 80-90% and on annealing the recrystallisation texture components were found to be 7° off the ideal cube texture (100)[001], together with the twin of this off-cube component. Verbraak[62,63] rolled a similar crystal 99% and found a similar annealing texture to that of Liu but 15° removed from the cube texture. Verbraak investigated the recrystallisation texture of rolled single crystals of copper of various initial orientations (100)[001], $(\bar{1}10)[110]$, $(\bar{1}12)[110]$, $(112)[11\bar{1}]$ and (001)[110]. He found the first three of these orientations gave complicated rolling textures approximating to the polycrystalline rolling texture, which recrystallised to the cube texture. He also noted that the crystal having an orientation $(112)[11\bar{1}]$ either remained intact on rolling or yielded a complementary {112}<111> component in which case the recrystallisation texture was found to be a cube texture. The (001)[110] crystal gave a double {112}<111> rolling texture with a minor (110)[001] component. In all cases where cube texture was present it was accompanied

by its twin orientations. Hibbard et al[15] rolled copper single crystals of various orientations which have been used to describe the texture of polycrystalline copper. They studied the recrystallisation kinetics at temperatures up to 320°C and found that the four orientations, $(358)[52\bar{3}]$, $(110)[\bar{1}12]$, $(112)[11\bar{1}]$ and $(123)[\bar{4}\bar{1}2]$ all of which had been rolled 95%, $(112)[11\bar{1}]$ recrystallised the most rapidly and $(110)[\bar{1}12]$ was the slowest to recrystallise. These authors also noted that the combined recrystallisation components did not approximate to the annealing texture of polycrystalline copper. Heller et al[64] studied the recrystallisation behaviour of {110}<112> aluminium single crystals. After deformation between 50-60% by plane strain these retained their original orientation, whereas a rolled aluminium single crystal showed a considerable orientation spread around the stable position. After annealing of rolled single crystals, oriented nucleation dominated the spontaneous recrystallisation process. Because the inhomogeneities in the deformed matrix had a <111> orientation relationship with the original $(\bar{1}\bar{1}0)[1\bar{1}2]$ orientation, the recrystallised grains also had a <111> orientation relationship with that orientation. The orientation determinations of the grains at the abraded side were essentially the same as those for the plane-strain deformed crystal. Recrystallised grain developed after artificial nucleation from layers with random orientations and appear to have the usual <111> orientation relationship. Lücke et al[65,66] in their work found that the recrystallisation texture of high purity (99.998% pure) aluminium single crystals with

original orientation $(2\bar{1}10)[42\bar{1}]$ and $(123)[41\bar{2}]$ deformed 80% reduction, are determined by 40° ⟨111⟩ orientation relationship.

However, the recent investigations on the microstructure and recrystallisation behaviour of a stable $(110)[\bar{1}12]$ and unstable (100)[011] copper crystal[67] show that after 90% homogeneous rolling reduction the two crystals showed different deformation structures. The recrystallisation textures of the stable orientation are determined by the relationship $(35^{\circ}-40^{\circ})$⟨111⟩ rotations about the poles of the rolling components. Whereas unstable crystal shows one main component and its twins, Figures (8, 9 a,b).

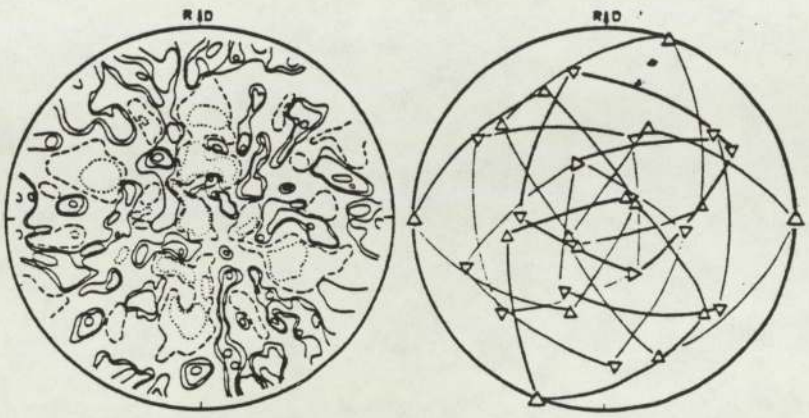

Figure (8) ⟨111⟩ - recrystallisation texture of the 90% rolled (110)[$\bar{1}$12] crystal after 30 min. at 230°C and -40°-⟨111⟩-rotations about all poles of the rolling component

Ref.(67)

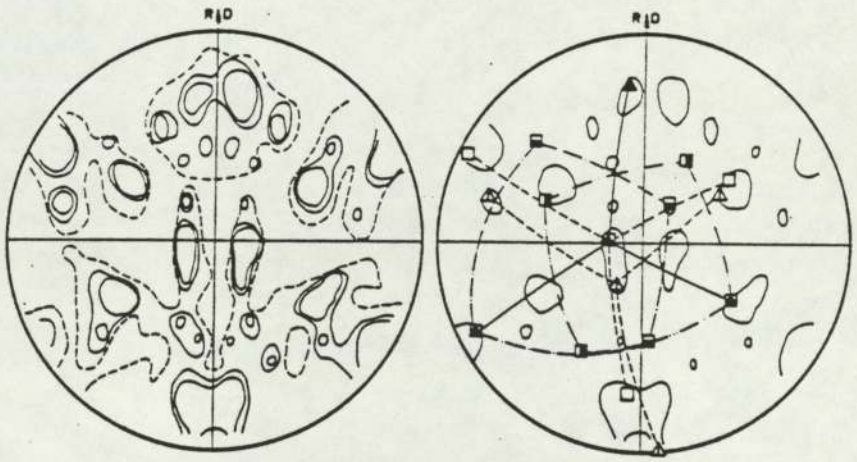

Figure (9) a) ⟨111⟩ - recrystallisation texture of the 90% rolled (100)[011] crystal after 30 min. at 190°C.

b) One variant of recrystallisation components found in (a)

▲ - {11,14,6}⟨14,8,7⟩

Δ {123}⟨14,11,12⟩ Ref.(67)

2.4.2 Recrystallisation Textures of Polycrystalline F.C.C. Metals and Alloys

Extensive work has been done in order to determine the recrystallisation texture of such polycrystalline F.C.C. metals as copper, aluminium and nickel and their various alloys. As in the case of deformation textures, most work relates to copper and its alloys. The particularly sharp cube texture, (100)[001], which is found in deformed pure copper after recrystallisation is of the most scientific interest. Early work by Cook et al[68] showed that for pure polycrystalline copper after prior deformation of up to 50%, the recrystallisation texture is almost random. However after 90% deformation the annealing texture resembles the deformation texture. At higher deformation the texture consists of the cube texture {100}<001> and its twins {122}<212>. In fine grained starting materials at high annealing temperatures the cube texture is found to be more perfect, and the twin density lower. In heavily rolled copper[69] with small grained starting material several cube oriented areas (100)[001] were observed in the rolled structures and these regions have a distinctive microstructure compared with the other oriented regions which makes them easy to identify, and these regions are very important in the subsequent recrystallisation process. After annealing this material developed very strong cube texture with its twin components {212}<122>. In early electron microscopic studies of rolling texture of copper using SAD patterns it was found that no cube-oriented crystallites could

be found after cold rolling. Recently many authors have found cube orientation in copper[36,69,70], in aluminium[71] and in AlMgSi alloys[70] after heavy reduction. The cube oriented areas in copper were detected by their special characteristic microstructures and exhibit a recovered structure. In high SFE metals such as aluminium, the cube oriented areas cannot be detected as easily as in copper (with low SFE), because of the large amount of recovery which occurs in metal or alloys of high SFE. In AlMgSi alloys[70] nucleation in the cube oriented regions does not have a major role, because of the presence of the coarse second phase particles and the nucleation will occur at the particles and oxides[72.73], so that the softening process will be controlled by these nuclei as described in detail in another section (2.7).

For aluminium of 99.99% purity, the recrystallisation texture is essentially the same as that for copper, although it is more difficult to produce 100% cube texture. It has been suggested that the effect of alloying on recrystallisation is related to the effect on the deformation texture. However Lui et al[31] found that the amount of solute necessary to completely suppress cube texture development is considerably less than the amount required to cause transition to the "alloy type" rolling texture. Beck et al found that when α-brass[74] and silver[75] are cold rolled to 96% reduction the annealing texture is described by the indices $(225)[73\bar{4}]$ or near $(113)[21\bar{1}]$.

In Copper-Zn alloys[76], the (225)[$73\bar{4}$] component originates as (214)[$52\bar{3}$], in a 3% Zn alloy. Increasing the zinc content to 6% causes a texture rotation to approximately (438)[$63\bar{4}$]. Similar texture transition occurs by alloying copper with aluminium[78], tin and germanium[30] show annealing texture transitions essentially similar to the copper-zinc alloys. Increasing the alloy content in each case caused the volume fraction of the cube texture component to decrease, and other recrystallisation texture components become important.

Merlini et al[79] have reported that cross-rolled copper does not recrystallise in the cube orientation. The copper rolled alternately in two perpendicular directions, gave a deformation texture {110}⟨223⟩. This was found to recrystallise to {519}⟨$4\bar{1}1$⟩. The eight equivalent components of this orientation are all related to the deformation texture component, by 30° rotations about ⟨111⟩ poles near the centre of the {111} pole figure.

The data in aluminium annealing textures are rather more complex than for copper. In aluminium however the behaviour depends upon purity, prior to heat treatment and deformation history. Deformation of 90% or more produces, after annealing, a cube texture coexisting with a "retained rolling texture"[42,74] Figure (10 a). For deformation of 50 to 90%, the annealing texture is the same as that for copper, and is entirely composed of the retained rolling texture components. The interest in commercial aluminium and its

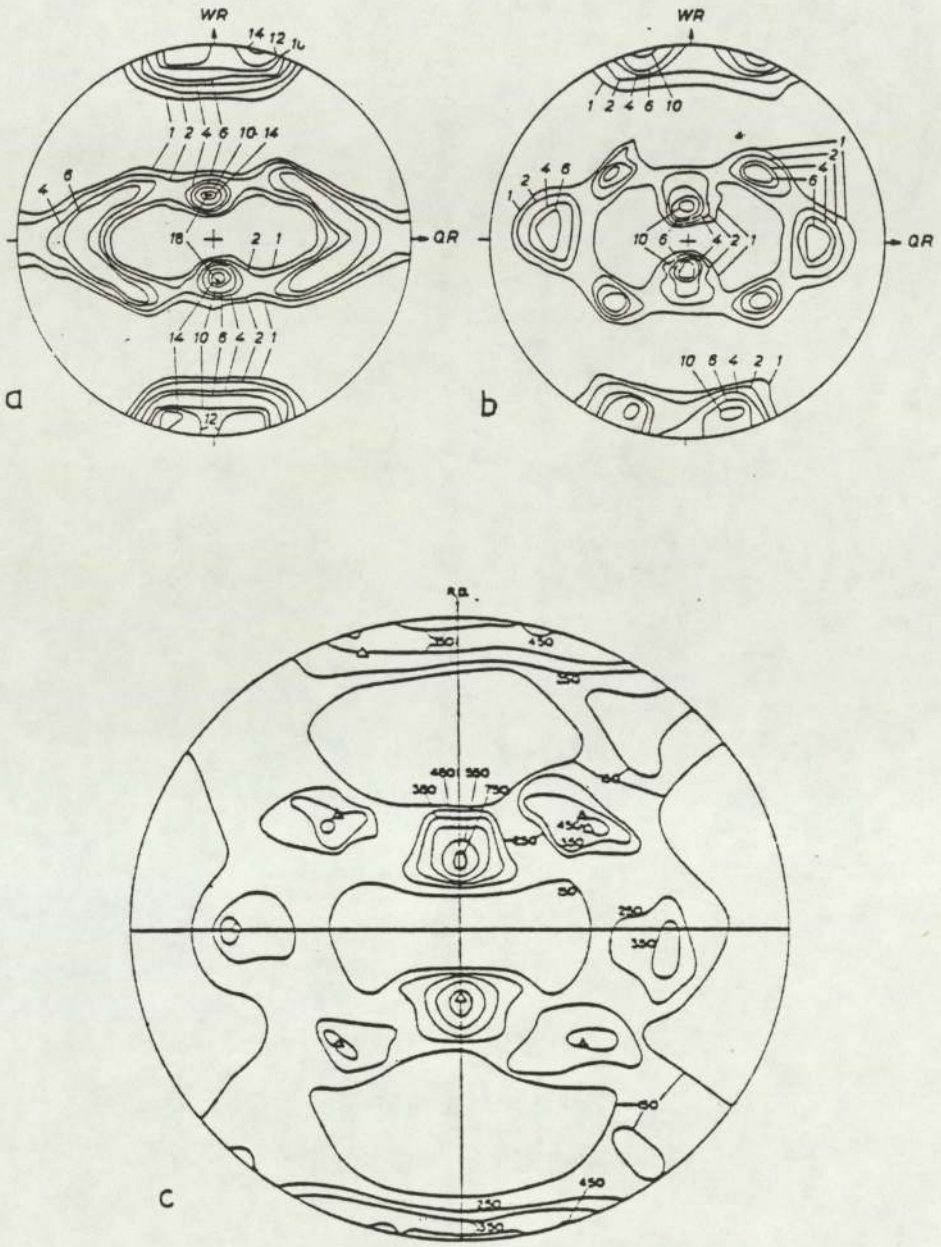

Figure (10) - (111) pole figures for annealing texture in commercial pure aluminium

a - Mixed texture consisting of rolling and cube texture (0.15Wt%Fe, 0.34Wt%Si). Continuous casting, hot rolled starting at 520°C to 8 mm, cold rolled to 0.5 mm, annealed 3 hrs. at 400°C.

b - Rolling texture (0.54Wt%Fe, 0.035Wt%Si). Pretreated as in (a) annealed 40 hrs. at 250°C.

c - Rolled 96% and annealed for 5 minutes at 300°C.
△ (7,12,22)[845] near (123)[1$\bar{2}$1]
⏃ (100)[001] orientation Ref.(27)

alloys lies in the relative proportions of the "cube" texture and the "S-texture"[80]. Figure (10 b) shows an example of rolling texture retained by means of recovery[81]. This component is similar to the main rolling texture component for aluminium called the "R-texture"[80]. The annealing texture for commercial aluminium rolled to 95% reduction and annealed for 5 minutes at 300°C is shown in Figure (10 c). The amount of the cube component in the annealing texture of pure aluminium can be increased by prolonged annealing or by raising the annealing temperature[42,82] when the cube component grows at the expense of the "S-texture".

Very extensive studies have been made regarding the effect of silicon and iron in commercial aluminium on its rolling and recrystallisation textures. Smallman[29] observed that silicon contents below the limit of solubility do not affect the rolling texture of aluminium. Blade[83] demonstrated that in his binary Al-Si alloys silicon is not effective in restricting grain growth and preventing the formation of cube texture during annealing. In contrast to silicon, iron has been found to have a significant effect on textures in commercial aluminium, but two opposing views have been advanced for the role which it plays. One is that iron in solution has a significant effect on texture development, while the other theory is that second phase particles restrict grain growth and so affect the final annealing texture. Bunk et al[84] studied the annealing texture of aluminium of various purities with Si:Fe ratios of 2:1, 1:1 and 1:2 and found that the

high silicon:iron ratio favoured the formation of cube texture. This was attributed to the smaller amount of iron in solution in the high Si:Fe material, and consequent development of a "pure metal" rolling texture from which the cube texture was produced on annealing. Blade[83] and Haessner et al[85] on the other hand, hold the view that it is iron in the form of precipitated particles rather than iron in solid solution which affects the annealing texture of commercial aluminium.

2.5 Theories of Recrystallisation Texture

Recrystallisation textures have been the subject of considerable controversy, with opinions split between those researchers who explain results on the basis of the preferred nucleation of certain recrystallised grains (oriented-nucleation), and those who consider orientation dependent growth as more important (oriented-growth). These two ideas form the basis of two theories that have been put forward to explain the development of primary recrystallisation texture. In the oriented-nucleation theory the nucleation process is supposed to be of primary importance in determining the range of available nuclei which can contribute to the recrystallisation temperature. In the oriented-growth theory on the other hand, the recrystallisation texture is considered to result from growth selection due to the orientation dependence of the rate of grain boundary migration.

Following the concept that recrystallisation textures

are determined by the orientation of the available nuclei, Burgers et al[23] tried to relate the nucleus orientations in turn to a model of the structure of the compressed aluminium single-crystal specimens. They assumed that on annealing deformed crystal the nuclei of the recrystallised grains developed from the most heavily deformed fragments which were located in the vicinity of active glide planes. Burgers considered that these fragments of highly deformed elements were rotated with respect to the main body of the crystal around <112> axes parallel to the active slip planes and normal to the active slip direction in each slip plane.

Barrett[86] made orientation determinations on 50 recrystallised grains in a compressed aluminium single crystal and found the orientation to correspond to approximately 45° rotation around <111> axes with respect to the orientation of the deformed crystal. The <111> rotational relationship in primary recrystallisation of aluminium has been confirmed by other workers[87]. Liu et al[14], in rolled single crystal copper of the (110)[1$\bar{1}$2] orientation, found, after annealing,the results seem to contradict Burger's theory of oriented nucleation. Beck et al[19,26] argue that Burger's theory should have predicted the same kind of rotations for both heavily rolled and lightly deformed single crystals, with less scatter in the latter case, because of the better deformation of slip planes and slip directions in crystals highly deformed in tension. Beck[88] has observed that the application of an oriented-nucleation mechanism to poly-

crystalline metals must encounter certain difficulties. Such a mechanism depends on a definite orientation relationship between the nuclei and matrix region immediately surrounding it, the range of nucleus orientations is bound to be at least as large as that of the matrix orientations. Thus, on the basis of the oriented-nucleation theory, a complex deformation texture, such as that of rolled polycrystalline copper, should, on annealing, yield an extraordinarily large number of nucleus orientations and consequently an extremely complicated recrystallisation texture. Furthermore, Lücke et al[51] studied the growth rate in commercial purity aluminium deformed by tension, and found a very pronounced orientation dependence of the growth rate with a maximum at 40^{o} rotation around <111> axes. They also found a corresponding growth selectivity among the recrystallised grains nucleated randomly by severe local deformation at one end of their long cylindrical single crystal specimen deformed 15% by tension. Dillamore et al[89] considered the orientation change during the deformation of polycrystalline material, and concluded that the recrystallisation textures are solely determined by the orientation of nuclei. Using the model relevant to the deformation texture they also explained the origin of annealing texture. The explanation may be as follows[121]:-

Since the orientation coordinate flow along the convergent surfaces is very slow, there will be many of these orientations lying on convergent surfaces when the deformation ceases. If recrystallisation nuclei develop from

grains with these orientations they will have an orientation fairly close to the stable rolling textures. Orientation near the divergent surfaces will be present in nuclei generated on the transition bands. The model by Dillamore et al shows that the nuclei due to nucleation within the grains and at grain boundaries are responsible for the retained rolling texture, and that the cube texture component can be generated in the transition bands. Dillamore et al[90] have determined the conditions under which lattice curvatures (in particular transition bands) would provide nuclei for recrystallisation. Nucleation was found to be favoured by thin long subgrains with low level misorientations across successive subgrains. The possibility of grain boundary nucleation as the origin of the characteristic alloy texture,the {113}<211> has also been suggested.

Liu[14] suggested that the mechanism leading to the formation of the cube texture was kinetically favoured so that it dominated the recrystallisation texture. But later work by Hibbard et al showed that the rotation leading to the cube texture does not have the maximum recrystallisation rate and in fact the (112)[$\bar{1}\bar{1}$1] orientation has the highest recrystallisation rate although it does not lead to a cube oriented product[15].

In order to overcome the objection in the preceding paragraph several authors[91] proposed that the nucleation orientation is dependent on the principal flow directions in the deformation process rather than

the deformation texture. The mechanism assumes that small local regions of cube orientation exist and that these regions recover fastest without an orientation change and serve as recrystallisation nuclei. In support of this, Burgers et al showed that cube oriented crystals polygonise faster on annealing than do similarly deformed crystals of other orientations for aluminium, but this was later shown to be untrue for copper. In any case this mechanism could lead to the cube texture, irrespective of the deformation texture, whereas cross-rolled copper, with about twice as many cube oriented nuclei as the normally rolled material gives a very weak cube component in its recrystallisation texture[79].

Another mechanism was suggested by Burgers et al[92] based on the "reverse Rowland transformation", i.e. two (112)[$\bar{1}$11] orientations shearing on annealing to give a (100)[001] orientation. Although the necessary starting orientations are present in heavily rolled copper, this mechanism is unlikely because of the low or non-existent driving energy and the high activation energy[93]. In any case Verbraak[92] admitted this could not happen in aluminium because of the high stacking fault energy.

The theory of oriented growth first suggested by Barrett[86] relies on the orientation dependence of grain boundary mobility being responsible for the <111> rotational orientation relationship between the recrystallised grains and the deformed aluminium crystal matrix, in which they grew on annealing. Beck et al[94]

used localised inhomogeneous deformation in a deformed matrix to provide random nuclei. They used 99.97% aluminium rolled 12% and then scratched and annealed at 350°C for one hour and found that the fastest growing grains were still those with a 40° <111> rotation.

Recently, detailed electron microscopy studies in heavily deformed copper and aluminium[36,95,96] have supported the view of Decker et al[97]. Hutchinson[98] has derived the recrystallisation orientations from all orientations of the copper type rolling texture (ODF) by 35° rotations clockwise and counter-clockwise about the four <111> poles of each orientation of the deformed matrix and found that the cube texture was not predicted and the closest it came to one of the predicted orientations was 15°. In F.C.C. metals the boundary with the greatest mobility is that produced by a 30° to 50° rotation about the <111> axes. Bunk[99] has indicated that the initial nucleation is not entirely random by pointing out that this theory does not explain why rotations about a full set of recrystallographically equivalent <111> axes are rarely found experimentally, instead of a rotation about a particular [111] axis.

Criticism of the "oriented-growth" theory is made on the basis that the growth relationship is not sharp enough to account for the well defined recrystallisation textures which are obtained. By considering the restrictions on the growth of nucleus texture, Dillamore[78] has shown that the sharpness of the recrystallisation texture can be due

to the conflicting conditions which would occur when nuclei grew into a multi-component matrix. He considered the most probable sites for nucleation to be grain boundaries and deformation bands. The major components of the annealing texture were considered to arise from nuclei which are capable of growth:-

a) into the orientations on either side of the boundary;
b) through the spread of these orientations;
c) into the remaining two of the four symmetrical components of the deformation texture.

The annealing texture orientations resulting from a $\{110\}\langle 112\rangle$ deformation texture are predicted as $(4,9,17)[3,8,5]$, $(4,9,0)[001]$ and $(112)[\bar{1}10]$. However the predominant component in the annealing texture, resulting from a deformation texture of $\{110\}\langle 112\rangle + \{112\}\langle 111\rangle$, is predicted to be that of the $\{100\}\langle 001\rangle$ cube orientation.

2.6 Recrystallisation of Two-Phase Alloys

Many commercial alloys such as steel, aluminium and copper alloys are phase mixtures rather than homogeneous solid solutions. Their recrystallisation behaviour depends on whether second phase particles are precipitated during recrystallisation or before plastic deformation, and on the nature, volume fraction and dispersion of the second phase. A dispersed second phase may exert opposing influences on the progress of recrystallisation of a deformed alloy:

1 - Nucleation of new grains may be accelerated especially if the second phase particles are comparatively large. If they are very small, nucleation is retarded or prevented altogether.

2 - Growth of new grains is always impeded, because of the drag exerted on a migrating grain boundary by dispersed particles, especially if these are small and numerous.

It is well established that dispersed, hard incoherent particles can either retard or accelerate recrystallisation of a metallic matrix. Köster[100] quotes a number of examples of this. When dispersed particles are quite coarse (several microns across) it appears that they generate a local concentration of the lattice distortion caused by the applied deformation, which in turn enhances the nucleation rate in the matrix close to the inclusion. Leslie et al[101] showed that coarse oxide inclusion in an iron-oxygen alloy enhanced nucleation. Also[102] similarly observed that precipitates of $FeAl_3$ particles of about 1 μm diameter in aluminium-iron alloys accelerated nucleation more than it retarded growth of new grains, so that recrystallisation as a whole was accelerated. Work was carried out by Doherty et al[103,104] on a dispersion of $CuAl_2$ in aluminium-copper alloys both in polycrystalline and single crystal form. They found that the θ-phase could either accelerate or retard recrystallisation, and they indicated that the nucleation rate was critically sensitive to particle spacing and that when the particle

spacing became small nucleation was very difficult, the situation is summarised in Figure (11 a,b). The inter-particle spacing was much more important than the particle size. Hard second phases will tend to increase the stored energy of deformed material through their effect of prompting dislocation multiplication during cold work. Retardation of recrystallisation can rise through two effects. Firstly, the second-phase particles may cause an inherently stable dislocation structure. Secondly, the particles may hinder dislocation (and network) rearrangement, thus hindering the formation of grain boundaries and their migration. Finely dispersed small particles have the effect of homogenizing the distribution of slip, so that the deformation structure contains no regions of severe plastic curvature and is thus inherently more resistant to recrystallisation. Rollason et al[105] took a crystal of Cu-3 Wt% Co which had been aged to generate a dispersion of incoherent Co particles, and deformed it into stage II (the structure in this stage is less inhomogeneous in two-phase crystals, and lattice misorientations were lower) of the stress-strain curve. It was then annealed for 98 hours at 950°C at which temperature all the cobalt particles would dissolve within a few seconds, yet it was seen that no recrystallisation occurred. It is unlikely that this effect would be important in polycrystalline materials, however, due to the complex nature of the slip occurring. This would lead to non laminar slip and thus to high inhomogeneities of deformation. Therefore, any high resistance to recrystallisation in polycrystalline materials must arise

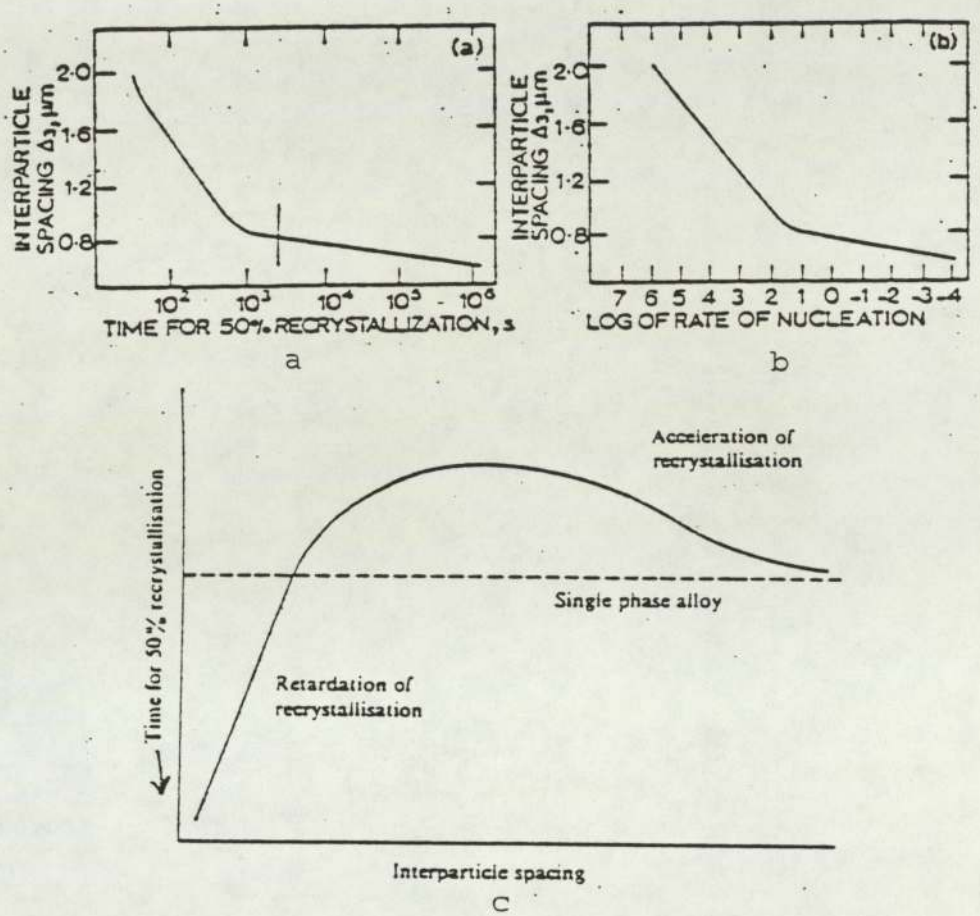

Figure (11) a - Variation of inter particle spacing with time for 50% recrystallisation in Al-$CuAl_2$ alloys. The time for the single-phase alloys is shown by the vertical line

b - Variation of the apparent rate of nucleation of recrystallisation with inter particle spacing in Al-$CuAl_2$ alloys. Ref.(103)

c - schematic diagram of the influence of dispersed particles on recrystallisation Ref.(108)

primarily from particle pinning effects.

Widely spaced particles caused an acceleration of recrystallisation as a result of increased work hardening in the two-phase alloy. If, during the growth of subgrains, the boundaries are pinned by particles before a mobile high angle boundary can be generated, the probability of any particular grain gaining a significant size advantage over its neighbours is minimised. In this case further subgrain growth is dependent on the coarsening of second phase particles. It can be seen that a fine particle dispersion will have a considerable retarding effect on nucleation. In fact a fine dispersion of second phase particles was found to suppress recrystallisation to a rate much slower than that appropriate to the residual solid solution level. Rollason et al[106] also examined the influence of particle size on deformation structure and recrystallisation behaviour. They showed that misoriented subgrains associated with the dispersed phase form on annealing only if the dislocation interactions during straining lead to the development of local lattice curvature in the matrix in these regions. In Humphreys' et al[107] observations on copper-zinc, two types of dislocation-particle interactions are found, depending on the size of the particles and the applied plastic strain. At large strains and/or particle sizes, dislocations form as secondary glide loops which involve a local lattice curvature adjacent to each particle; when the dispersed particle size and/or strain is small, only primary prismatic dislocations exist, which do not involve local

curvature of the matrix lattice, and in this case no recrystallisation embryos are observed after annealing. Figure (11 c) (due to Köster)[108] summarises the influence of inter-particle spacing on the recrystallisation kinetics of two-phase alloys.

Coarse dispersion (i.e. large particles, widely spaced) have the effect of accelerating recrystallisation because of the increased dislocation density and the presence of local lattice curvature. Mould et al[109], in experiments on two-phase aluminium-iron alloys, found that the recrystallisation rate increased as the iron content increased for a given inter-particle spacing. This was due to an enhanced nucleation rate as the iron content rose, while the growth rate stayed approximately the same. They also found that decreasing the grain size increased the recrystallisation rate due to increased nucleation at grain boundaries and at particle/matrix interfaces.

Gawn et al[110] have carried out careful quantitative metallographic analysis in an iron-carbon alloy, carbide particles act as nucleation sites for recrystallisation. They also showed that a critical particle size is necessary for this effect. The first systematic approach to particle stimulated nucleation was presented in a work by Humphreys[111] which studied the condition under which dispersed particles can provide nuclei for recrystallisation of deformed aluminium, Figure (12) summarises Humphreys' results. Single crystals of aluminium containing

Figure (12)

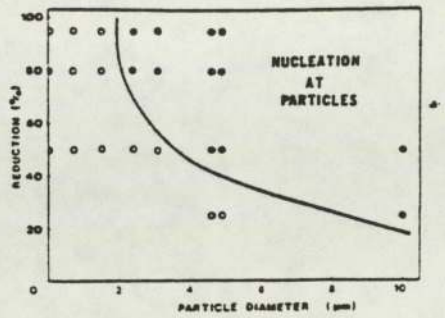

Figure (13)

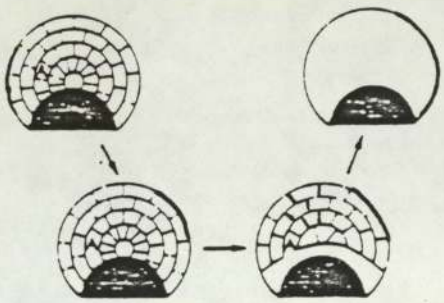

Figure (14)

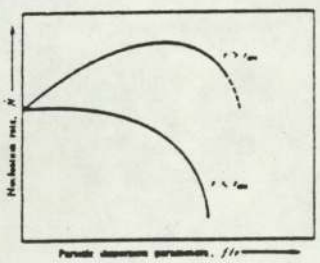

Figure (12) The conditions of deformation and particle size for which nucleation is observed to occur at particles. Closed circles indicate observations of nucleation at particles. Ref.(111)

Figure (13) The annealing behaviour of a deformation zone adjacent to a particle Ref.(111)

Figure (14) The variation of nucleation rate of recrystallisation with f/r according to the model of Nes (1976) Ref.(115)

0.45 Wt% Cu and varying amounts of silicon were chosen and various cold-rolling reductions were applied to the crystals and annealed at 300°C (at which temperature the dispersed phase was stable). He observed nucleation at pre-existing subgrains within the deformation zone at the particle/matrix interface. Nucleation occurred by a rapid sub-boundary migration until the deformation zone was consumed. At this stage the nucleus may or may not grow, depending on its size and orientation. His observations lend support for the local lattice curvature around them. Figure (13) indicates diagramatically the observed annealing behaviour within the deformation zone adjacent to a particle; a nucleus A in the deformation zone grows at an early stage towards and around the particle. After the deformation zone has been consumed, the driving force for recrystallisation arises from the matrix dislocation density.

Rollason et al relating to Humphreys' data[105] concluded that for optimum recrystallisation resistance SiO_2+Cu and $CuAl_2$ the dispersed particles should have a diameter smaller than 0.3μm in order to suppress the development of local lattice curvature during deformation. Nes et al[112] studied the recrystallisation behaviour of two different aluminium alloys, aluminium-zinc-magnesium and aluminium-manganese. In the case of the former, the precipitate particles were present prior to recrystallisation, in the latter the two processes took place simultaneously. The recrystallisation behaviour of aluminium-zinc-magnesium was observed and the following found:-

After 20% cold deformation and at (400-500°C) nucleation of new grains took place at particles on grain boundaries and these spread at high temperature till the material was completely recrystallised at 550°C. Additional intragranular nucleation was also observed at high temperatures by subgrain coalescence and nucleation at Al_3Zn particles. As a result, the microstructure was fine grained. This behaviour was termed "static" interaction. The aluminium-manganese exhibited a "dynamic" interaction where recrystallisation of 85% cold rolled material yielded a small number of nuclei and the final microstructure consisted of large grains, approximately equiaxed.

Nes[113] studied the recrystallisation behaviour of an aluminium-manganese alloy containing a duplex particle structure consisting of a coarse distribution of large cast inclusions and a finer dispersion of smaller particles due to precipitation prior to recrystallisation. He assumed that nucleation of new grains occurs very rapidly at the large inclusions which is termed a "site-saturated" process, i.e. that the final grain size is determined by the number of nucleation events. Nes derived an expression relating the grain nucleation rate to the particle dispersion and the subgrain size distribution prior to recrystallisation. This was shown to account for the experimentally determined relationship between the recrystallised grain size and particle dispersion. This expression assumes also that the heterogeneous form of new grains required sub-boundary migration to form a viable nucleus. The expression is:-

$$N = N_o \left[1 - \lambda \left(\frac{\bar{\rho}^2}{\sigma\sqrt{2}\left[\frac{4r}{3f\alpha} - \bar{\rho}\right]} \right) \right]$$

WHERE:

N	Number of nucleation events
N_o	Number of nucleation events in the absence particles.
σ	standard deviation in the Subgrain size distribution
$\bar{\rho}$	Average subgrain size
f	Volume fraction of fine particles dispersion
α	A constant of order unity.

Scharf et al[115] investigation of the recrystallisation behaviour of in an Al-Mg-Si alloy has quantitatively determined the variation in nucleation rate with the particle dispersion level, $\frac{f}{r}$. The effect of varying the dispersion levels on the nucleation rates for the situations when r is greater or less than r_{crit} (r_{crit} being the critical size above which the particle may act as a nucleation site). Figure (14) summarises the effects of dispersed particles upon the kinetics of recrystallisation.

In direct in-situ study using high voltage electron microscopy (HVEM) it was found that during annealing the recrystallisation formed at a pre-existing subgrain within the deformation zone and the nucleation occurs by rapid sub-boundary migration[116-118] which is similar to the results found by Herbst et al[73].

The work by Herbst et al[73] and Humphreys[111,119] shows that the cold working generated large misorientation in

the deformation zones up to 30^{o} for rolling reduction range between 65% to 90%. Thus a particle stimulated nucleation site depends on particle size and amount of cold deformation, i.e. the amount of misorientation increase with the size of the particle and the applied strain. Humphreys[119] found the deformation zone extends to about the particle diameter.

2.6.1 Retardation of Boundaries by Fine Dispersed Phase

Zener[120] was the first to point out that the ability of a given volume fraction of dispersed phase to slow a grain boundary migrating under a fixed driving force is a function of the fineness of dispersion, and that this in turn limits the grain size attainable in grain growth (when the driving force continuously diminishes as growth continues). When a migrating boundary of specific surface energy σ_B intersects a spherical inclusion of radius r, the retarding force per unit area of grain boundary (F_r) is given by:

$$F_r = \frac{3 f \sigma_B}{2 r}$$

where: f - volume fraction of the particles.

The growth of new grains will thus be retarded by a factor of the form $\frac{f}{r}$, since this growth involves migration of higher angle boundaries. Clearly the drag will be much higher for a fine dispersion than a coarse one of the same volume fraction. This expression is not relevant to solute

atoms, because foreign atoms are not sessile in the lattice (as second phase particles are) but can move through the lattice by diffusion. Also a grain boundary can be overcome, or even very small particles, with the aid of thermal activation.

2.6.2 Precipitation During Recrystallisation

When recrystallisation and precipitation occur in a similar time span the processes exert a mutual influence[108]. Thus precipitate particles hinder the formation and migration of the "recrystallisation front" while the lattice defects themselves promote the nucleation of precipitates. The time for recrystallisation, t_r, assuming a constant nucleus size, is given by equation[100]

$$t_r = A \exp\left(\frac{Q_r(N)}{KT}\right)$$

Where A is a factor containing the driving force for the reaction, entropy, geometry, and Q_r is the activation energy for the formation of recrystallisation front. It decreases somewhat with increasing dislocation density N, and the incubation time for precipitation t_p, is given by:

$$t_p = B \exp\left(\frac{Q_n(C.T)+Q_D}{KT}\right)$$

Where $Q_n(C.T)$ is the activation energy for nucleation of the second phase, and Q_D - is the activation energy for diffusion, and B - is constant (similar to A).

When $\frac{1}{T}$ is plotted against Ln t such a graph is shown in

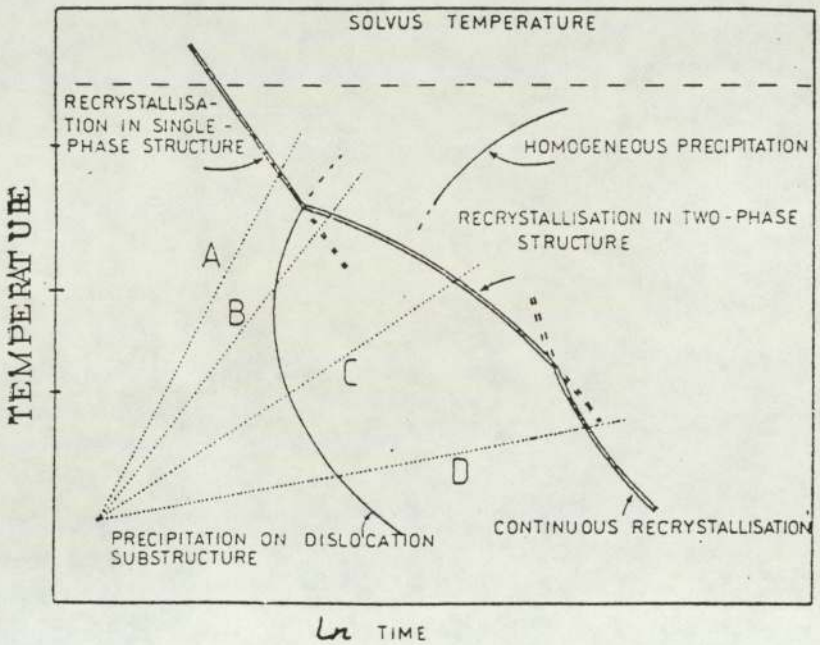

Figure (15) Schematic Time-Temperature-Transformation diagrams for recrystallisation and precipitation in a supersaturated solid solution. Different heating rates are indicated by the dotted lines A, B, C and D of different slopes.

Ref.(121)

Figure (15). There are three temperature ranges in the recrystallisation behaviour that can be distinguished:-

1 $T > T_1$ Normal recrystallisation will proceed, and there is no effect of particles at this stage. The transformation may be regarded as the recrystallisation of solid solution.

2 $T_1 > T > T_2$ Normal recrystallisation occurs, but precipitation will take place in the complete recrystallisation structure. So the only effect that the second phase has is that of the solid solution. If precipitation does occur after recrystallisation is complete it will greatly inhibit grain growth because the grain boundaries are pinned by the precipitate particles.

3 $T < T_2$ Just below T_2 a fine scale precipitation occurs before recrystallisation[121], with particles forming preferentially on the deformation substructure. Nucleation of recrystallisation is greatly retarded, because of sub-boundary pinning and as a result the final grain size is increased.

At lower temperatures the volume fraction of second phase increases and particle coarsening has to take place before unpinning of nuclei can occur. Growth of recrystallised grains is impeded and so more nuclei become involved as each growing nucleus becomes pinned. The final grain size is small as a result. At the lowest temperature it is possible sometimes for complete recovery of the deformation substructure to occur by polygonisation and growth of

subgrain as the second phase particles coarsen. This process has been termed continuous recrystallisation[100]. Precipitation following primary recrystallisation influences the grain growth.

2.7 Influence of Second Phase on Rolling and Recrystallisation Textures

In recent years many assessments have been made of the textures produced in metals and alloys having a F.C.C. structure. However, little work has been published on the subject of second phase particles and their effect on resulting textures in these structures.

The relative proportions of cube texture and retained rolling texture in aluminium are dependent upon processing and variations in purity. Most workers are agreed about the effect of impurities found in commercial aluminium, although iron is claimed to be the most effective impurity causing variations on the annealing textures. Increasing the iron content decreases the strength of the cube texture[98] especially when in solid solution, precipitation of Al_3Fe may occur.

Blade[122] has found that the very favoured nucleation of cube grains in pure aluminium is suppressed considerably by additions of iron and silicon. This[98] may be due to suppression of transition band nucleation or grain boundary precipitation inhibiting the growth of nuclei formed before precipitation; as a result a small grain size is expected and is, in fact, observed. Bunk et al[84] suggested that

iron restricts recrystallisation to a cube texture by its effect on the rolling texture, and they also mentioned the importance of silicon in this respect. Supersaturation of iron favours the formation of an "S-texture" while the precipitation of the iron as an intermetallic compound prior to the final rolling sequence, favours the cube texture. Iron may be precipitated[20] by slow cooling after casting or a low hot rolling temperature, and low temperature intermediate annealing.

Gokyu et al[123] observed that recrystallisation texture in aluminium-copper alloys was dependent upon the solution treatment prior to cold rolling, but that the cold rolling textures remain unaffected. Specimens which had not been solution treated, recrystallised to {100}<001> and {113}<332>, whereas solution treated specimen recrystallised to {110}<001> and {110}<110>. These textural differences were attributed to precipitate distribution during primary recrystallisation, and the suppression of random nucleation around precipitate particles.Goodman et al[124] have shown that in an 18.6% chromium 9.5% nickel stainless steel,the cube texture produced on annealing could be influenced by the precipitation of carbide particles. It was concluded from their results that finely dispersed carbides impeded the growth of the cube oriented grains.

Clark et al[125] examined pure nickel containing small quantities of cobalt and chromium. They showed that for a given amount of cold deformation, a more pronounced

rolling texture, around the (123)[41$\bar{2}$] orientation, is produced in a dispersion hardened nickel than in high purity nickel. The annealing texture of dispersion hardened nickel is cube, with pronounced twin components. Dillamore et al[20] however, have argued that the reductions used were rather low and the annealing textures were either random or retained rolling texture type. Hatherly et al[126] have also considered the effect of second-phase on texture development. If the texture is to be altered, the distribution of second-phase particles must either be present before cold rolling begins or be precipitated during annealing. In the former case the distribution might be expected to perturb the predicted rotations and in the latter case the sequence of annealing processes may be affected. It is well established that in aluminium commercial purity where nucleation is expected to be associated with large AlFeSi-primaries; recrystallisation may result in strong textures[127]. Humphreys[128] has proposed that particles larger than about 1μm present during cold rolling will tend to produce random annealing textures. Herbst et al[73] studied the development of the recrystallisation texture in an Al-Mg-Si alloy containing large, undeformable particles. They found that after annealing for 30 minutes at 350^{o}C the recrystallisation texture was random. Even after a long time of annealing the random recrystallisation texture remains

In a recent work by Grewen et al[72] and Noda[70] on AlMgSi it was found that the presence of a coarse second phase particle influences recrystallisation texture.

These particles reduced cube texture in AlMgSi because the process of softening was controlled by nucleation at coarse particles and at oxides. Nuclei orientations were random and this tended to randomise the recrystallisation texture. From this point it is clear why a sharp cube texture can be developed only in aluminium of high purity without particles before rolling. These results agree well with the oriented nucleation theory and not with oriented growth. Herbst et al[73] have studied the development of preferred orientation from nuclei originated from the deformation zones around large particles in an AlMgSi alloy. They found that no preferred orientation could be detected and there was a weak texture after full recrystallisation. The effect of the presence of both small and large particles on texture developments has been observed in a commercial Al-Mn alloy[129,130]. It was found that the orientation of the nuclei were scattered around the cube orientation, and the fraction of the cube oriented grains increased with increasing grain size in the final product, in agreement with oriented nucleation theory.

Hornbogen et al[131] have summarised the effect that second phase particles have on recrystallisation and therefore on the resulting annealing textures. Particles, which are present before deformation, and possess incoherent interfaces, can accelerate the formation of recrystallisation nuclei. On the other hand, the precipitation of particles prior to recrystallisation hinders the rearrangement of dislocations and retards the formation of recrystallisation nuclei. The presence of second phase

particles may therefore influence primary recrystallisation texture in the following ways:-

1 - A precipitate which can cause recrystallisation in situ (continuous recrystallisation)(in cases of high particle drag) does not markedly change the texture from that of the deformation texture.

2 - Coarse dispersion of incoherent particles in a matrix lattice with strong anisotropy of grain boundary velocity, lead to optimal conditions for growth activity and therefore to strong, well developed recrystallisation textures.

3 - Both precipitation at the recrystallisation front or discontinuous precipitation lead to great isotropy of boundary velocity and therefore to the disappearance of rolling textures during recrystallisation.

2.8 Shear Band Formation

It was observed many years ago, that in heavily deformed metals shear band formation is often a common feature. Adcock[132], however, who first reported shear bands in heavily rolled copper nickel alloys in 1922, showed also that these inhomogeneities of deformation were preferred sites for nucleation during subsequent annealing. Grewen et al[133] and Hatherly[134] have independently recognised different forms of "shear" banding, in heavily rolled metals. Grewen et al[133] have observed macroscopic shear bands in copper and copper-0.6 Cr alloy deformed

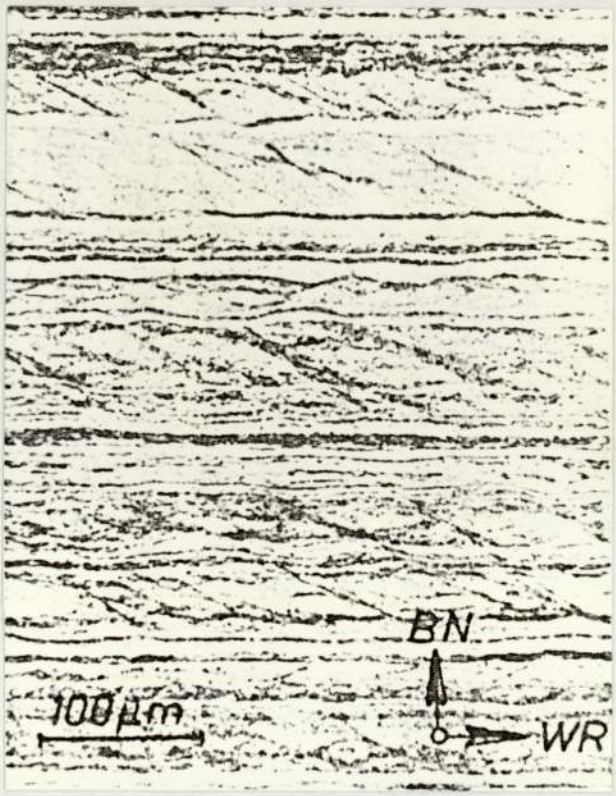

Figure (16) - Shear bands in rolled copper-0.6 Wt% Cr alloy rolled 95%,

BN = ND, WR = RD

Ref.(133)

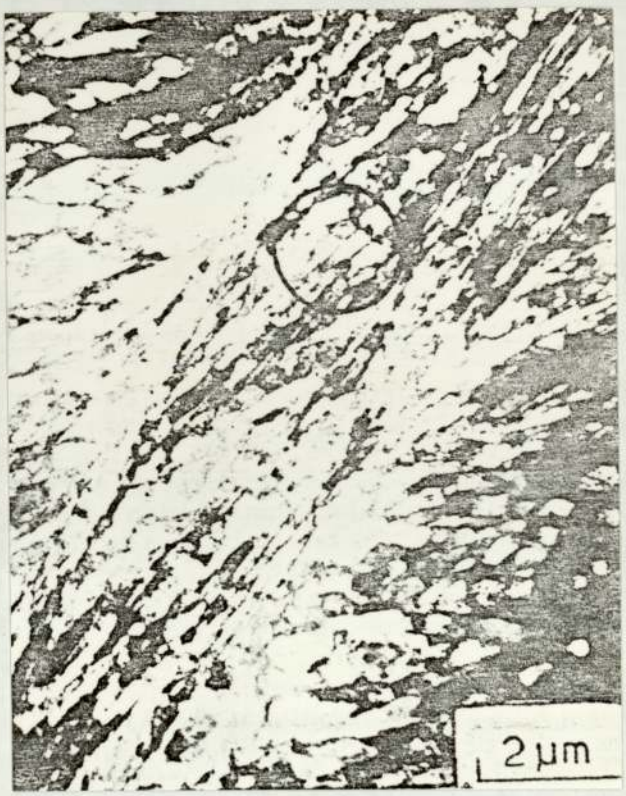

Figure (17) - TEM micrograph in copper-0.6 Wt% Cr alloy rolled 95%.

Transverse section showing the elongated subgrains of the shear band.

Ref.(133)

by rolling to a strain of about ε=3. They were described as coarse bands and about 2μm wide, making an angle 20^{o}-35^{o} to the rolling direction, parallel to the transverse direction, Figure (16,17), and these consist of elongated cells parallel to the shear band. Diffraction pattern analysis showed that the shear bands are not associated with a particular crystallographic plane like microbands, but the shear bands are extensive inhomogeneous deformation producing local shear texture {111}<112>, {001}<110> and {112}<011>. Extensive electron microscope studies have shown that shear bands contribute significantly to the process of deformation in low SFE metals and alloys[134,135]. Shear bands also occur, but less extensively in high SFE metals[133]. Geometrically similar shear bands have been reported in several high SFE (untwinned) materials, e.g. aluminium[136]. The material within the shear bands appears to be sharply misoriented with respect to the surrounding matrix[133,137]. It has been determined that shear bands containing fine crystallites can suffer large shears. In the case of high SFE materials the origin of the shear band lies in the ability of the material to undergo work softening and the shear band morphology differs from the low SFE materials. In each case the shear bands develop as sheet like features that are 35^{o} to the rolling plane and parallel to the transverse direction and not on the plane of maximum shear stress (45^{o} to the rolling direction). In a recent report Houtte et al[138] have shown that inhomogeneous deformation by shear band formation needs less work than homogeneous plane strain deformation in

some strongly textured metals. They suggest that shear bands are poorly defined in high SFE metals which is not supported by other work.

Shear bands are a common feature of the microstructure of rolled aluminium, particularly those containing magnesium. Brown[137] has shown in heavily rolled aluminium and aluminium-0.8% Mg alloy that after 80% reduction, occasional shear bands start to propagate from one grain to another producing displacement of grain boundaries about (1~5μm). Only one set of bands was present making an angle of about 35^{o} or about 110^{o}. However, the TEM observations of shear bands in medium-high SFE metals are very few in the literature, and most of the observations, which have been reported, show the same feature. Probably this is partly due to the difficulty of obtaining a thin foil containing shear bands because either the shear bands tend to polish faster than the other deformation microstructures, or the frequency of the shear bands is not high enough. It seems that shear bands are much easier to observe by optical metallography.

The sheet-like bands always form with a specific orientation relationship to the specimen geometry. This relationship was found by measuring the inclination of the shear bands to the rolling plane trace in both RD and TD sections. Wakefield et al[34] detected that shear bands in rolled Cu-6.4 Wt% Al alloy in longitudingal sections appear after about 60% reduction; they are inclined about 35^{o} to the rolling direction, and parallel

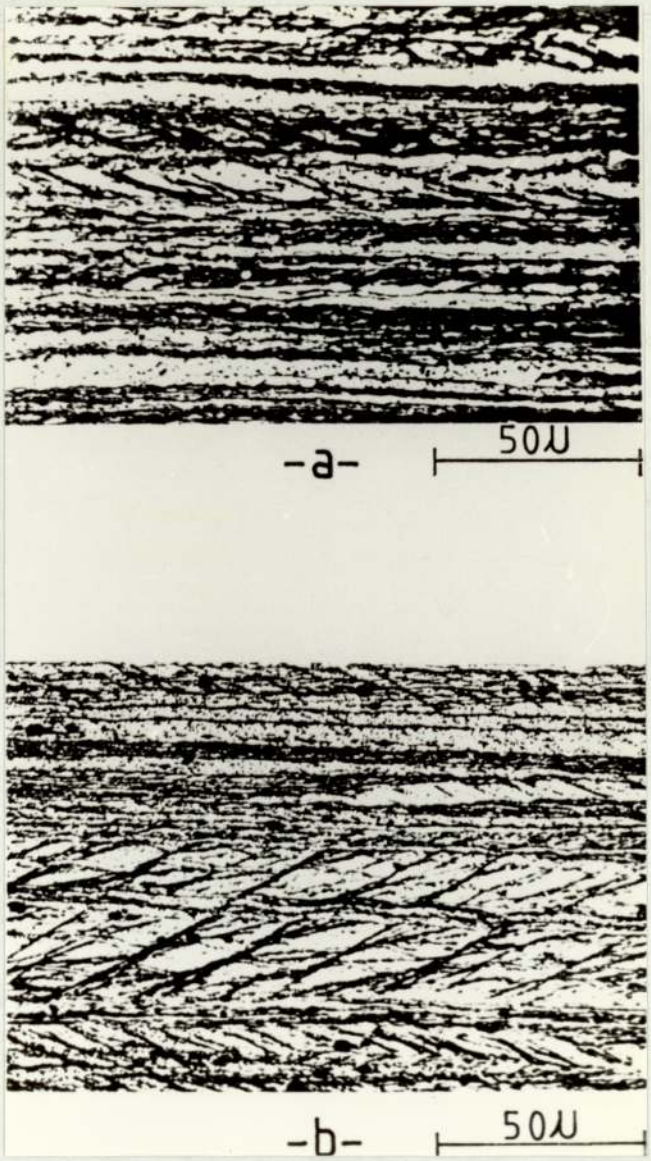

Figure (18) - Optical microstructures in Copper A

a) - rolled to 90% at -100°C,
initial grain size 85 mm

b) - rolled to 90% at room temperature
initial grain size 300 mm.

Ref.(139)

to the transverse direction. Duggan et al[135] and Hutchinson[39] found that in 70:30 brass only one set of shear bands started to form first after rolling 50% reduction, but after 70% reduction two sets of shear bands were formed and their frequency after 90% reduction increased.

In the recent work by Ridha et al[139], heavily rolled copper, with different initial grain size and purity were cold rolled at room temperature to 90% reduction. Material B with coarse grain size exhibited shear bands whereas material A with small initial grain size showed no shear bands. By lowering the rolling temperature and increasing the grain size of material A the microstructures changed. Figure (18 a,b) showing the microstructure in material A with coarse grain size gives similar deformation microstructure to copper B. They concluded that the shear bands were formed preferentially in materials with coarse grained starting material and suppressed in materials of fine grain size. Similar observations were observed by Hutchinson et al[140] in silicon-iron.

The inhomogeneous deformation in single crystals with various orientations have been studied by many workers. The microstructure of rolled single crystals of copper with a different orientation, Brown et al[141], show that the shear bands appear after about 20% reduction except in the crystal of orientation (110)[1$\bar{1}$2] which exhibited bands only after 90% reduction.

Morii et al[142] detected that shear bands in α-brass single crystals with (211)[$\bar{1}$11] orientation were formed after about 53% reduction, they were inclined about 40° with the rolling direction and increased in number as the rolling reduction increased. After >75% reduction two sets of shear bands were formed. The (211)[$\bar{1}$11] α-brass crystal showed the same feature as that observed in the (513)[$\bar{1}$21] single crystal of α-brass[143].

Silver single crystals with orientation (211)[$\bar{1}$11] and (101)[$\bar{1}$21][144] were rolled at room temperature. The microstructure of crystal (211)[$\bar{1}$11] showed shear bands formed after about 30% reduction which increased in frequency as the rolling deformation increased. These shear bands penetrated the whole specimen thickness making an angle of 40° with respect to the rolling plane. Reduction to more than 75% gave two sets of shear bands. In contrast no shear bands were observed in the single crystal with orientation (101)[$\bar{1}$21] rolled up to 95% reduction.

According to TEM of rolled α-brass[135,142,143] and Cu-Al alloy[144] the microstructure of the shear bands has been observed to consist of fine polycrystalline aggregates with high misorientation due to intensive shearing deformation which leads the crystal within the shear band regions to be fragmented.

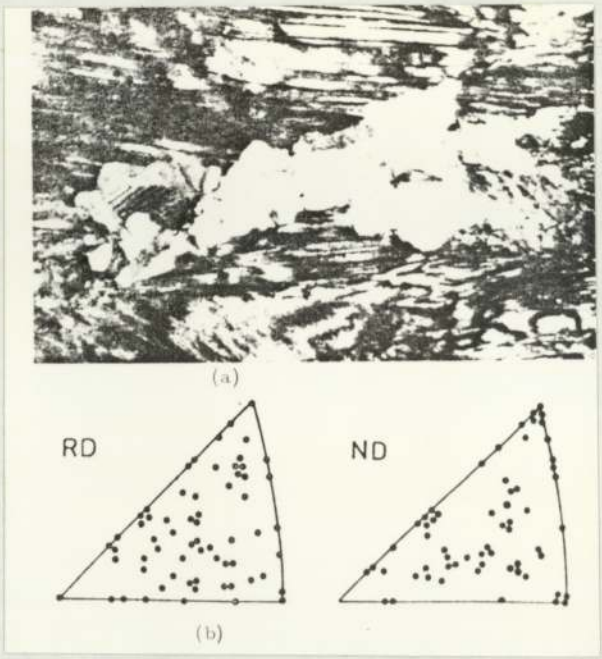

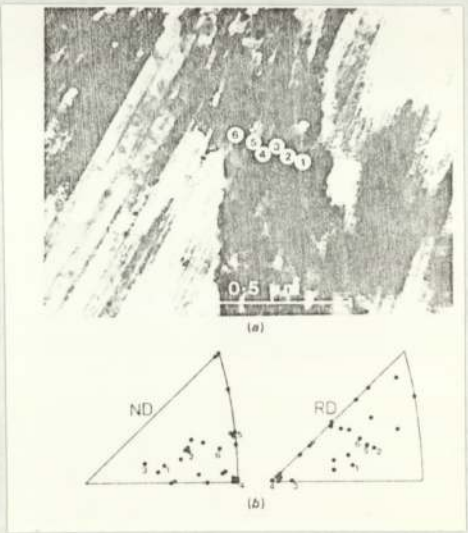

Figure (19) a - Longitudinal section rolled 60% and annealed 3 min at 300°C

b - Orientation of recrystallised grain in shear bands, 60%, annealed 3 min at 300°C. Ref.(145)

Figure (20) Analysis of orientation in shear bands

a - Single shear band showing location of STEM diffraction patterns

b - Orientations from location in a) and other shear band sites Ref.(135)

2.8.1 Nucleation at Shear Bands

The high dislocation density and sharp lattice curvature in shear bands make them highly favourable sites for nucleation in heavily deformed metals. Adcock[132] who was the first to report shear bands in heavily deformed cupro-nickel, showed that, recrystallisation on annealing occurred in the shear bands. Recently similar observations have been reported by Grewen et al[133] in Cu-0.6 Wt% Cr, and by Duggan et al[145] in 70:30 brass. On annealing, inside the HVEM they showed that numerous recrystallised grains formed within the shear bands and especially at the area of the intersection of the two shear bands. They found that recrystallisation always commenced in the shear bands without preference for edge or central regions as shown in Figure (19 a). The density of shear bands in heavily deformed high SFE materials is usually not large enough to provide all the nuclei needed for recrystallisation.

In heavily rolled copper annealed at 100°C for 10 hours the recrystallised grains were found to occur within shear bands[139]. Also work by Hutchinson et al[140] showed that the recrystallised grains occur preferentially within shear bands in both polycrystalline and single crystal materials of silicon-iron alloy.

2.8.2 The Effect of Shear Band on Deformation and Recrystallisation Texture

Recent work by [39,133,135,142-144] has indicated the possible contribution of shear bands to deformation texture development, and the further possibility of recrystallisation textures being derived from shear band orientations. Also [133,145] have deduced from SAD patterns that large misorientation exists between the crystallites, and that shear texture components are present within the bands. Grewen et al[133] have found the expected shear texture orientations in the larger crystallites of the shear bands in a precipitation hardened Cu-Cr alloy including {110}<001>. The only analysis of crystallite orientations using the more appropriate scanning transmission electron microscope (STEM) technique[39,135] has given the results as shown in Figure (20 b). These indicate that there is a wide scatter in orientation, but with a distinct tendency for orientations near {110}<001>. This orientation has also been observed by Grewen et al[133] in a Cu-Cr alloy. Other orientations were also reported including {112}<111> but these were not well populated.

Morii et al[142] studied the development texture of deformation microstructure in α-brass single crystal with orientation $(211)[\bar{1}11]$. After 40% reduction mechanical twinning developed and the $(211)[\bar{1}11]$ orientation changed to $(211)[\bar{1}11] + (255)[5\bar{1}\bar{1}]$ and gradually to the $\{111\}\langle 211\rangle$ duplex orientation. After 75% reduction the orientation

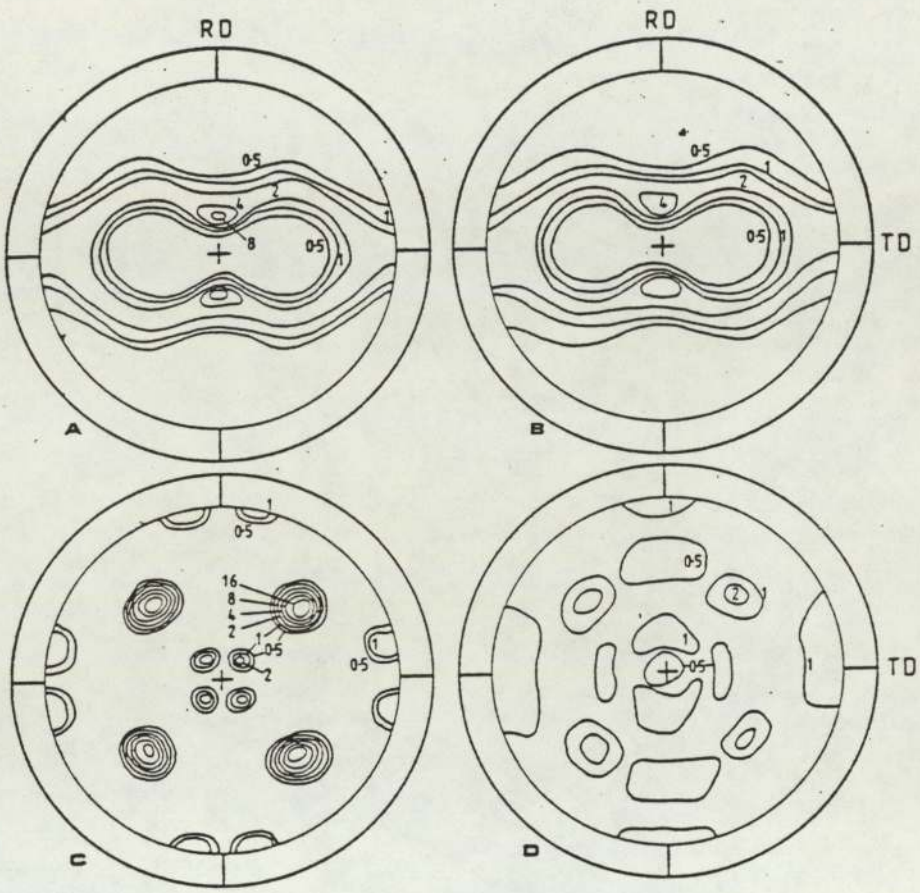

Figure(21) - (111) pole figures for samples of copper

a) Copper A rolled 90%
b) Copper B rolled 90% at room temperature
c) Copper A fully recrystallised
d) Copper B fully recrystallised

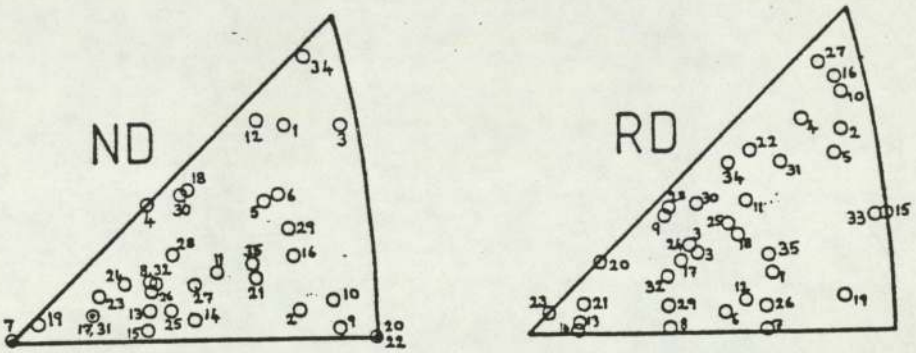

Figure (22) - Orientation of recrystallised grains formed within shear bands in copper B

Ref.(139)

{111}<211> rotated into the {011}<100> and {011}<211> orientations. This was ascribed to the textures developed within the regions of shear bands during deformation at high reduction. Similar results were found in silver single crystal[144] of the same orientation. The changes in orientation were explained on the basis of activation and development of shear bands.

In recent work Ridha et al[139] examined heavily rolled copper. The rolling texture of copper B which exhibit shear bands during deformation was weaker than copper A which was free of shear bands. The recrystallisation texture of copper A shows very sharp cube texture in addition to its twins {122}<212>. In contrast, copper B shows weak cube texture and diffuse spread of orientation, Figure (21).

Ridha[69] summarised the effect of the presence of the shear bands on rolling and recrystallisation texture in copper in two ways which weaken the cube texture:-

1 - The shear bands forming in copper break up the cube oriented regions into smaller lengths so that their special advantages for preferential nucleation are lost.

2 - During annealing nucleation occurs within the shear bands and the orientation of these nuclei are random which randomises the recrystallisation texture, Figure (22).

Hutchinson et al[140] showed that cold rolled single crystals of silicon iron with (111)[11$\bar{2}$] orientation

exhibit shear bands during rolling. Recrystallisation texture of these crystals shows very strong Goss components, (110)[00$\bar{1}$]. They concluded that the shear bands recrystallise first on annealing to produce new grains which have the Goss orientation. The recrystallisation texture after complete recrystallisation was the same as that of the nuclei within the shear bands.

CHAPTER THREE

EXPERIMENTAL PROCEDURE

3.1 Materials and Initial Treatment

The materials were provided by the British Aluminium Company Limited. They were received as chill cast blocks 152.4 x 25.4 x 304.8 mm in size, made from a high base purity of not less than 99.8% Al, and containing a standard titanium-boron grain refining addition. The two alloys used in the present work were Al-0.75% Mg-0.43% Si (A), and Al-5.1% Zn-1.0% Mg (B). The actual chemical compositions are given in Table 1.

Table 1

Chemical Composition of Materials Used (Wt%)

Samples	Si	Fe	Cu	Mn	Mg	Cr	Zn	Ti
A	0.44	0.05	<0.01	<0.01	0.68	<0.01	0.01	0.03
B	0.04	0.06	<0.01	<0.01	0.98	<0.01	4.98	0.03

The starting materials were annealed in a muffle furnace for one hour at a temperature of 500^{o}C, then the slabs were hot rolled using a two-high rolling mill. Between each reduction the slabs were re-heated to ensure re-crystallisation and prevent the development of a strong texture at this stage. Total hot rolling reduction was

about 50% to a final thickness of 13 mm. This was followed by a solution treatment using air circulatory frunace for about 2 hours at 530°C for materials A, and at 465°C for material B and water quenching. This produced an initial grain size of about 294μm and 56μm for materials A and B respectively. For material A, a series of preliminary experiments were carried out to find which treatment gave suitable precipitate morphologies (i.e. the particles were required to be large and widely spaced). The following heat treatment schedule was finally adopted:

1 - Solution treatment at 530°C

2 - Anneal at 450°C for 48 hours then slow furnace cool to 350°C, held at this temperature for 72 hours and water quench (A_I)

An alternative to 2 was to

3 - Anneal at 530°C for 2 hours then slow furnace cool to 350°C, held at 350°C for 72 hours and water quench (A_{II}) in order to get another precipitate morphology.

3.2 Cold Rolling

The specimens in both solution-treated and aged condition for material A were cold rolled by 10-90% and for material B as solution treated were rolled by 80-90% reduction. Cold rolling was performed on a small two high mill. Oil lubrication was applied to the rolls in order to reduce friction between the rolls and the specimens, which would minimise any change in texture through the thickness of the cold rolled slabs.

3.3 Techniques for Investigation

A wide range of experimental techniques were used to examine the deformation microstructure, rolling texture, orientation of single crystals and recrystallisation behaviour during annealing for both aluminium alloys (single crystals and polycrystalline)and single crystals of pure aluminium.

3.3.1 Optical Metallography

Samples were removed from the bulk material using a diamond cutting wheel at low speed to minimise surface damage. The small amount of damage produced was removed during subsequent preparation. The specimens were ground and mechanically polished on successively finer silicon carbide papers, finishing on 1200 grit. Polishing was accomplished using 6μm and 1μm diamond paste. To obtain scratch-free surfaces, the samples were electropolished for about 5 minutes in 5% perchloric acid in 2-Butoxythanol solution held at a temperature in the range $-20^{o}C$ to $-10^{o}C$, using a potential of 30 to 40 volts in a stainless steel beaker as cathode. To produce grain contrast the polished surface was anodised and the microstructure was viewed under polarised light with a ¼ wave plate to enhance the optical contrast. The anodising was performed in an aqueous solution of 2.5% Fluoroboricacid in water at room temperature. A potential of 20 volts was applied. Suitable contrast was achieved after about two minutes of this treatment.

3.3.2 Scanning Electron Microscopy

A Cambridge S2A scanning electron microscope was used in the back-scattered mode to examine the size, shape and distribution of precipitation in solution treated and aged specimens of material A_I after cold rolling to different reductions in order to study the behaviour of the second phase rotation with respect to the various reductions. This technique was also used to examine the microstructure of partially recrystallised specimens of material B. This technique employs electron channelling contrast and has a number of advantages over optical and transmission microscopy which can be summarised as follows:-

(a) Large areas could be examined on the specimen, and specimen preparation is easy, so that representative statistical studies can be made.

(b) Image formation depends on electron channelling which differes from crystal to crystal, so that the deformed and recrystallised regions can be identified.

(c) Channelling patterns can be obtained from recrystallised grains >3μm in diameter so that their crystallographic orientation could be determined.

(d) The process of recrystallisation can be observed by heating the specimen inside the microscope. Also it is a powerful technique with a 5 K magnified image with good resolution and forms as a link between optical and transmission electron microscopy.

The longitudinal section specimens were mechanically

polished and electropolished as described in the previous section. Grain orientations in partially recrystallised specimens were determined by selected area channelling patterns (SACP).

3.3.3 Transmission Electron Microscopy

Routine examination of aged and deformed samples and partially recrystallised specimens were carried out using a Jeol 100 B with an accelerating voltage of 100kV, equipped with a -60^{o} single tilt and 360^{o} rotation specimen stage. The microscope also had a scanning transmission (STEM) attachment. To determine the orientation of fine substructures, the STEM attachment of a Philips EM 400 STEM was used operating at 120 kV. The Jeol 100 TEM was calibrated for magnification and rotation relative to the diffraction patterns using Mo_2O_3 single crystals on a carbon support film.

Grain and substructure orientations were determined by selected area Kikuchi electron diffraction patterns (SAKDP), which gave accurate measurements of crystallite orientations. The rolling direction of every foil was identified in the electron micrographs and diffraction patterns from images of the edge of the specimen cut perpendicular or parallel to the rolling direction.

For thin foil specimen preparation, longitudinal sections of about 0.4 mm thick were cut from the rolled sheet

specimens by the diamond cutting wheel. The section was mechanically thinned to about 50μm by grinding on water lubricated 600 and 1200 grade abrasive paper. Great care has been taken throughout this preparation especially during the final stage of mechanical polishing. Further thinning was done by electropolishing using the same conditions as in the previous section (3.3.1) using the window technique.

3.3.4 Texture Determination

Barrett[86] has shown that texture variation can occur through the thickness of cold rolled aluminium sheet. It was therefore important to remove half the thickness of the cold rolled sheet before texture examination was carried out. Quantitative pole figures were determined by the Schultz X-ray reflection method using a Siemens texture goniometer, in conjunction with a Siemens X-ray generator and detector system. The Schultz method involves the specimen undergoing two simultaneous rotations, one being about an axis normal to the rolling plane (ψ-rotation) and the other being about an axis lying in the plane of the sheet (ϕ-rotation). The diffracted radiation was monitored continuously by a proportional counter and recorded on a chart as variation in diffracted intensity, proportional to the density of {hkl} planes reflecting, with specimen rotation. However, the Schultz method is only accurate for ϕ-angles of up to 60^{o}. Above this figure the intensities cannot be determined accurately. By correcting the intensity levels, contours may be plotted

with reasonable accuracy for values from 0 to 75°. The radiation used for the texture analysis was copper Kα. Quantitative {111} and {200} pole figures were determined for the specimens rolled to 50-90% reduction.

Square specimens about 2 cm across were cut from the rolled materials. In order to remove half of the thickness each specimen was lacquered on one face and then etched in a solution of 40% NaOH at a temperature of ~70°C to increase the rate of reaction.

3.3.5 X-Ray Examination

A quantitative X-ray diffraction technique was used to determine the lattice parameter of Mg_2Si particles.

(a) - Powder Camera:-

A Philips X-ray generator was used with Mo filtered CuKα radiation at 40 kV and 20 mA. Specimens were prepared by using fibres of glass coated with adhesive and then rolled in the particles of Mg_2Si. Separation of Mg_2Si particles was achieved by dissolving the aluminium matrix in a solution of NaOH and collecting the residue by using centrifugal separation.

3.3.6 Production of Single Crystals of Aluminium Alloys

In order to overcome the difficulty of identifying directions in polycrystalline material when carrying out transmission electron microscopy on strained material,

single crystals of Al-Mg-Si and Al-Zn-Mg were grown in the solution state.

The method used was a repeated strain anneal, similar to that described by Hosford et al[146]. Strips of alloy were rolled to 5 mm thickness, and pieces measuring 200 mm long and 15 mm wide were cut from the strip and strained ~1% using a Dennison Tensile Machine. The strained material was then annealed at 530°C for 16 hours and water quenched. They were then strained ≤2% and annealed at 550°C for two days and water quenched. After about two cycles of this treatment, grains with diameters of the order of 15 mm were present in the strip. The orientations of the larger grains were determined by the Laue back reflection technique with a film to specimen distance of 3 cm and unfiltered Mo radiation. These crystals could then cut out. After machining the orientations were again checked.

In order to roll the relatively small initial single crystals, it was necessary to mount each crystal in other material of the same thickness to hold the specimen during the rolling. For rolling of the crystals a small roll diameter was used with an oil lubricant. The rolling was carried out up to a reduction in thickness of 70 to 80%. In order to obtain a well-defined rolling direction, the specimens were guided on one side on entering the rolls. After the desired degree of rolling, the specimens were removed from the material holder. The crystal orientations

used in the present work are tabulated in Table 2

Table 2

Orientation of Single Crystals

Material	Crystal symbol	Nominal orientation	Deviation from orientation (deg)
2-PHASE Al-Mg-Si	A	(110)[001]	< 2
	B	(231)[$\bar{1}2\bar{4}$]	< 2
	C	(014)[$34\bar{1}$]	1
Pure Al	D	(110)[001]	
Al-Zn-Mg	E	(110)[001]	1
	F	(110)[$\bar{1}1\bar{2}$]	2
	G	(231)[$1\bar{2}4$]	5
	H	(241)[$1\bar{1}2$]	4

CHAPTER FOUR

EXPERIMENTAL RESULTS

4.1 Optical Metallography

Metallographic examination of the microstructures was carried out on the Al-Mg-Si and Al-Zn-Mg specimens after solution treatment for 2 hours at a temperature of 530°C and 465°C respectively, in an air circulation furnace. The grain size for each specimen was estimated at about 294μm and 56μm. In order to produce coarse, hard and widely separated Mg_2Si particles in Al-Mg-Si specimens, two different treatments were carried out. In the first specimens were aged at 450°C for 48 hours, furnace cooled to 350°C, held at 350°C for 72 hours and then water quenched. This material was designated A_I. In the second treatment specimens were partially solution treated at 530°C for 2 hours, furnace cooled to 350°C, held at 350°C for 72 hours and then water quenched. This material was designated A_{II}. The different structures produced by these treatmens are shown in Figure (23). Second phase particles separated from the matrix by the first treatment are shown in Figure (24) and appear as square platelets.

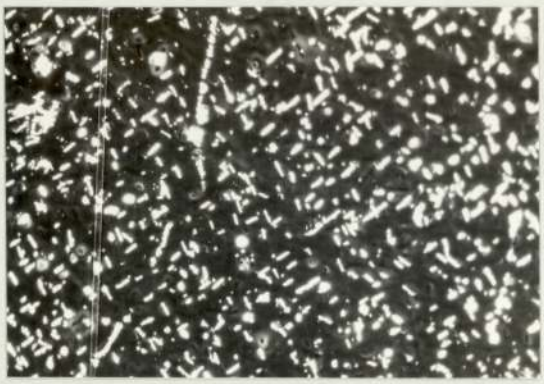

Figure 23 Microstructure of Al-Mg-Si alloy solution treated at 530°C/2hrs. prior to rolling

a) Aged at 450°C/48 hrs + 350°C/72 hrs W.Q. (A_I)

b) Aged at 530°C/2 hrs + 350°C/72 hrs W.Q. (A_{II}) X 196

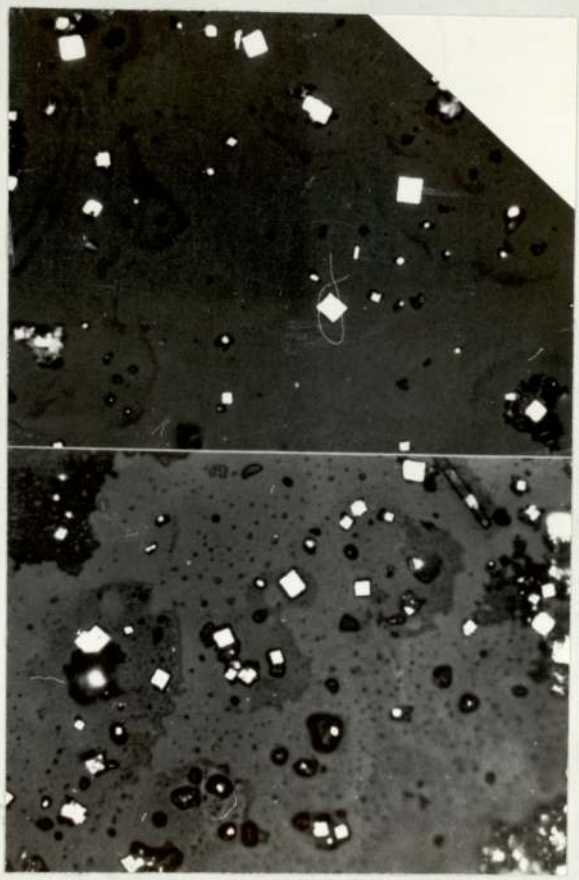

Figure 24 Optical micrograph showing the shape of Mg_2Si particles after separation from the matrix X420

4.2 Deformation and Annealing Microstructure

4.2.1 Polycrystalline Materials

4.2.1.1 Al-Mg-Si Alloy

The microstructure developed during cold rolling of Al-Mg-Si specimens:- The unaged condition with large initial grain size, shows a few shear bands after 90% reduction, usually within individual grains, Figure (25 d). Specimens in the aged condition with similar initial grain size do not show such shear bands, Figure (25 c), and the microstructure is considerably different. Deformation microstructures at different degrees of reduction 50 to 90 percent showed that the grains were gradually elongated in a direction parallel to the rolling direction with increased applied strain, as shown in Figure (25 a-c). In order to investigate the effect of the Mg_2Si particles produced by the second treatment, (material A_{II}) similar reduction were applied by rolling and the deformation microstructure showed no shear bands, Figure (25 e,f).

Because of the difficulty in observing, during the early stage of recrystallisation the formation of nuclei near to the particles by optical microscopy, this treatment is described in the TEM section (4.6).

4.2.1.2 Al-Zn-Mg Alloy

The deformation microstructure in the unaged Al-Zn-Mg

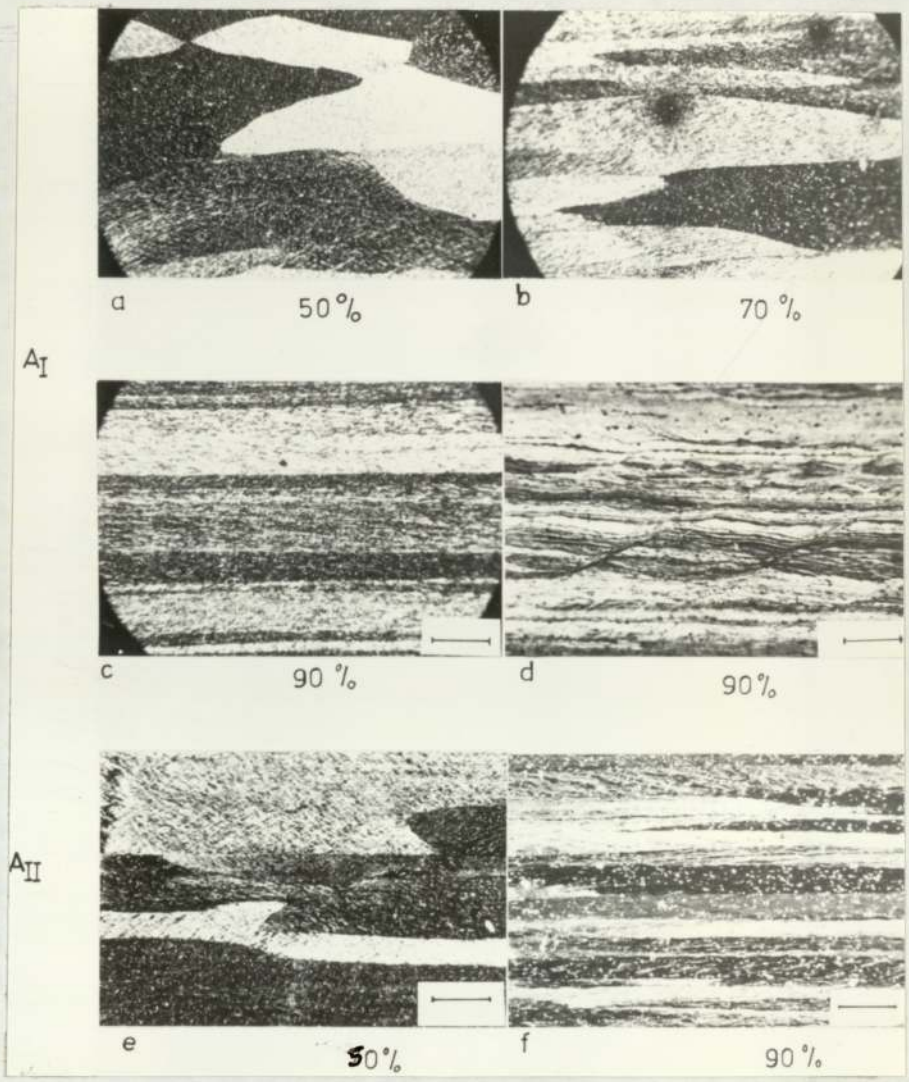

Figure 25 Optical microstructures in Al-Mg-Si in longitudinal section anodised in aqueous Fluoroboric acid

a) Material A_I rolled 50% reduction
b) Material A_I rolled 70% reduction
c) Material A_I rolled 90% reduction X 112
d) Al-Mg-Si as solution treated rolled 90% reduction X87
e) Material A_{II} rolled 50% reduction X41
f) Material A_{II} rolled 90% reduction X78

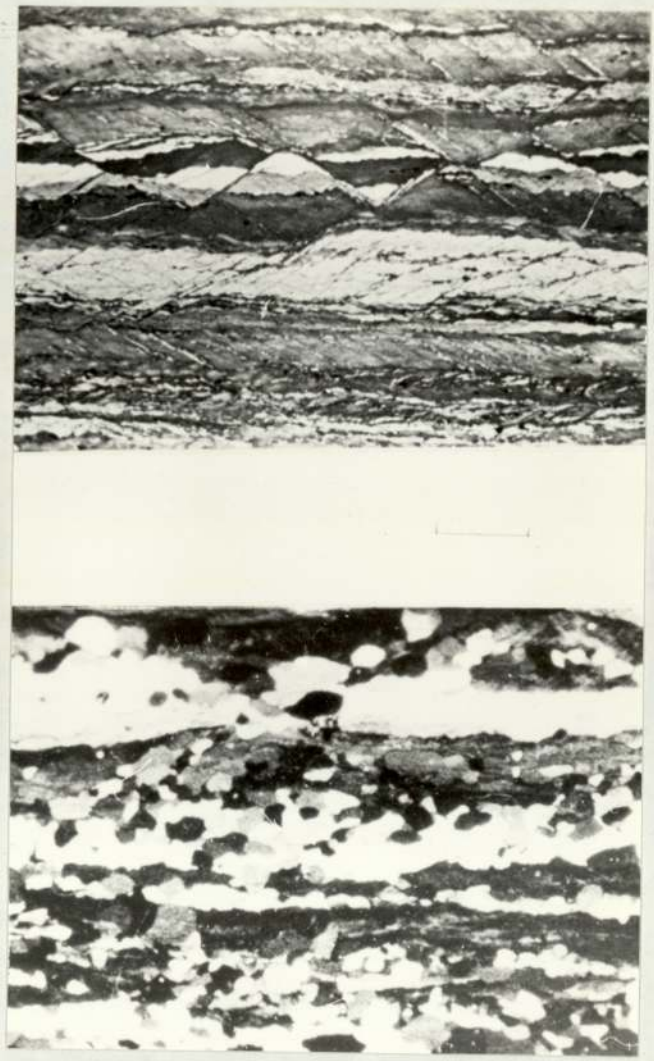

Figure 26 Optical microstructure of Al-Zn-Mg alloy anodised in aqueous Fluoroboric acid in longitudinal section

a) As rolled 90% reduction

b) As partially recrystallised showing recrystallisation along the shear bands

X128

alloy with small initial grain size after cold rolled to 90% reduction at room temperature, exhibited numerous shear bands, many of which existed within individual grains, although some extended into other grains. Such features of the deformed structure are shown in Figure (26 a). The aged specimen showed a rather similar appearance.

After annealing the rolled specimens for short times of about 25 seconds in a salt bath at 350°C to partially recrystallise, the annealing microstructures showed development of recrystallised grains along the shear bands, until the whole bands were fully recrystallised. The specimens were recrystallised rapidly even in a short time, Figure (26 b).

4.2.2 Single Crystals

4.2.2.1 Al-Mg-Si Alloy

Three single crystals A, B and C with initial orientations (110)[001], (231)[$\bar{1}2\bar{4}$] and (014)[$34\bar{1}$] were studied. These three crystals were aged to a similar condition to the polycrystalline Al-Mg-Si material (A_I), to contain coarse, non-deformable particles prior to rolling. They were then rolled to about 71% reduction in thickness at room temperature. The deformation microstructures show no sign of shear bands formed in any of these crystals.

The annealing microstructures of the partially recrystallised material is explained in the TEM section.

4.2.2.2 Pure Aluminium Crystal (D)

High purity aluminium single crystals accurately oriented (110)[001] were rolled at room temperature to about 75% reduction. The deformation microstructures showed a high density of what appeared to be very fine cross-slip bands, with no sign of inhomogeneous deformation by shear bands. Figure (27 a) shows the longitudinal section through the deformed structure. During subsequent annealing this crystal became more reluctant to recrystallise at 350°C, comparable with a similarly deformed polycrystalline aluminium alloy. A remarkably high temperature was needed to cause recrystallisation to occur, so the annealing temperature was increased to 400°C. The specimens were then completely recrystallised after 300 s with large resulting grain size. There was clear evidence that no shear bands were formed in high purity aluminium single crystals with this orientation.

4.2.2.3 Al-Zn-Mg Crystals

1 - Crystals(E) with (110)[001] orientation were cold rolled at room temperature to 80% reduction. Optical micrographs of the deformed structures showed only one or perhaps two sets of deformation bands because of the symmetry of this orientation. One set was inclined at 35° to the rolling direction, the second set was more difficult to detect, Figure (27 b). These bands became a little clearer when the rolled specimens were partially annealed at 350°C for 180 s. The microstructure showed a few

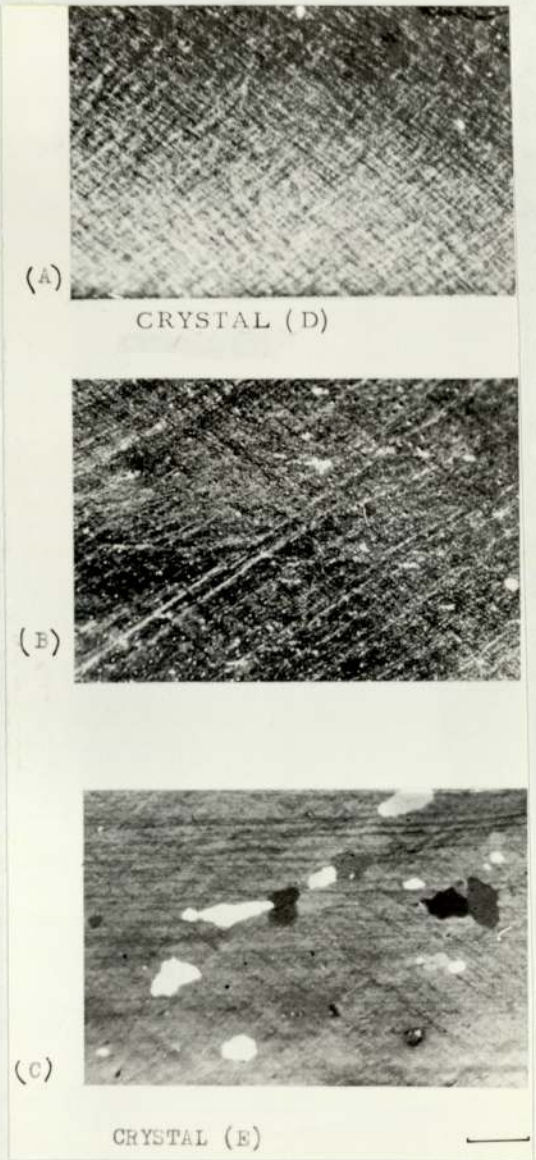

Figure 27 Optical microstructure of rolled crystals in longitudinal section anodised in aqueous Fluoroboric acid

a) Crystal D rolled 75% reduction, showing the slip bands
b) Crystal E rolled 80% reduction
c) Crystal E as partially recrystallised showing the early stage of recrystallisation after 3 mins. at 350°C

× 82

recrystallised grains started along the band, with others widely scattered through the specimen, Figure (27 c). The delayed recrystallisation, and small number of recrystallised grains provided clear evidence that there were no shear bands in this crystal of the Al-Zn-Mg alloy.

2 - The deformation microstructure of a crystal (F) with $(110)[\bar{1}1\bar{2}]$ orientation rolled to 80% reduction at room temperature showed a high density of dark etching, sheet-like shear bands with various thicknesses. Only one set of shear bands was observed, inclined at about 35^{o} with respect to the rolling direction. These passed through the whole thickness of the specimen which signified localisation of the inhomogeneous deformation during rolling.

New shear bands developed during rolling were less broad than those first formed, and these narrow shear bands were formed by bran ing from the original bands or formed at some distance from them. Some of these narrow bands crossed the original large shear bands. Large numbers of small, narrow bands inclined at large angles to the layer bands were also detected. These filled the spaces between the original bands, Figure (28 a). In a view normal to the rolling direction, the shear bands made an angle with the transverse direction at about 10^{o}, and they are not parallel to the transverse direction as has been observed by other workers[132-135] Figure (28 b) shows an example of these shear bands.

The rolled specimens were annealed in a salt-bath furnace

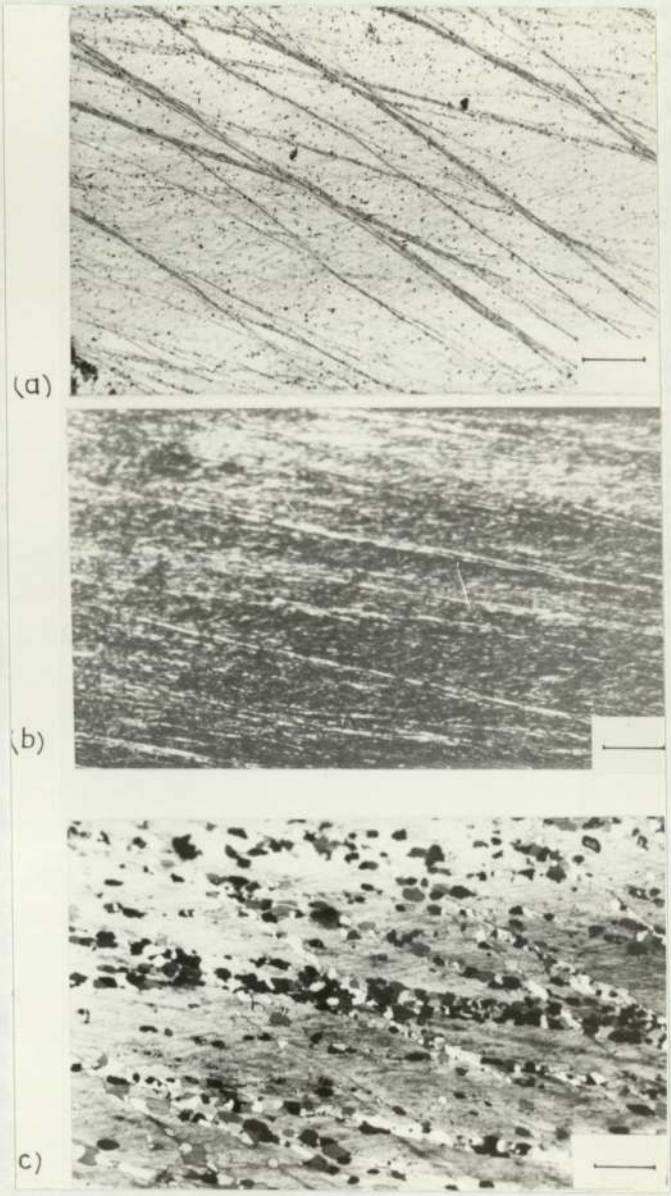

Figure 28 Optical micrograph showing the structure of rolled crystal F, anodised in aqueous Fluoroboric acid

a) Rolled 80% reduction (Longitudinal Section) X58

b) Section parallel to the Transverse Direction) X80

c) As partially recrystallised (Longitudinal Section), showing the recrystallisation along the shear bands X58

at a temperature of 350°C for 60 s to partially recrystallise. The annealed microstructure revealed that this crystal was rapidly recrystallised and these small recrystallised grains formed along the shear bands. The size and number of recrystallised grains was increased by increasing the length of annealing time. Figure (28 c) shows the partially recrystallised specimen annealed for 90 s. A large number of recrystallised grains is shown at the intersection of shear bands.

3 - Examination of the longitudinal section of crystal (G) deformed 80% reduction in thickness at room temperature, showed widely spaced, narrow and severe shear bands. They were inclined at about 35° to the rolling direction. The shear bands were of two types, one clearer and sharper than the other and crossing the whole specimen thickness. The others did not pass through the whole section, possibly because the deformation was not high enough to let these bands develop fully. A few shear bands either split from the original shear bands which formed early, or developed independently at a later stage of deformation. The shear bands in this crystal were less frequent than in the previous crystal, as shown in Figure (29 a). In a section normal to rolling direction the shear bands were not parallel to the transverse direction, but inclined at an angle of about 5 to 8 degrees to T D. Examples of these peculiar shear bands are shown in Figure (29 b).

During subsequent annealing at a temperature of 346°C for a period of 80 s, this crystal recrystallised very rapidly

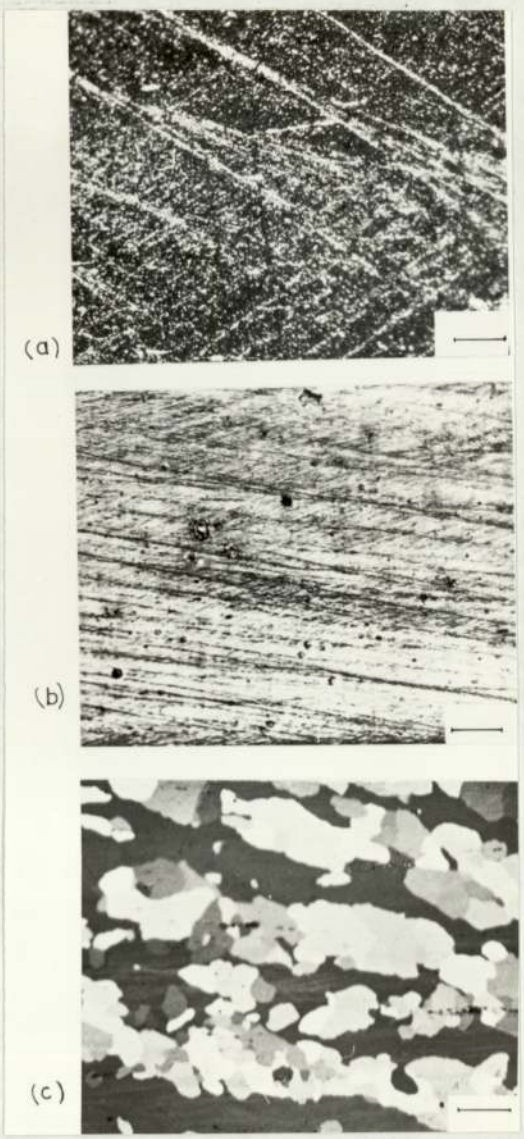

Figure 29 Optical micrograph showing the structure of rolled crystal G, anodised in aqueous Fluoroboric acid

a) Rolled 80% (Longitudinal Section) X 76

b) Section parallel to the Transverse Direction X 90

c) As partially recrystallised (Longitudinal Section), showing the recrystallisation along the shear bands X 112

and the recrystallised grains occurred along the shear bands, Figure (29 c). Although this crystal recrystallised very quickly, the size of the recrystallised grains was much larger than that developed in the other crystals. Figure (29 c) shows three fully recrystallised shear bands.

After 20 minutes annealing at 350°C for complete recrystallisation the annealed structure was as shown in Figure (31 a).

4 - Figure (30 a) shows the structure of crystal (H) after cold rolling to 80% reduction at room temperature. The deformed structure contained a very high density of shear bands running across the whole specimen thickness, inclined at about 35° to the rolling plane. These shear bands were similar to those formed in crystal (F) but were more severe and narrower. In addition, new shear bands deviated from the original bands, and were narrower than those formed earlier. Possibly other very fine bands were observed. Many of these shear bands crossed each other. These shear bands were not parallel to the transverse direction, and made an angle of about 2° to 5° with the T D as shown in Figure (30 b). The annealing microstructure shown in Figure (30 c) was similar to that in crystal (F). The specimens were annealed at 350°C for 90 s, and the recrystallised grains occurred preferentially within the shear bands so that the bands become rows of these new grains. The density of the recrystallised grains was greater in the crossing point of these shear bands. Figure (31 b) shows the structure of fully recrystallised

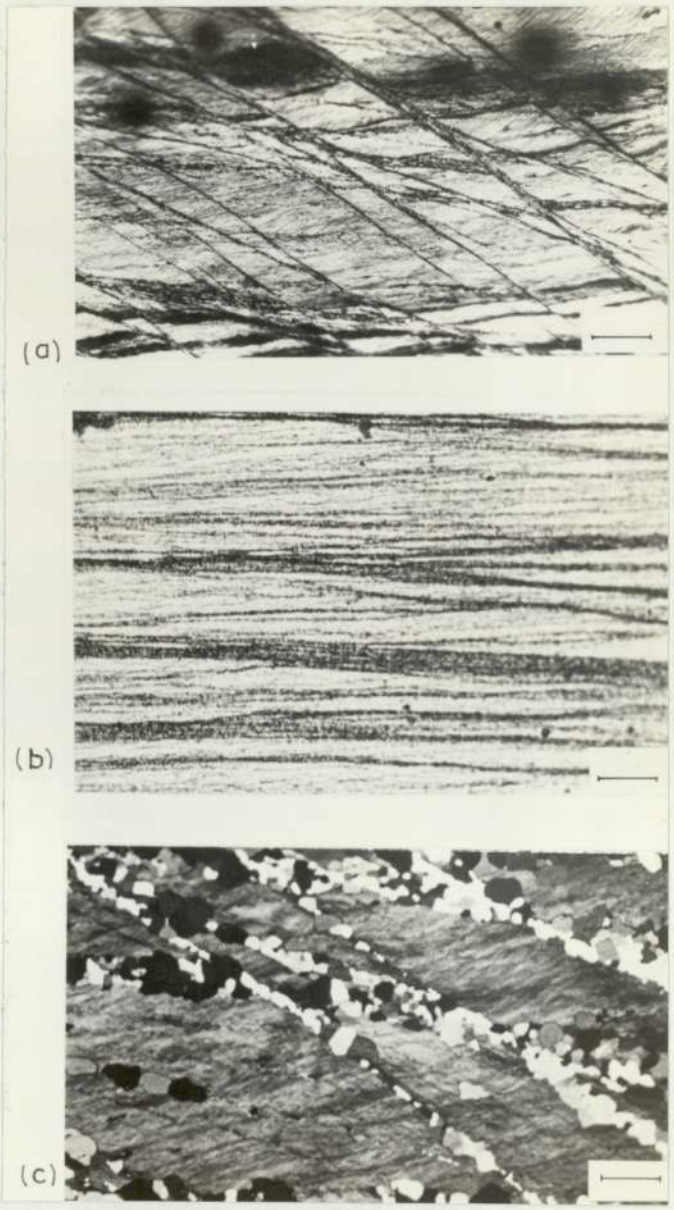

Figure 30 Optical micrograph showing the structure of rolled crystal H, anodised in aqueous Fluoroboric acid

a) Rolled 80% (Longitudinal Section) X 64

b) Section parallel to the Transverse Direction X 90

c) As partially recrystallised (Longitudinal Section), showing the recrystallisation along the shear bands X 112

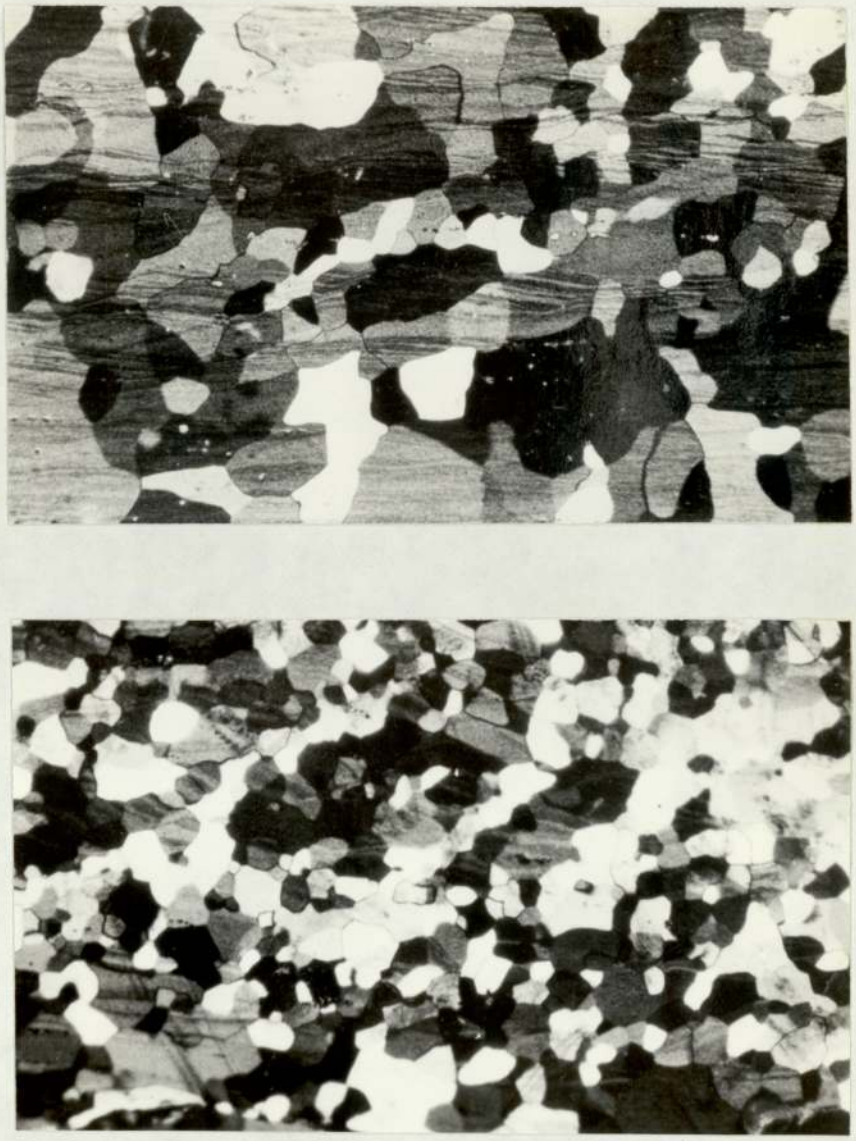

Figure 31 Optical micrograph of fully recrystallised Al-Zn-Mg in longitudinal section, anodised in aqueous Fluoroboric acid

a) Crystal G

b) Crystal H X 84

specimen.

4.3 Scanning Electron Microscopy

4.3.1 Effect of Applied Strain on the Non-Deformable Second-Phase Particles in Al-Mg-Si Alloy

In the Al-Mg-Si alloy, coarse, hard, square-shaped, plate-like particles were formed prior to rolling, as described in section (3.1). A severe compatibility problem occurs between soft, easily-deformed material such as the matrix, and hard, non-deformable particles. In such cases, any rotation of these particles must occur independently of the matrix rotations, i.e. inhomogeneous deformation will be produced. In order to investigate the behaviour of such particles with applied strain, longitudinal sections were cut from samples of Al-Mg-Si alloy which had been deformed to 10-90% reduction in thickness. The specimens were prepared as described in section (3.3.2). The orientation distribution of Mg_2Si particles at low strains was not much affected. With increasing applied strains, a gradual rotation of these particles was observed. Particles with a certain orientation relative to the RD, i.e. $(10\text{-}80)^{o}$, would be able to rotate in such a way as to lie parallel to the rolling direction. Occasionally, particles lay perpendicular to the rolling direction. Particles in such cases were hard to rotate and instead tended to buckle in such a way as to accommodate to the deformation state.

A statistical study was made to find the initial angles

between the particles and the rolling direction, and the final orientation, of these particles at different degrees of deformation. Measurements were carried out in one hundred fields at a magnification of 1 K. The results of this study were plotted in Figure (32). It is clear that on increasing the applied strain more particles lay parallel to the R D. Theoretical analyses were made in order to fit with the experimental results. See Appendix A.

4.3.2 Determination of Second Phase Parameters

The dispersion parameters which affect the nucleation of recrystallisation in second-phase Al-Mg-Si material, are: volume fraction (V_F), interparticle spacing (λ), and the size of the particles, which is here the length (L). There are many different definitions used to calculate these parameters. In the present work point counting was adapted by using a square grid superimposed on the SEM micrograph on about 10 fields at 1 K magnification, Figure (33 a). The lengths of the large particles were measured, the results were plotted in a histrogram. The mean length of the particles was found to be $\bar{L} = 5.95\mu m$. Figure (33 b) shows the particle length distributions.

Interparticle spacings(λ) were calculated in the same way as that used by Humphreys[111], i.e. by measuring the number of the particles per unit area of plane surface of the micrograph (N_s). Then $\lambda = \frac{1}{\sqrt{N_s}} \sim 12.85\mu m$.

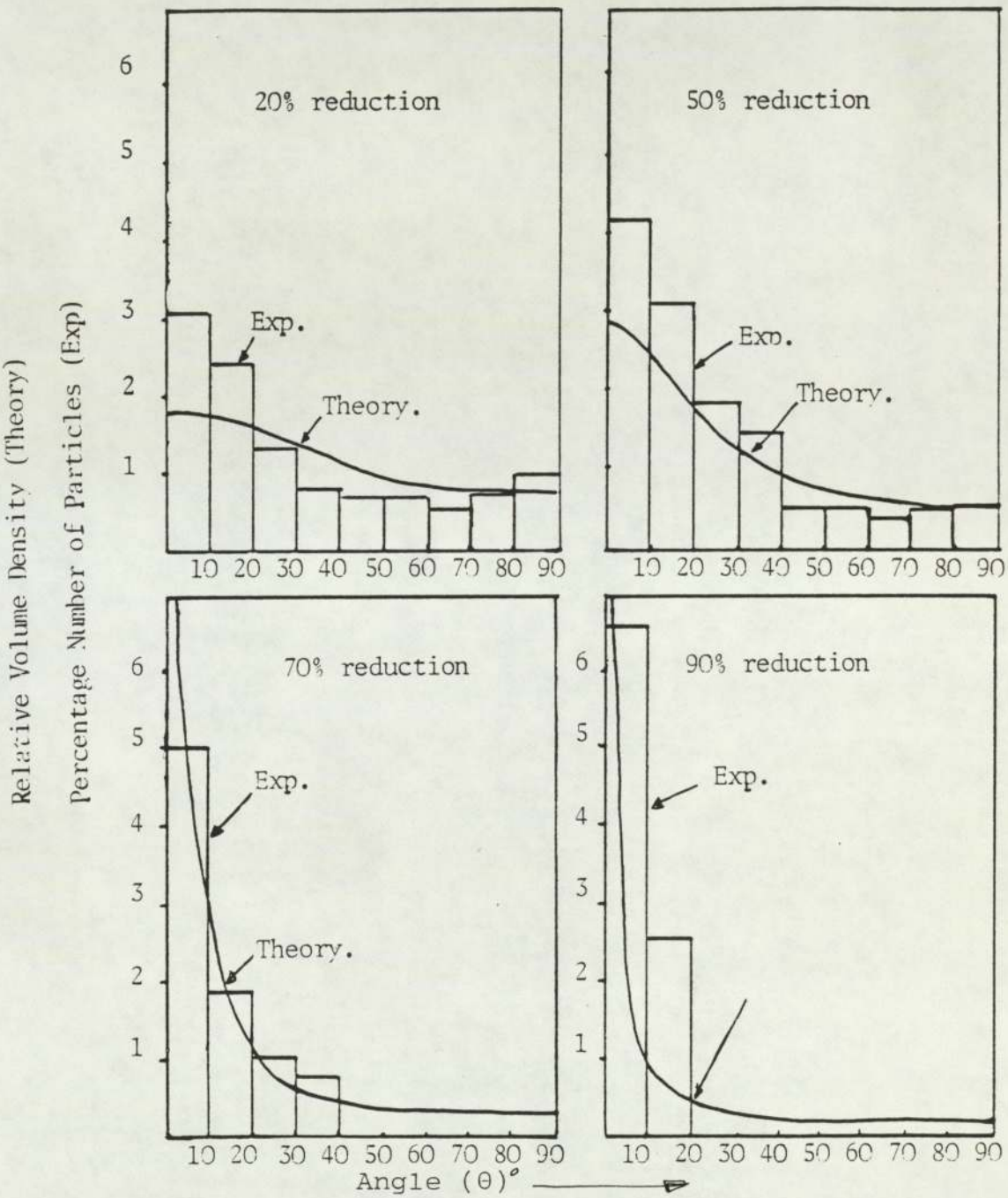

Figure 32 Results of calculation of the orientation distribution of the Mg_2Si particles as a function of the angle, the rolling direction and the applied deformation

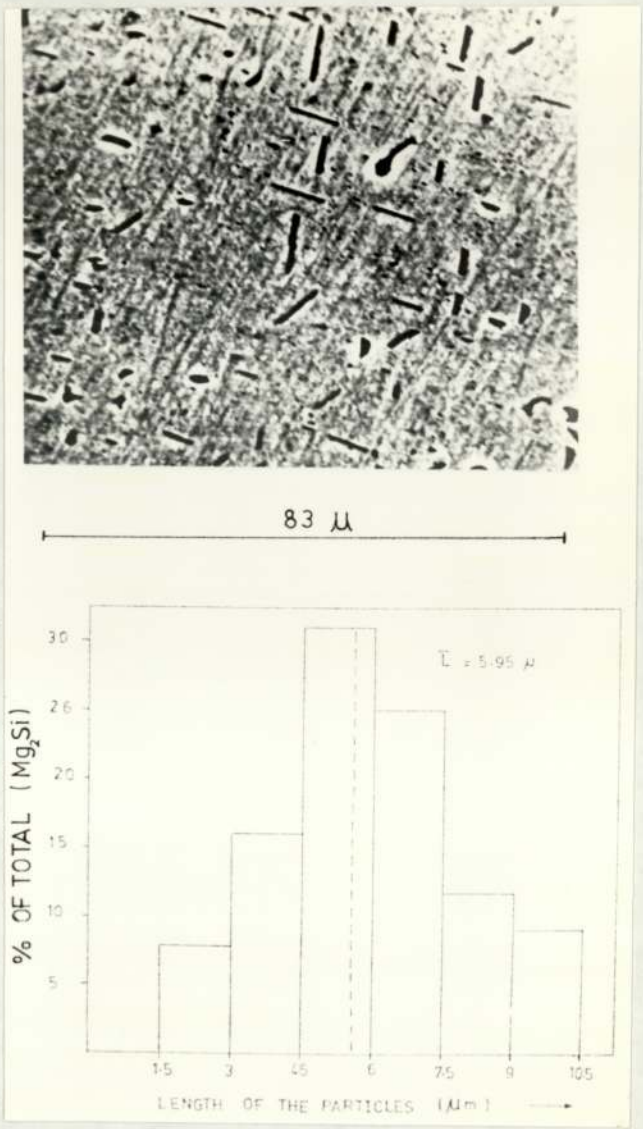

Figure 33 a) A composite of SEM/BSE micrograph showing the Mg_2Si in Al-Mg-Si

b) Frequency distribution of particle length of Mg_2Si in Al-Mg-Si alloy

The volume fractions (V_F) were measured on micrographs from planer sections, using a square grid. The number of intersections of the grid falling in the Mg_2Si phase are counted, compared with the total number of points laid down. The volume fraction V_F was found to be approximately $15.5x10^{-2}$.

4.3.3 Orientation Determination of the Recrystallised Grains Within the Shear Bands of a Single Crystal in Al-Zn-Mg Alloys

Longitudinal sections of the three crystals in the as-partially-recrystallised were used for optical microscopy. They were prepared for the SEM as described in section (3.3.2). The specimens were examined in SEM in the BSE mode in order to determine the orientation of the small recrystallised grains formed within the shear bands by the channelling pattern technique.

1 - Crystal (F):- Figure (34 a) shows an example of the partially recrystallised structure after a short anneal, and the new grains were formed within the shear bands. The grains whose orientation was determined are labelled. Some grains were nucleated on a shear band and others originated from the matrix. Several other areas were examined, and the orientations of all the grains measured are plotted in the unit triangle of Figure (34 b). Despite the spread in orientation these results agree with those of the components determined from pole figures after full recrystallisation of the specimen.

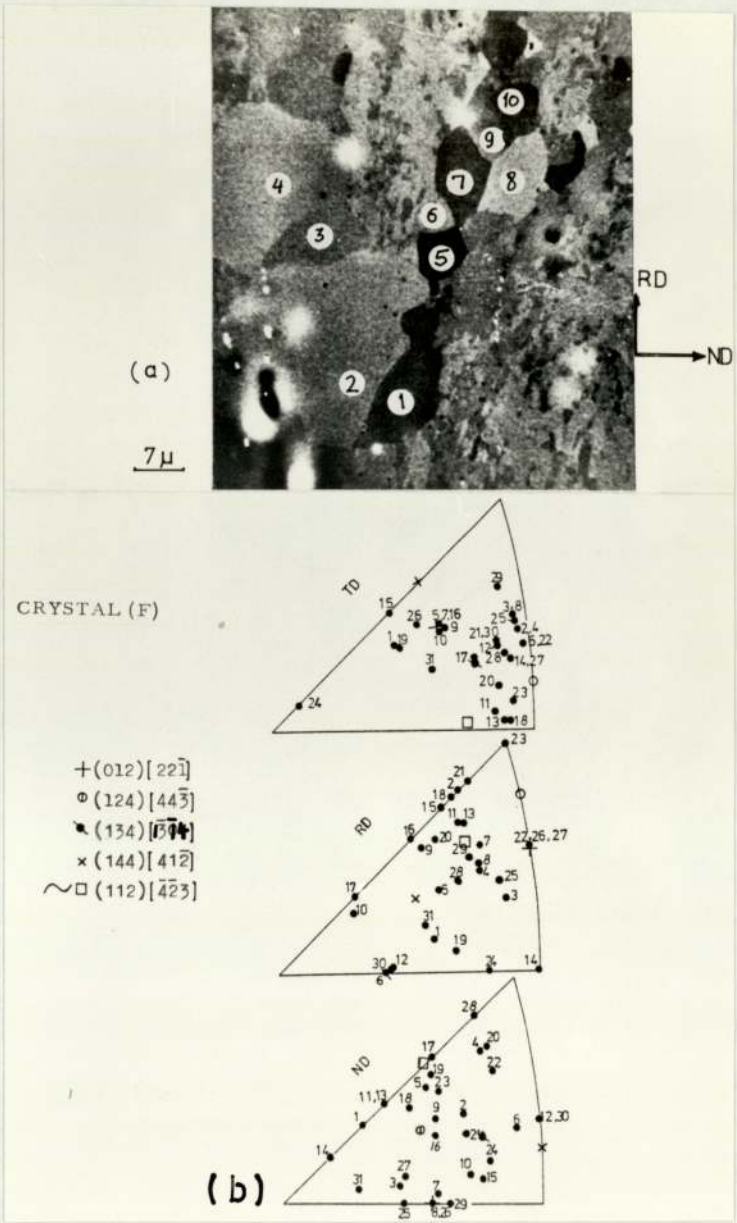

Figure 34 A composite of SEM/BSE micrograph in Al-Zn-Mg crystal F after rolling reduction 80% and partially annealed in longitudinal section

a) back-scattered electron image showing recrystallisations within the shear bands

b) orientations of selected grains indicated in (a) and other areas determined from selected area channeling patterns (Selected area Kikuchi patterns)

2 - Crystal (G):- Examination of the partially recrystallised specimen showed that the recrystallised grains occurred preferentially within the shear bands. The micrograph also shows that there are more than two bands of new grains. The recrystallisation behaviour of this crystal was different from the previous crystal in that it recrystallised very fast, with the production of large grains. The orientations of these new grains, formed along the shear bands which are shown labelled in Figure (35 a), together with others, were determined by (SACP) and the results were plotted in Figure (35 b). Examination of these orientations of the new grains showed that they differed from those of the fully recrystallised sample, i.e. there was no association between the first formed grains and the fully recrystallised grains.

3 - Crystal (H):- This crystal also showed similar features when partially recrystallised as described before, and the recrystallisation occurred within the shear bands and spread through the specimen. Compared with crystal (G) the recrystallised grains were smaller, but were larger than those in crystal (F). The orientations of the recrystallised grains labelled in the area shown in Figure (36 a) and from other areas, were determined by using SACP,and the results were plotted as shown in Figure (36 b). A wide scattering in these orientations is evident, but there was some distinct tendency for the T D to lie near (112). However these orientations determined from the recrystallised grains formed within the shear

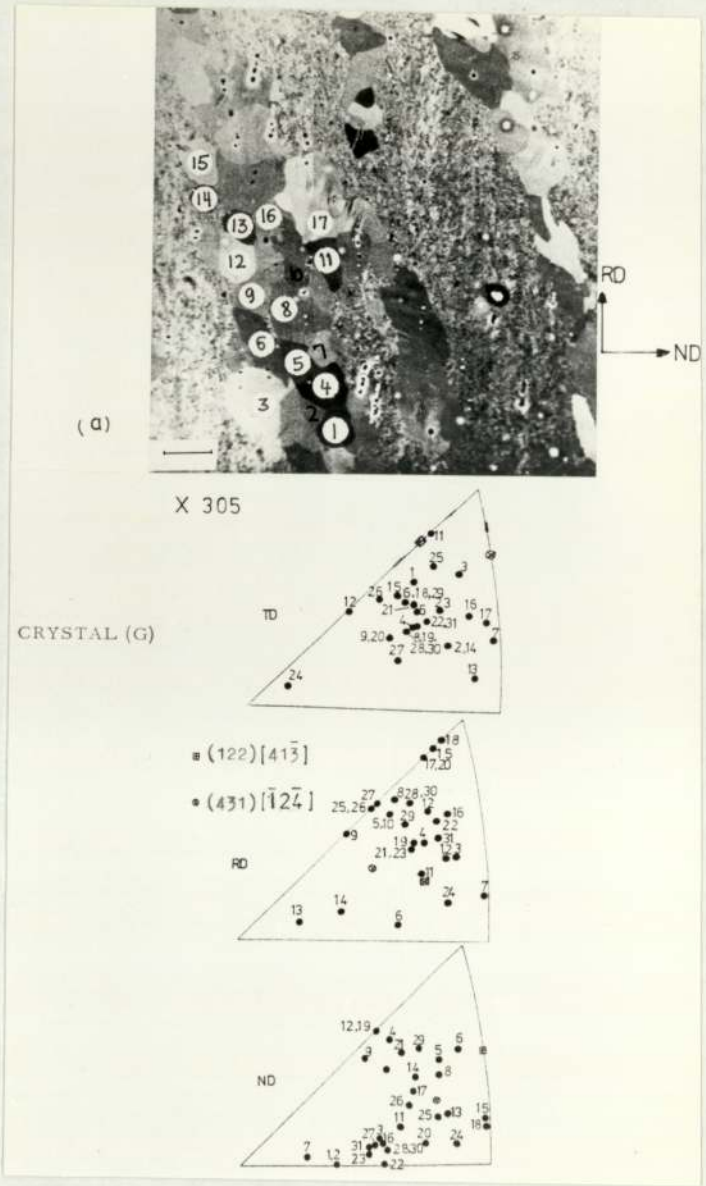

Figure 35 A composite of SEM/BSE micrograph in Al-Zn-Mg crystal G after rolling reduction 80% and partially annealed in longitudinal section

a) back-scattered electron image showing recrystallisations within the shear bands

b) orientations of selected grains indicated in (a) and other areas determined from selected area channeling patterns. (Selected area Kikuchi patterns)

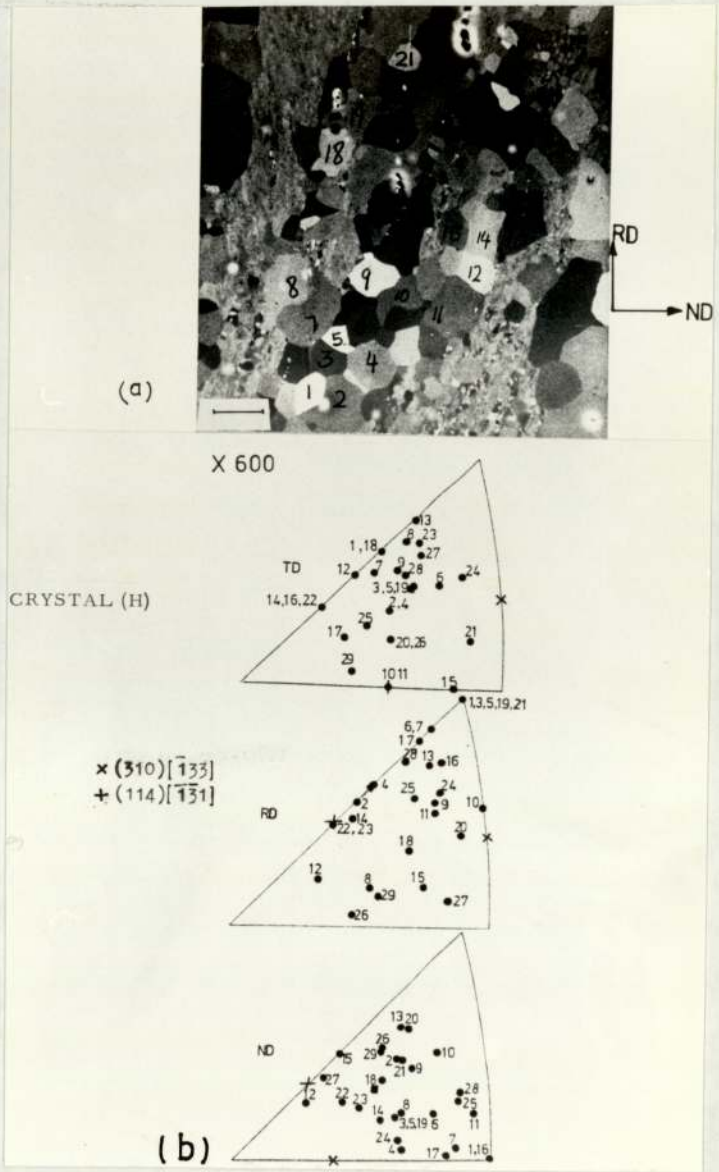

Figure 36 A composite of SEM/BSE micrograph in Al-Zn-Mg crystal H after rolling reduction 80% and partially annealed in longitudinal section

a) back-scattered electron image showing recrystallisation within the shear bands

b) orientations of selected grains indicated in (a) and other areas determined from selected area channeling patterns. (Selected area Kikuchi patterns)

band do not show any association with the texture of the fully recrystallised specimen.

4.4. X-Ray Examination

An x-ray diffraction technique was used to determine the lattice parameter and the crystal structure of Mg_2Si. Bragg's law was used to index the x-ray traces which correspond to an f.c.c. lattice. The structure cell was confirmed as f.c.c. and the true lattice parameter was determined by using powder methods. The specimens were prepared as described in section (3.3.5). From each diffraction line the lattice parameters were determined and the results were plotted on a graph against an angular function of the $\frac{1}{2}\left(\frac{\cos^2\theta}{\sin\theta}\right) + \frac{\cos^2\theta}{\theta}$) and then extrapolating the curve to $\theta = 90^{\circ}$.

4.5 Recrystallisation Kinetics in Single Phase and Two Phase Aluminium Alloys

Recrystallisation curves of aluminium alloys rolled 90% reduction at room temperature and annealed in a salt bath furnace at 350°C for various lengths of time are shown in Figure (37), for single phase and two-phase Al-Mg-Si and Al-Zn-Mg alloys. It is clear that in the material with no second phase i.e. curve (C), shows an incubation period and the early stage of recrystallisation was retarded compared with those materials with a second phase, curve (A) or shear bands formation curve (B). After an incubation period in curve (C) the recrystall-

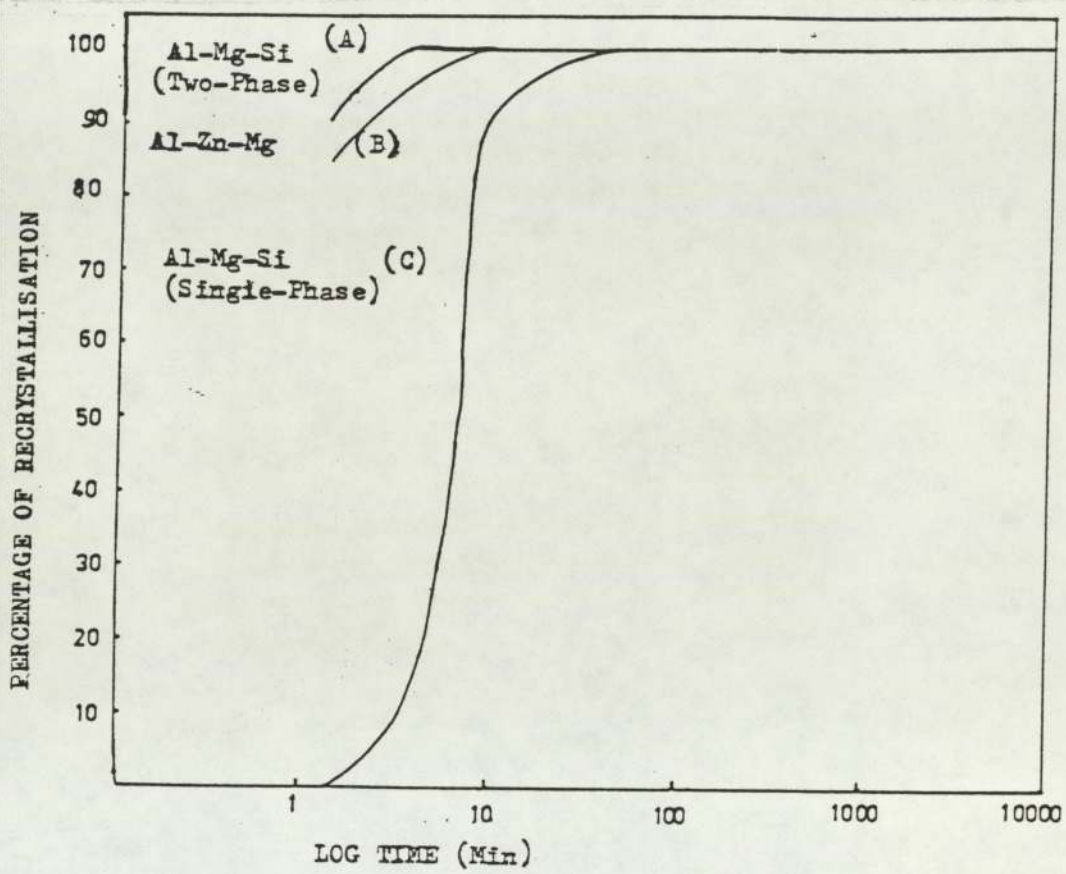

Figure 37 Isothermal recrystallisation curve in single phase, second phase Al-Mg-Si and Al-Zn-Mg alloys, rolled 90% reduction at room temperature, annealing temperature 350^{o}C

isation rose rapidly. Initially nuclei of strain-free grains begin to grow from a number of sites in the cold-worked matrix, the number of sites increases with time, and new nuclei continue to form until the entire cold-worked matrix is consumed. Accelerated recrystallisation was observed in Al-Zn-Mg material but the fast recrystallisation occurred in the Al-Mg-Si alloy which reached nearly 90% recrystallisation after only 1 minute at 350°C.

4.6 Transmission Electron Microscopy

4.6.1 Morphology and the Habit Plane of the Mg_2Si Particles

Specimens for TEM were prepared as described in section (4.3.3). The results of this observation can be seen in Figure (38), which show equilibrium Mg_2Si precipitates in the Al-Mg-Si alloy which were formed after ageing for 48 hours at 450°C, then furnace cooled to 350°C and held at that temperature for 72 hours. Figure (38 a) shows thin plates of Mg_2Si lying on habit planes nearly parallel to the beam. Figure (38 b) shows all three orientations of the platelet particles labelled A,B and C. 'A' is a small, square plate lying parallel to the foil surface, 'B' and 'C' are holes caused by the etching away during thinning, but indicate that the plates were lying on two other variants of the {100} habit plane, in this case the {100} and {010}. A diffraction pattern was obtained from the same area and is shown in Figure (38 c), with (001) orientation. It is difficult to identify any diffraction

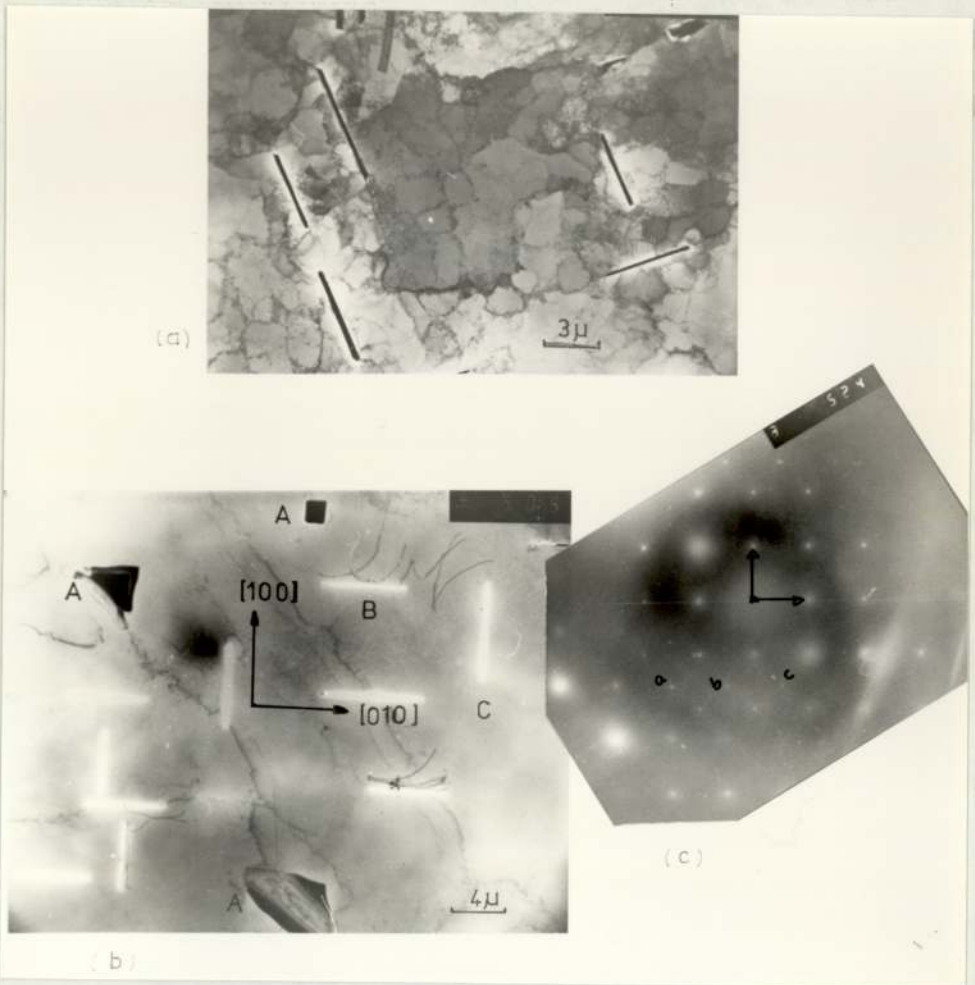

Figure 38 TEM micrograph of Al-Mg-Si alloy as aged before rolling.

a) platelets of the equilibrium Mg_2Si

b) different area showing three orientations of Mg_2Si visible at A,B and C, (001) matrix orientation

c) A selected area electron diffraction pattern from area (b)

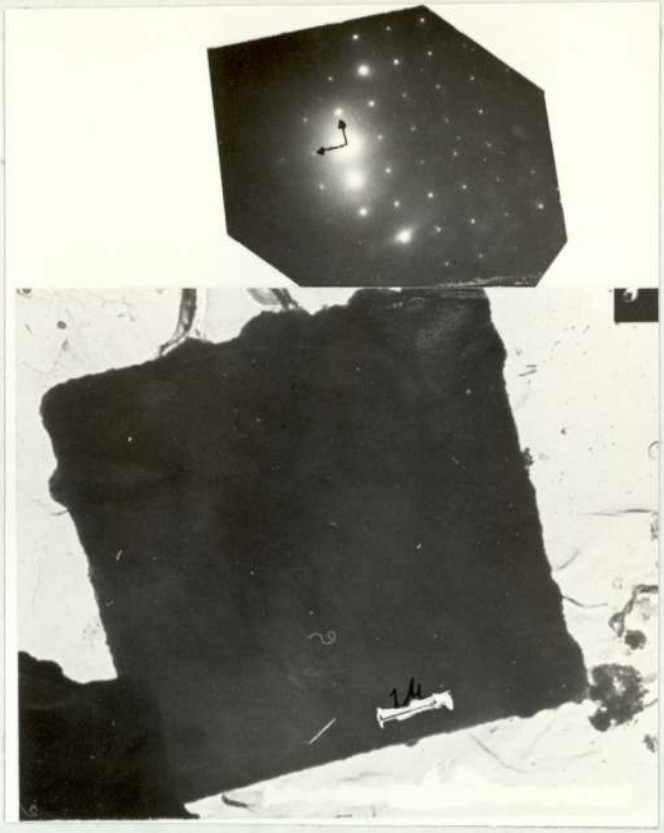

Figure 39 Electron micrograph of individual particle of Mg_2Si and microdiffraction pattern from same particle

spots from the Mg_2Si particles, to find the orientation relationship between the Mg_2Si and the matrix. During this examination it was hard to get a diffraction pattern from the particles, so the particles were separated from the matrix by dissolution of the material. Specimens for TEM were prepared by placing a drop of solution containing Mg_2Si in suspension onto a carbon support film and examining this in the TEM. The results of this examination are shown in Figure (39) which shows an example of an individual Mg_2Si square-shaped platelet. A diffraction pattern from the same platelet is shown in Figure (39). The structure was identified as consistent with the f.c.c. structure cell.

4.6.2 Deformation Structure

4.6.2.1 Al-Mg-Si Alloy

TEM investigation was carried out on cold-rolled Al-Mg-Si alloys at room temperature in the range (50-90%) reduction, in longitudinal sections where second phase particles had been induced prior to rolling. TEM specimens were prepared as described in section (4.3.3.1). The deformation structure depends on the size and type of particles present in deformed material. The Al-Mg-Si alloy contained coarse, non-deformable platelets of Mg_2Si which were oriented parallel to <100> direction. So the area very close to the particle surface does not deform i.e. no slip occurred at the particle-matrix interface. Homogeneous slip would be inhibited by the

presence of these particles. So during particle rotation the particle/matrix interface element carried with the particle must rotate towards the rolling plane. The deformation microstructure of Al-Mg-Si deformed to different strains showed the gradual development of a well-defined cell structure. The cell boundaries become distinct at a strain (ε=2.3), and the cell size decreased with increasing strain. Figure (40) shows the sequence of deformed structures. At low strain i.e. (ε=0.7), the microstructure mostly showed large elongated slub-shaped subgrains with dislocations inside them. There was also evidence of dislocation tangles near the particles. Certain regions contained a high dislocation density, but cell structure had not formed and there were only a few small subgrains with sharp boundaries, with very small dislocation free areas, Figure (40 a). The direction of the large subgrains was parallel to the R D. After large deformation, the microstructure was nearly uniform and consisted of small subgrains oriented parallel to the R D, as shown in Figure (40 b). At this level of strain the majority of the particles lay parallel to the R D, and because the particles were platelet shaped and nearly straight, the microstructure some distance from the precipitates was aligned parallel to the R D. But if the particles had a habit plane parallel to the plane of rolling the band like matrix microstructure was locally disturbed near the particles so that it flowed above and below the plates,curved and then joined together and became nearly straight and parallel to the R D. It is clear that at high strain some recovery took place during

Figure 40 TEM micrographs showing deformation microstructure (Longitudinal Section) of Al-Mg-Si rolled

a) 50%

b) 90%

either specimen preparation or specimen examination inside the microscope. Recovered structures are evident in the electron micrograph of Figure (40 b).

A general view of the deformation structure of the crystals A, B and C containing coarse, non-deformable second-phase particles, was band-like with well defined cell structures of various sizes and widths. Figures (41 a,b,c) are a montage of electron-micrographs from rolled crystals to about 71% reduction in longitudinal sections, and are typical of the deformation structure. It is quite clear from the TEM micrographs in polycrystalline material and single crystals, that no shear bands were formed in agreement with the optical observations. In all cases the major difficulty in TEM studies of the deformation zone, was the impossibility of observing the structure of the deformation zone. This area was very sensitive to chemical attack and it polished faster than the rest of the deformed matrix which made detection of Kikuchi lines very difficult.

In order to study the orientations in area around the particles in more detail, many selected area Kikuchi patterns from small subgrains were obtained from accurate measurements of orientation. At 50% reduction the microstructure of subgrains is not as clear as at higher reductions.

Thin foils of specimens of 70% and 90% reduction from Al-Mg-Si polycrystalline materials were prepared as

(a)

Figure 41 (a) Montage of Al-Mg-Si single crystal A cold rolled 71% (Longitudinal Section) showing the deformation microstructure

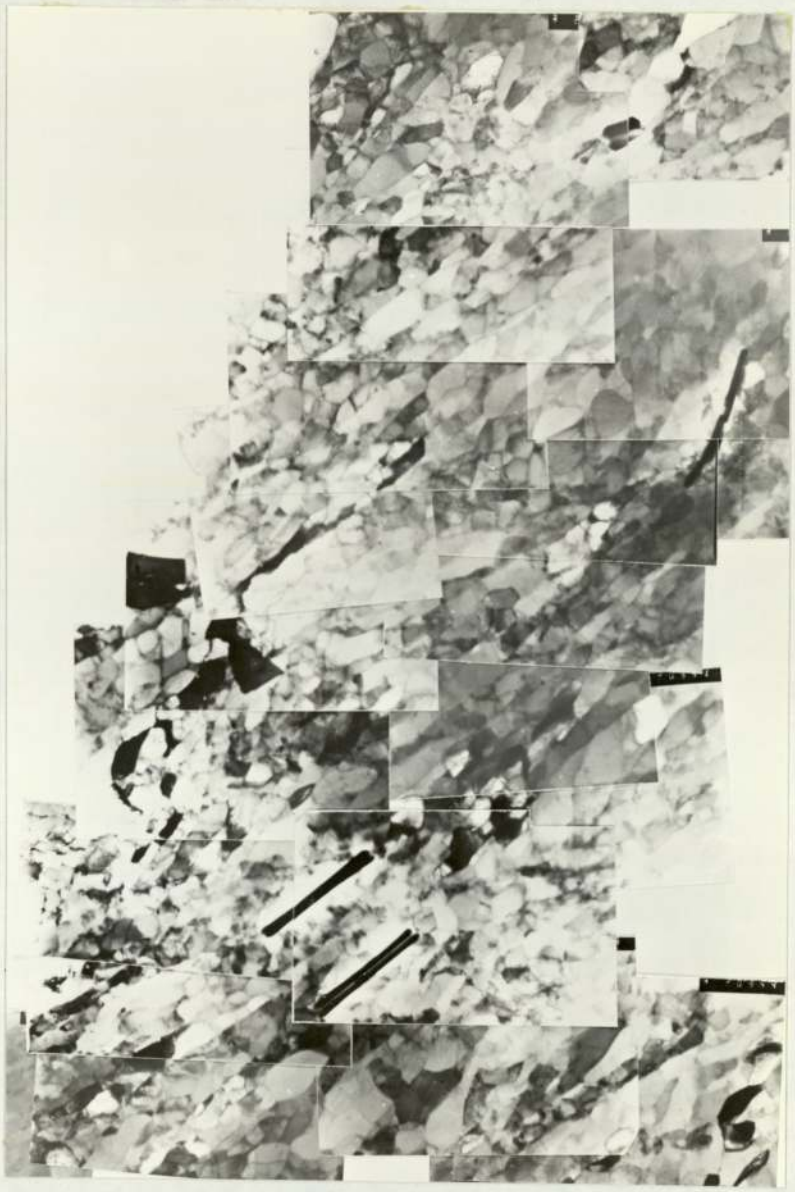

(b)

Figure 41 (b) Montage of Al-Mg-Si single crystal B cold rolled 71% (Longitudinal Section) showing the deformation microstructure

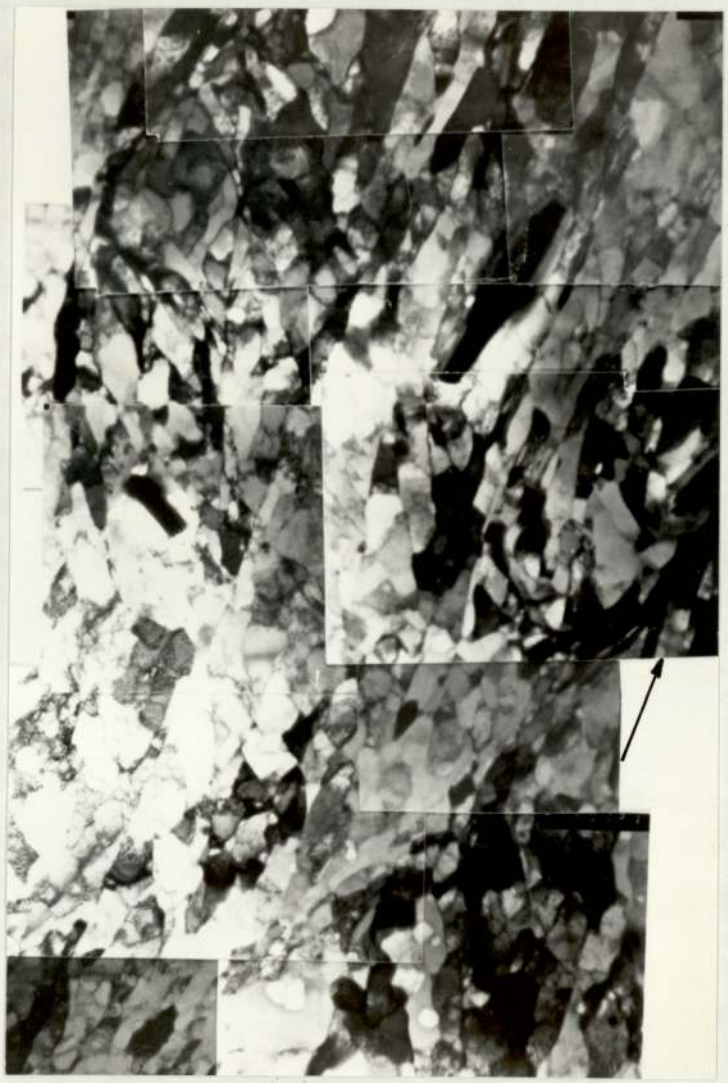

(c)

Figure 41 (c) Montage of Al-Mg-Si single crystal C cold rolled 71% (Longitudinal Section) showing the deformation microstructure

described in section (4.3.3.1) in longitudinal sections. The subgrain orientations around the particles were determined from areas labelled in Figures (42a,43a). Because this region was strongly distorted a nearly random orientation of subgrains was observed, as shown in Figures (42b,43b). At high reductions, the recovery process was observed to lead to sharp subgrains as shown in Figure (43b). This effect was not observed at lower reductions up to 70%.

In order to get more understanding of the orientations in the vicinity of the particles, single crystals of Al-Mg-Si were prepared as described in section (3.3.6) with various orientations containing coarse, hard second phase particles prior to rolling. These were deformed to about 70% reduction at room temperature to the final thickness of about 0.9 mm. Thin foils from the longitudinal sections were prepared as described in section (3.3.3) from each rolled crystal although the success rate in getting good thin foils from the narrow thickness was small. The deformation state in rolled crystal (A) with an initial orientation close to (110)[001] is shown in Figure (44 a,b). An extensive study of the orientation variation around the particles was made on a number of specimens using selected area Kikuchi patterns (SAKP). Figure (44b) shows a different Mg_2Si particle which was not oriented near to the rolling direction. The orientations of 68 subgrains around the particles were determined, and the results are plotted in Figure (44c). It is clear that a distinct population of orientations

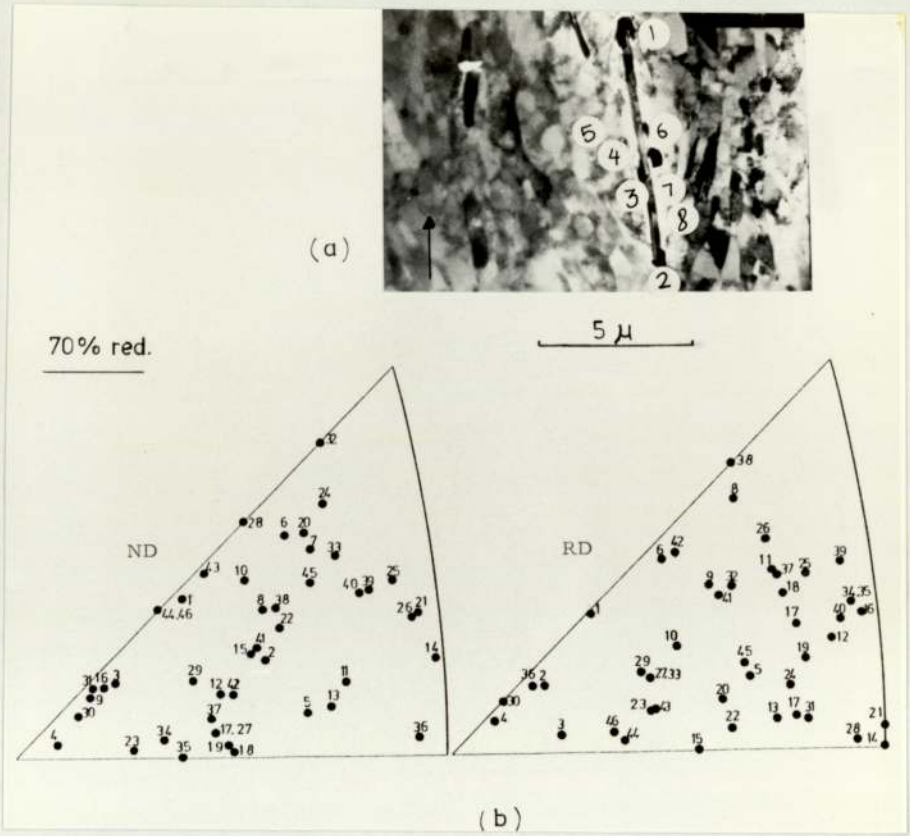

Figure 42 Electron micrograph of 70% cold rolled Al-Mg-Si alloy (Longitudinal Section)

a) locations of selected area Kikuchi patterns

b) orientations of the subgrain determined from area (a) and other areas

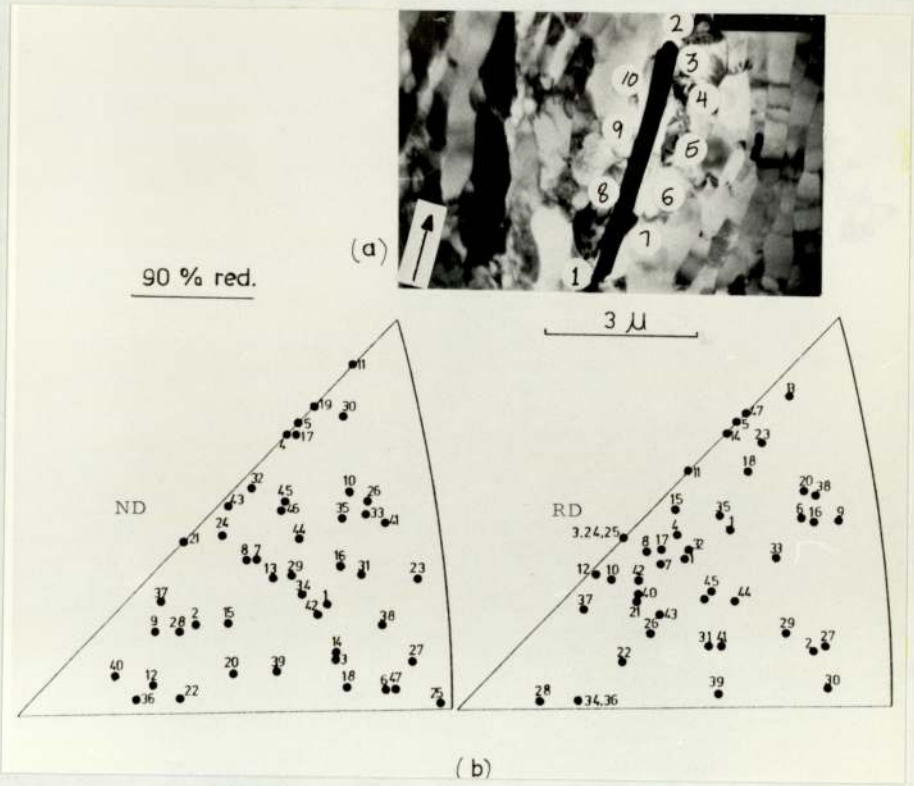

Figure 43 Electron micrograph of 90% cold rolled Al-Mg-Si alloy (Longitudinal Section)

a) locations of selected area Kikuchi patterns

b) orientations of the subgrain determined from area (a) and other areas

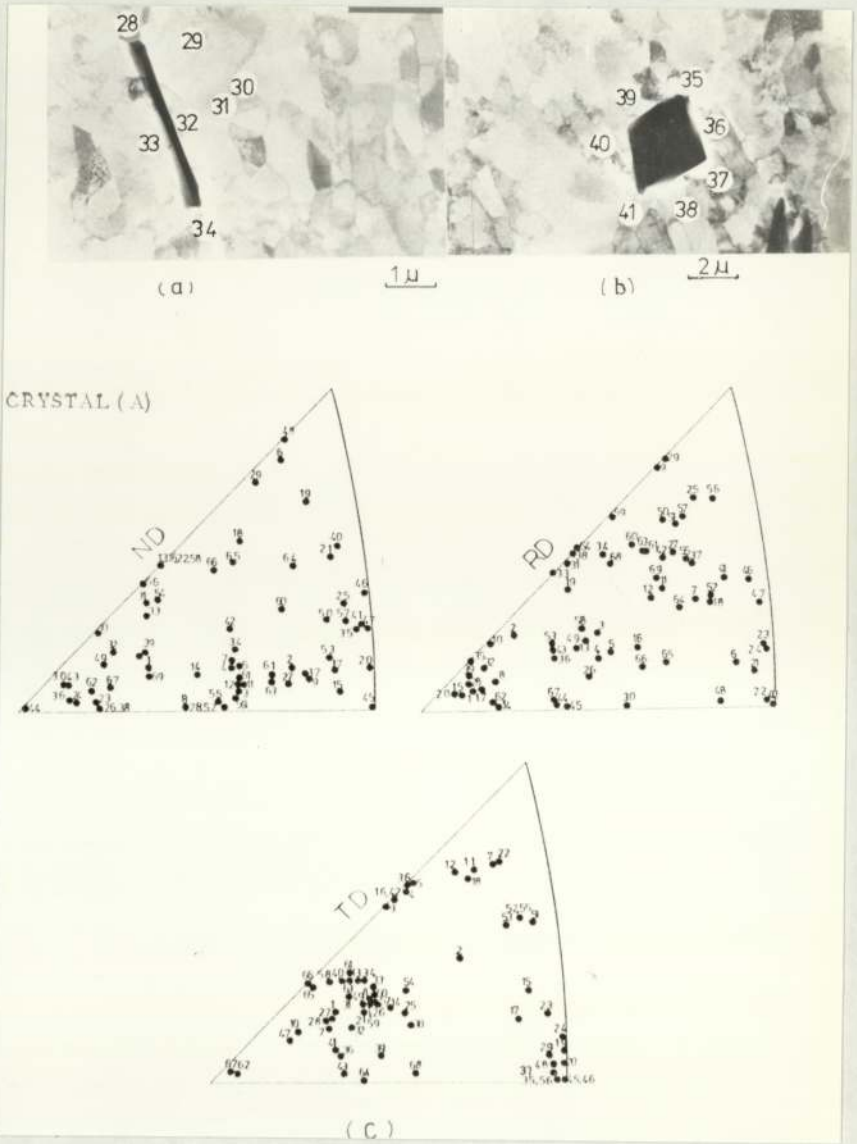

Figure 44 TEM micrographs of 71% cold rolled crystal A of Al-Mg-Si (Longitudinal Section)

a,b) locations of selected area Kikuchi patterns

c) orientations determined from areas (a,b) and other areas

was present, but with a wide scatter. In the transverse direction there is in addition to the orientations accumulated near (011), also some scattered patches of orientation. Also there was an orientation near to (001).

In crystal (B) with $(231)[\bar{1}2\bar{4}]$ orientation, the deformation microstructure is shown in Figure (45 a,b). The orientations of subgrains around the particles were determined by selected area Kikuchi patterns and the results are plotted in Figure (45c) in three unit triangles, one for the rolling plane orientation and the other for the rolling direction and the normal direction. There was a wide spread, with patches of orientation present.

For the last unstable single crystal with orientation $(041)[34\bar{1}]$, the deformation structure is shown in Figure (46a). The orientations of the subgrains around the particles from the same area as in Figure (46b) were measured. The subgrains orientations were widely spread.

4.6.3 Annealing Structure of Al-Mg-Si Alloy

The TEM investigation was carried out on specimens rolled to 70% and 90% reduction, and annealed in a salt bath furnace at 300°C for 10 s and 5 s respectively. The recrystallisation behaviour of Al-Mg-Si which contained large, non-deformable particles was determined by nucleation which occurs preferentially in the vicinity of the particles, where the local deformation and dislocation density were high.

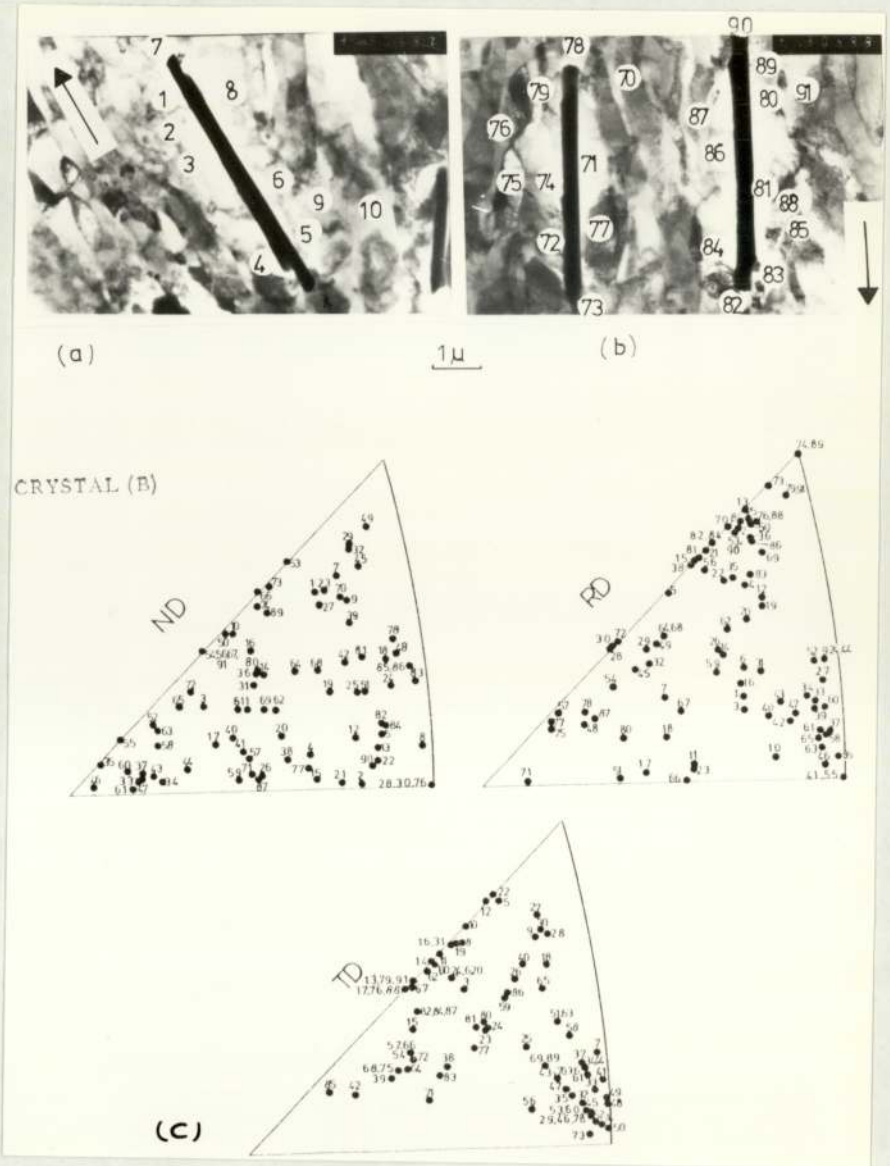

Figure 45 TEM micrographs of 71% cold rolled crystal B of Al-Mg-Si (Longitudinal Section)

a,b) locations of selected area Kikuchi patterns

c) orientations determined from areas (a,b) and other areas

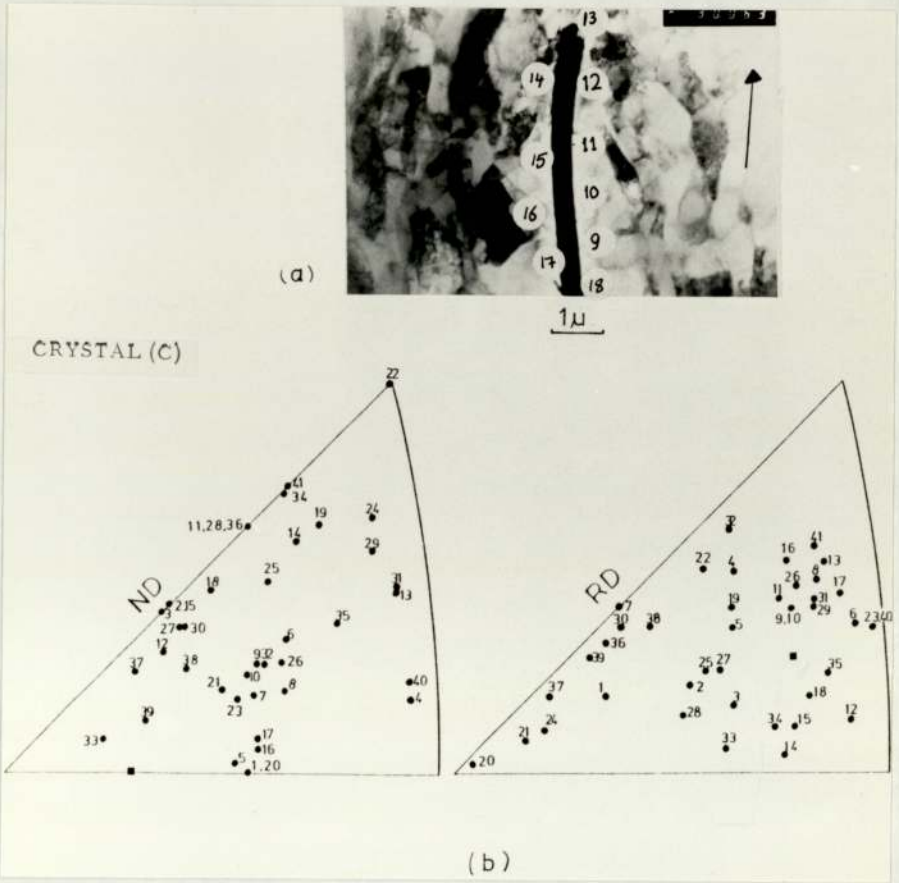

Figure 46 TEM micrographs of 71% cold rolled crystal C of Al-Mg-Si (Longitudinal Section)

a) locations of selected area Kikuchi patterns

b) orientations determined from area (a) and other areas.

After 70% reduction, the TEM micrographs showed three different events of nucleation adjacent to the particles. In most cases more than one grain nucleated at each particle, as shown in Figure (47a) where there are three nuclei located near to the particle. In Figure (47 b.c) large nuclei were formed at one end of the particles and grew quickly in the deformation zone until the whole zone was consumed, and nuclei surrounded the whole particle. Nucleation in the deformed matrix was difficult to observe. Sometimes where there was one large nucleus, as shown in Figure (47b), it is difficult to know whether there was one nucleus formed or whether others formed but were consumed by one rapidly growing nucleus. The growth direction of these nuclei formed near to the particles within the deformation zone, was nearly parallel to the rolling direction. In order to get more information about the orientation of nuclei formed adjacent to the particles, more than one area was investigated using selected area Kikuchi patterns, and the results of these orientation determinations are shown in Figure (47d) and it appears that these are effectively random.

After 90% reduction, the partially recrystallised specimen showed that nucleation occurred adjacent to the particles and more than one nuclei was observed to form at each particle. At this level of deformation, recovery processes have been observed such as are shown in Figure (48 a,b). The orientations of the recrystallised grains were determined by selected area Kikuchi patterns and the results were plotted and shown in Figure (48c),

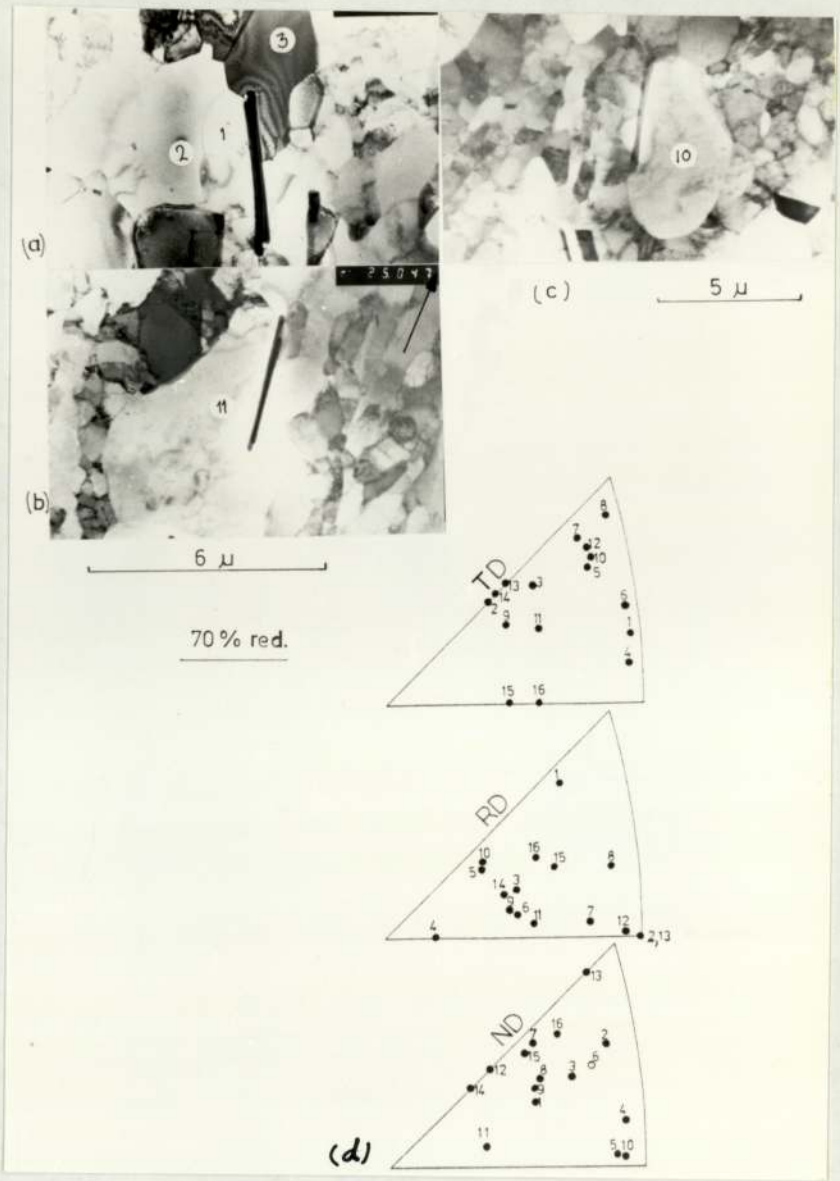

Figure 47 TEM micrographs of partially recrystallised specimen of 70% reduction in Al-Mg-Si alloy

a,b & c) locations of selected area Kikuchi patterns

d) orientations of recrystallised grains

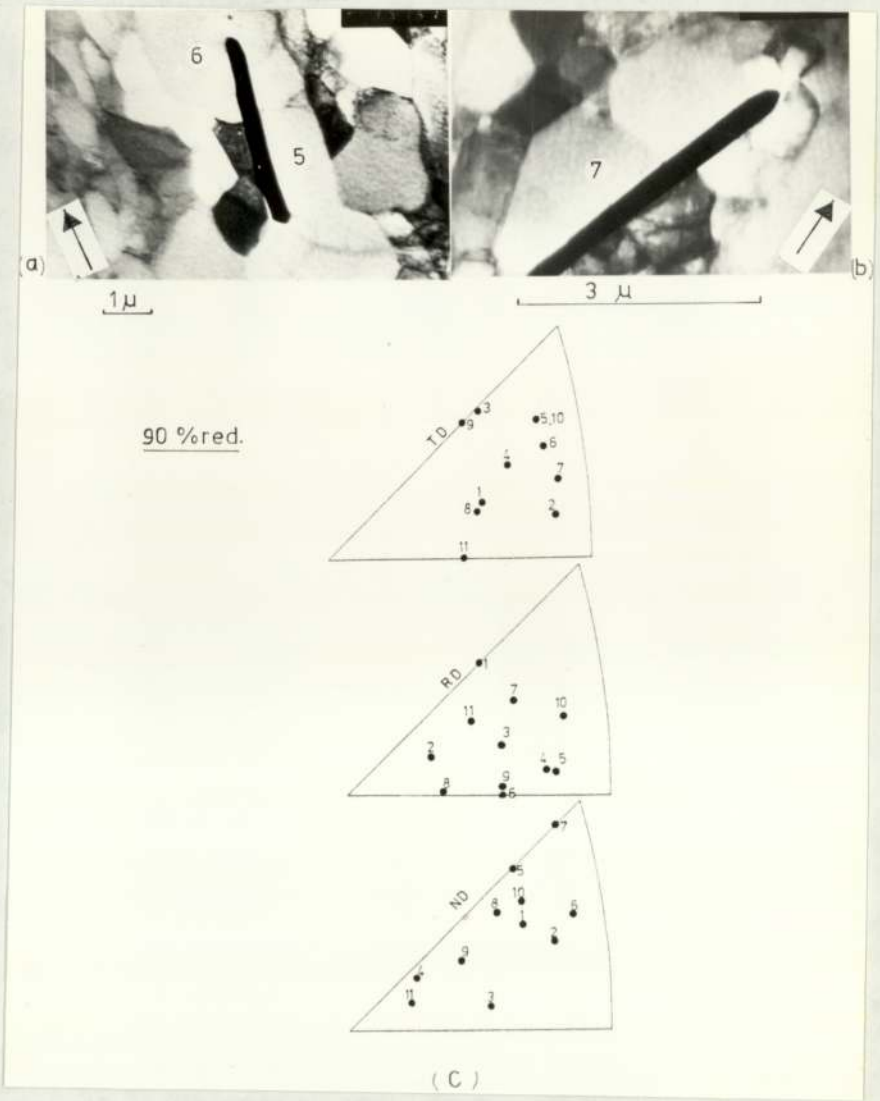

Figure 48 TEM micrographs of partially recrystallised specimen of 90% reduction in Al-Mg-Si alloy

a,b) locations of selected area Kikuchi patterns

c) orientations of recrystallised grains

which shows large scattering in orientation distribution.

Single crystals of various orientations were rolled to 70% reduction and then annealed in a salt bath furnace at 300°C. In crystal (A) of (110)[001] orientation, rapid recrystallisation occurred after 5 s, and the recrystallised grains were formed in the vicinity of the particles where the large lattice rotation was produced during rolling. Figure (49 a) shows the nucleation at and surrounding the particle, while the deformed matrix is still present. Probably a little recovery took place, but no nucleation had occurred within the deformed matrix. However, it seems that although nucleation must have occurred in the deformation zone, it did not necessarily take place at the interface. More than one grain was nucleated at each particle with different orientation, and these are shown in Figure (49d). Figure (49 e,f) shows an example of particles which make an angle of 90° with the rolling direction and have buckled during deformation. The orientation of the nuclei was determined using selected area Kikuchi patterns, and the results are plotted as shown in Figure (49c).

A similar observation was made in crystals (B) and (C) after annealing for 15 s at 300°C, where the nuclei formed near to the particles, either at one end or both, or sometimes beside the particles. Also the photographs show that after the nucleation had started, the deformation structure was still present, Figures (50a, 51a,b). More than one nuclei was present. The orientations of these

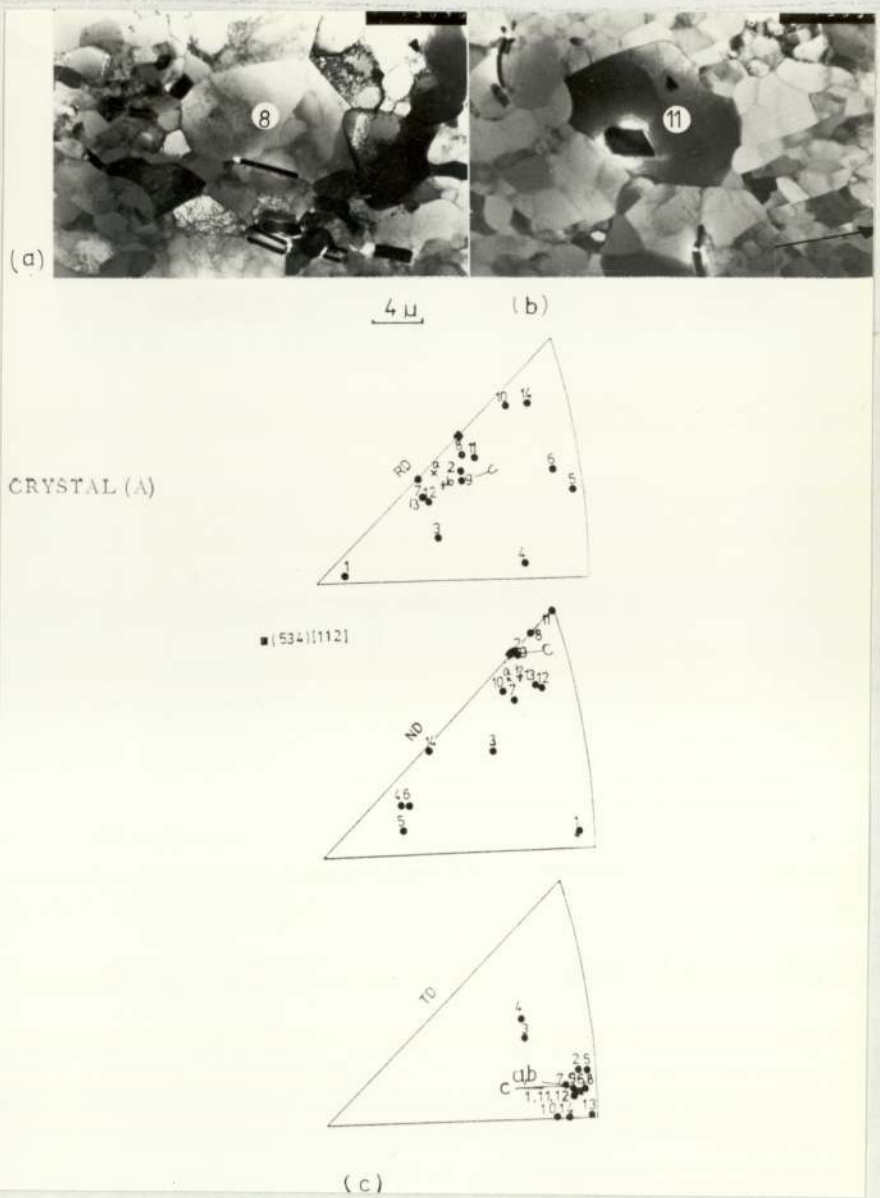

Figure 49 TEM micrographs of partially recrystallised specimen of crystal A rolled 71% of Al-Mg-Si

a,b) locations of selected area Kikuchi patterns

c) orientations of recrystallised grains

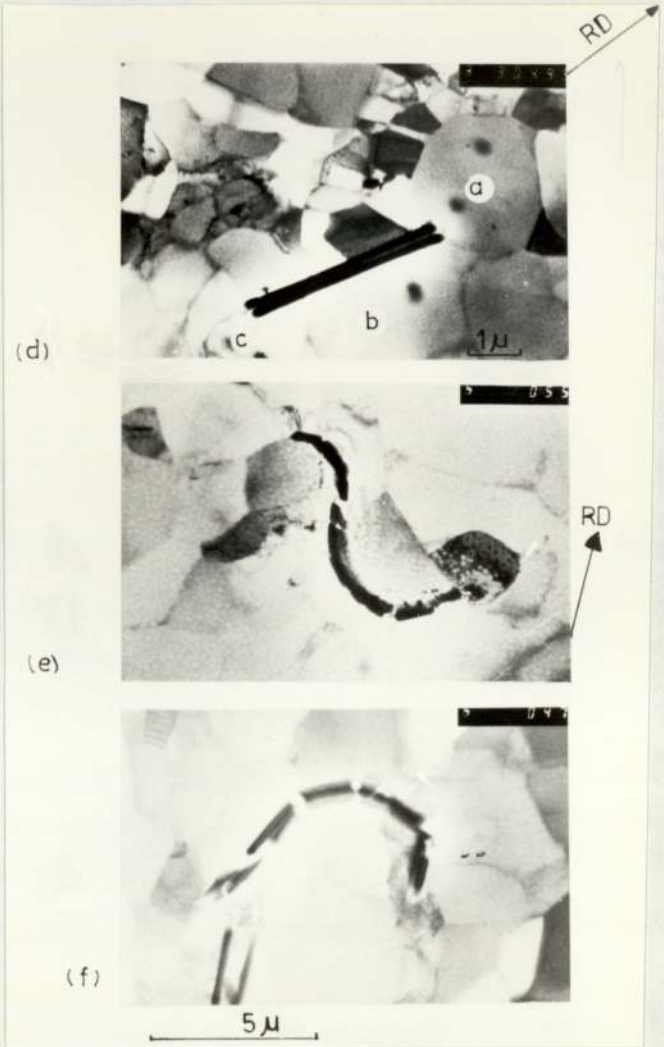

Figure 49 (cont.) TEM micrographs of partially recrystallised specimen of crystal A rolled 71% of Al-Mg-Si

d) three nuclei formed around one particle

e,f) buckling of the particle during rolling

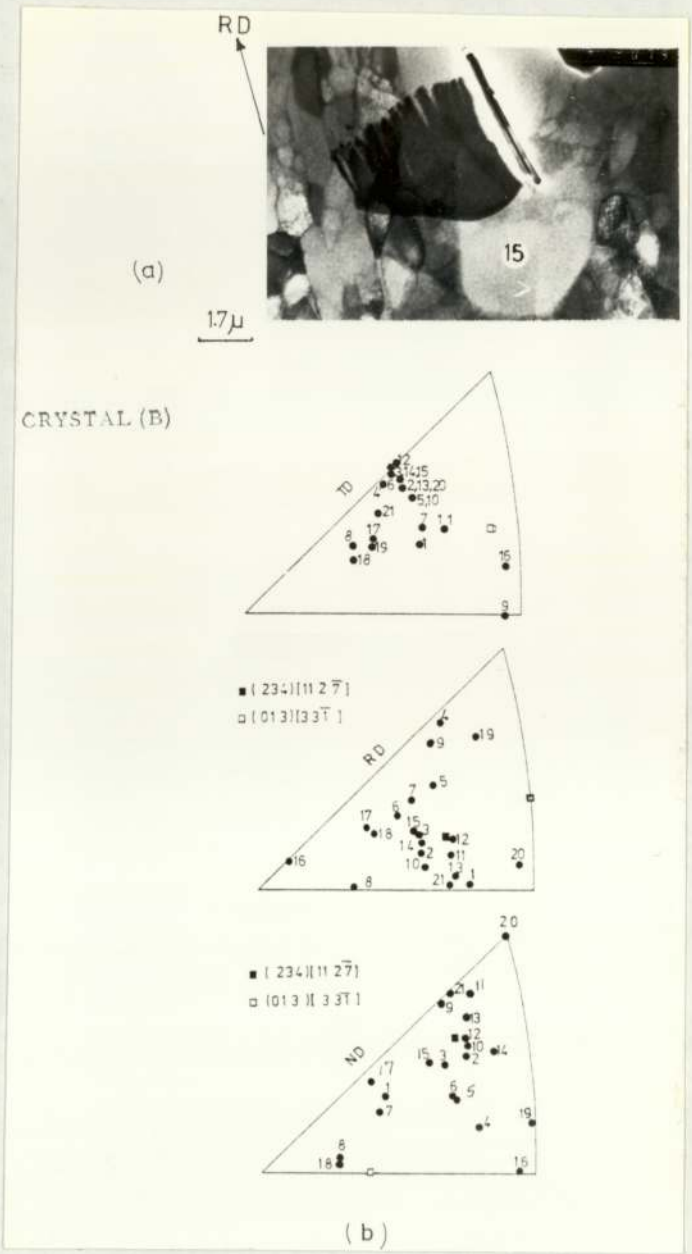

Figure 50 TEM micrographs of partially recrystallised specimen of crystal B rolled 71% of Al-Mg-Si

a) locations of selected area Kikuchi patterns

b) orientations of recrystallised grains

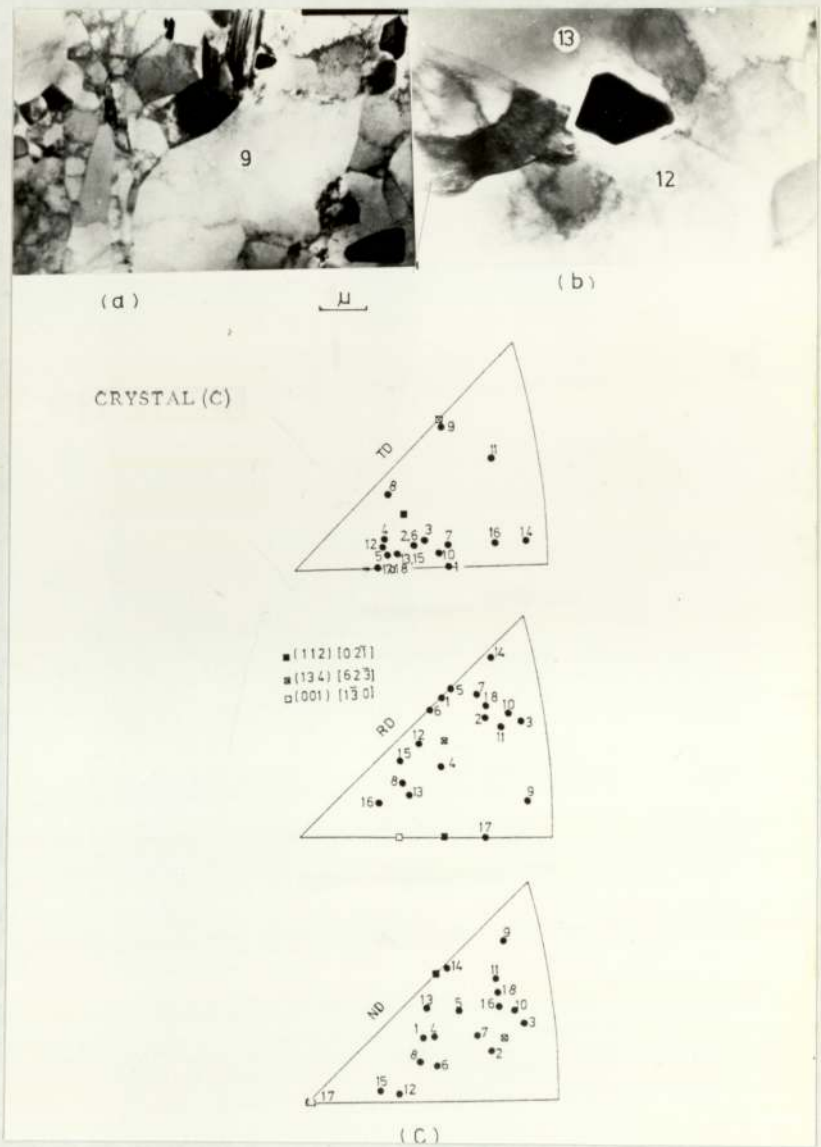

Figure 51 TEM micrographs of partially recrystallised specimen of crystal C rolled 71% of Al-Mg-Si

a,b) locations of selected area Kikuchi patterns

c) orientations of recrystallised grain

nuclei were determined by selected area Kikuchi patterns, and the results are plotted as shown in Figures (50 b, 51c)

4.6.4 Single Crystals of Al-Zn-Mg Alloy

Examination of the microstructure of cold-rolled crystals at room temperature up to 80% reduction revealed different features of each crystal, depending on the original orientation.

In crystal (E) with (110)[001] orientation, the microstructure developed thin, sheet-like ribbons or isolated bands parallel to each other running across the cell structure. The length of these bands was difficult to determine; some were traced in the microscope for 16 to 25μm. The thickness of these bands varied also between 0.3-0.7μm. Figure (52 a,b) shows an example of the rolled structure in this crystal, also the micrograph showed two narrow sets present, which agreed well with optical observation. Figure (53 a) is a montage of micrographs s showing the deformed structure of crystal (F) which had the typical microstructure after 80% reduction. A very few shear bands were present with narrow wavy shape. In this crystal it was found that shear bands dissolved preferentially during electropolishing and it was difficult to estimate their length or their width very accurately. The structure within the shear band was hard to distinguish, and also these shear bands tend to split into narrow bands which diverged from the original shear bands.

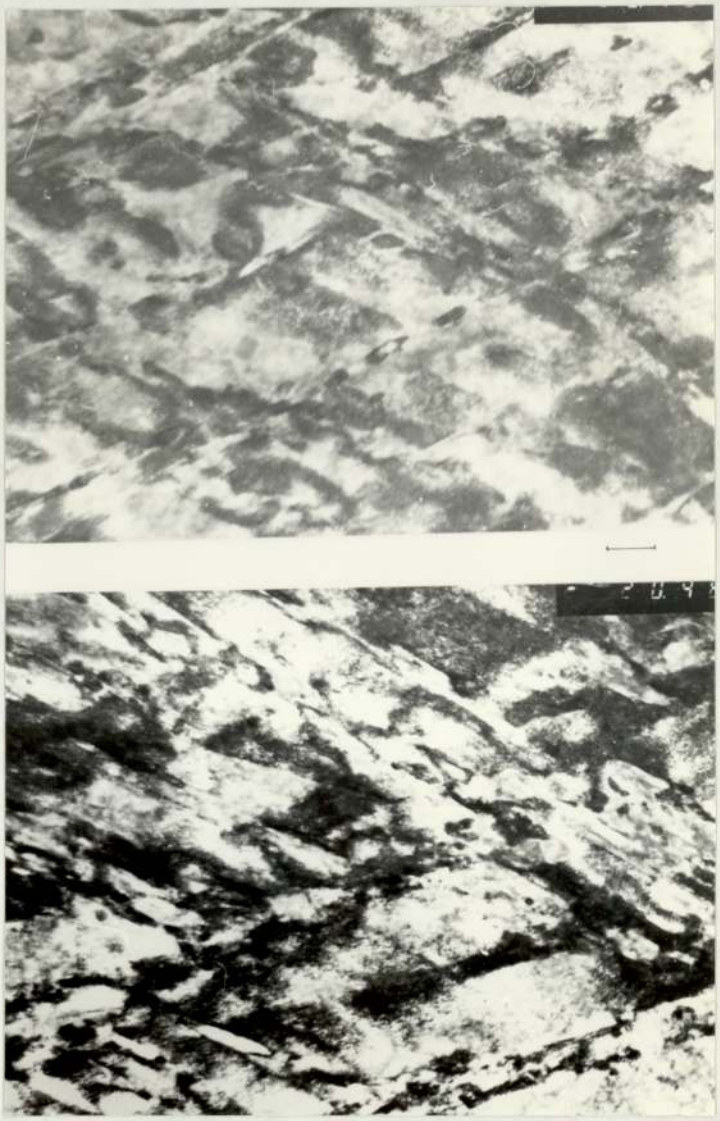

Figure 52 TEM micrograph showing deformation microstructure (Longitudinal Section) of crystal E rolled 80%

a,b) narrow and very long microbands in two directions X 12.6K

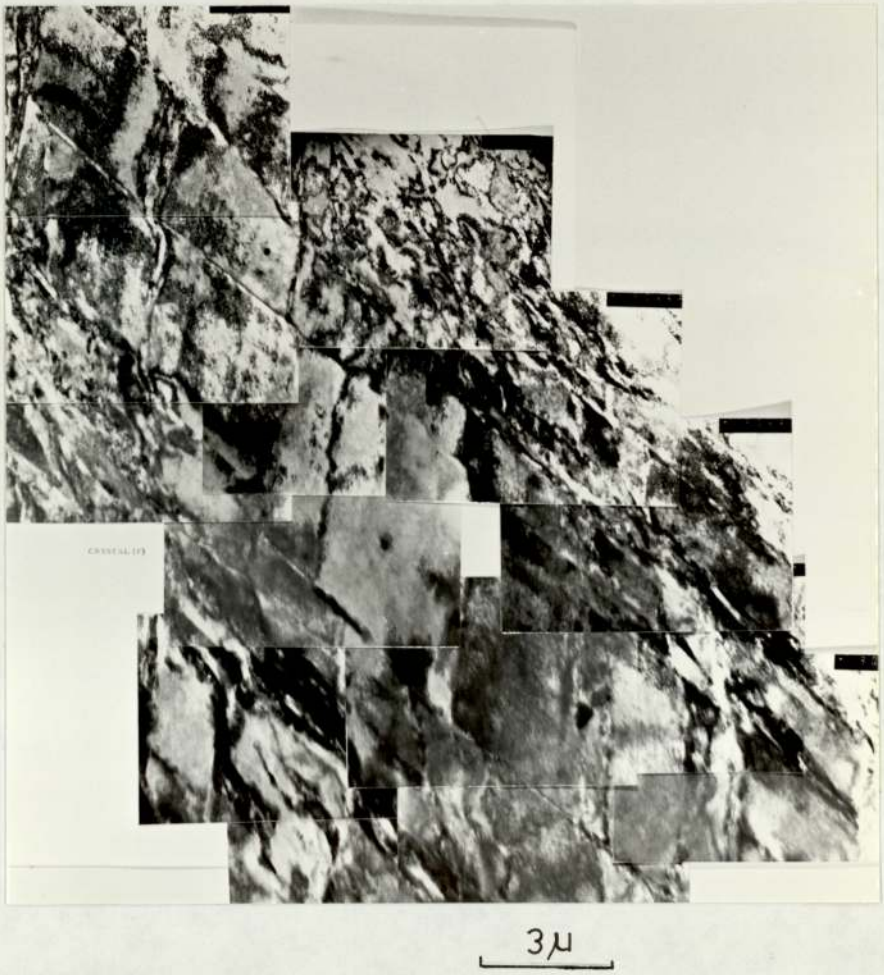

Figure 53 (a) Montage of Al-Zn-Mg single crystal F rolled 80%, showing the deformation microstructure (Longitudinal Section)

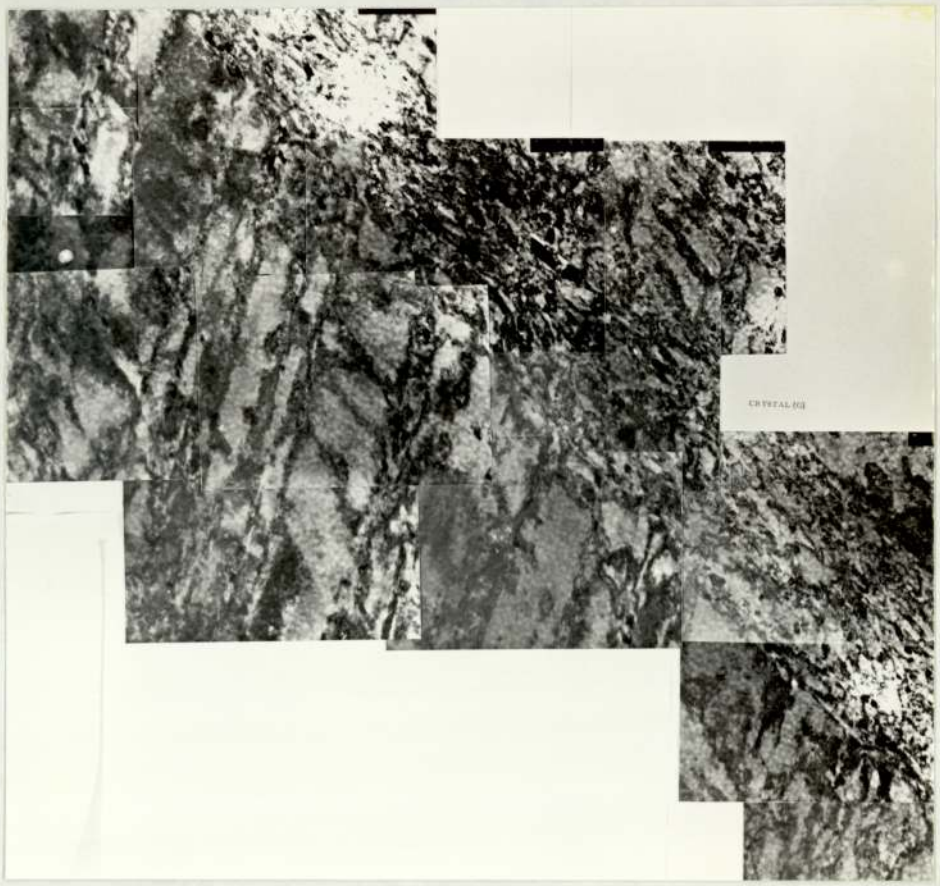

Figure 53 (b) Montage of Al-Zn-Mg single crystal G rolled 80%, showing the deformation microstructure (Longitudinal Section)

The deformation structure in crystal (G) was different from that in previous crystals, the shear bands were observed to be much thicker, with clear structure inside the shear bands. They were usually very long, and one about 35μm was formed running across the specimen. Figure (53 b) shows a montage of photographs from crystal (G) after deformation of 80% reduction.

In crystal (H), the deformation structure showed a very high density of shear bands, which were more sharp and severe than in the previous three crystals. In addition to the shear bands there were many thin sheet-like bands running across the original shear bands, with high dislocation density. Figure (54 a,b) shows that different kinds of shear bands were formed after 80% reduction. In Figure (54 a) are shown some kind of shear bands which were either split from the early-formed shear bands on the right or from the shear bands on the left making the shape of the letter N. The microstructure inside the shear bands consisted of very small, thin elongated fine crystallites.

In order to determine the orientations of the very small crystallites within the shear bands, a STEM technique was used for this purpose. Selected area Kikuchi patterns were obtained from the areas labelled in Figure (55 a) in the crystal (F), deformed 80% by cold rolling. The results of these orientation determinations from the area shown in Figure (55 a) and others were plotted in Figure (55 b). The orientations of these crystallites were

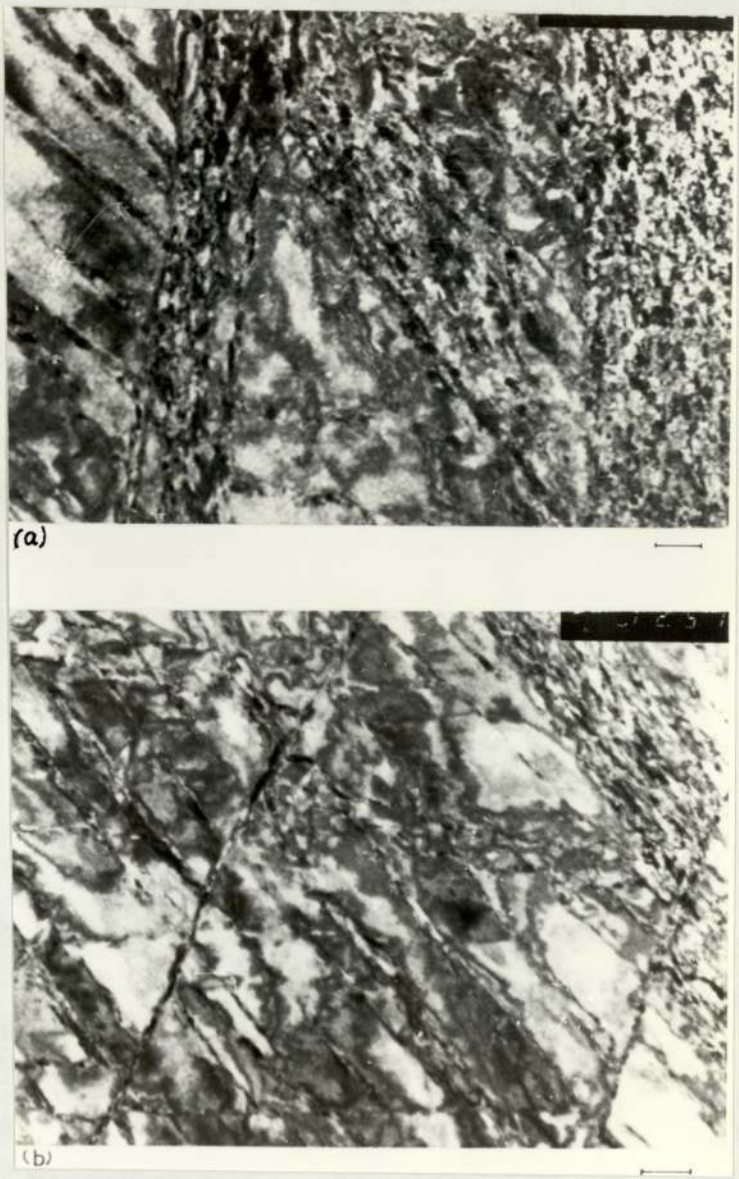

Figure 54 a,b TEM micrographs showing deformation microstructure (Longitudinal Section) of Al-Zn-Mg crystal H rolled 80%

X 11K

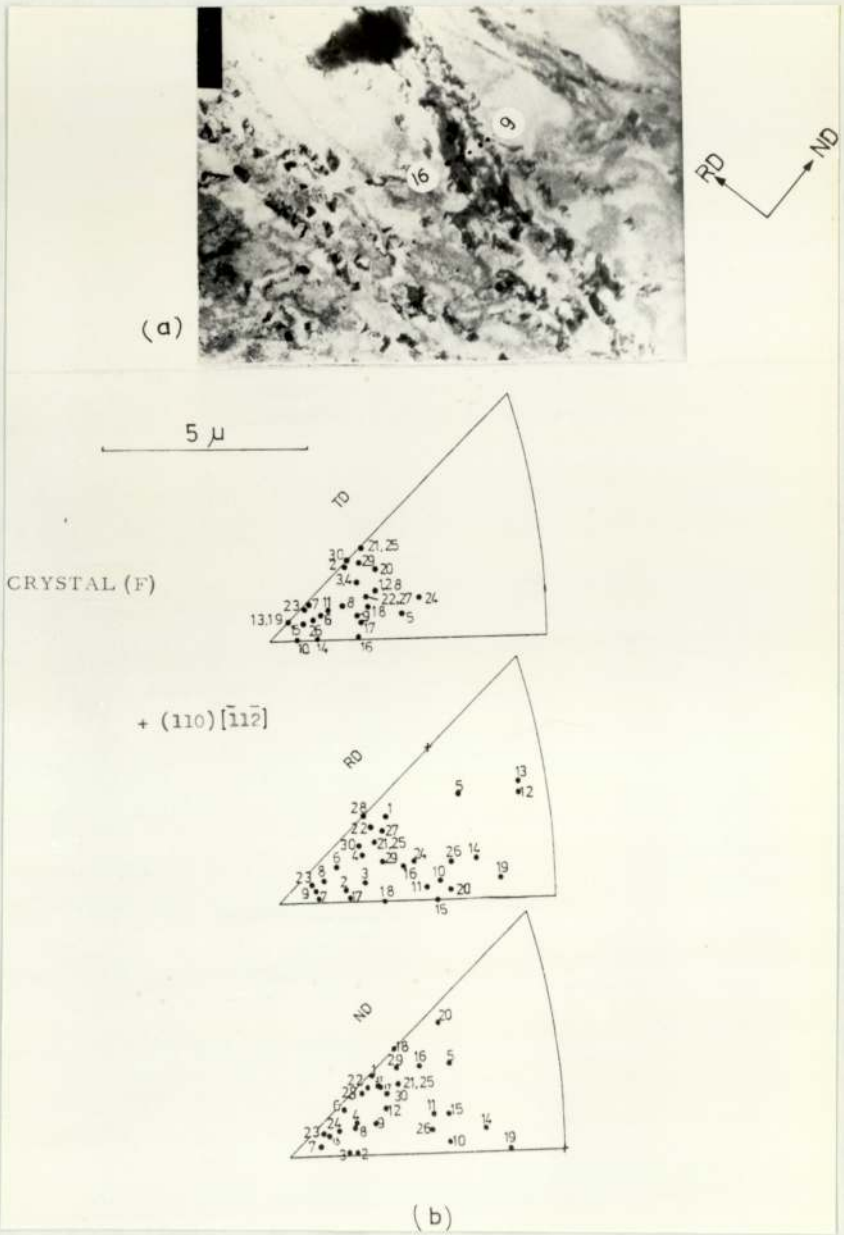

Figure 55 Analysis of orientations in shear bands in crystal F of Al-Zn-Mg alloy (Longitudinal Section)

a) Single shear band showing locations of STEM diffraction patterns

b) Orientations from locations in (a) and other shear band sites

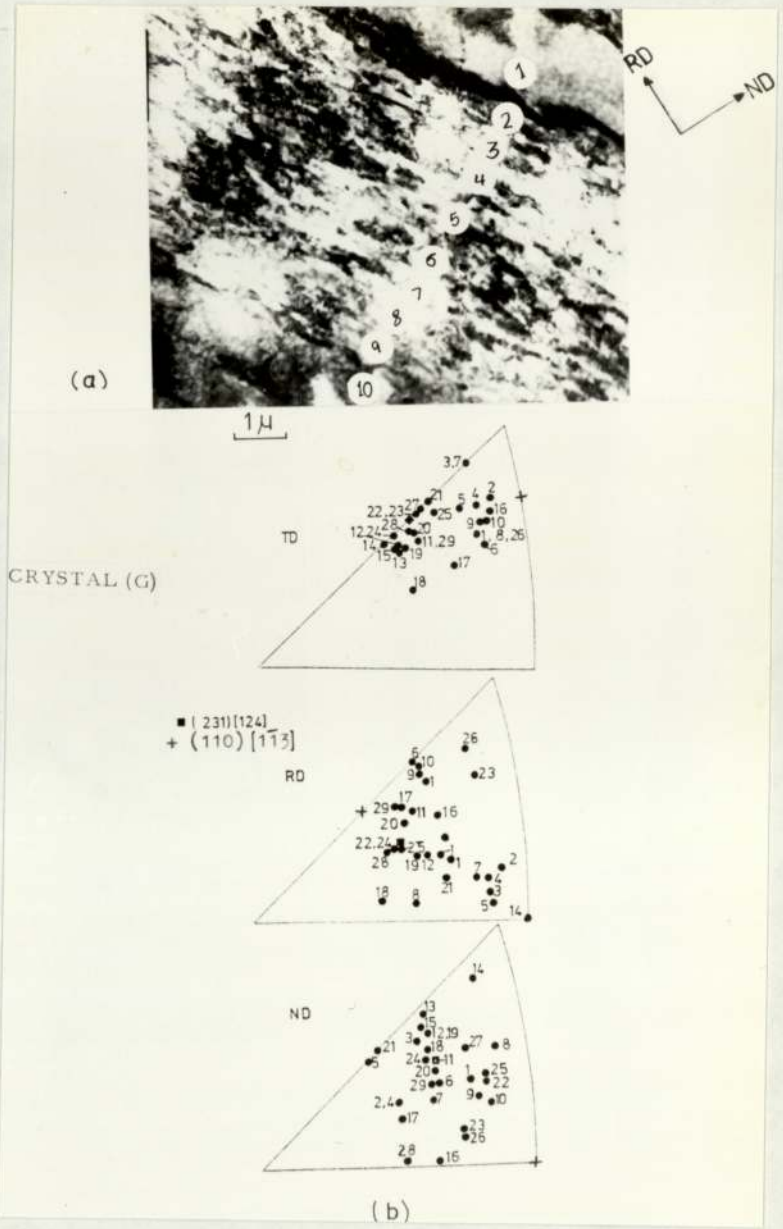

Figure 56 Analysis of orientations in shear bands in crystal G of Al-Zn-Mg alloy (Longitudinal Section)

a) Single shear band showing locations of STEM diffraction patterns

b) Orientations from locations in (a) and other shear band sites.

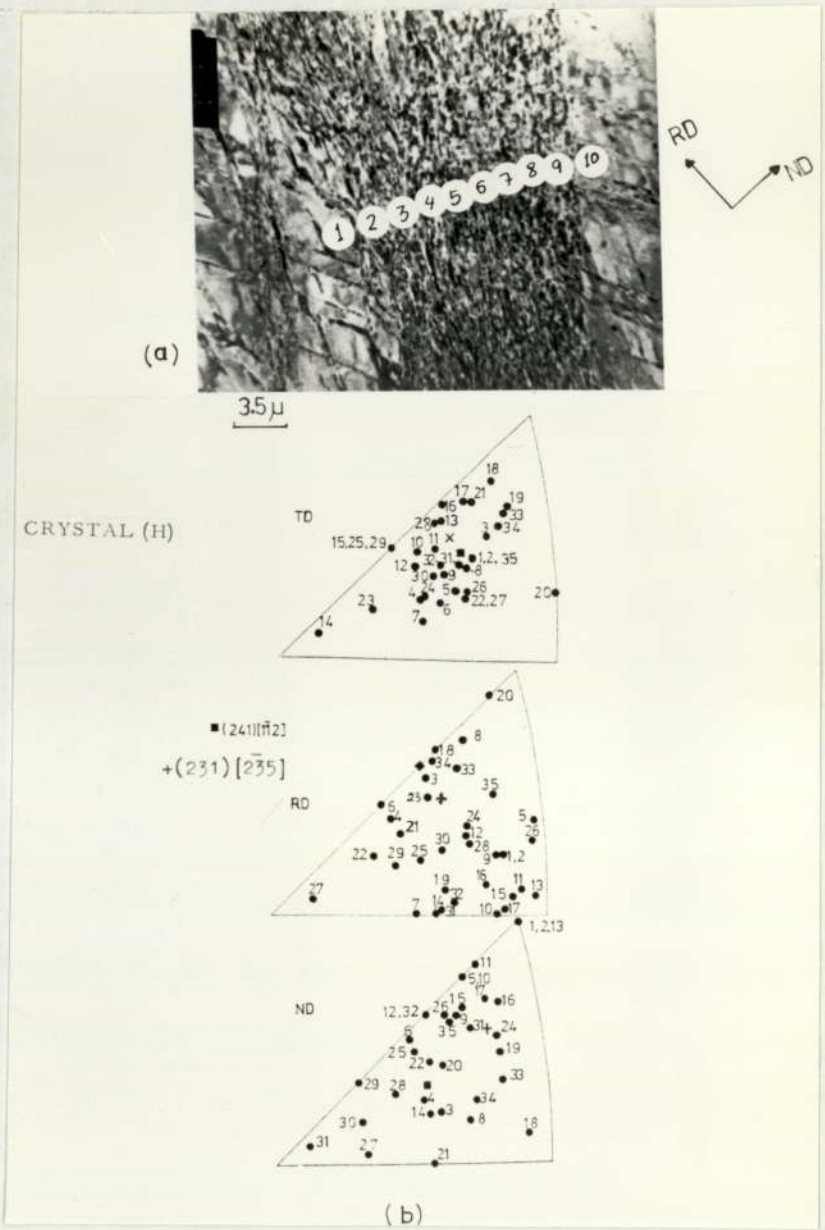

Figure 57 Analysis of orientations in shear bands in crystal H of Al-Zn-Mg alloy (Longitudinal Section)

a) Single shear band showing locations of STEM diffraction patterns

b) Orientations from locations in (a) and other shear band sites.

widely spread but not random orientation.

Similar methods were applied to crystals (G) and (H) to determine the orientations of the crystallites within the shear bands from the area labelled in Figures (56 a, 57a) and from other areas. The results are plotted as shown in Figures (56 b, 57b). Again a wide spread was obtained but the distribution was not random.

4.7 Rolling and Annealing Textures

4.7.1 Polycrystalline Al-Mg-Si Alloy

{111} and {200} pole figures for three rolling reductions (50, 70 and 90%) of Al-Mg-Si alloy were determined. The results in Figure (58), show the various stages in the development of the final single phase Al-Mg-Si texture. When particle formation was induced prior to deformation, the rolling textures after similar reductions are illustrated in the {111} and {200} pole figures of Figures (59 A,B,E,F,I & J). These pole figures represent the development of deformation textures in second phase Al-Mg-Si material A_I, which were nearly similar textures in both cases. The only detectable difference was that textures in second phase material A_I were a little weaker and more diffuse. A similar texture was developed in material A_{II} which contained different second phase particles from A_I. In both of these cases the textures closely resembled that of single phase material rolled to the same deformation levels at room temperature.

Figure 58

{111} pole figures of Al-Mg-Si solution treated, cold rolled:-

A) 50% B) 70% C) 90%

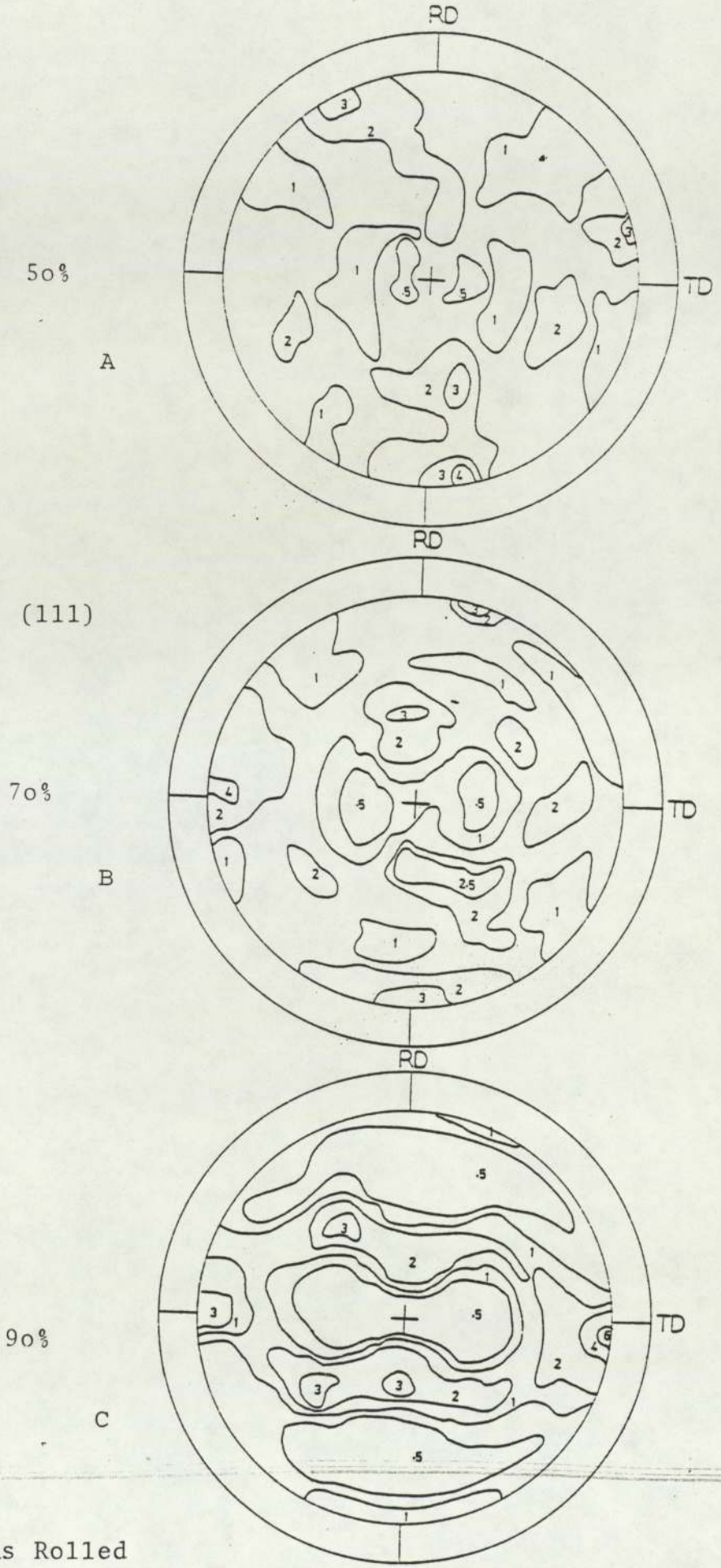

Figure 58

Figure 59

{111} and {200} pole figures of Al-Mg-Si aged condition material A_I

A) {111} cold rolled 50%

B) {200} cold rolled 50%

C) {111} cold rolled 50% Fully Recrystallised

D) {200} cold rolled 50% Fully Recrystallised

E) {111} cold rolled 70%

F) {200} cold rolled 70%

G) {111} cold rolled 70% Fully Recrystallised

H) {200} cold rolled 70% Fully Recrystallised

I) {111} cold rolled 90%

J) {200} cold rolled 90%

K) {111} cold rolled 90% Fully Recrystallised

L) {200} cold rolled 90% Fully Recrystallised

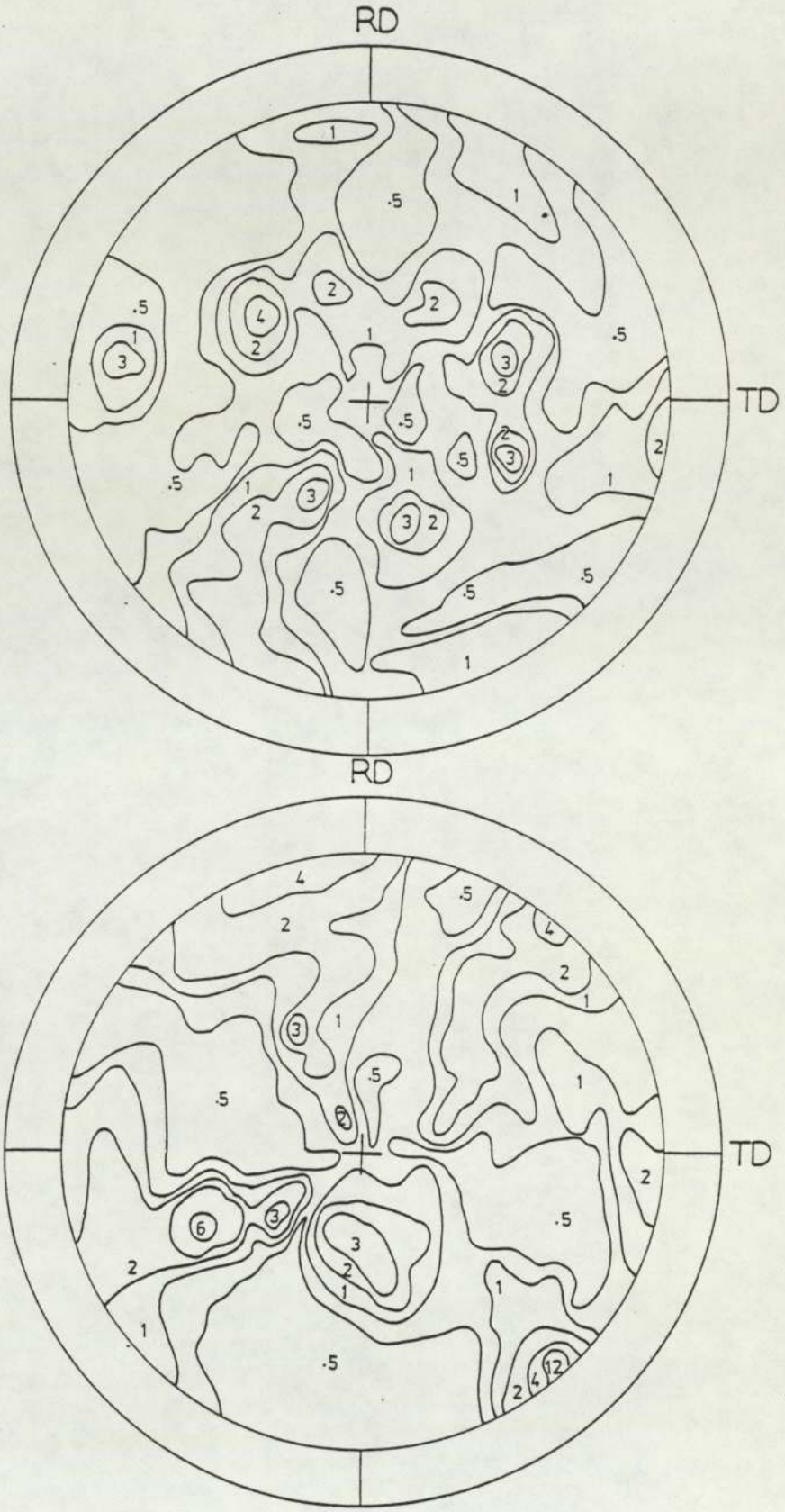

(A)

50%

(B)

As Rolled

Figure 59

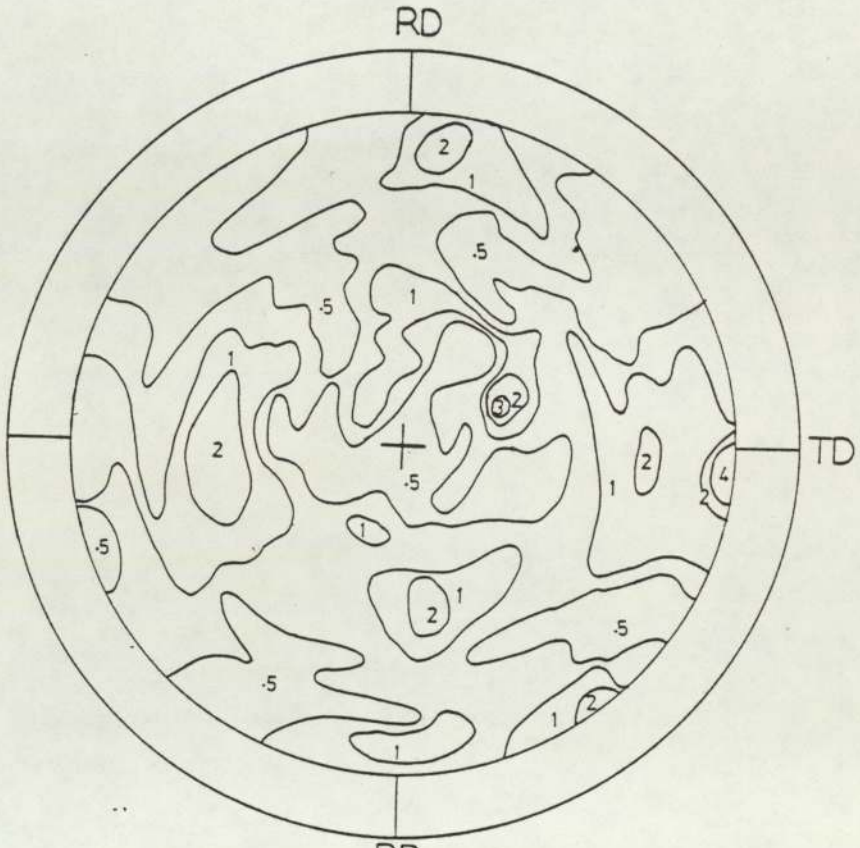

(C)

50%

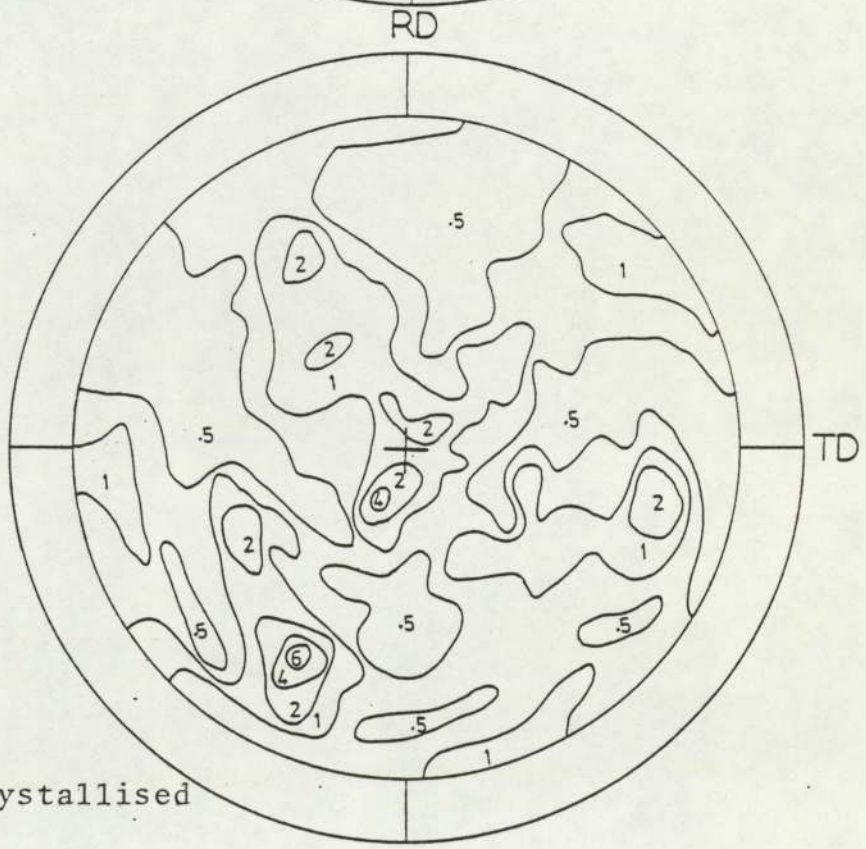

(D)

As Fully Recrystallised

Figure 59

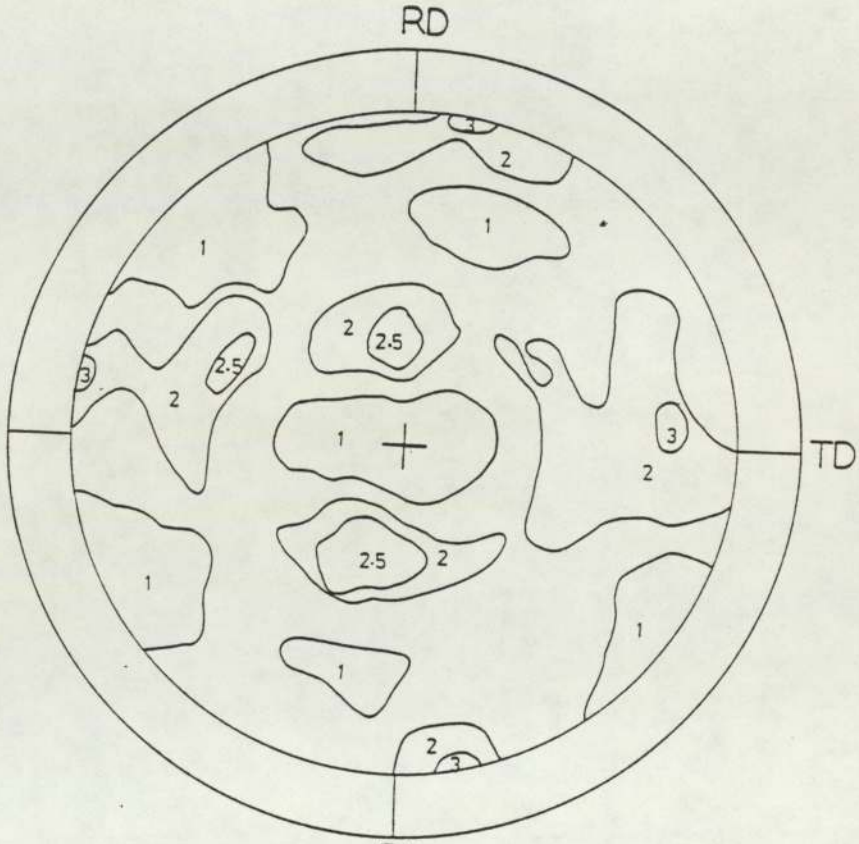

(E)

70%

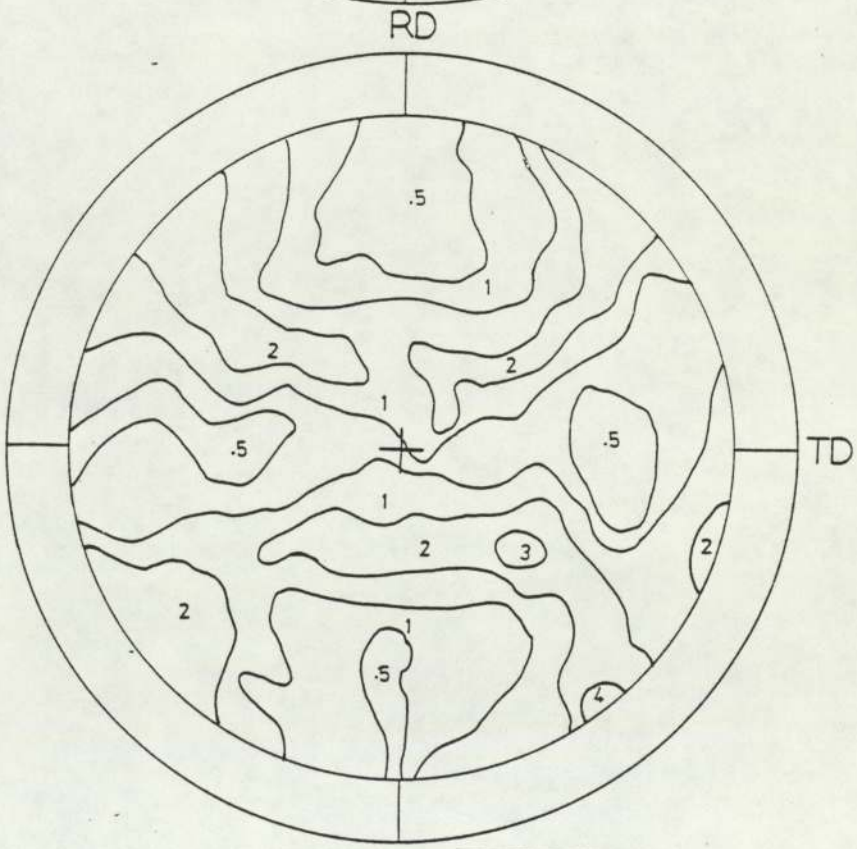

(F)

As Rolled

Figure 59

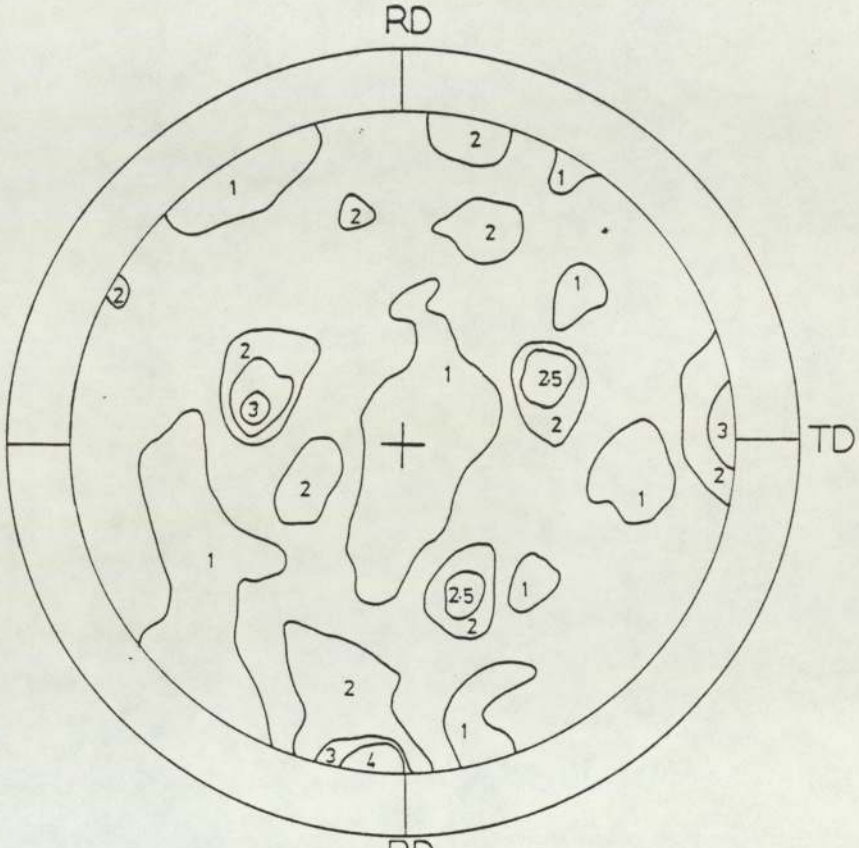

(G)

70%

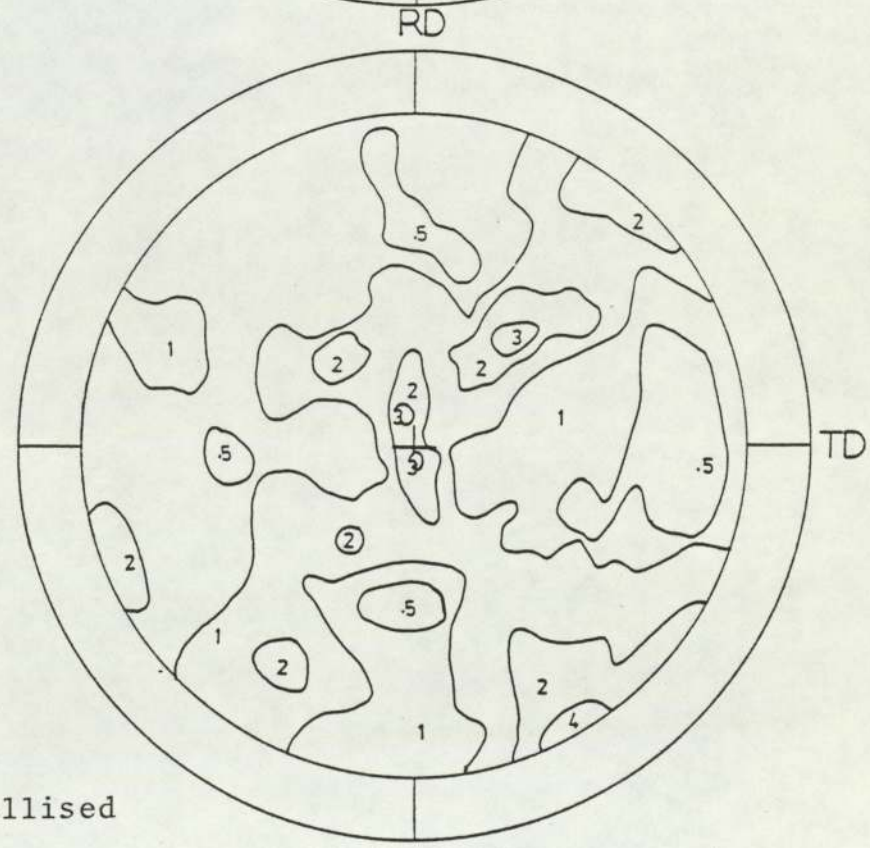

(H)

As Fully Recrystallised

Figure 59

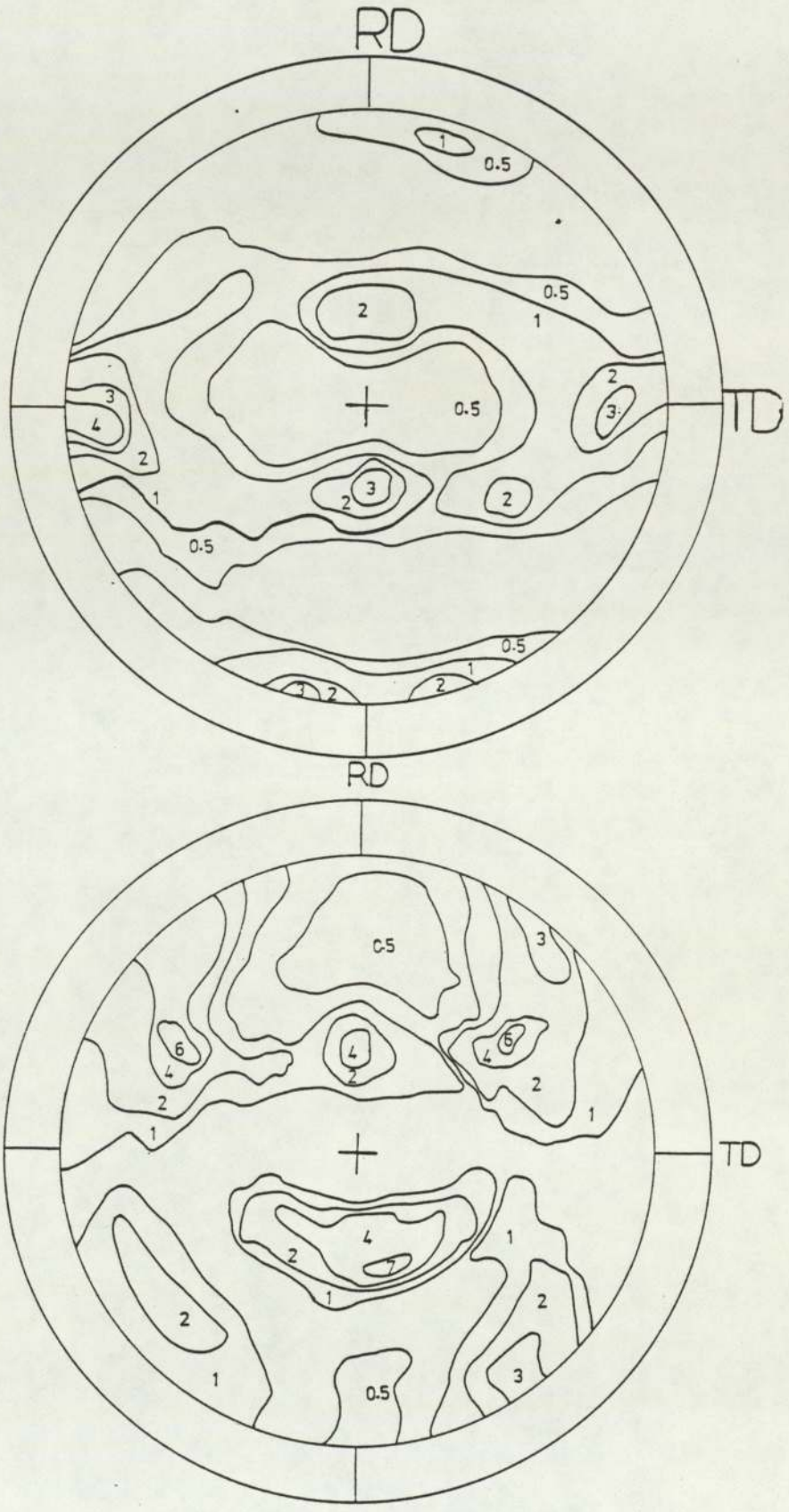

(I)

90%

(J)

As Rolled

Figure 59

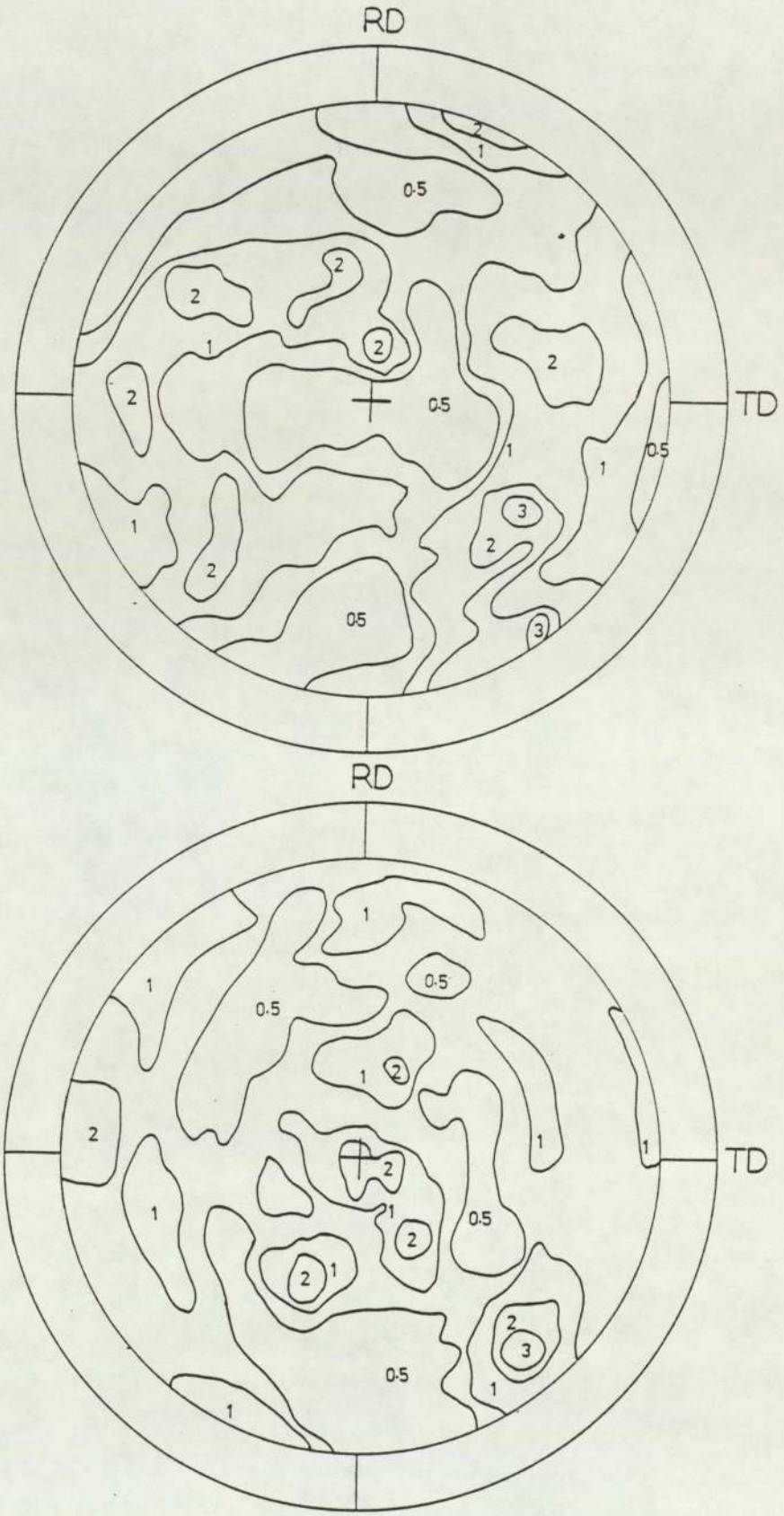

(K)

90%

(L)

As Fully Recrystallised

Figure 59

Figure 60

{111} and {200} pole figures of Al-Mg-Si, aged condition material A_{II}

A)	{111}	cold rolled 50%	Fully Recrystallised
B)	{200}	cold rolled 50%	Fully Recrystallised
C)	{111}	cold rolled 70%	Fully Recrystallised
D)	{200}	cold rolled 70%	Fully Recrystallised
E)	{111}	cold rolled 90%	Fully Recrystallised
F)	{200}	cold rolled 90%	Fully Recrystallised

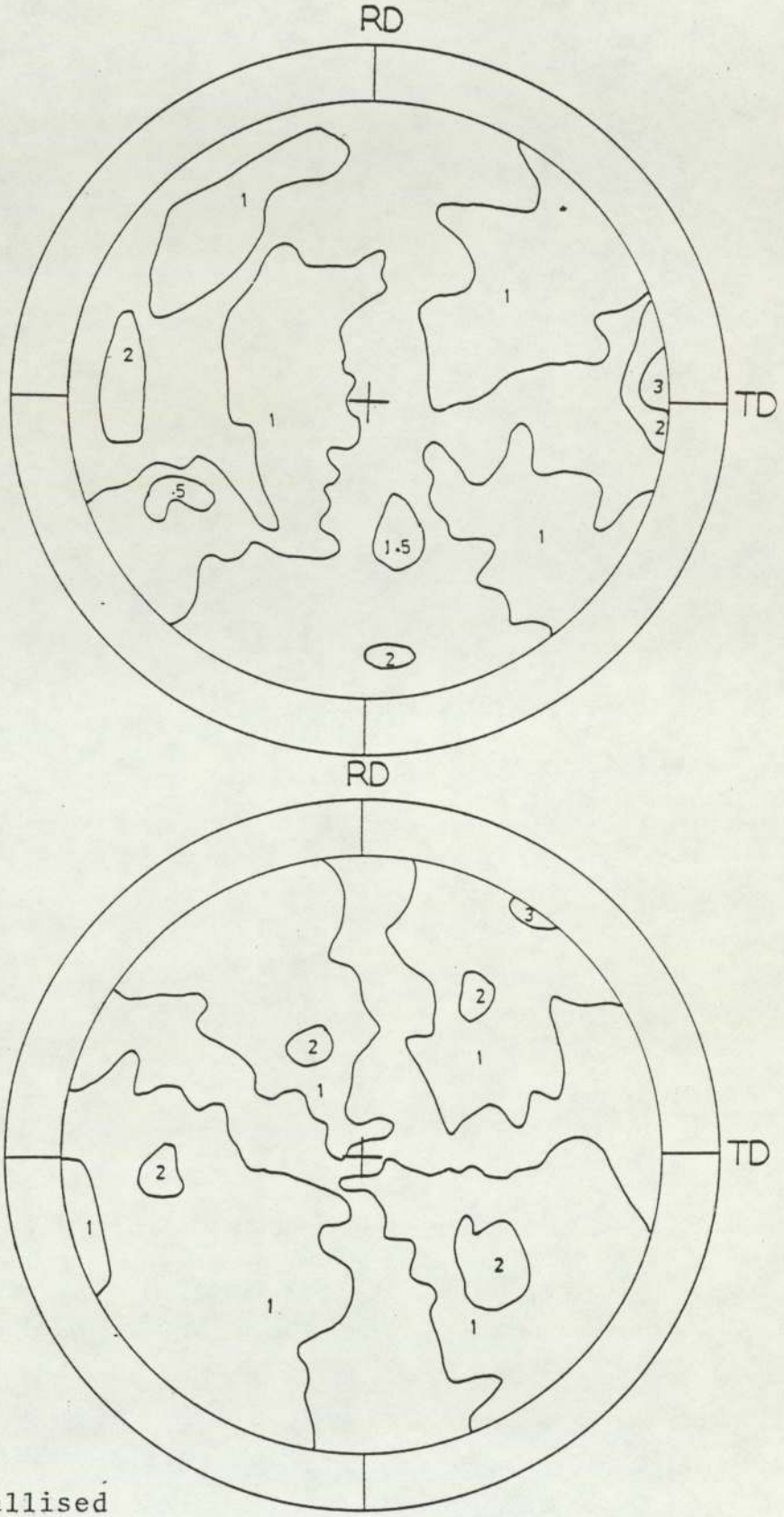

(A)

50%

(B)

As Fully Recrystallised

Figure 60

(C)

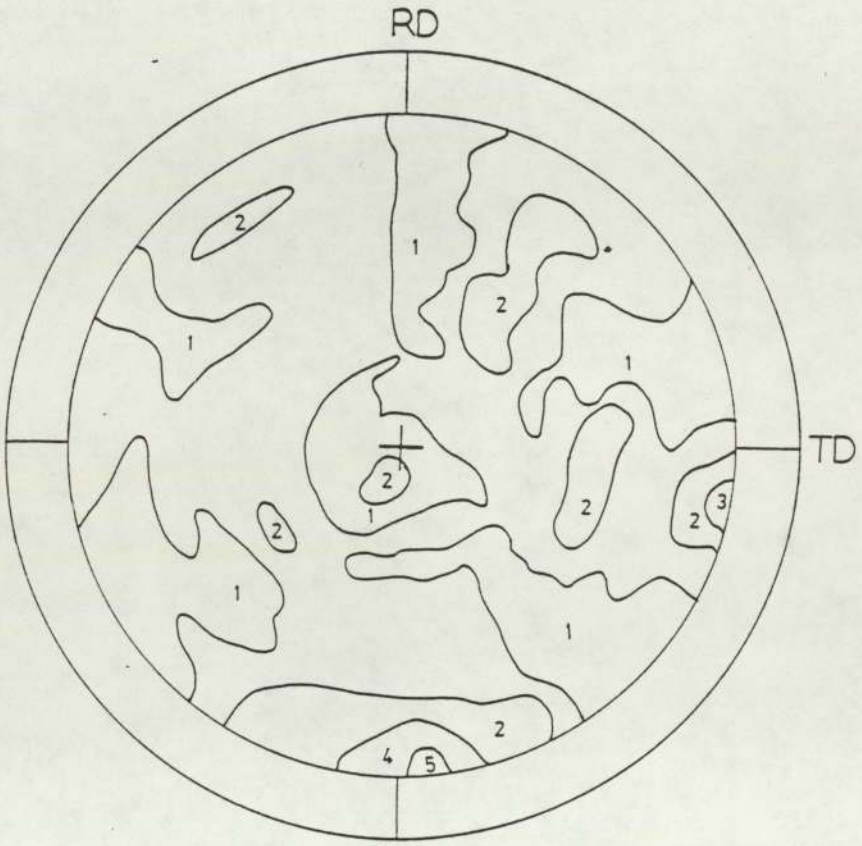

70%

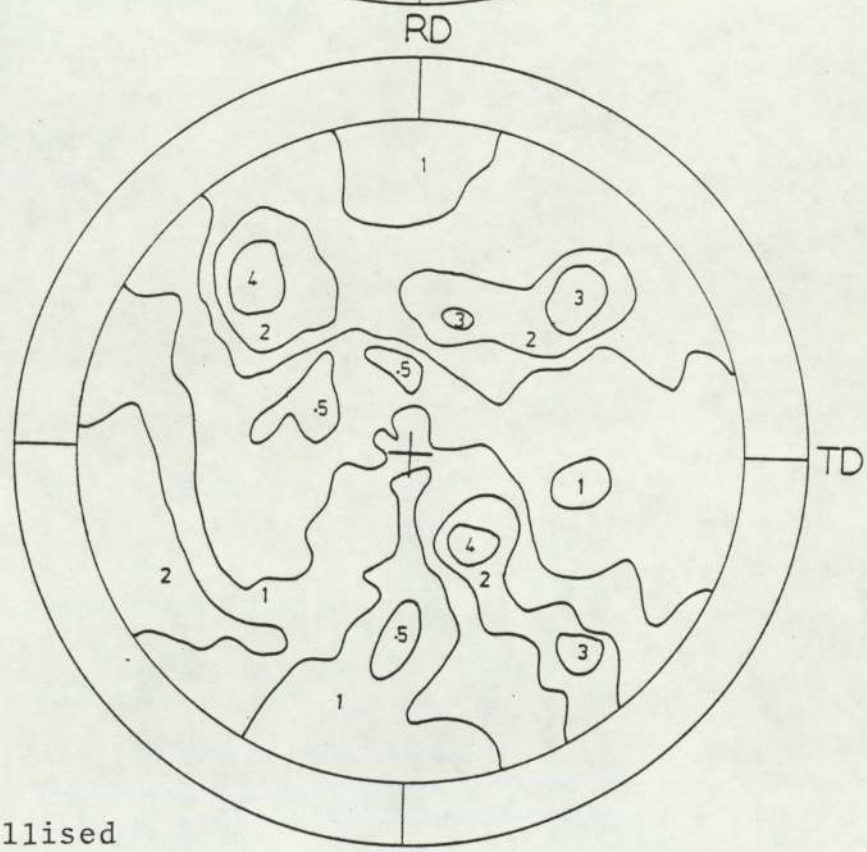

(D)

As Fully Recrystallised

Figure 60

(E)

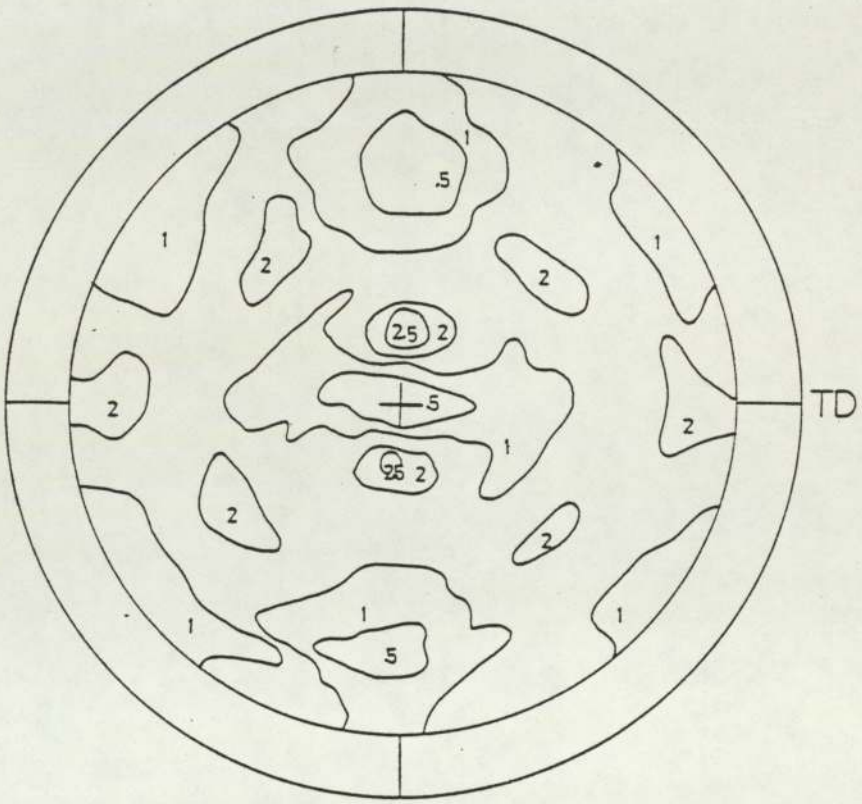

90%

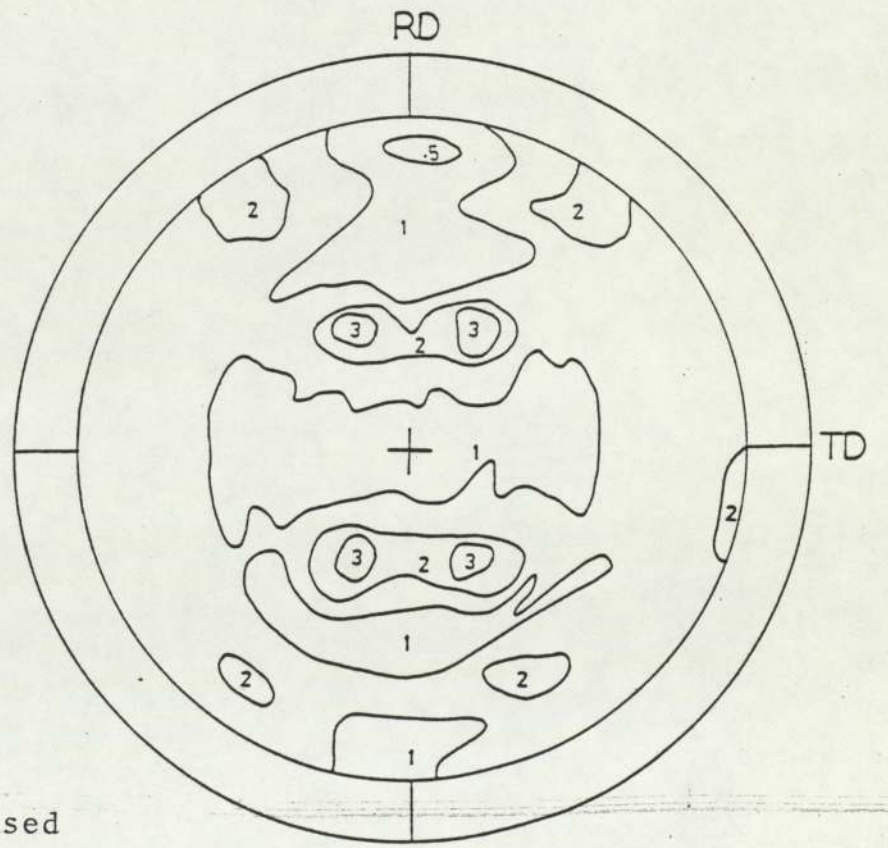

(F)

As Fully Recystallised

Figure 60

The cold rolled specimens of both aged conditions were annealed at a temperature of 350°C for 5, 4 hours and 180 s to 50, 70 and 90% reduction respectively, in a salt bath furnace. The type of annealing texture developed was controlled by the pre-existing deformation texture and structures. The {111} and {200} pole figures for fully recrystallised materials are illustrated in Figures (59 C, D,G,H,K,L & 60 A-F). Both cases developed a nearly random texture despite the fact that this alteration had no significant effect on the rolling texture.

4.7.2 Single Crystals of Al-Mg-Si Alloy

{111} and {200} pole figures for three single crystals whose orientation is shown in Table (2) were determined. These crystals were aged in a similar manner to the polycrystalline material to produce a coarse second phase structure, prior to cold rolling.

Crystal (A) was rolled at room temperature to about 73% reduction in thickness in (110) plane with the [001] direction lying in the rolling direction. The rolling texture is shown in the Figure (61 A,B). Despite its stability to the rolling deformation it also showed some spread along the rolling direction.

Specimens were cut from the edge of the rolled crystal with great care and the cutting damage was removed by etching before annealing. The rolled strip was annealed in a salt bath furnace at 350°C for 4 hours to fully

recrystallise the material. The annealing texture is shown in the (111) and (200) pole figures of Figure (61 C,D). By careful analysis of the pole figures, it was found that the main recrystallisation components which developed were four separated orientations of type $\{534\}\langle 112\rangle$, and spread along the transverse direction. Two of these components with clockwise rotation were much stronger than the other two with anti-clockwise rotation.

Crystal (B) with an orientation $(231)[\bar{1}2\bar{4}]$ was deformed to about 71% by cold rolling at room temperature. Figure (61 E,F) shows the (111) and (200) pole figures of rolling texture, and the results of the pole figures show that this crystal had essentially retained its original orientation plus some spread along the rolling direction. Figure (61 G,H) showed the (111) and (200) pole figure of this crystal after recrystallising for 4 hours at 350°C. The recrystallisation texture was found to consist of two components of $(234)[11\bar{2}\bar{7}]$ and $(013)[33\bar{1}]$.

Crystal (C) of $(014)[34\bar{1}]$ original orientation was deformed to about 71% by cold rolling at room temperature. In contrast to the other orientations mentioned above, this was an unstable orientation. Upon rolling, this orientation splits up into the two nearly symmetrical components $(114)[53\bar{2}]$ and $(114)[\bar{8}\bar{4}3]$ with spread along the rolling direction. The (111) and (200) pole figures are shown in Figure (61 I,J). The recrystallisation texture obtained from the deformed unstable crystal after 4 hours at 350°C is shown in Figure (61 K,L). The main

Figure 61

{111} and {200} pole figures of Al-Mg-Si single crystals cold rolled 71%

Crystal A

A) {111} As Rolled

B) {200} As Rolled

C) {111} As Fully Recrystallised

D) {200} As Fully Recrystallised

Crystal B

E) {111} As Rolled

F) {200} As Rolled

G) {111} As Fully Recrystallised

H) {200} As Fully Recrystallised

Crystal C

I) {111} As Rolled

J) {200} As Rolled

K) {111} As Fully Recrystallised

L) {200} As Fully Recrystallised

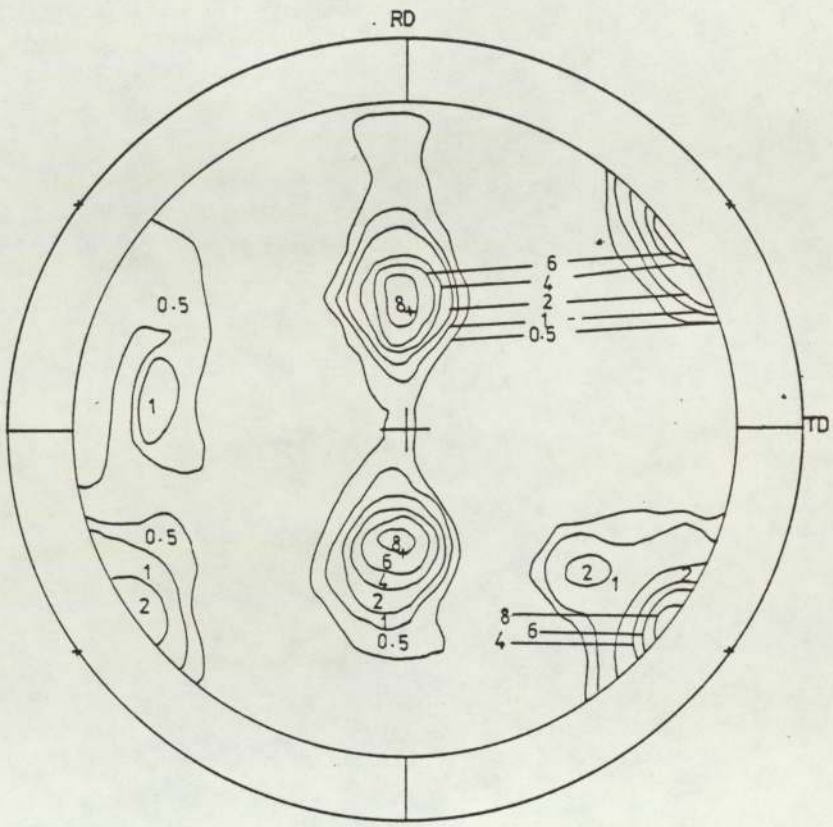

(A)

Crystal A

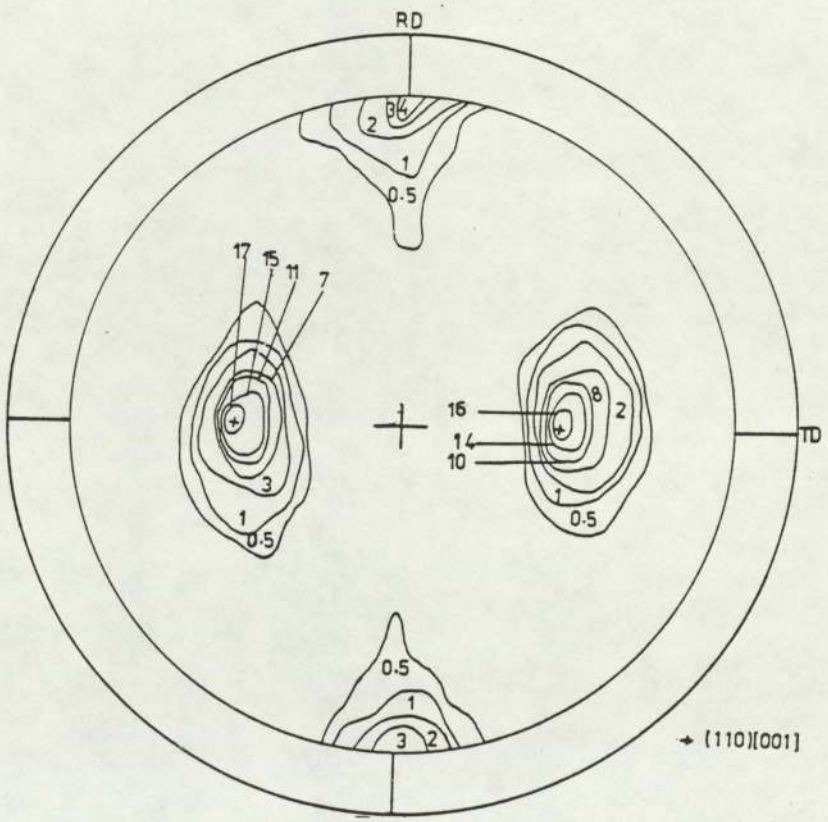

(B)

As Rolled

Figure 61

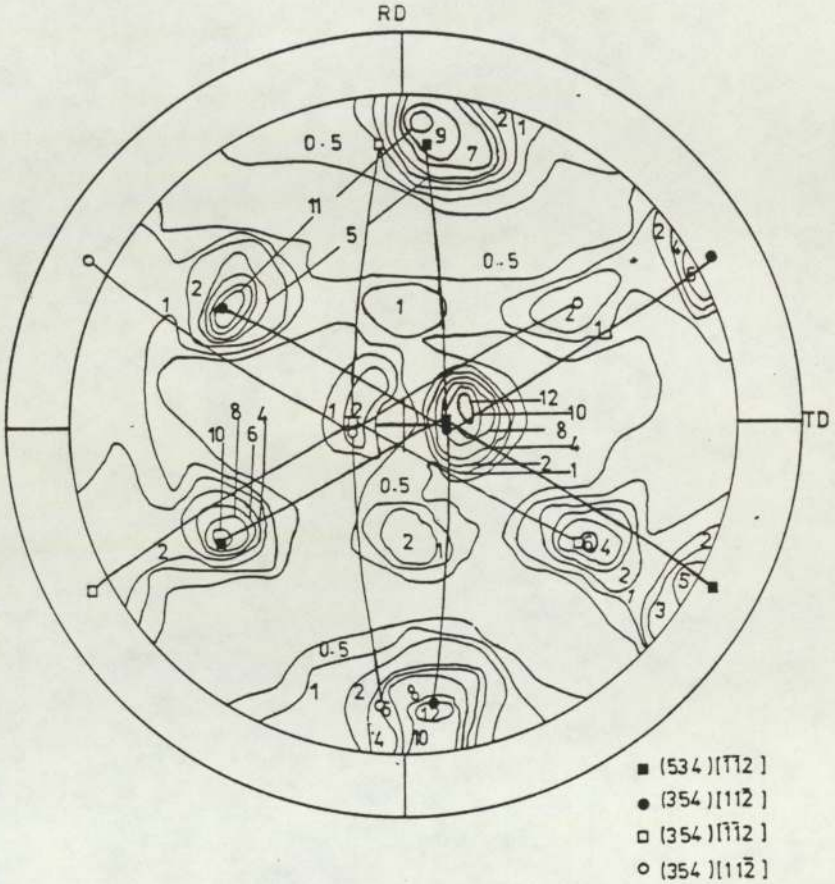

(C)

Crystal A

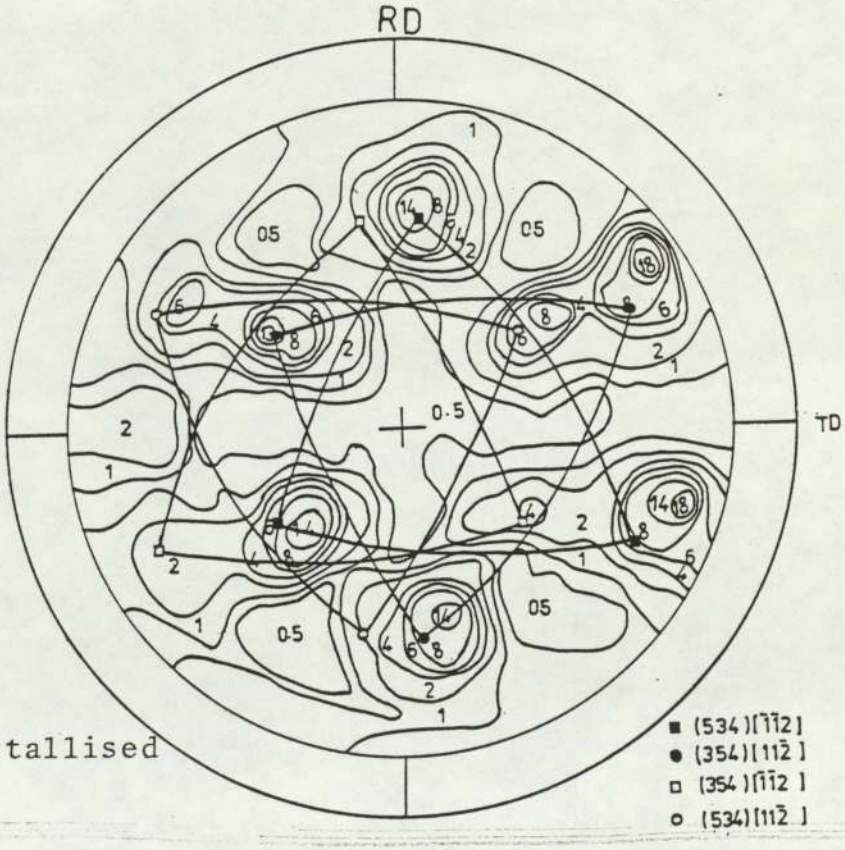

(D)

As Fully Recrystallised

Figure 61

(E)

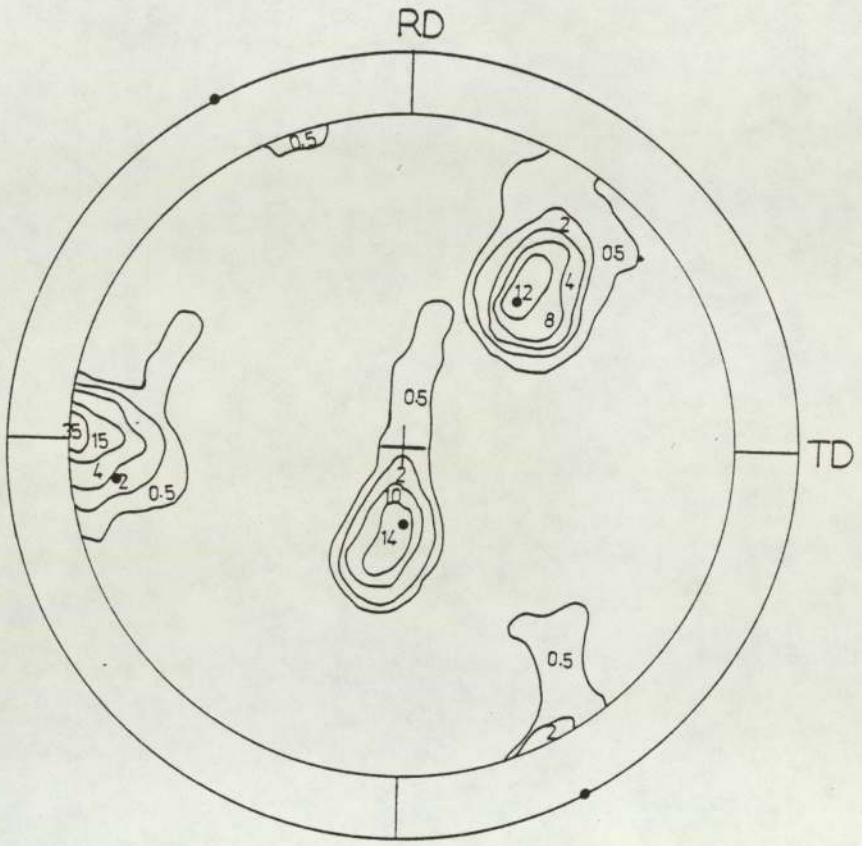

Crystal B

(F)

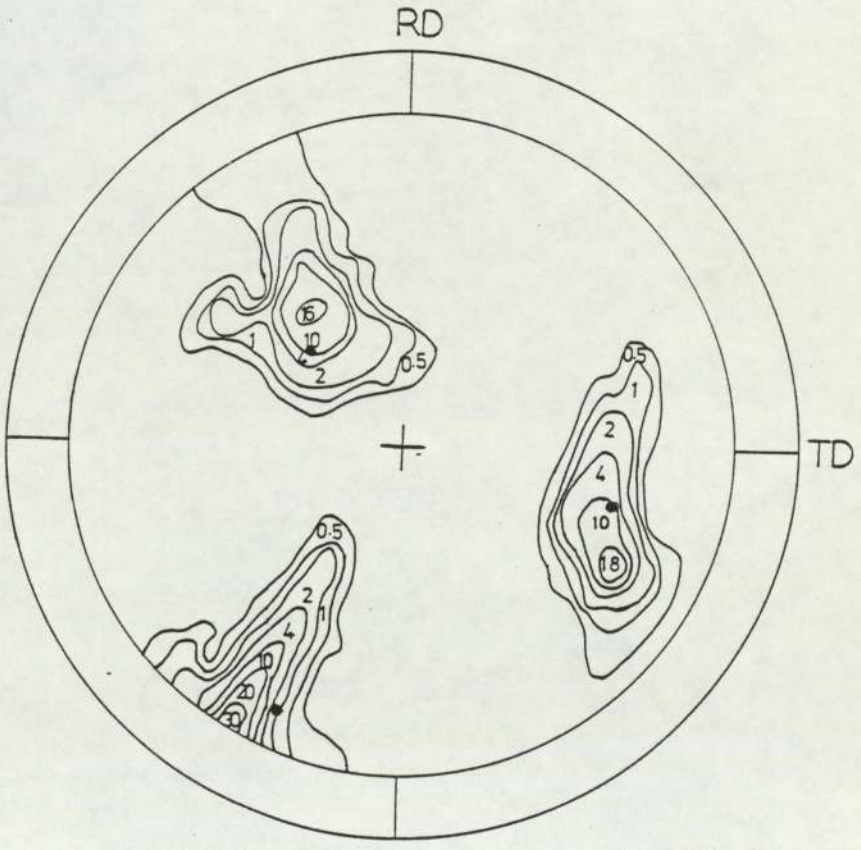

As Rolled

• (231)[1̄2Z]

Figure 61

(G)

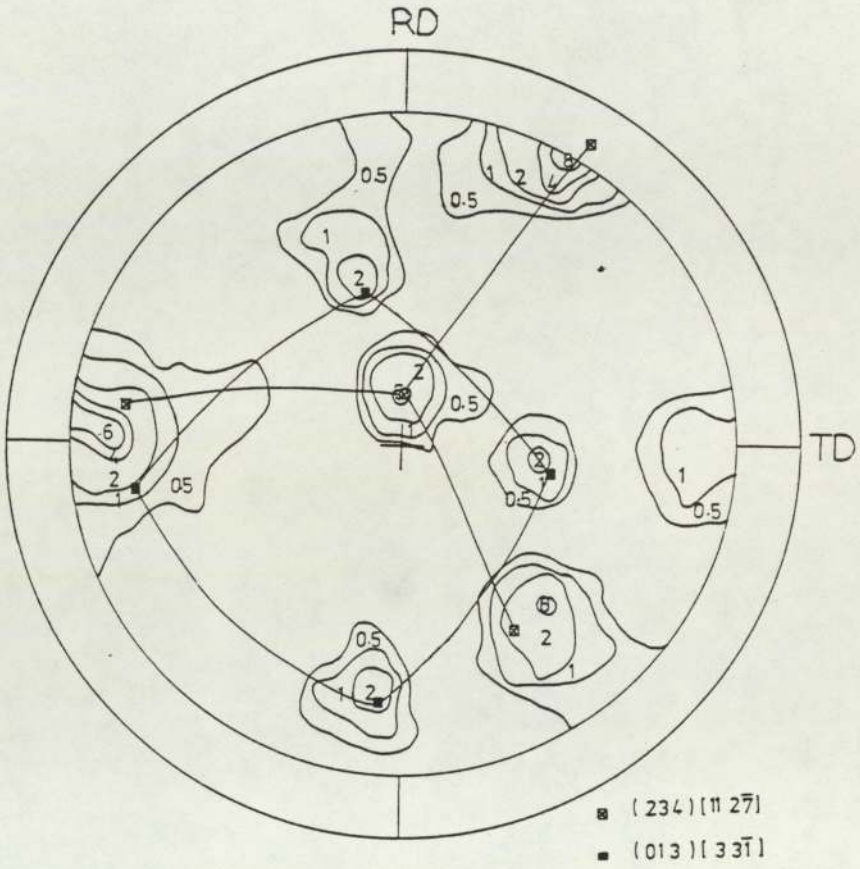

Crystal B

(H)

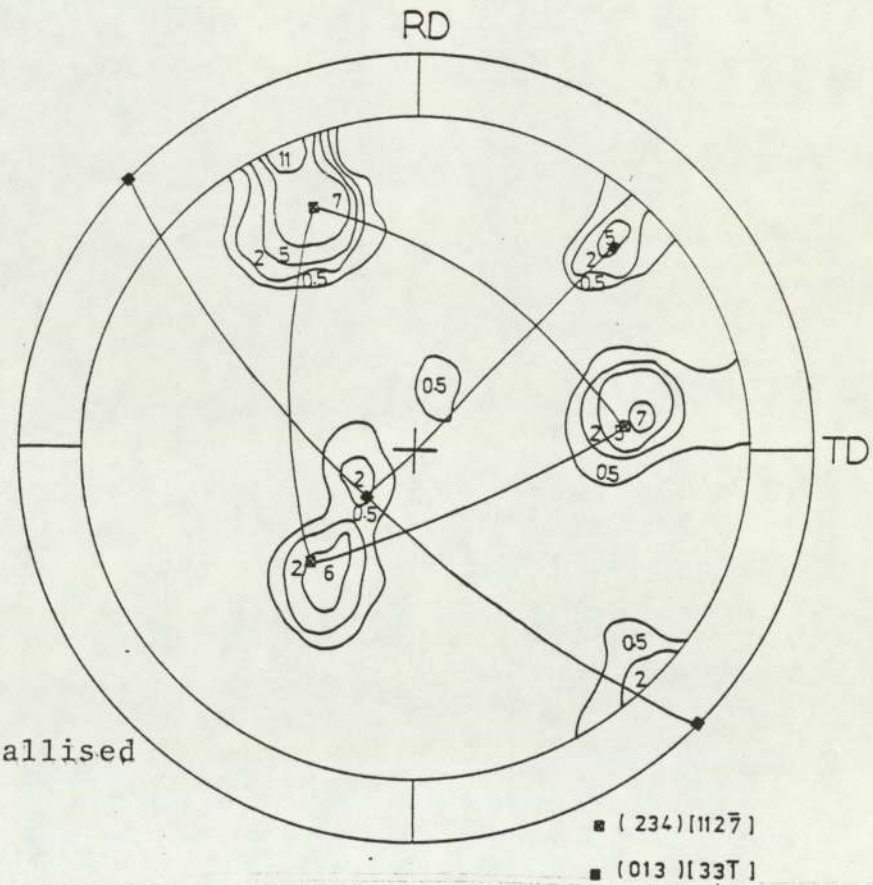

As Fully Recrystallised

Figure 61

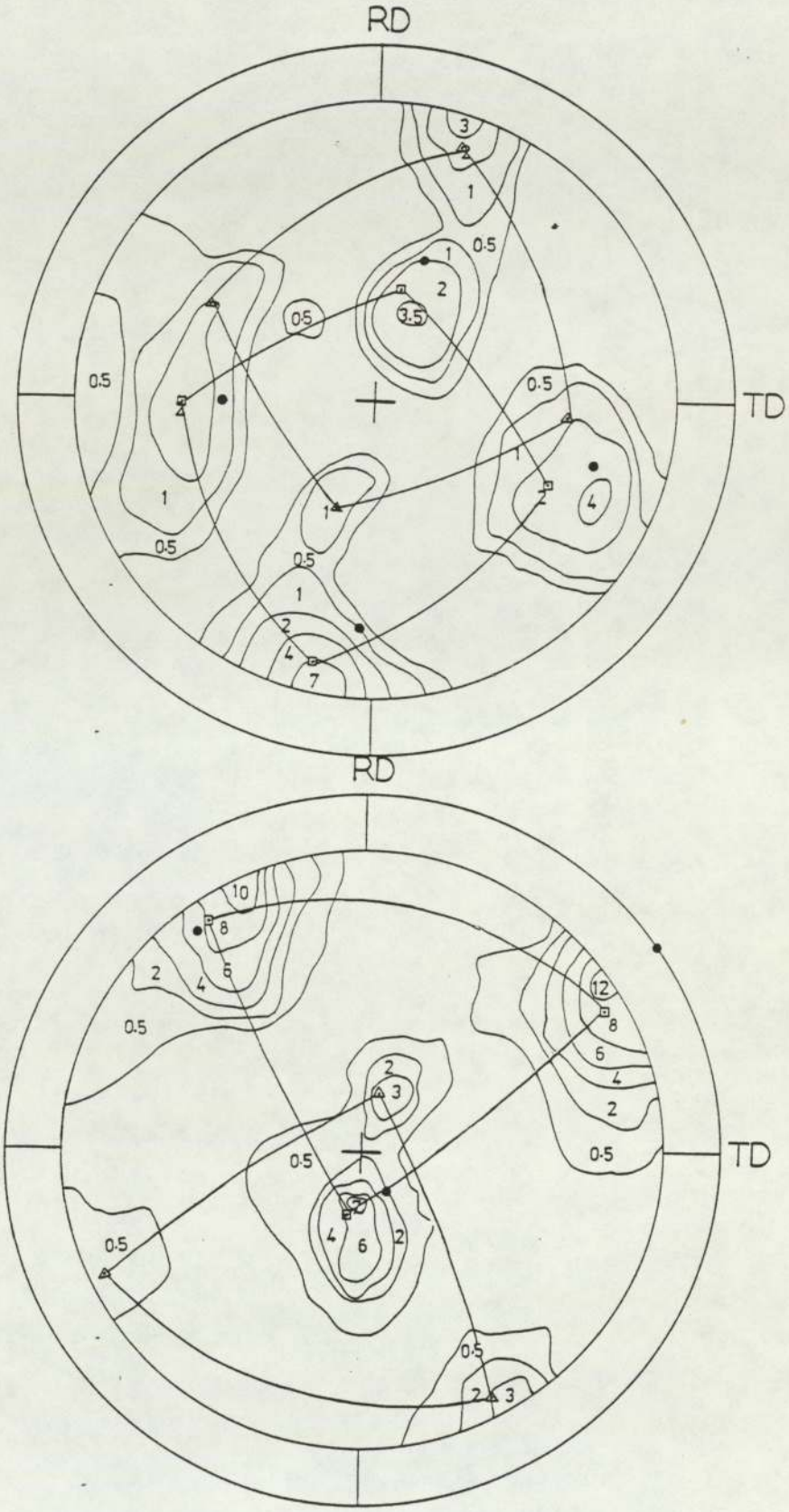
RD
TD
(I)
Crystal C
RD
TD
(J)
As Rolled
● (014)[34̄1] — ORIGINAL ORIENTATION
▣ (114)[53̄2] ▲ (11 4)[8̄43]

Figure 61

(K)

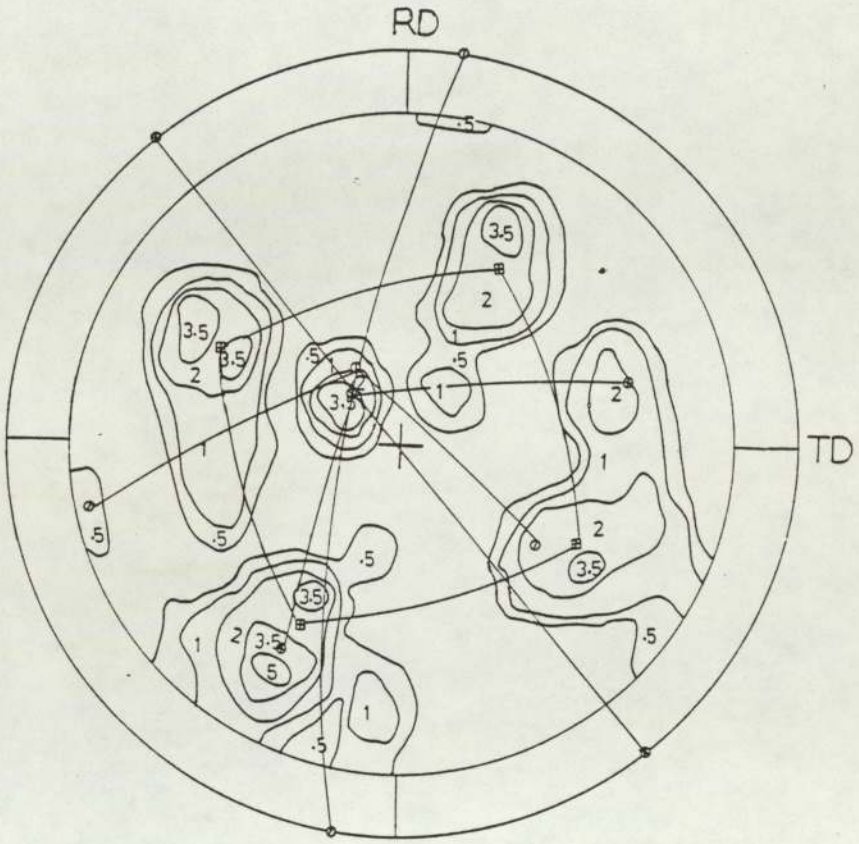

Crystal C

(L)

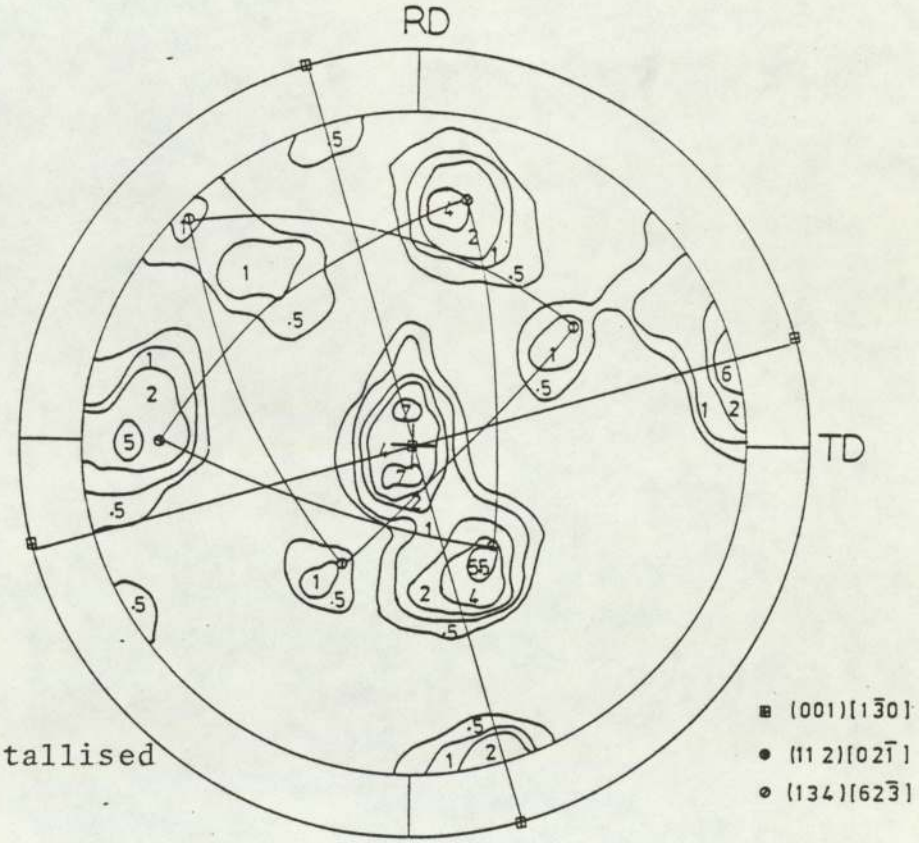

As Fully Recrystallised

Figure 61

recrystallisation components, are (001)[1$\bar{3}$0], (112)[02$\bar{1}$] and (134)[62$\bar{3}$] plus spread towards the rolling direction.

4.7.3 Single Crystal of High Purity Aluminium

A high purity aluminium single crystal (D) of (110)[001] orientation which was oriented exactly parallel with the rolling plane and rolling direction was deformed about 75% by cold rolling at room temperature. The original orientation was retained, and the texture was remarkably sharp with a maximum intensity of 38 X random. The (111) and (200) pole figures are shown in Figure (62 A,B) The most significant observation of this crystal was that it was resistant to recrystallisation at 350^{o}C and needed heating to 400^{o}C to induce recrystallisation. The (111) and (200) pole figures are shown in Figure (62 C,D) showing the annealing texture was random.

4.7.4 Polycrystalline Al-Zn-Mg Alloy

The {111} and {200} pole figures for Al-Zn-Mg alloy rolled 90% at room temperature is shown in Figure (63 A,B) The rolling texture developed in this alloy was essentially similar to that of Al-Mg-Si alloy rolled to the same deformation level. The rolled specimen was annealed at 350^{o}C for 180 s in a salt bath furnace. The (111) and (200) pole figures of annealing texture showed a weaker texture with diffuse spread of orientation than observed in Al-Mg-Si alloy of Figure (58 C)

Figure 62

{111} and {200} pole figures of pure aluminium single crystal cold rolled 75%

A) {111} As Rolled

B) {200} As Rolled

C) {111} As Fully Recrystallised

D) {200} As Fully Recrystallised

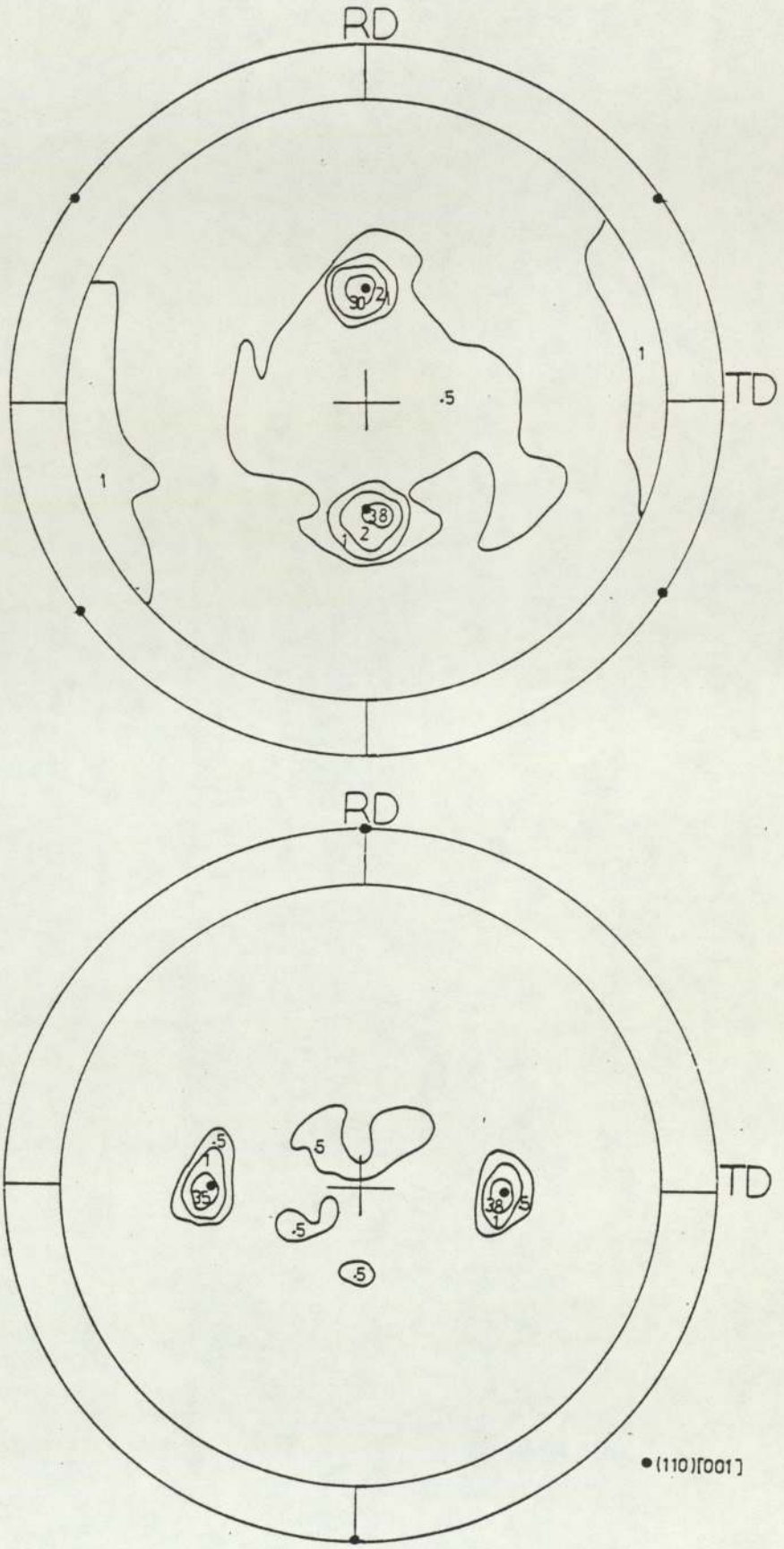

Figure 62

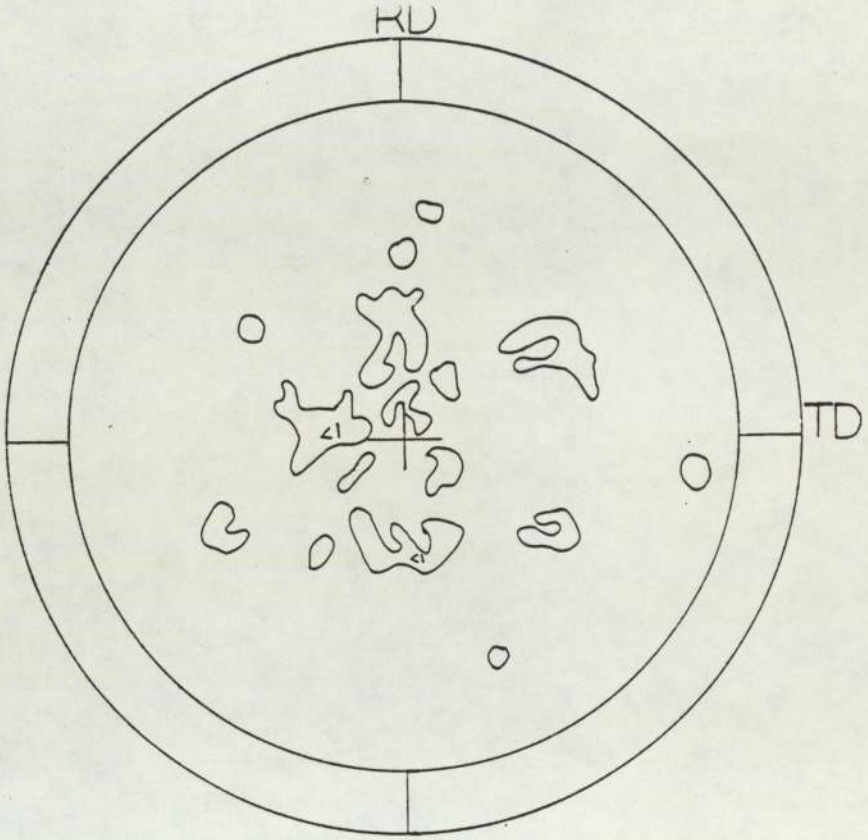

(C)

Crystal D

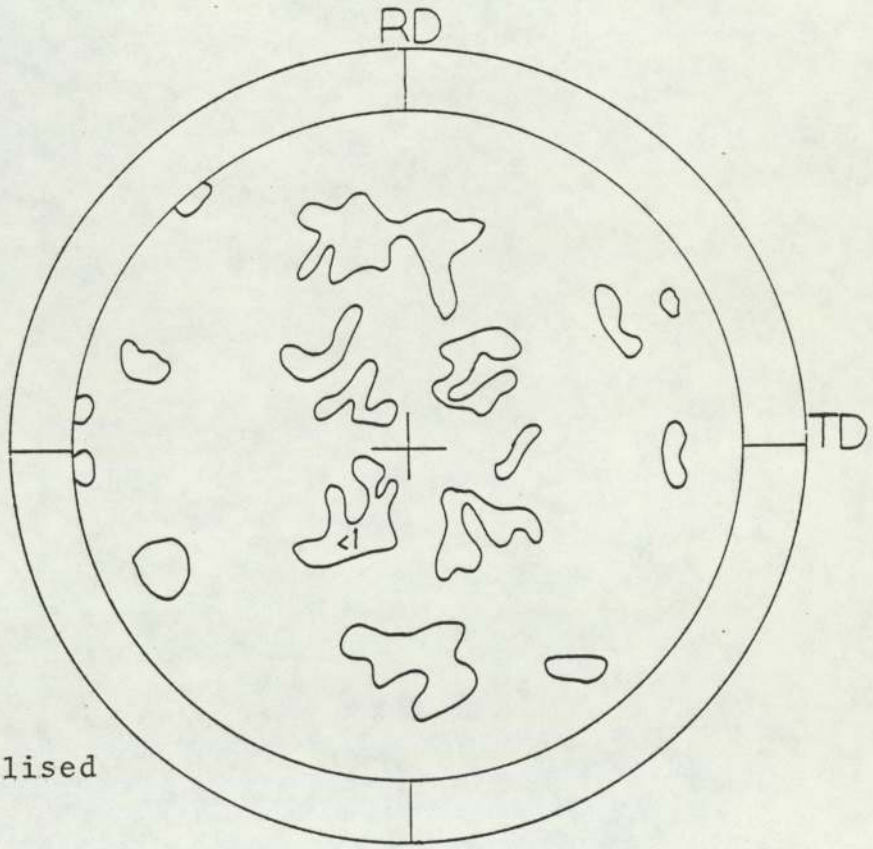

(D)

As Fully Recystallised

Figure 62

Figure 63

{111} and {200} pole figures of Al-Zn-Mg alloy cold rolled 90%

A) {111} As Rolled

B) {200} As Rolled

C) {111} As Fully Recrystallised

D) {200} As Fully Recrystallised

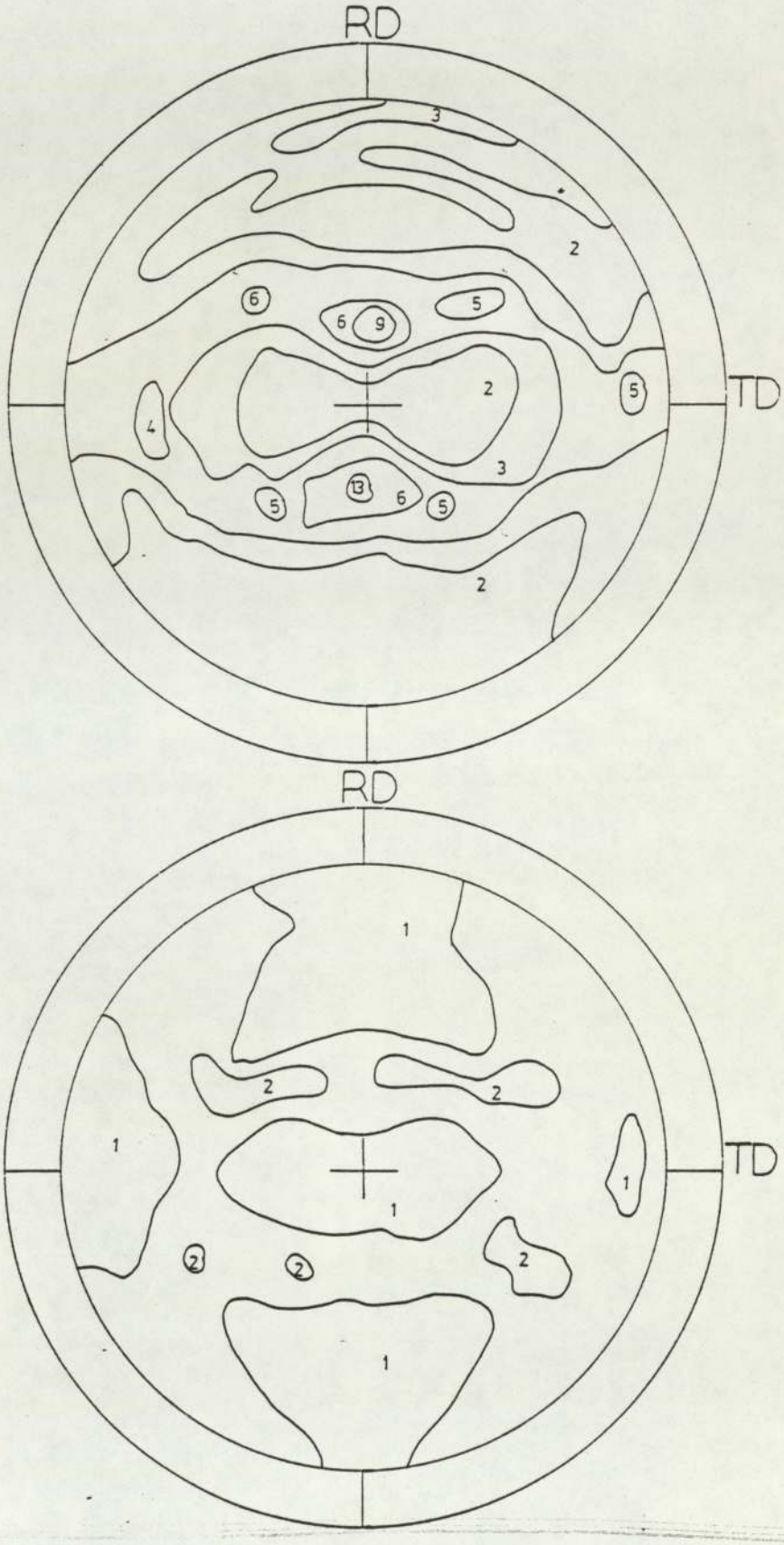

(A)

90%

(B)

As Rolled

Figure 63

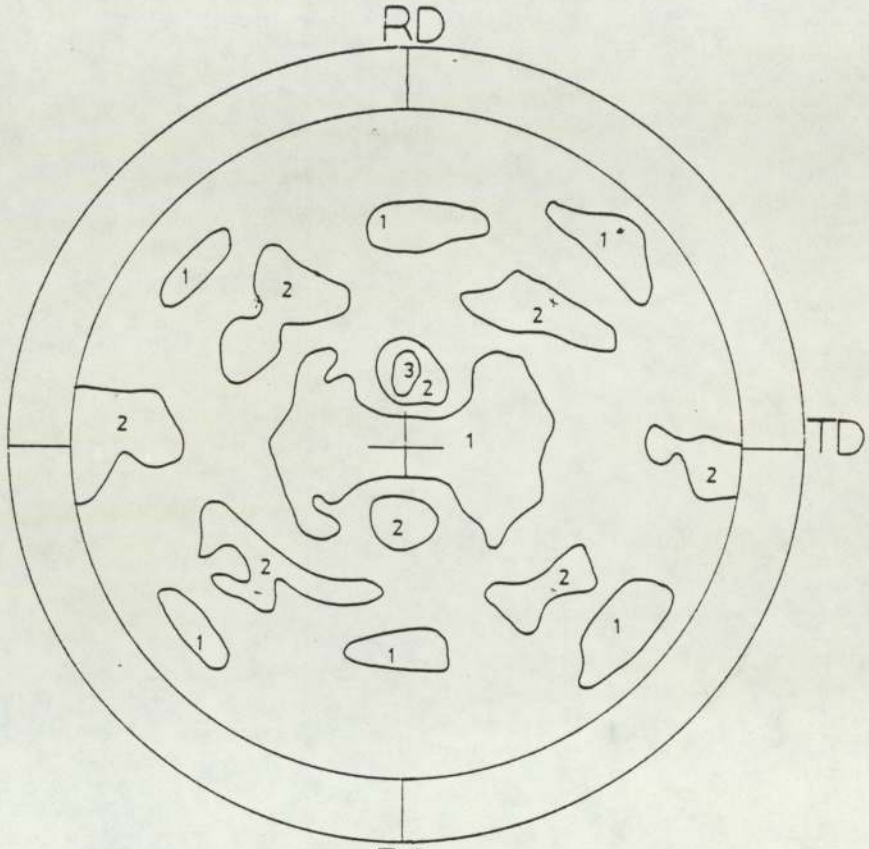

(C)

90%

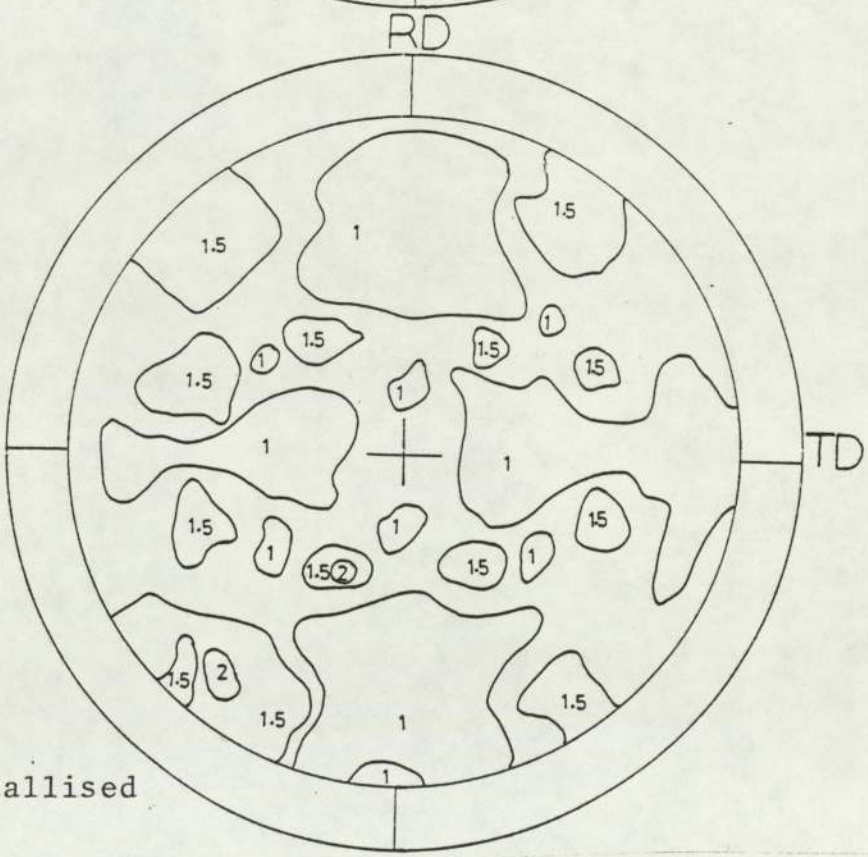

(D)

As Fully Recrystallised

Figure 63

4.7.5 Single Crystals of Al-Zn-Mg Alloy

1 - Crystal (E) of (110)[001] orientaion, remained stable during deformation at room temperature up to 80% by cold rolling, with a little spread along the rolling direction. The (111) and (200) pole figures are shown in Figure (64 A,B). After subsequent annealing at 350°C for 20 minutes, the corresponding recrystallisation texture consisted of two symmetrical components $(134)[2\bar{2}1]$ and $(\bar{1}\bar{3}4)[\bar{2}2\bar{1}]$ with some scattered orientation, as shown in Figure (64 C,D)

2 - Crystal (F) had an initial orientation of $(110)[\bar{1}1\bar{2}]$. This crystal also maintained its original orientation with respect to the rolling deformation to about 80% reduction with a little scatter and spreading along the transverse direction. The (111) and (200) rolling textures are shown in the pole figures of Figure (64 E,F)

The resulting recrystallisation texture after 20 minutes annealing at 350°C was very complicated, with about four components, $(012)[22\bar{1}]$, $(124)[44\bar{3}]$, $(134)[13\bar{1}4]$, $(144)[41\bar{2}]$ and finally $(112)[\bar{4}\bar{2}3]$, developed during annealing, Figure (64 G,H)

3 - The next crystal (G) was oriented near to $(231)[1\bar{2}4]$ orientation, which deviated about 5° away from the nominal position. After 80% reduction by cold rolling, the corresponding deformation texture was near to $(110)[1\bar{1}3]$, as shown in Figure (64 I,J). After 20 minutes annealing at 350°C in a salt bath furnace, the recrystallisation

texture consisted of two components, $(122)[41\bar{3}]$ and $(431)[1\bar{3}5]$. The (111) and (200) pole figures are shown in Figure (64 K,L)

4 - The final single crystal is (H) which had an orientation $(241)[1\bar{1}2]$ with deviation about 4^{o} away from the true position. The rolling texture after deformation 80% by cold rolling, showed $(231)[2\bar{3}5]$ plus some spread toward the rolling direction. The (111) and (200) pole figures are shown in Figure (64 M,N). The rolled specimen was annealed at 350^{o}C for 20 minutes, the recrystallisation texture again showed two different components of $(310)[\bar{1}33]$ and $(114)[\bar{1}\bar{3}1]$, with some spread along the transverse direction, the (111) and (200) pole figures are shown in Figure (64 O,P)

Figure 64

{111} and {200} pole figures of Al-Zn-Mg single crystals cold rolled 80%

Crystal E

A) {111} As Rolled

B) {200} As Rolled

C) {111} As Fully Recrystallised

D) {200} As Fully Recrystallised

Crystal F

E) {111} As Rolled

F) {200} As Rolled

G) {111} As Fully Recrystallised

H) {200} As Fully Recrystallised

Crystal G

I) {111} As Rolled

J) {200} As Rolled

K) {111} As Fully Recrystallised

L) {200} As Fully Recrystallised

Crystal H

M) {111} As Rolled

N) {200} As Rolled

O) {111} As Fully Recrystallised

P) {200} As Fully Recrystallised

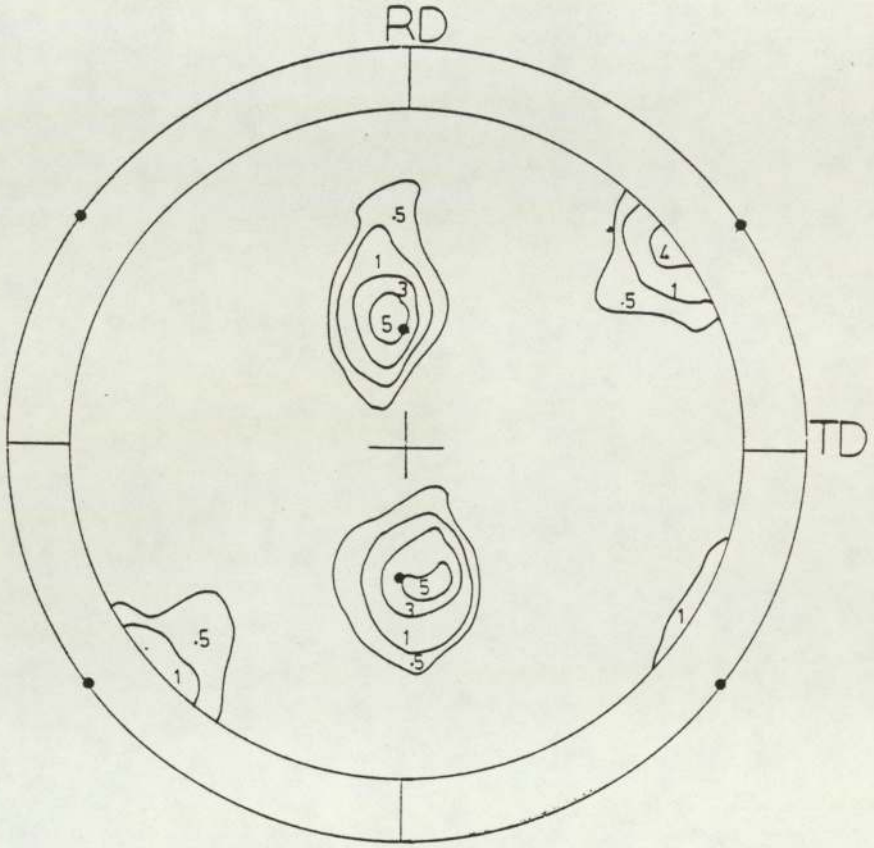

(A)

Crystal E

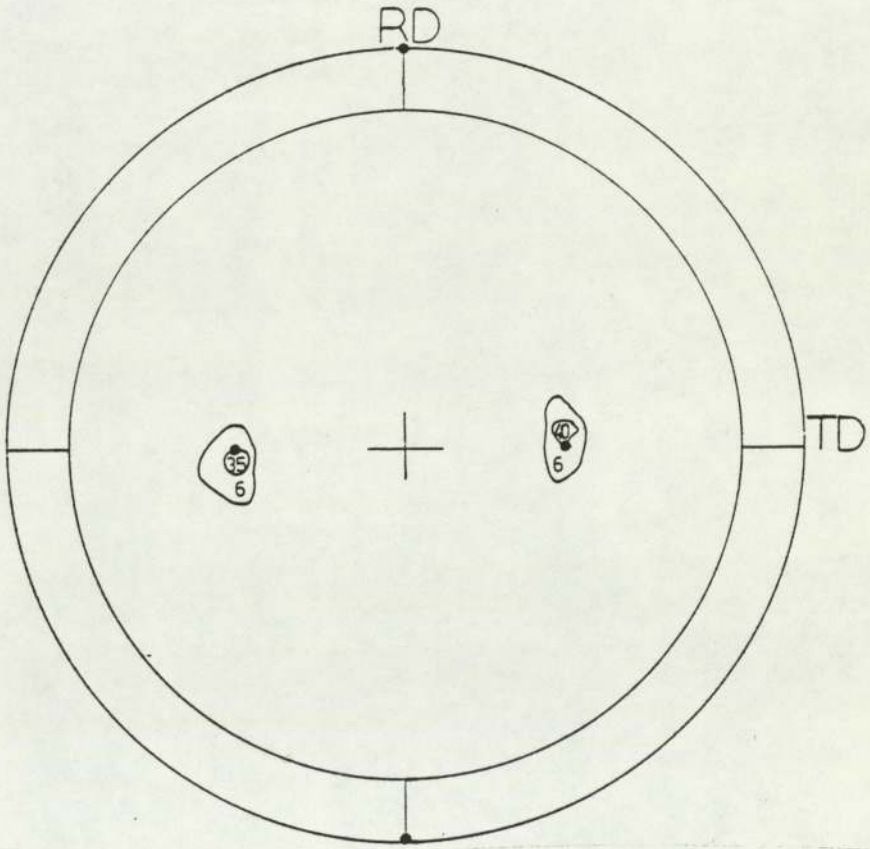

(B)

As Rolled

(110) [001]

Figure 64

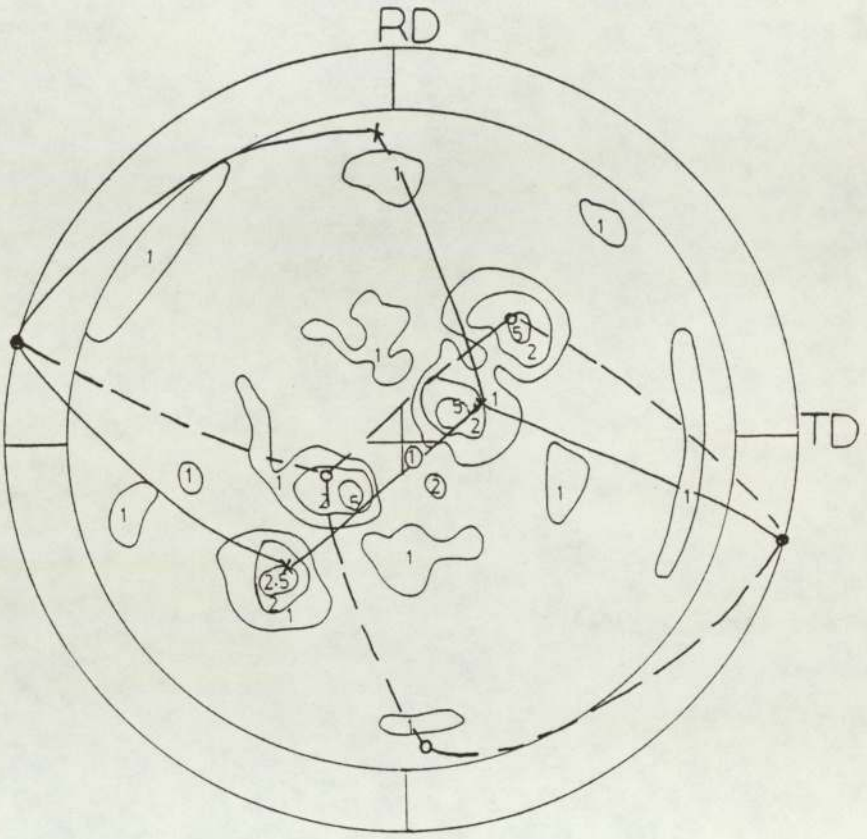

(C)

Crystal E

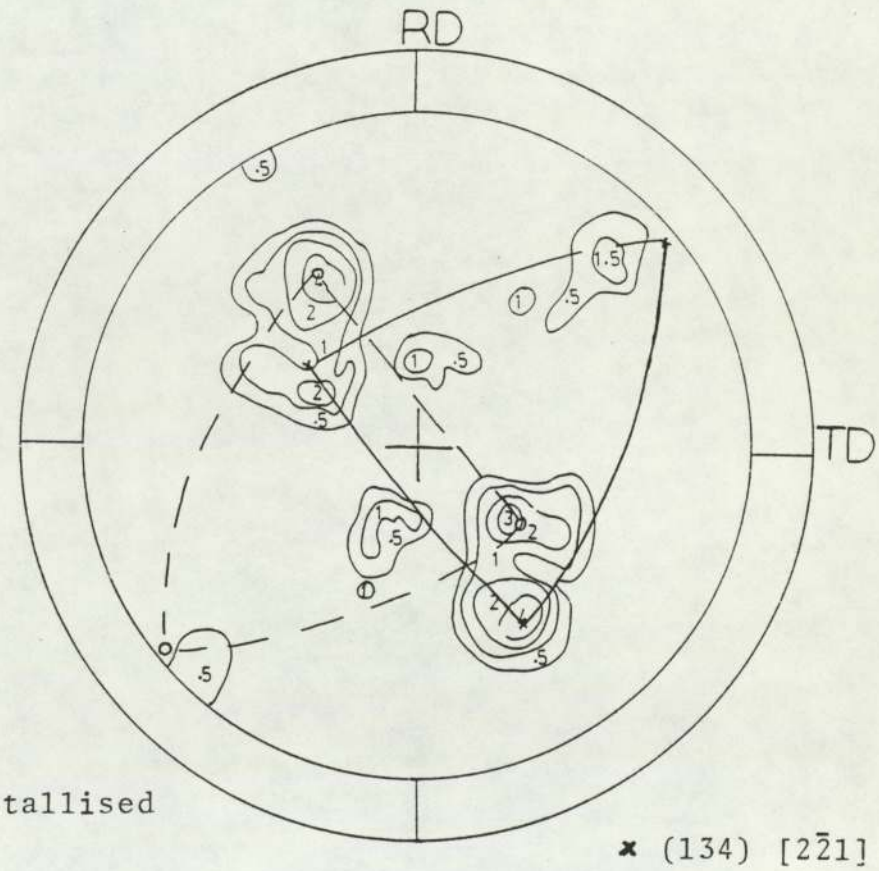

(D)

As Fully Recrystallised

× (134) [2$\bar{2}$1]

o (134) [$\bar{2}$2$\bar{1}$]

Figure 64

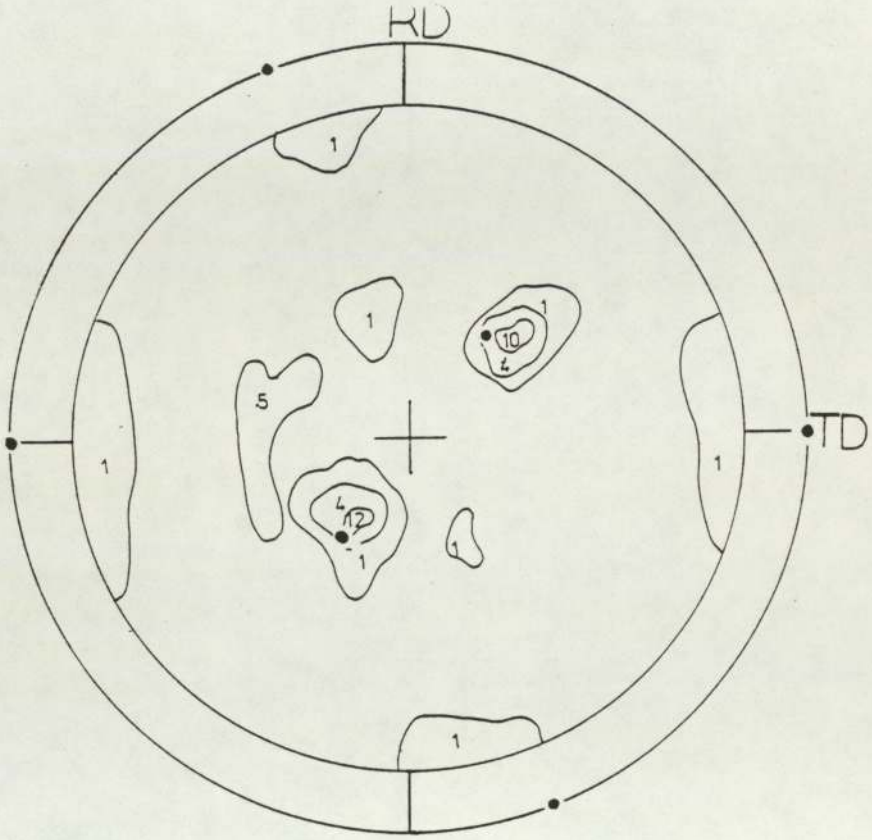

(E)

Crystal F

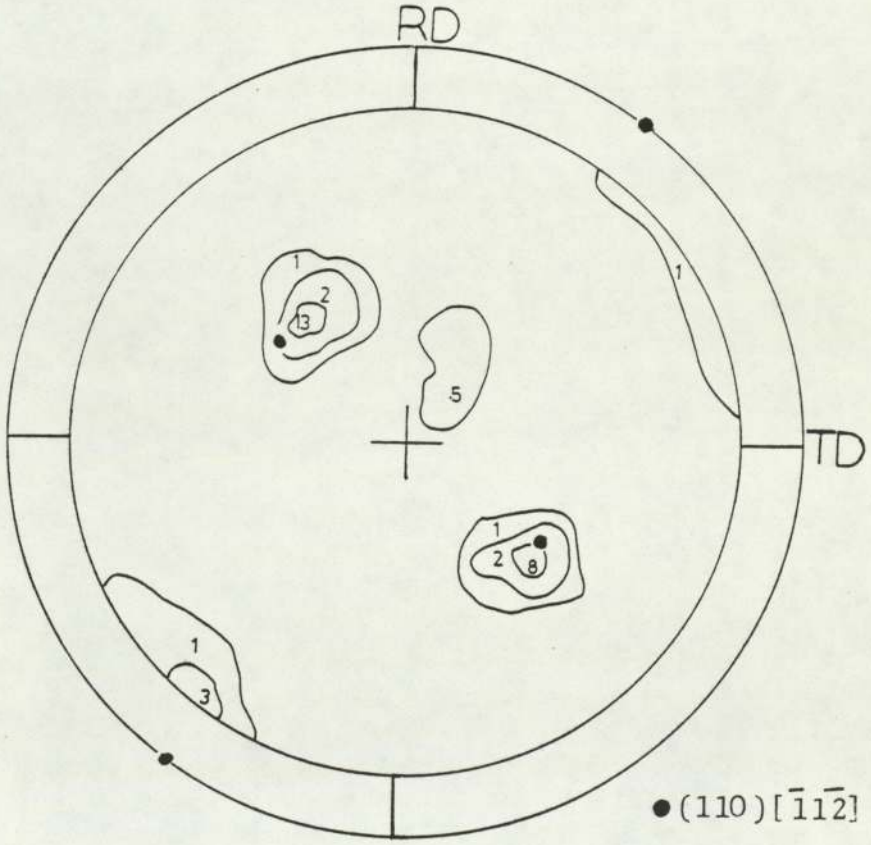

(F)

As Rolled

●(110)[$\bar{1}1\bar{2}$]

Figure 64

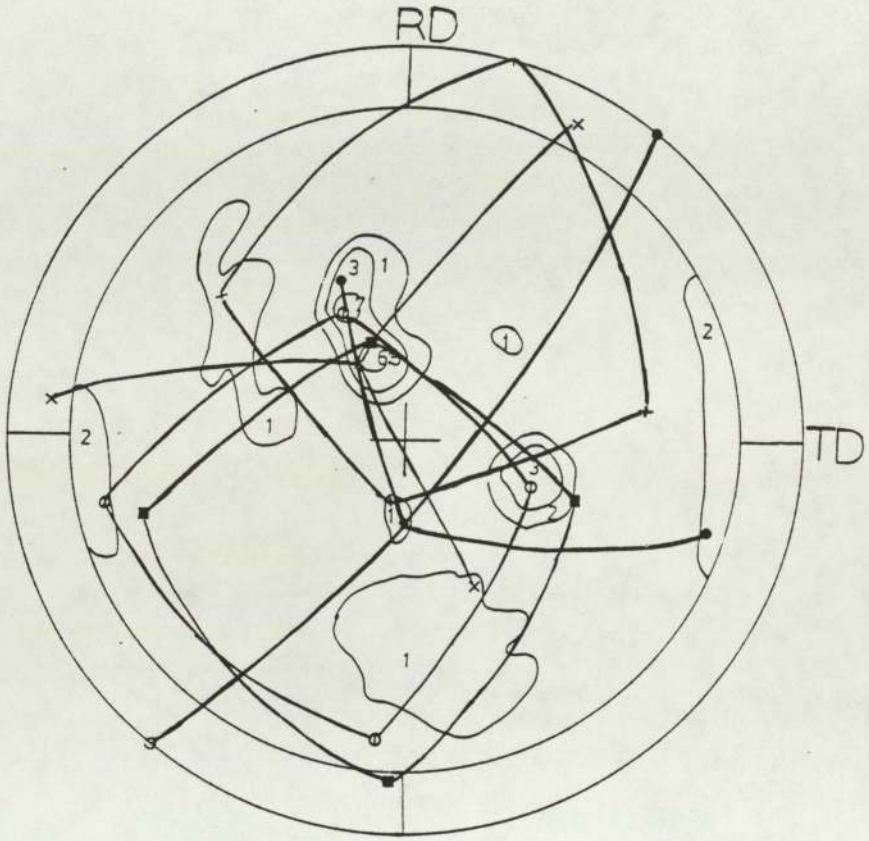

(G)

Crystal F

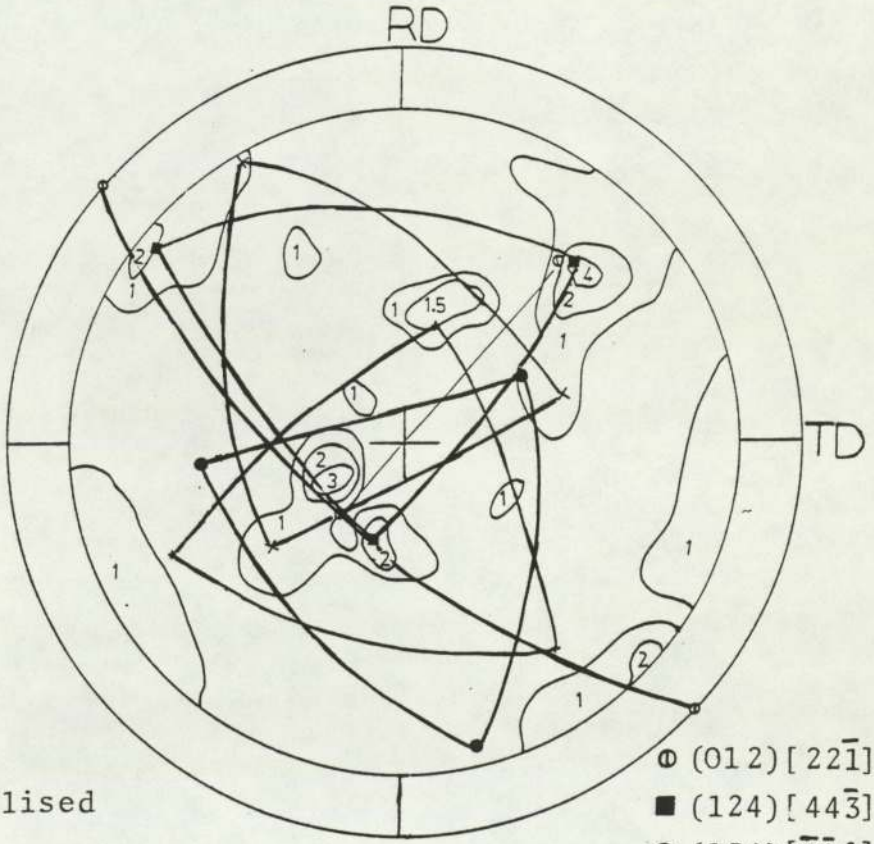

(H)

As Fully Recrystallised

Φ (012)[22$\bar{1}$]
■ (124)[44$\bar{3}$]
● ($\bar{1}$3$\bar{1}$4)
× (144)[41$\bar{2}$]
+ ($\bar{1}\bar{1}$2)[$\bar{4}\bar{2}$3]

Figure 64

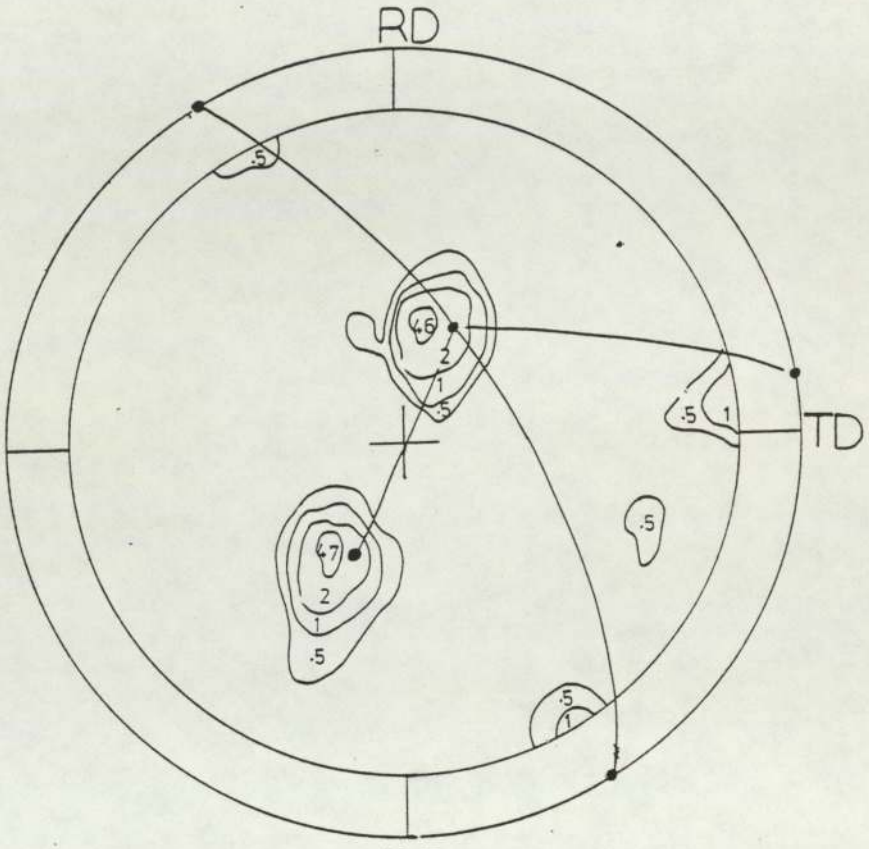

(I)

Crystal G

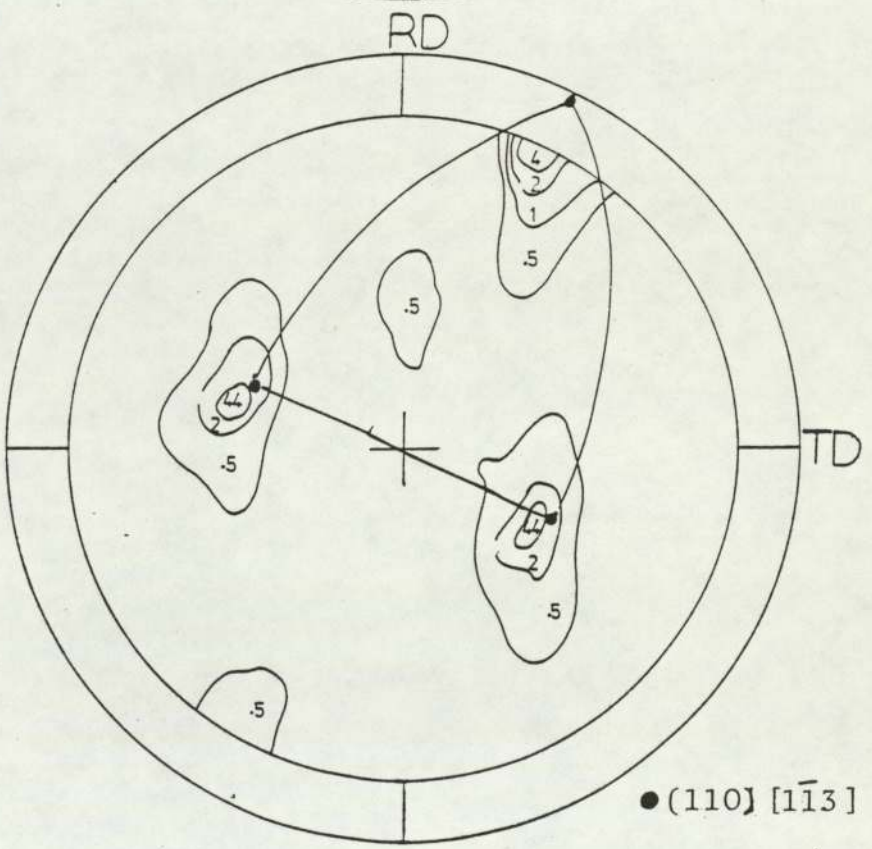

(J)

As Rolled

● (110) [1$\bar{1}$3]

Figure 64

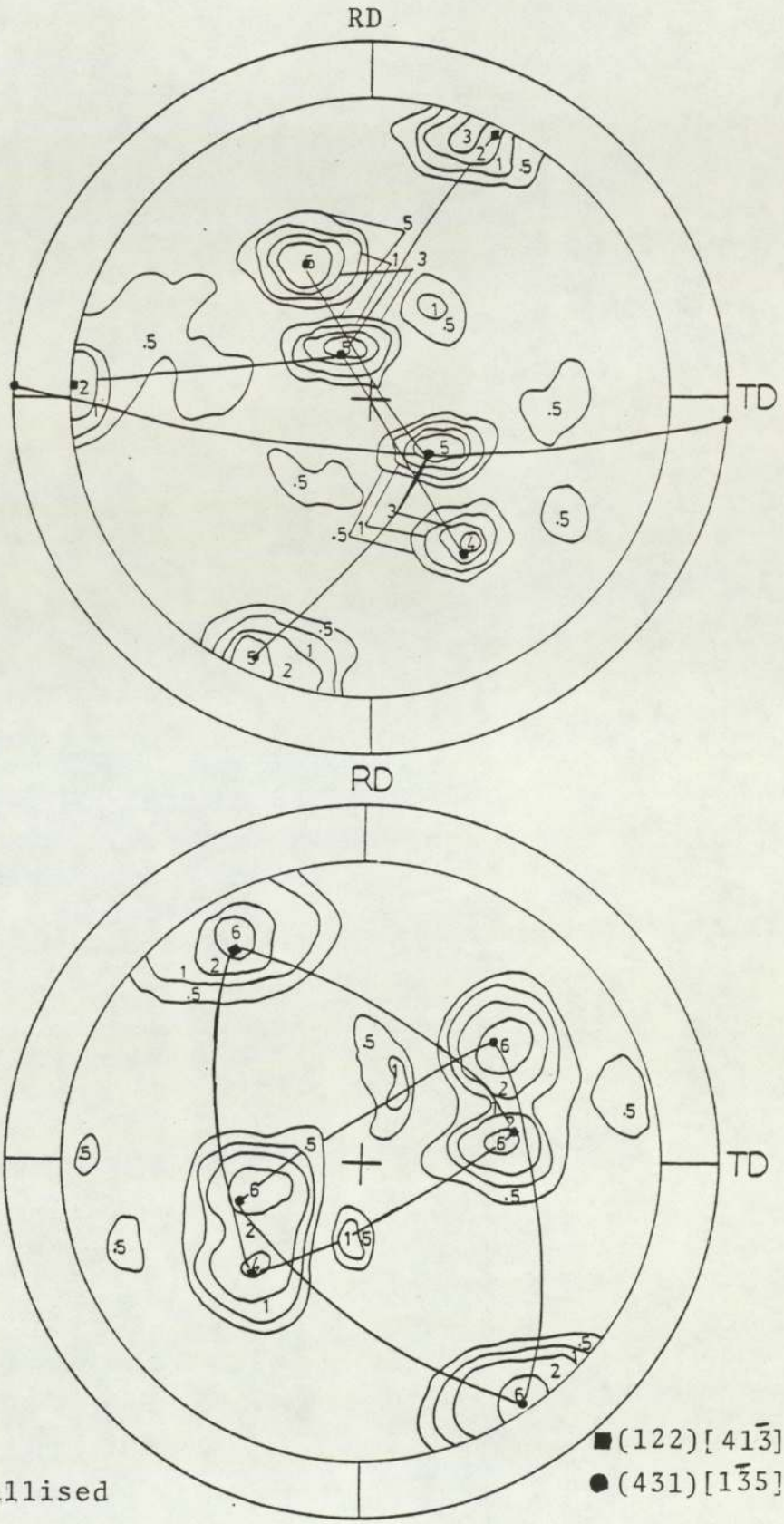

(K)

Crystal G

(L)

As Fully Recrystallised

Figure 64

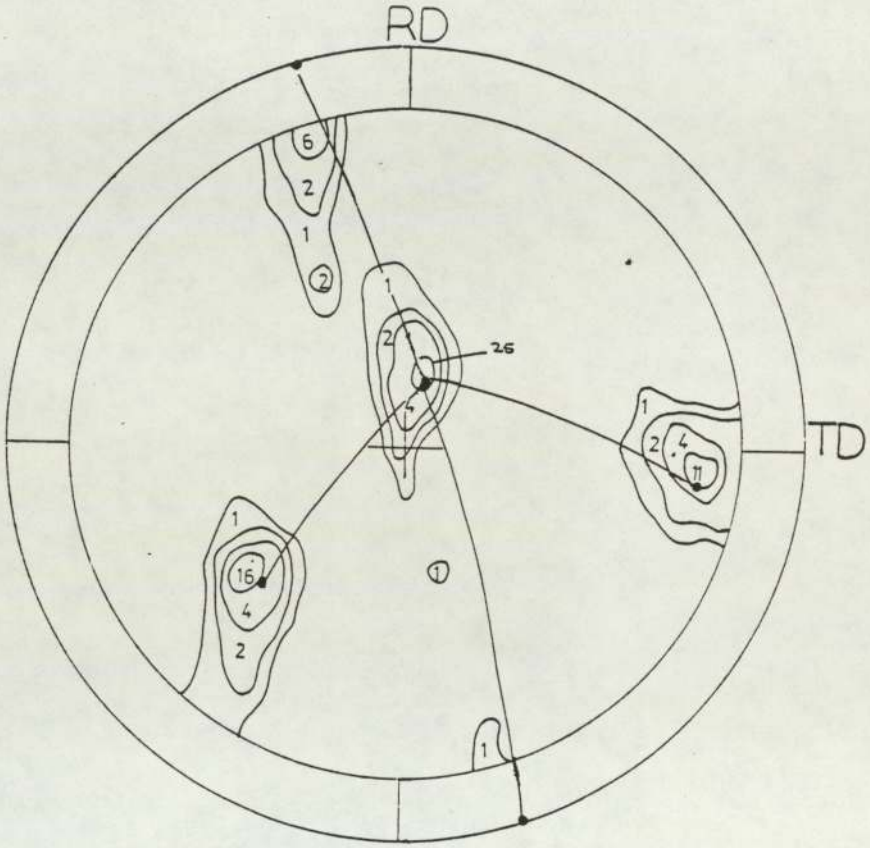

(M)

Crystal H

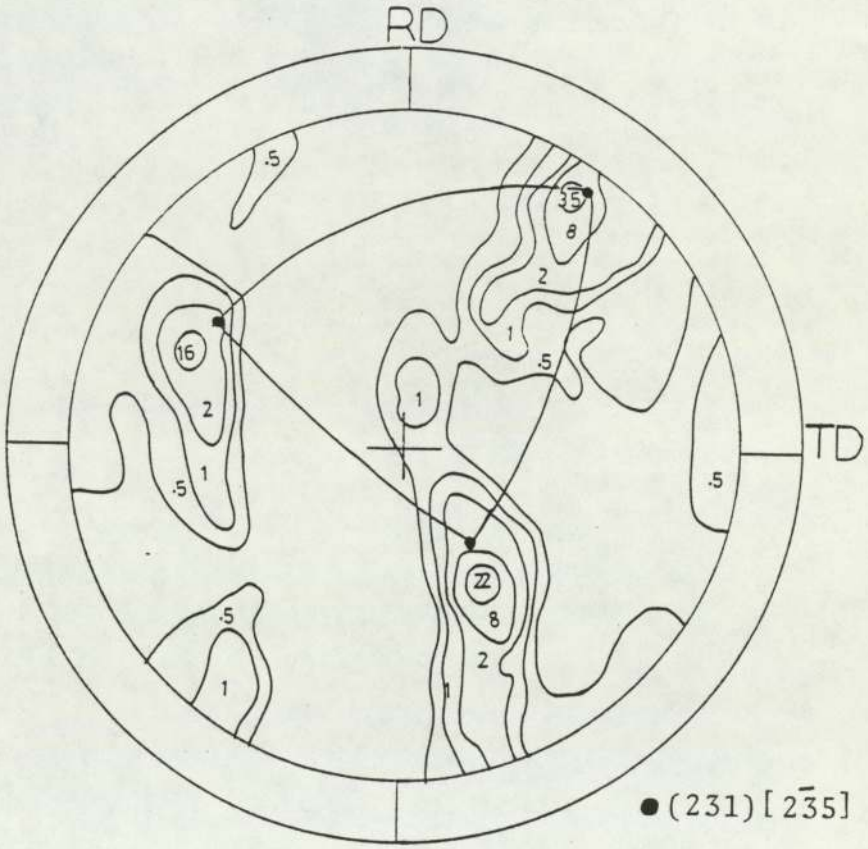

(N)

As Rolled

●(231)[2$\bar{3}$5]

Figure 64

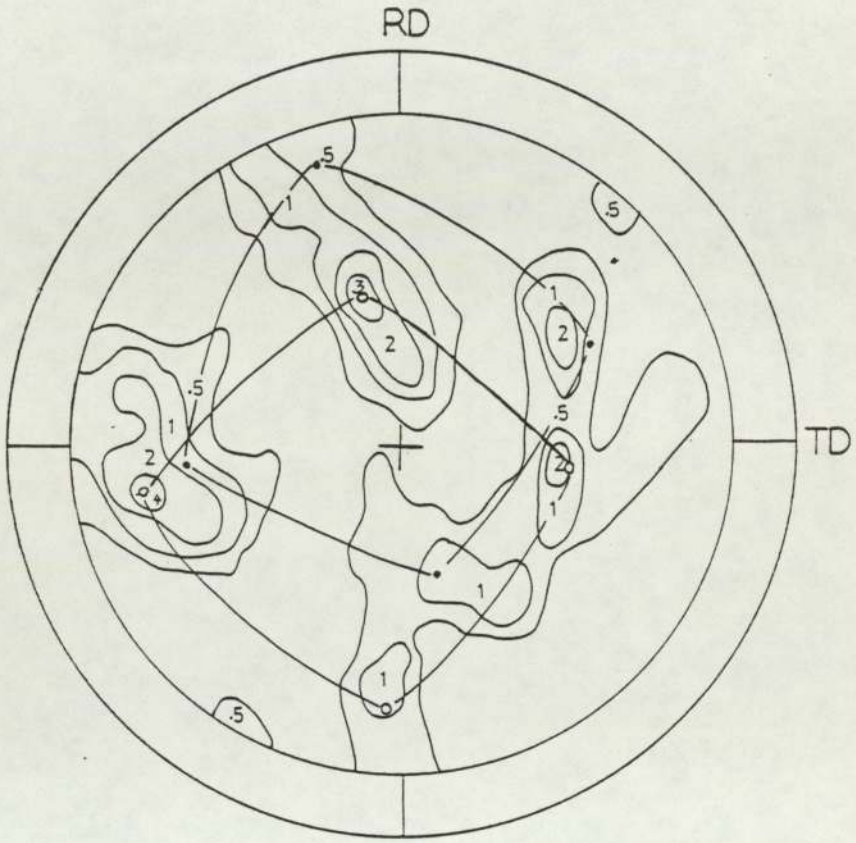

(O)

Crystal H

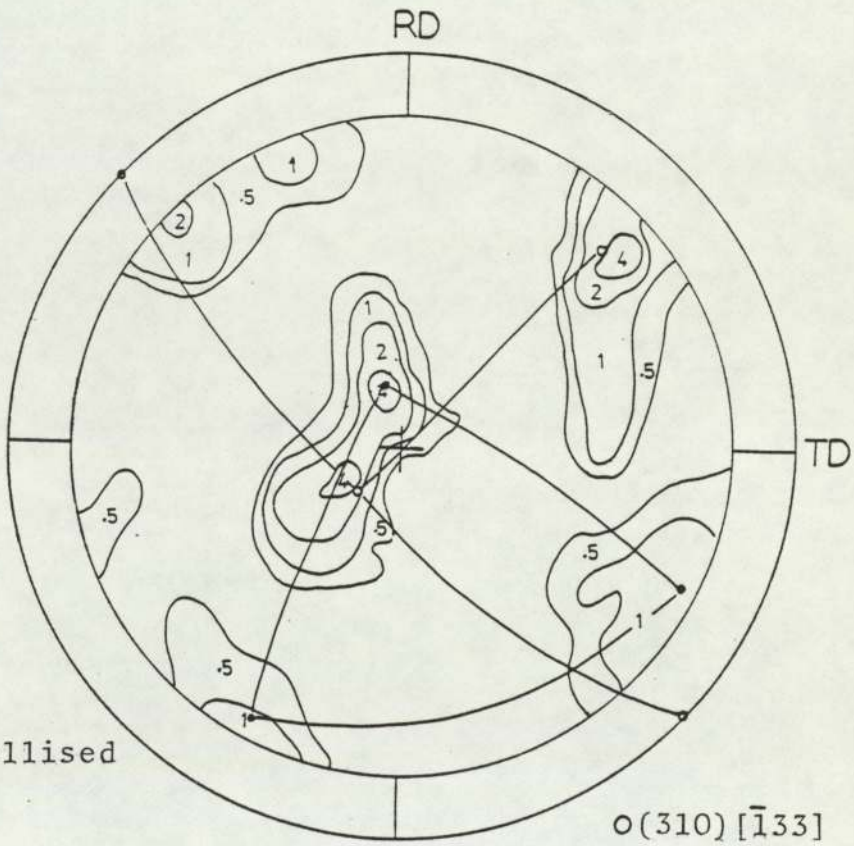

(P)

As Fully Recrystallised

o (310) [$\bar{1}$33]

● (114) [$\bar{1}\bar{3}$1]

Figure 64

CHAPTER FIVE

DISCUSSION AND CONCLUSIONS

5.1 Al-0.75% Mg-0.43% Si Alloy

Perhaps the most apparent result of the present work is that the formation of the equilibrium (β) Mg_2Si precipitates in Al-Mg-Si alloy on ageing will disturb the structure during deformation and also affect the subsequent annealed state due to their influence on nucleation and grain growth. The influence of the presence of second phase particles in Al-Mg-Si material prior to deformation depends on their size, volume fraction and inter-particle spacing in addition to their hard, non-shearable nature. This is clear from Figure (23), which is an optical micrograph of the Al-Mg-Si alloy in two different treatments.

The combination of optical microscopy, SEM, TEM and X-ray examination has shown that the semi-coherent Mg_2Si particles, have the fcc structure with a lattice parameter of 6.365 $\mathring{A}$, and were formed as square platelets on the matrix {100} planes. The orientation relationship with the matrix was found to be[11,12]

$$(100)_\beta \;//\; (100)_{Al} \quad \text{and} \quad [110]_\beta \;//\; [100]_{Al}$$

These particles have a mean length of about 5.95μm, Figure (33 b) and thickness about 0.8μm, and are hard and non-deformable. During deformation the particles lying at certain angles rotated into parallelism with the

directions of the flow and with increasing applied strain, more particles lay parallel with the rolling direction, RD. The rolling direction experimental results of the orientation distribution of the particles with respect to the rolling reduction showed a little agreement with theoretical results, this deviation may possibly be attributed to those particles making an angle of 90^{o} with the rolling direction, and instead of rotating they have started to buckle during deformation to maintain the deformation processes.

The results in Chapter (4) indicated that unaged Al-Mg-Si specimen rolled 90% reduction in thickness, showed a few shear bands in its deformation structure, while no shear bands formed in aged specimen, Figure (25 c,d). Despite this difference in their deformation structure the recrystallisation kinetics, as determined by optical microscopy, showed that aged specimen with large, non-deformable particles recrystallised faster than as-quenched specimen, as shown by curves A and C in Figure (37). This is possibly attributed to the presence of very coarse particles of Mg_2Si prior to rolling, which gave rise to great heterogeneity of the microstructure during rolling deformation. This would increase the dislocation density and thus the stored energy, and produce local lattice curvature around the particles. This will stimulate nucleation which is responsible for the acceleration of recrystallisation, resulting in a fine grain size. In unaged specimen with starting material of large grain size,

on annealing an incubation period occupied some time, and then recrystallisation started rapidly, probably due to the large grain size which reduced the availability of nuclei to form, so the recrystallisation was retarded in the early stage of anneal. Similar observations have been reported in the Al-Cu[103,104] and Al-Mg alloy[128].

The difference in the deformation structure in unaged and aged specimens may be due to the presence of the large particles prior to deformation, Figure (25 c,d,f). The formation of shear bands in unaged specimen was similar to those formed in Al-Cu alloys[136,147]. This is attributed to the age hardening in Al-Mg-Si alloy which occurs at room temperature, and produced too fine a scale of precipitates so that these precipitates will shear during plastic deformation and thus allow localised softening to occur. This effect will cause the instability in the matrix and formation of shear bands. But when these precipitates have grown to a large size, no shear bands are formed as in Figure (25 d,f). Dillamore et al[147] explain the formation of shear bands in aged Al-Cu alloy as due to the work softening. Also Brown[137] attributed the formation of shear bands in Al-Mg and pure aluminium to a decreasing work hardening rate. Thus the formation of shear bands depends upon the size, nature and the volume fraction of the particles in addition to the distribution of these particles prior to rolling. When these particles are not uniform, the slip tends to concentrate in bands in which the volume fraction of the second phase is lower than in the rest of the matrix.

Crystals A and B were single crystals of Al-Mg-Si which were deformed about 71% reduction at room temperature, and contained coarse particles before rolling. The orientations were (110)[001] and (231)[$\bar{1}2\bar{4}$] and they showed no sign of shear bands which is consistent with the TEM observation.

In a high-purity aluminium single crystal with (110)[001] orientation, no shear bands have been observed after deformation to about 75% reduction at room temperature, only very fine cross slip bands were visible in the surface, Figure (27 A). Probably this crystal was oriented for easy deformation. This was supported by the observation of the annealed microstructure, which indicated that this crystal was resistant to recrystallisation and required a high temperature of up to 400^{o}C to complete recrystallisation. Because of the easy flow during deformation this lead to a reduced stored energy which is necessary to form new grains. Also in very pure materials a small fraction of the stored energy is utilised for recovery in comparison to the amount required for less pure materials, so the comparatively large recovery process in the early stage of annealing will retard recrystallisation.

5.2 Al-5% Zn-1% Mg Alloy

In Al-Zn-Mg alloy, the deformation structure was quite different from that observed in Al-Mg-Si alloy. A large number of shear bands were formed after deformation 90%

by cold rolling, in both as-quenched and overaged conditions. This similarity in the deformed structure may be due to the dissolution of most of the second phase at the ageing temperature, and this view is consistent with the TEM observations that they were distributed on a very fine scale.As mentioned earlier, in Al-alloys age hardening occurs at room temperature and forms fine precipitates which are sheared during deformation.

The incidence of shear band formation in high Stacking Fault Energy (SFE) alloys are lower than in low Stacking Fault Energy alloys (e.g. copper compared to aluminium), and these bands are sheet-like and exist within individual grains although some extended into other grains. However the structure was not divided into a series of rehomboidal prisms as has been observed in brass[39,135], but instead the structure consisted of an array of elongated deformation bands and it is believed that these are different than those observed in low Stacking Fault Energy materials, especially in materials where the shear bands must be accompanied by mechanical twinning during deformation[133-135,143,144]. In untwinned materials such as aluminium and aluminium-alloys, the origin of the shear bands perhaps lies in the ability of the material to sustain further work hardening.

The results given in section (4.2.2) show that recrystallisation of heavily rolled Al-Zn-Mg alloy begins within the shear bands, Figure (26 b), where these regions are

associated with a high density of dislocations (high stored energy) and local misorientation, and these have acted as favourable nucleation sites, resulting in a fine, equiaxed grain size. It is well established that recrystallisation occurs preferentially within the shear bands[132,139,140,145] as was observed in the present work. This will have accelerated recrystallisation in Al-Zn-Mg alloy, curve (B) of Figure (37).

The deformation structure in Al-Zn-Mg single crystals after 80% reduction, exhibited different microstructures, depending on their original orientation. In crystal E with (110)[001] orientation, the deformed structure showed very fine, narrow bands, making an angle of about 35^{o} to the rolling direction, Figure (27 B). Compared with the pure aluminium single crystal (D) after 75% reduction, Figure (27 B) shows a similar structure with only fine slip bands. This was confirmed by the TEM observation, where Figure (52) shows narrow bands with probably two very narrow cross bands running between them. The recrystallisation of this crystal was slow but still faster than in the crystal D at the same annealing temperature. Also the fact that this recrystallised most slowly is evidence that there were no shear bands formed. This was possibly due to the orientation of this crystal to give single slip with respect to the rolling direction which leads to a reduction in the stored energy necessary for nucleation.

In contrast, in crystal F with (110)[$\bar{1}1\bar{2}$] orientation the deformed structure was remarkably different from that

which has been observed in previous crystals. The incidence of the shear bands was high and these were inclined at an angle of about 35^{o} with the rolling direction, not parallel to the transverse direction, but running through the whole specimen thickness, Figure (28 a,b). According to Dillamore et al[147] the (110)[001] and (110)[112] should be symmetrical in their behaviour and would form two sets of shear bands with equal widths, but this was contrary to the present observation.

This crystal recrystallised rapidly compared with the previous crystal and the new recrystallised grains were obviously formed within the shear bands where the high strain concentration occurred, Figure (28 c). By increasing the annealing time, more nuclei continued to form along the shear band and the recrystallised grain size increased. Adcock[132] showed that shear bands are potent sites for nucleation of recrystallisation. Similar observations have been reported by many workers[39,135,136,139,140].

A complete softening by recovery without recrystallisation has been reported for aluminium crystals[17,21], and slow recrystallisation for both aluminium[19] and copper[14,15]. In the present work, it was found that this crystal recrystallised very rapidly with small grained microstructure.

Liu et al[16] showed in deformed pure copper and Cu-4%Al, that no shear bands were formed even after 99% reduction, only slip bands. Also in copper crystal[141] and in high

purity silver crystal[144] rolled between 85 to 95% reduction at room temperature, the deformation structure showed neither twin lamellae nor the shear bands.

The deformed structure of crystal (G) showed that fewer shear bands were formed, but these were more severe and narrow, and were inclined at about 35° to the rolling direction, but not parallel to the transverse direction, Figure (29 a,b). The annealing microstructure of Figure (29 c) showed that the recrystallised new grains occurred preferentially within the shear band. The behaviour of this crystal was different from the previous two crystals (E) and (F), which recrystallised very fast to form a coarse grained microstructure.

In the last crystal of Al-Zn-Mg, (H), the deformed structure showed a high density of shear bands which were inclined at an angle of about 35° with respect to the rolling direction, and again not parallel to the transverse direction, Figure (30 a,b).

During annealing the recrystallisation grains were found to form within the shear bands, to produce a fine-grained microstructure. Figure (30 c) showed that copious nucleation had occurred in shear bands. The recrystallisation behaviour was similar to that observed in crystal (F) but different from that of (E) and (G).

From the present results, it was clear that the high Stacking Fault Energy metals such as aluminium and

aluminium-alloys behaved quite differently from the low or medium Stacking Fault Energy metals. In similar orientations different microstructures were developed during deformation, and subsequently different recrystallisation kinetics resulted. Also it is indicated that the formation of shear bands depended on the initial orientation.

Grewen et al[133] considered only grains having either of the two stable end orientations, that is (112)[$\bar{1}$11] or (110)[$\bar{1}$12], and their observations showed that in grains with (112)[$\bar{1}\bar{1}$1] orientations, shear bands made an angle of 20 - 5° or 33° - 5° to the rolling direction. While in grains with (110)[$\bar{1}$12] orientation the angle between the shear band and the rolling direction was 30° - 5°. Consequently they concluded that shear bands are crystallographic, and their direction is governed by the orientation of the grains. This is in contrast with present results which show shear bands are non-crystallographic , which has been observed first by Adcock[132] and has been found since in many metals and alloys. In all cases the shear bands developed as sheet-like features that make an angle between 30° to 35° with respect to the rolling direction, but they are not parallel to the transverse direction, and they do not form on the expected plane of maximum shear stress (45° to the rolling direction). Dillamore et al[147] have shown that shear bands formed at 45° to the rolling plane trace if the materials contained a weak texture. It was argued that shear bands form as the result of a load instability due to

geometric softening.

Table (3) summarises the observed features in the deformed structure of single crystals with different orientations.

Table (3)

Crystal Symbol	Initial Orientation	Deformed Structure (70-80% Reduction)
A	(110)[001]	No shear bands
B (Al-Mg-Si)	(231)[$\bar{1}2\bar{4}$]	No shear bands
C	(014)[34$\bar{1}$]	No shear bands
D (Pure Al)	(110)[001]	No shear bands
E	(110)[001]	A few narrow bands
F	(110)[$\bar{1}1\bar{2}$]	Numerous shear bands occur with an angle 35° with RD; not parallel to TD.
G (Al-Zn-Mg)	(231)[1$\bar{2}$4] (110)[1$\bar{1}$3]	Less incidence shear bands, more severe with an angle 35° with RD, not parallel to TD
H	(241)[1$\bar{1}$2] (231)[2$\bar{3}$5]	High level of shear bands making an angle 35° with RD and again not parallel to TD.

Dillamore et al[90] have pointed out that the deformation bands may arise in four ways. In particular, they will occur whenever local differences in stress state activate different combinations of slip systems to produce the same imposed strain in different parts of the crystal. Different slip rotations will then occur and a relative misorientation is produced. From this point of view

deformation bands of this type are inevitable in rolled single crystals because of the presence of surface friction stresses.

5.3 Scanning Electron Microscopy - Back-Scatter Electron In Al-Zn-Mg Single Crystals

In Chapter (4) the examination results indicated that in Al-Zn-Mg single crystals of various orientation, shear bands formed after deformation of about 80% by cold rolling at room temperature, with the exception of crystal (E) of (110)[001] orientation.

In the early stages of recrystallisation of the three crystals, F, G and H, the nucleation of new grains occurred along the shear bands as have been observed by optical microscopy and SEM/BSE, Figure (33, 34, 35). This behaviour may be expected because of the sharp lattice curvature produced by the shear process[133,145] and high dislocation density (stored energy) associated with them.

An orientation analysis was carried out by selected area channelling patterns (SACP) from these first new recrystallised grains formed within the shear bands for each crystal. Crystal F of (110)[$\bar{1}1\bar{2}$] orientation, Figure (33b), showed, in spite of some scattering, the orientation of the recrystallised grains formed along the shear bands which agreed quite well with the results of pole figures determined after complete recrystallisation. Similar observations have been reported in cupro-nickel[132],

Cu-0.6 Wt% Cr[133], 70:30 brass[39], and Silicon-Iron[140].

In the last two crystals (G) and (H), their orientation change after deformation. After a short anneal there is no doubt about the formation of the nuclei within the shear bands, as observed by optical microscopy and SEM, Figures (34 a,35 a). As mentioned earlier, crystal G was recrystallised very rapidly compared to crystals F and H resulting in a large grain size. The orientation of these new recrystallised grains labelled in Figures (34 a,35 a), and from other areas, is shown in Figures (34 b,35 b). There were only a few orientations near to the final orientation after complete recrystallisation, i.e. the annealing texture is not clearly associated with orientations from these first formed nuclei as in previous crystals. This may possibly be attributed to multiple nuclei which were formed in these regions, which restrict the ability of each other to grow, while other nuclei developed elsewhere in the deformed structure and grew more rapidly than those formed first, to dominate the final recrystallisation texture. In photograph, Figure (31 a,b) from specimens of crystals G and H after complete recrystallisation, which showed that the new recrystallised grain were smaller than the grains within the deformed matrix. Alternatively this effect could be due to the instability of these crystals during deformation where their orientation deviated from the true position, which makes it difficult to interpret the results clearly. The formation of peculiar shear bands later is possibly another reason, but these are not easy to predict.

Hutchinson et al[135,145] have suggested that shear bands contribute significantly to the development of annealing texture, but such an effect has not been observed in these results. Similar observation for copper[139] showed that the introduction of shear bands in copper prevented the development of a strong cube texture, their presence destroying the long transition bands needed for nucleation of cube oriented grains. Also in 70:30 brass, Duggan et al[145] have shown that a virtually random array of nucleus orientations is produced when recrystallisation is confined to the shear bands. Dillamore[149] has reported that the orientation of the grains within the shear bands is not associated with fully recrystallised texture and he attributed this to the fact that the multitude of nuclei found to form within the shear bands leads to a fine - grained structure, which may be consumed subsequently by other grains formed within the matrix.

5.4 Transmission Electron Microscopy

5.4.1 Al-Mg-Si Alloy

During deformation of Al-Mg-Si polycrystalline and single crystals the microstructure was free of shear bands. Because the specimens were aged prior to rolling to produce coarse, hard, widely separated precipitates, the deformation will depend on the plasticity of each phase. The deformation will occur first in the soft phase and with more difficulty in the hard particles. This leads to the compatibility problem between the hard second phase

and the soft matrix so that the slip first occurs in the matrix, therefore the distribution of the strain will be nonuniform, and high local deformation will be produced in the vicinity of the particles, resulting in a high dislocation density. These regions are referred to as the deformation zone[111].

The appearance of the deformation zone in aluminium alloys has been recently studied by Humphreys[111] and Herbst et al[73]. The subgrain size is considerably smaller in the area around the particles than elsewhere. In the present work this was observed to be mainly near to one end of the edge of the particles or at both sides. Since the effect of the presence of coarse, second phase particles is to disturb the deformation microstructure, by disturbing the motion of dislocation, therefore the distribution of the cells is not uniform, especially after 50% reduction, Figure (40 a), which showed some subgrains free of dislocation where others were not. After a higher reduction of about 90%, i.e. higher stored energy, the rearrangements of dislocations were speeded up as shown in Figure (40 b). The deformation microstructure of all the single crystals A, B and C was similar with only slight differences in the sizes of the subgrains, Figures (41 a,b,c)

The orientations determined from the subgrains around the particles in 70% and 90% reduction specimens were nearly random, Figures (42, 43 b). Because of inhomogeneous deformation occuring near to the particles, this lead to

many orientations and a large orientation spread will develop in the vicinity of the particles. A similar observation has been reported by Humphreys[111], Grewen et al[72] and Herbst et al[73].

The orientation analysis of rolled single crystal(A) Figure (44 b) of orientation (110)[001], showed that the orientation around the particles was not random, but there was a wide scatter and some clustering of different orientation as shown in Figure (44 c), in addition to population of orientation near the original orientation. In crystal (B) of (231)[$\bar{1}2\bar{4}$] orientation, it was found that the orientation distribution of the subgrains adjacent to the particles split into about two orientations near to the [110] and the other about on a curve between [115] to nearly [111] in transverse direction in addition to the population near to [112] transverse direction, Figure (45 b), while in the normal direction and rolling direction there is a wide scattering with some preferred orientation near to <110> in the transverse direction and rolling direction. While in crystal (C), with an orientation (014)[34$\bar{1}$] which was originally unstable during deformation, a wide scattering of orientation with some patches of population of different orientations is shown by Figure (46 b). It was difficult to find precisely what orientation, due to the instability of this crystal during deformation.

It has been widely reported that the nucleation of recrystallisation occurs preferentially in deformation

zones adjacent to large particles where the lattice is misoriented and because of the high elastic energy this will be the preferred site for nucleation on subsequent recrystallisation.

The annealed specimen of 70% reduction showed that the nuclei were formed within the deformation zone adjacent to the coarse particles where the sharp lattice curvature was present, and some of them started on each side near the end or fom one end and consumed the deformation zone to finish at the opposite end of the particle. This is shown by Figure (47 c). Alternatively they may continue to grow till the particle was entirely surrounded as in Figure (47 b). In the 90% reduction specimen, the development of nuclei on annealing was aided by a high local dislocation density near to the particles, and the nuclei were formed within the deformation zone around the particles. More than one nucleus was observed to form, Figure (48 a,b), in spite of the recovery during annealing and it was hard to find nuclei formed within the deformed matrix far away from the particles in the surrounding area. Due to the large scattering in orientation around the particle, the orientation of these nuclei was found to be random, because only the subgrains present near to the particles could act as nucleation sites. Similar observations have been reported by Humphreys[111,118] and Herbst et al[73]. Multiple nucleation was observed to form at one particle. The work by Herbst et al[73] agrees well with the present work, which does not agree with the conclusion of Grewen et al[72] that a single nucleus is

formed at each particle.

The orientations of nuclei when the recrystallisation has only just begun in annealed crystals (A) and (B) are shown in Figures (49 c,50 b), which show that some of these orientations resemble those of the mature grains after complete recrystallisation. Because the area surrounding the particles was more complicated in deformation structure, so due to this case, probably, multinuclei were formed in this region which restricted each other for growing. Since these remained very small they were consumed by other nuclei formed within the scattered orientation around the particles, which were able to grow faster and gave the final annealing texture. Or possibly due to the recovery in this area during a short anneal, where the high stored energy was present. More than one nucleus was formed adjacent to one particle, Figure (49 d) this observation is not in agreement with that of Humphreys[111] on Al-Cu-Si single crystals. He explained that the deformation zone in deformed single crystal seems to be less complicated than in polycrystalline material, therefore only one grain will be formed. In crystal (C) also,nucleation was observed to occur in the vicinity of the particle and more than one recrystallised grain was nucleated near to the particle. The orientations of these nuclei showed a wide spread with little population around the final orientation, Figure (51 c). A very small group of orientations from cube-oriented grains was also observed. This could be explained in terms of the particles being probably located within transition bands, as

described by Nes et al[129], and because the process of softening is controlled by the nucleation at coarse particles which will prevent the development of the cube-oriented grains. A similar observation has been reported in Al-Mg-Si alloy[70,73].

5.4.2 Al-Zn-Mg Alloy

In section (4.7) the examination results of deformed Al-Zn-Mg single crystals exhibit different behaviour with respect to rolling deformation after 80% reduction. The deformation structure of the (110)[001] oriented crystal (E), showed two sets of narrow bands which are shown in Figure (52 a,b). In contrast the (110)[$\bar{1}1\bar{2}$] crystal, in spite of the effect of the polishing on the shear bands, but still some are visible, Figure (53 a). While in the last two crystal (G) and (H), the deformed structure showed very wide shear bands running through the whole specimen thickness, as in Figures (53b, 54a,b), where the incidence of the shear bands are more in crystal (H) compared with other crystals. From this observation it is clear that the inhomogeneous deformation of shear bands depends on the orientation of the crystal. The microstructure of the bands consists of fine crystals with high misorientation due to the high strain concentration.

The orientation of these crystalline regions (Figure 55 b) showed a wide spread, with a distinct tendency near {114}. The methods of Bishop and Hill[149] have been used in order to predict which slip systems are operating. The

results of such analysis found that only a single slip system operates with rotation around [12$\bar{1}$] axis, where a small circle was drawn to find the rotation paths. According to this method it was found that this does not fit with the STEM results shown in Figure (55 b). In the last two crystal (G) and (H) it was found that the orientations of the crystallites within the shear bands, Figures (56 b,57 b), in addition to the large spread and scattering in orientation, were in agreement with the texture determined from X-ray pole figures. A similar procedure of using Bishop and Hill methods, was used for both crystals, and it was found that crystal (G) deformed by single slip with rotation around the transverse direction, while in crystal (H) double slip systems operated and the rotation was around the transverse direction. There has been some discussion recently about shear bands and their contribution to deformation processes and the microstructure and texture of rolled material[39,145]. No attempt is made to discuss the details of the shear bands in high Stacking Fault Energy materials such as aluminium and aluminium alloys, and their contribution to the texture.

5.5 Texture

5.5.1 Rolling and Annealing Al-Mg-Si Alloy

The development of the deformation texture during cold rolling of a solution treated and overaged Al-Mg-Si with large grain size starting material is similar to that of

'pure metal' texture. The rolling textures developed in second-phase material were almost the same as for single phase material in which a low concentration of shear bands was found to form, and in both cases the textures were weaker than in 'pure metal' type texture, Figures (58&59 A,B,E,F,I,&J)

The generation of the 'pure metal' texture after 50% reduction is possibly due to the presence of the precipitates which set up regions of high strain around the particle, thus initiating cross slip earlier and therefore resulting in the onset of the 'pure metal' type texture sooner than for a pure aluminium specimen. Since the presence of the coarse particles disturbs the deformation, resulting in inhomogeneous deformation this will affect the rolling texture and subsequently the annealing texture.

Wasserman et al[148] found that the hard particles have a remarkable influence in prohibiting the formation of a deformation texture of the matrix metal. Because the bonding of the particle to the adjacent matrix crystals is so firm, the normal crystallographic slip processes are disturbed. From Figure (65) which shows the immediate surroundings of an undeformable particle, no deformation of the matrix is evident within a very thin layer. But within a distance of about 5μm a transition from almost randomly disoriented matrix to the substructure with the normal deformation texture takes place. So that the more particles are present, the more disturbed zones exist.

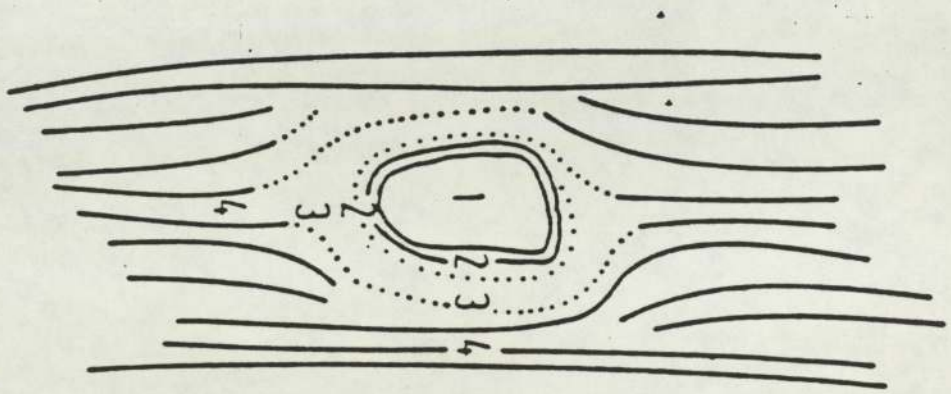

Figure (65) Undeformable particle and its influence on matrix texture. 1 - Particle, undeformed,
2 - Matrix, undeformed, no texture,
3 - Matrix, deformed, no texture,
4 - Matrix, highly deformed, texture

Ref. (148)

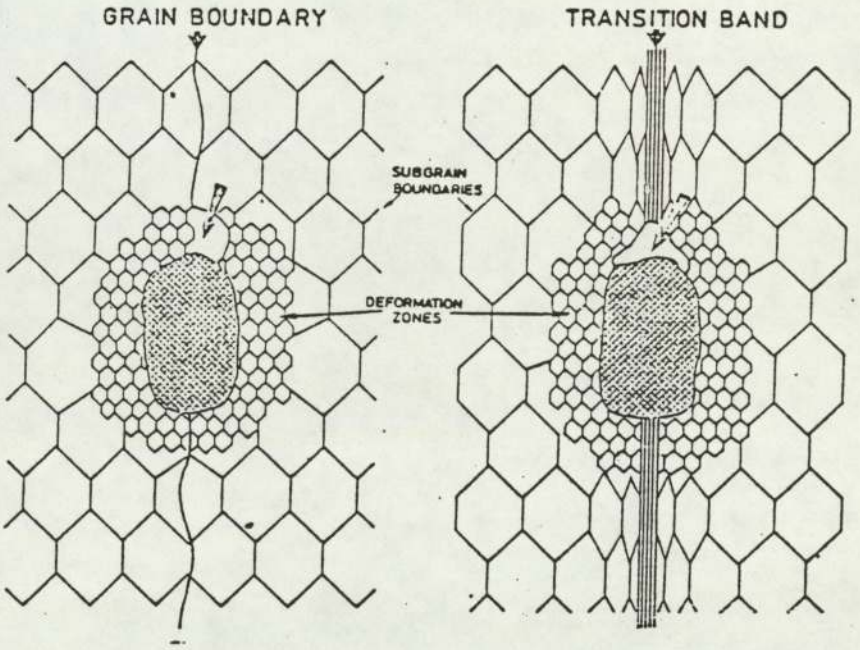

Figure (66) Sketches illustrating typical sites for nucleation of recrystallisation in polycrystalline materials,
a)-Particle/grain boundary nucleus and
b)-Particle/transition band nucleus

Ref. (129)

The annealing textures of deformed specimens, Figures (59 C,D,G,H,K,L & 60 a-f) for material A_I and A_{II} were basically similar, but with the first treatment some cube component was present which had disappeared from material A_{II}. The presence of the hard, coarse second-phase particles prior to deformation increased the randomness of annealing texture. This was possibly due to the particles acting as centres for high internal energy accumulation in the matrix which resulted in the formation of many new centres for recrystallisation and then gave scattering at orientations. By comparison with the TEM, the investigation of the early stages of annealing showed that the orientaion of the new grains formed adjacent to the particles was random, i.e. there was no preferred orientation, which agrees with the annealing textures determined from X-ray pole figures. A similar observation has been reported by many workers on Al-Mg-Si alloys and Cu-Ag-Si alloys[72,73,117]. They found large misorientations near to the particles following cold work, with subgrain nuclei formed at orientations up to 20^{o} away from the surrounding matrix material. Humphreys[118,128] has proposed that particles larger than about 1μm which are present during cold working will tend to produce random annealing textures,and the orientations of the recrystallised grains are found to be in the orientation spread present in the deformation zone, as observed in the present work. This result strongly supports the oriented nucleation mechanism rather than that of oriented growth. Similar results have been reported by many workers[70,72,73]. The development of random arrays of nuclei in randomly oriented

zones around the particles should provide the conditions for selective growth but the absence of a marked recrystallisation texture supports the theory of oriented nucleation. Also many works have been published on the effect of the second-phase on the recrystallisation behaviour in Al-Mn alloys[113,114,129,130].

The presence of impurities in commercial aluminium was found to be causing variations in the annealing texture. Hutchinson[98] found that the increasing iron content decreased the strength of the cube texture especially when in solid solutions. Blade[122] investigated the recrystallisation behaviour of super pure and commercial purity aluminium, by lowering the heating rates, more cube texture developed, because cube nuclei began to grow at lower temperatures. He also found that the cube nuclei were suppressed considerably in pure aluminium by iron and silicon. Bunk et al[84] suggest that iron suppresses recrystallisation to a cube texture by its effect on the rolling texture.

Gokyu et al[123] found the recrystallisation texture in Al-Cu alloys was dependent upon the solution treatment prior to cold rolling, while the cold rolling texture remained unaffected. These effects were attributed to precipitate distribution during primary recrystallisation, and the suppression of random nucleation around precipitate particles. Generally speaking, the effect of solid solution is to weaken the sharp, "pure-metal" texture and lead to the retention of rolling textures. Hatherly et al[126] have

also considered the effect of the second-phase on texture development. In commercially pure aluminium it was found that the nucleation expected to be associated with large Al-Fe-Si particles on recrystallisation resulted in a strong texture[127], which is in contrast with the present work.

Coarse particles act as preferential sites for nucleation, and because the cube oriented grains in aluminium recover more strongly and rapidly than the differently oriented area, the final texture is dominated by the orientation from growing nuclei initiated in the vicinity of these big particles. From this point of view it was considered that this is why a sharp cube texture can be developed only in high purity aluminium without particles prior to rolling. Large numbers of particles completely inhibited the formation of cube texture.

The (110)[001] oriented crystal (A) is stable up to about 70% reduction by cold rolling and the original orientation is retained with just a little spread along the rolling direction, Figure (61 A,B). The recrystallisation texture of the deformed crystal consisted of four separate orientations of the type with components $\{534\}\langle 112\rangle$. Two of them are weak and the other two strong, with little spread along the transverse direction, Figure (61 C,D). There is some spread observed but it is too weak to identify in detail. While in crystal (B) of $(231)[\bar{1}2\bar{4}]$ orientation the corresponding deformation texture is stable during deformation and retained its original orientation

with spread along the rolling direction, Figure (61 E,F) These spreads which were present in crystals (A) and (B) were possibly due to the presence of the coarse, second-phase particles prior to deformation. This orientation was found to be stable up to 95% reduction[14]. The annealing texture contained two different components of $(234)[11\bar{2}\bar{7}]$ and $(013)[33\bar{1}]$ plus a spread along the transverse direction, Figure (61 G,H). Recrystallisation textures in each crystal depended on their original orientation. Since crystals (A) and (B) containing second-phase particles prior to rolling deformation resulted in inhomogeneous deformation, and these coarse particles rotated during deformation, so high local deformation will occur in the vicinity of the particles with large lattice curvature, i.e. there was a more complicated structure near to these particles, therefore a spread of orientation was produced, as has been reported by other workers[72,73, 111,117,119]. Because of this, these areas become more favourable sites for nucleation during primary recrystallisation. By comparison, the results determined from X-ray pole figures together with the TEM results showed that these components arose from the orientation spread around the particles, possibly, as mentioned earlier, the area close to the particles was more complicated and many orientations were present resulting in the formation of multiple nuclei which restricted each other from growing, whereas other nuclei,formed within the spread of orientation around the particles, grew and consumed these little recrystallised grains.

In the last crystal (C), with (014)[34$\bar{1}$] orientation, which was unstable during deformation, the rolling texture splits into two nearly symmetrical components of (114)[53$\bar{2}$] and (114)[$\bar{8}\bar{4}$3]. Because of the instability of this crystal, the recrystallisation texture was different from that in previous crystals. The recrystallisation texture consisted of three components of (001)[1$\bar{3}$0], and (112)[02$\bar{1}$] and (134)[62$\bar{3}$] plus a spread along the transverse direction. It is difficult to correlate these components accurately with the nuclei orientations formed within the deformation zone around the particles. The (001)[1$\bar{3}$0] component was possibly due to the nucleation sites adjacent to the particle being located in transition bands as explained by Nes[129] and schematically illustrated in Figure (66 b).

According to the oriented nucleation model[23,89] the nuclei are considered to be part of the deformed matrix and these nuclei completely determine the recrystallisation texture. In contrast, the oriented growth model[193] disregards the details of the nucleation process and assumes that nuclei of any arbitrary orientation are present at the beginning of recrystallisation. However, the presence of these oriented grains within the deformation zone shows that the oriented growth did not play any important role[72,73,141] as has been observed in the present work. Lücke et al[65] explain the recrystallisation textures of rolled single crystals of high purity aluminium with original orientation (211)[12$\bar{4}$] and (123)[41$\bar{2}$] after 80% reduction by the 40^{o} <111> orientation relationship.

5.5.2 Pure Aluminium Single Crystal (D)

Crystal (D) of (110)[001] orientation retained its original orientation after 75% reduction. The rolling texture was remarkably sharp with a slight spread along the rolling direction, Figure (62 A,B). The significant result of this crystal was its resistance to recrystallisation under the same conditions as other crystals. This reluctance to undergo recrystallisation was probably due to homogeneous deformation. The recrystallisation texture showed random texture, Figure (62 C,D). By comparison with the previous crystal (A), which contained coarse particles before rolling, it showed a completely different behaviour. This might be due to the different deformation behaviour in these two crystals.

5.5.3 Al-Zn-Mg Alloy

The Al-Zn-Mg alloy developed a similar rolling texture to the 'pure metal' type, Figure (63 A,B). Any difference which had occurred in the development of deformation texture may be explained in terms of the formation of shear bands. The development of annealing texture is controlled by the pre-existing deformation texture and structure, and may be influenced by solid solution alloying elements. The recrystallised texture after 90% reduction of the Al-Zn-Mg alloy showed weak maxima of 3 X random with a diffused spread of orientations, Figure (63 C,D). This was probably due to the formation of a high density of shear bands, and these act as preferential nucleation

centres for recrystallisation. The importance of deformation bands and shear bands for nucleation of recrystallisation in rolled material is well established (39,132,133,139,140,145). In view of the importance of shear bands in the recrystallisation texture, Ridha et al(139) have recently shown that the formation of shear bands in copper (B) developed very weak cube texture with a diffuse spread of orientations. These shear bands prevent strong cube texture developing by destroying the cube oriented regions. A similar observation was made in work on 70:30 brass(145).

The (110)[001] oriented crystal (E) is stable with respect to the rolling deformation, with little spread along the rolling direction, Figure (64 A,B). The recrysallisation texture consisted of two separate components of the type {134} <221> plus some spread which was too weak to identify, Figure (64 C,D). The microstructure developed no shear bands during rolling; only very narrow bands were visible.

Comparing these results with those from the previous crystals (A), containing coarse particles prior to rolling, and (D) of pure aluminium, it was found that the recrystallisation texture was completely different. In the first crystal,recrystallisation occurred rapidly due to the inhomogeneous deformation, while crystal (D) which deformed homogeneously showed a random texture, and the crystal (E) (probably deformed less homogeneously) had a recrystallisation texture with two components. Thus it appears that

the recrystallisation texture depends on the deformation structure.

The rolling texture of crystal (F) with (110)[$\bar{1}1\bar{2}$] orientation, shows stability during deformation, and retained its original orientation with a little scatter and spread along the transverse direction, Figure (64 E&F) This orientation has been investigated by many workers[13-16, 25] and it was found that it possesses a high stability with respect to rolling. Lutts et al[17] found that in high purity aluminium it retained its original orientation after 80% reduction, and they reported that there is "remarkably little scatter" if the initial orientation of the specimen deviated within one degree of the (110)[1$\bar{1}$2] orientation. Similar observations have been reported by Liu et al[19] in high purity aluminium single crystal after rolling up to 99.6% reduction, where the crystal deviated from (110)[1$\bar{1}$2] by 3°. Dillamore et al[20] considered these results as an indication of the instability of the (110)[1$\bar{1}$2] orientation in aluminium crystals, in contrast with copper single crystals. They suggested that this is due to the ease of cross-slip in aluminium compared with copper. Hu et al[21] have observed a remarkably sharp texture in a crystal of zone-refined aluminium rolled at -78°C to 80% reduction. This is possibly because at a lower temperature the incidence of cross-slip is reduced or alternatively that at heavy deformation, surface effects may predominate.

Since the microstructure contained high density of shear

bands during deformation, so these shear bands became sites for nucleation during annealing. Due to this, the crystal was found to recrystallise very rapidly with a small resulting grain size. The recrystallisation texture consists of five components of $(012)[22\bar{1}]$, $(124)[44\bar{3}]$, $(134)[\bar{3}01]$, $(144)[41\bar{2}]$ and the final component was $(112)[\bar{4}\bar{2}3]$, Figure (64 G,H). These were the same as those of the nuclei within the shear bands, so that the presence of shear bands controls the recrystallisation texture in this crystal through their effect on preferential nucleation. Recently a similar observation has been reported by Hutchinson et al[140] in Silicon-Iron single crystals. The recrystallisation process was dominated by oriented nucleation.

The last two crystals (G) and (H) had the nominal orientation $(231)[1\bar{2}4]$ and $(241)[1\bar{1}2]$ but they deviated from the original orientation by 5^{o} and 4^{o} respectively. Upon rolling, these orientations were found to change into $(110)[1\bar{1}3]$, Figure (64 I,J) and $(231)[2\bar{3}5]$, Figure (64 M.N) with a little spread along the rolling direction. It is reported that the $(231)[1\bar{2}4]$ orientation was stable and retained its original orientation during deformation[26], and this was also observed in the present work, crystal (B). So according to this the changing in their orientation was probably due to the large deviation from their original nominal orientation. During annealing, crystal (G) recrystallised very rapidly compared to the crystals (F) and (H) with large grain size where the incidence of the shear bands in crystals (F) and (H) was higher than in

crystal (G). The recrystallisation texture consisted of two components for both crystals, (122)[41$\bar{3}$] and (431)[1$\bar{3}$5] in crystal (G), Figure (64 K,L) and in crystal (H) (310)[$\bar{1}$33] and (114)[$\bar{1}\bar{3}$1] with spread along the rolling direction, Figure (64 O,P). The origin of the recrystallisation texture is not associated with the orientation of the first formed nuclei within the shear bands as observed with the previous crystal (F). It has been suggested that shear bands should contribute significantly to the development of annealing texture. In copper Ridha et al[139] have recently shown that the introduction of shear bands prevents the development of strong cube texture. Also in 70:30 brass[145] it has been shown that a virtually random array of nucleus orientations is produced when recrystallisation is confined to the shear bands. The results given here certainly show that nucleation occurred first in shear bands, but was not random, and the final annealing texture was not derived from these first formed nuclei. As explained in section (5.3) this is probably due to the copious nucleation found in the shear bands which gives a fine grained structure which restricts each others growth and prevents them from growing to a large size whilst at the same time other isolated nuclei form in other regions and grow rapidly to consume the fine grains and produces the final annealing texture.

CONCLUSION

1 - The coarse, non-deformable square platelet particles in Al-Mg-Si with mean length about 6μm were rotated during deformation and lay parallel to the rolling direction.

2 - The structure of the Mg_2Si particle is f.c.c. with lattice parameter $a_o = 6.365 \overset{o}{A}$.

3 - The existence of such particles prior to cold rolling affected the deformation structure and the subsequent rolling and annealing texture. The result was the development of a weak rolling texture and a random final annealing texture.

4 - The nuclei of the new grains formed on annealing preferentially in the vicinity of the particles.

5 - Multiple nucleation events occurred near to each large precipitate particle.

6 - The recrystallisation texture was the same as the orientation of the nuclei formed adjacent to the particle.

7 - No shear bands were formed in rolled crystals of $(110)[001]$ and $(231)[\bar{1}2\bar{4}]$ orientation after about 71% reduction, and they retained their orientation. During primary annealing, nucleation occurred adjacent to the particles, and the orientations of these nuclei were

similar to those observed in the fully recrystallised specimen.

8 - During cold rolling of pure aluminium single crystals with orientation (11$\bar{0}$)[001] no shear bands formed after about 75% reduction at room temperature, and it was found that this crystal was difficult to recrystallise.

9 - In rolled crystals with orientaions (110)[$\bar{1}1\bar{2}$], (231)[$1\bar{2}4$] and (241)[$1\bar{1}2$] shear bands developed after 80% reduction at room temperature except in the crystal with orientaion (110)[001]. During primary annealing the recrystallised grains formed preferentially within the shear bands. The recrystallisation texture in crystal (F) was derived from new grains which nucleated within the shear bands, but this was not the case for the other crystals.

10 - The shear bands developed in rolled crystals depend largely on their initial orientation.

11 - Orientations of the crystallites within the shear bands are not random.

12 - Deformation inhomogeneity in Al-Zn-Mg alloy was shown by the development of microbands (crystal (E)) and shear bands (crystals (F,G & H)) which were inclined at about 30-35^{o} to the rolling direction and were not parallel to the transverse direction.

13 - The rolling textures in Al-Mg-Si and Al-Zn-Mg alloys conformed to the usual "pure metal" type typical of high Stacking Fault Energy materials.

APPENDIX (A)

Rotation of Precipitate During Plane Strain (Rigid Plate)

For finite rotation, consider the precipitate end point deforming as a material point:-

giving

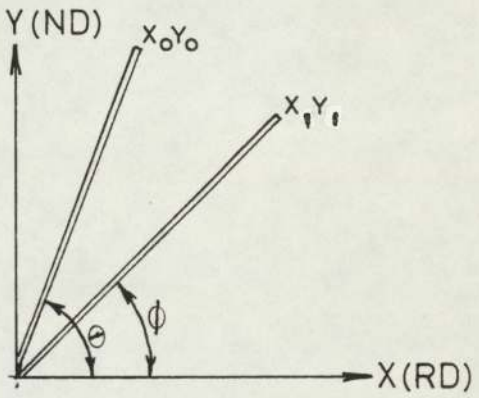

$$\tan\theta = \frac{y_o}{x_o}, \quad \tan\phi = \frac{y_1}{x_1}$$

$$\frac{\tan\phi}{\tan\theta} = \frac{y_1}{y_o} \cdot \frac{x_o}{x_1}$$

$$\ln\left(\frac{\tan\phi}{\tan\theta}\right) = \ln\left(\frac{y_1}{y_o}\right) + \ln\left(\frac{x_o}{x_1}\right) = 2\varepsilon$$

Where ε is the negative strain value.

Proceeding with this

$$\tan\phi = e^{2\varepsilon} \tan\theta$$

$$\phi = \tan^{-1}\left(e^{2\varepsilon} \tan\theta\right)$$

The distribution function $f(\theta)$ will be transformed such that the equality of integrals:-

$$\int_{\phi_o}^{\phi_1} g(\phi)\, d\phi = \int_{\theta_o}^{\theta_1} f(\theta) \cdot d\theta$$

is maintained in the limit $\theta_1 = \theta_o + d\theta$, so giving

$$g(\phi) = f(\theta)\, \frac{d\theta}{d\phi}$$

which gives

$$g(\phi) = f(\theta) \cdot \exp.(2\varepsilon)/\cos^2\theta \left[1+(\exp(2\varepsilon).\tan\theta^2)\right]$$

as the transformation between the angular distribution functions prior to and following straining.

REFERENCES

1. H.Brooks — Metal Interface Amer, Met. Soc. Met. 20, 1952

2. J.H.Van Der Merwe — Proc. Phys. Soc. 63 A, 616, 1950

3. A.Kelly & R.B.Nicholson — Precip. Hard. Prog. in Material Sci. 10, 154, 1963

4. A.Kelly & R.B.Nicholson — ibid p.155

5. T.Federigh & G.Thomas — Phil. Mag. (7), , 127, 1962

6. F.R.N.Nabarro — Proc. Phys. Soc., 52, 90, 1940

7. F.R.N.Nabarro — Proc. Roy. Soc., A175, 519, 1940

8. W.Boas & J.K.MacKenzie — Prog. Met. Phys., 2, 90, 1950

9. L.F.Mondolfo — Al. Alloys - Structure & Properties Butterworth, 1979

10. H.K.Hardy & T.J.Heal — Prog. Met. Phys., 5, 143, 1954

11. G.Thomas — J.I.M., 90, 57, 1961/62

12. M.H.Jacobs — Phil. Mag., 26, 1, 1972

13. C.S.Barrett & F.W.Steadman — Trans. AIME, 147, 57, 1942

14. Y.C.Liu & W.R.Hibbard,Jr. — ibid, 197, 673, 1953

15. W.R.Hibbard,Jr. & W.R.Tully — Trans. Met. Soc. AIME, 221, 336, 1961

16. H.Hu, R.S.Cline & S.R.Goodman — (Recrystallisation grain growth & textures), 295, 1966, As.M. Metals, Park, Ohio

17. A.H.Lutts & P.A.Beck — Trans. AIME, 200, 257, 1954

18. S.Kohara, P.A.Beck & M.N.Parthasarathi — Trans. Met. Soc. AIME, 212, 875, 1958

19. Y.C.Liu & W.R.Hibbard Jr. — Trans. AIME, 203, 1249, (1955)

20. I.L.Dillamore & W.T.Robert — Met. Rev., 10, 271, (1965)

21. H.Hu, [illegible] & B.B.Rath — Trans. AIME, 236, 1193, (1966)

22. C.A.Verbraak — Acta Met., 6, 580, (1958)

23. W.G.Burgers & P.C.Louwerse — Z.Physik, 67, 605, (1931)

24. R.M.Brick — Trans. AIME, 137, 193, 1940

25. H.Alborn, J.Grewen & G.Wassermann — Z.Metallked, 55, 598, (1964)

26. M.N.Parthasarathi & P.A.Beck — Trans. Met. Soc. AIME, 221, 831, (1961)

27. H.Hu & P.A.Beck — J.Met., 2, 1214, (1950)

28. H.Hu, P.R.Sperry & P.A.Beck — Trans. AIME, 194, 76, (1952)

29. R.E.Smallman — J.I.M., 84, 10, (1955/56)

30. Y.C.Liu & R.H.Richman — Trans. Met. Soc. AIME, 218, 688, (1960)

31. R.H.Richman & Y.C.Liu — ibid, 221, 720, (1961)

32. H.J.Bunge — Z.Metallked, 56, 872, (1965)

33. J.S.Kallend & G.J.Davies — Texture, 1, 51, (1972)

34. P.T.Wakefield, A.S.Malin & M.Hatherly — J. Aust. Inst. Met., 22, 145, (1977)

35. [illegible]

36. R.K.Ray, W.B.Hutchinson, F.M.C.Besag & R.E.Smallman — J. Micro, 97, 217, (1973)

37. V.Schmidt, K.Lücke & J.Pospiech — "Texture and properties of Mater." 4th ICOT, The Met. Soc., Cambridge 147, (1975)

38. H.Hu & S.R.Goodman — Trans. AIME, 227, 627, (1963)

39. W.B.Hutchinson, B.J.Duggan & M.Hatherley — Met. Tech., 6, p.398, (1979)

40. T.L.W.Richards — J.I.M., 84, 503, (1955/56)

41. F.Haessner — Z.Metallked, 54, 98, (1963)

42. T.L.L.Richards & S.F.Pugh — J.I.M., 88, 399, (1959/60)

43. I.L.Dillamore & W.T.Robert — Acta. Met., 12, 281, (1964)

44. R.E.Smallman & D.Green — ibid, 145

45. Y.C.Liu — Trans. AIME, 230, 656, (1964)

46. J.F.W.Bishop — J.Mech. Phys. Solids, 3, 130, (1954)

47. E.A.Calnan — Acta. Met., 2, 865, (1954)

48. G.Wassermann — Z.Metallked, 54, 61, (1963)

48a. H.Hu, R.S.Cline & S.R.Goodman — J.appl.phys., 12, 1392, (1961).

49. J.Hirsch, K.H.Virnich & K.Lücke — ICOTOM(6), 375, (1981)

50. S.Kohora, P.A.Beck & M.N.Parthasara thi — J.Appl. Phys., 29, 1125, (1958)

51. B.G.Liebmann, K.Lücke & G.Mas ing — Z.Metallked, 47, 57, (1956)

52. B. .Liebmann & K.Lücke — Trans. AIME, 206, 1413, (1956)

53. H.Yoshida, K.Lücke & B. .Liebmann — Acta. Met., 7, 51, (1959)

54. G.D.Graham & R.W.Cahn — Trans. AIME, 206, 504, (1956)

55. G.D.Graham & R.W.Cahn — ibid, P. 517

56. R.E.Green, B. .Liebmann & H.Yoshida — Trans. Met. Soc. AIME, 215, 610, (1959)

57. C.S.Barrett, C.D.Graham & J.M.Lommel — Acta. Met., 7, 699, (1959)

58. F.Haessner — Z.Metallked, 52, 651, (1961)

59. G.Czjzek & F.Haessner — ibid, 51, 567, (1960)

60. K.Lücke & F.Haessner — Acta Met., 3, 204, (1955)

61. Y.C.Liu — Trans. AIME, 209, 836, (1957)

62. C.A.Verbraak — Z.Metallked, 51, 646, (1960)

63. C.A.Verbraak — Acta. Met., 8, 65, (1960)

64. H.W.F.Heller, G.Wolff J.H.Van Dorp & C.A.Verbraak — Met. Sci., 15, 333, (1981)

65. J.Hansen, H.Mecking & K.Lücke — Acta Met., 24, 633, (1976)

66. K.Lücke, R.Rixen & M.Senna — ibid, p. 103

67. G.D.Kohihoff, J.Hirsch U.V.Schlippenbach & K.Lücke — ICOTOM (6), 489, (1981)

68. C.S.Barrett — "The Structure of Metals" 1953

69. A.A.Ridha — Ph.D.Thesis, University of Aston, (1981)

70. T.Noda & J.Huber — Z.Metallked, 69, 570, (1978)

71. E.Heller, J.Slakhorst & T.Verbraak — ibid, 68, 31, (1977)

72. J.Grewen & J.Huber — ibid, p.647

73. P.Herbst & J.Huber — Proceeding of the 5th ICOTOM-Achen , (1978)

74. P.A.Beck & H.Hu — J.[illegible].M., 4, 83, (1952)

75. H.Hu, R.S.Cline & S.R.Goodman — Trans. Met. Soc. AIME., 224, 96, (1962)

76. H.Hu — ibid, 221, 130, (1961)

77. A.Merlini & P.A.Beck — Trans. AIME, 203, 385, (1955)

78. I.L.Dillamore — Acta. Met., 12, 1005, (1964)

79. A.Merlini & P.A.Beck — ibid, 1, 598, (1953)

80. K.Lücke — Z.Metallked, 45, 86, (1954)

81. J.Grewen — ibid, 59, 212, (1968)

82. J.Grewen — Metall., 19, 664, (1965)

83. J.C.Blade — J.I.M., 90, 374, (1961/62)

84. W.Bunk & P.Esslinger — Z.Metallked, 50, 278, (1959)

85. F.Haessner, G.Masing & H.P.Stüwe — ibid, 47, 743, (1956)

86. C.S.Barrett — Trans. AIME, 137, 128, (1940)

87. N.K.Chen & C.H.Mathewson — ibid, 194, 501, (1952)

88. P.A.Beck — ibid, 203, 1270, (1955)

89. I.L.Dillamore & H.Katoh — Met. Sci., 8, 73, (1974)

90. I.L.Dillamore, P.L.Morris, C.E.Smith & W.B.Hutchinson — Proc. Rey. Soc., 329 A, 405, (1972)

91. C.T.Wei, P.A.Beck & M.N.Parthasarathi — J.Appl. Phys., 28, 874, (1957)

92. W.G.Burgers & C.A.Verbraak — Acta. Met., 5, 765, (1957)

93. P.A.Beck & H.Hu — "Recrystallisation, grain growth & texture" ASM, 393, (1966)

94. P.A.Beck, P.R.Sperry & H.Hu — J.Appl. Phys., 21, 420,(1950)

95. T.Noda & J.Huber — Z.Metallked, 69, 570, (1978)

96. H.Heller,J.Slakhorst & T.Verbraak — ibid, 68, 31, (1977)

97. B.F.Decker & D.Harker — J.Appl. Phys., 22, 900, (1951)

98. W.B.Hutchinson — Met. Sci., 8, 185, (1974)

99. J.E.Bunk — J. M., 4, 263, (1952)

100. U.Köster — J.Met. Sci., 8, 151, (1974)

101. W.C.Leslie , J.T.Michalak & F.W.Aul — Iron and Its Dilute Solid Solution, 119, (1963)

102. J.C.Blade quoted by R.D.Doherty & J.W.Martin — J.I.M., 91, 332, (1963)

103. R.D.Doherty & J.W.Martin — ibid, p.332

104. R.D.Doherty & J.W.Martin — Trans. Met., 57, 874, (1964)

105. T.C.Rollason & J.W.Martin — Acta. Met., 18, 1267, (1970)

106. T.C.Rollason — J.Mat. Sci., 5, 127, (1970)

107. F.J.Humphreys & A.T.Stewart — Surface Sci., 31, 389, (1972)

108. U.Köster — "Recrystallisation of Metallic Material" Ed. F.Haessner, Riieder Stuttgrat, 215, (1971)

109. P.R.Mould & P.Cotterill — J.Mat. Sci., 2, 241, (1967)

110. D.T.Gawne & G.T.Higgins — ibid, 6, 403, (1971)

111. F.J.Humphreys — Acta. Met., 25, 1323, (1977)

112. E.Nes & Embury

113. E.Nes — Scripta. Met., 10, 1025, (1976)

114. E.Nes — Metallurga I Odlewnictwo - TOM 5, Zeszyt 2, 209, (1979)

115. G.Scharf & W.Gruhl — Z.Metallked, 60, 413, (1969)

116. R.K.Ray, B.J.Duggan & W.B.Hutchinson — Acta. Met., 23, 831,(1975)

117. J.R.Porter & F.J.Humphreys — Met. Sci., 13, 83, (1979)

118.	F.J.Humphreys	Recrystallisation & grain growth Multi-phase & particle containing materials, p.35, Riso Nat. Lab. Denmark (1980)
119.	F.J.Humphreys	Met. Sci., 13, 136, (1979)
120.	C.Zener quoted by C.S.Smith	Trans. Met. Soc. AIME, 15, 175, (1948)
121.	W.B.Hutchinson & I.L.Dillamore	Ref.(114) p.257
122.	J.C.Blade	J. Inst. Met., 12, 55,(1967)
123.	I.Gokyu, H.Abe & N.Veyama	Nippon Kinzoku Gakkai-Si, 29, 51, (1965)
124.	S.R.Goodman & H.Hu	Trans. Met. Soc. AIME, 233, 103, (1965)
125.	C.A.Clark & P.B.Mee	Z.Metallked, 53, 756, (1962)
126.	M.Hatherly & I.L.Dillamore	J.Aust. Inst. Met., 20, 71, (1975)
127.	K.Lucke & R.Rixen	Z.Metallked, 67, 338, (1976)
128.	F.J.Humphreys	Metals Forum, 1, 123, (1978)
129.	E.Nes	Ref.118, p.85
130.	E.Nes & B.Anderson	NTNF/SI-7801 38-1, 37, (1980)

131. E.Harbogen & H.Kreye — Texture in Research & Practice, Ed. J.Grewen & G.Wasserman, 274, (1969)

132. J.Adcock — J.I.M., 27, 73, (1922)

133. J.Grewen, T.Noda & D.Sauer — Z.Metallked, 68, 260, (1977)

134. M.Hatherly — Conf. on High Strain Deformation/ University of Birmingham, 1976

135. B.J.Duggan, M.Hatherly W.B.Hutchinson & P.T.Wakefield — Met. Sci., 12, 343, (1978)

136. S.Nourbaksh & J.Nutting — Acta. Met., 28, 357, (1980)

137. K.Brown — J.I.M., 100, 341, (1972)

138. P.V.Houtte & E.Aernoudt — Mat. Sci. Eng., 23, 11, (1976)

139. A.A.Ridha & W.B.Hutchinson — Acta. Met., 30, 1929, (1982)

140. T.Haratani, W.B.Hutchinson, I.L.Dillamore & P.Bate — Met. Sci., 18 No.2, 57, (1984)

141. K.Brown & M.Hatherly — J.I.M., 98, 310, (1970)

142. K.Morii, M.Mera & Y.Nakayama — Trans. J.I.M., 18, 7, (1977)

143. S.Yoshioka, M.Mera & K.Morii — J.Jap.IM., 39, 394, (1975)

144. K.Morii, M.Mera & Y.Nakayama — Trans. J.I.M., 21, 20, (1980)

145. B.J.Duggan, W.B.Hutchinson & M.Hatherly — Scripta Met., 12, 293, (1978)

146. W.F.Hosford & R.H.Zeisloft — Met. Trans., 3, 113, (1972)

147. I.L.Dillamore, J.G.Robert & A.C.Bush — Met. Sci., 13, 73, (1979)

148. G.Wasserman, H.W.Bergmann & G.Frommeryer — Proceeding of the 5th ICOTOM 1, 37, (1978) Achen

149. J.F.W.Bishop & R.Hill — "Deformation Geometry for Materials Scientists" Ed. by Reid & Nicholas, P.145, 1973

ACKNOWLEDGEMENTS

I am greatly indebted to Dr.S.Murphy for his expert guidance and continual encouragement, especially during the writing up of the thesis.

I wish to express my sincere appreciation to my supervisor Dr.W.B.Hutchinson.

The author wishes to express her gratitude to Professor I.L.Dillamore former Head of Metallurgy and Material Engineering, Professor J.T.Barnby Head of the Metallurgy and Material Engineering for the provision of laboratory facilities, and to Dr.P.Bate for the many helpful suggestions and advice.

My thanks are also due to Dr.I.Jones and Dr.M.Hall for their guidance in scanning transmission and scanning electron microscopy at Birmingham University, and to the technicians of the department for their help.

I wish to express grateful thanks to my husband for his encouragement and my little daughter for her patience throughout the period of research. Last but not least, I am grateful to my eldest brother for his support and invaluable encouragement.

The author also thanks the Iraqi Government for financial support.

Finally, thanks are due to Mrs.A.Howell for typing this thesis.